# Modelling Water Quality for Water Distribution Systems

A thesis submitted for the degree of

Doctor of Philosophy

by

Stefan Heinrich Maier

Department of Manufacturing and Engineering Systems

Brunel University, Uxbridge

February 1999

*Dedicated to my parents,*

*Hanna and Heinz Maier*

# Acknowledgements

Special thanks go to my supervisor, Dr. Roger Powell, for guiding and supporting me throughout this project. He always made time for helpful discussions and his enthusiasm was an inspiration to me. I am also very thankful to my industrial supervisor, Tony Woodward, who was equally supportive, helpful and challenging.

Much support for my work came from the team of people at Thames Water Utilities Ltd. that was working on the pipe rig during the time of my experiments. I am indebted to all of them for their help, frequently starting at six o'clock in the morning, but in particular the contributions of Anaïck Delanoue, Dr. David Holt and Dr. Sarah McMath were invaluable.

I am also much obliged to Thames Water Utilities Ltd. who provided, among other things, the experimental set-up, the large-scale "TORUS" pipe rig, and granted me the use of the obtained and previous data.

Last but not least, many discussions with my father, Prof. Heinz Maier, and my friends and colleagues, especially Dr. Johannes Andersen and Silvio Hrabar, did help me to clarify (or discard) my ideas. All my family and my friends both in England and back home in Germany were an invaluable support throughout the time of my research work at Brunel and I am very privileged to have them.

# Abstract

Maintaining water quality in distribution systems has become a prominent issue in the study of water networks. This thesis concentrates on disinfectant and particle counts as two important indicators of water quality.

The models discussed in this work are based on data collected by the author. The experimental set-up and procedure are described and observations of particle counts, particle counter size distributions, monochloramine as disinfectant, temperature, heterotrophic plate counts and epifluorescence microscopy counts are reported.

A model of the response of particle counts to an increase in flow is developed. This model is obtained from specification derived from the data and assumptions, and is validated by its interpretability and its fit to data. A local shear-off density and an initial biofilm shedding profile were introduced and thus a linear model for this part of the water quality dynamics could be obtained. A procedure for the identification of the parameters of the local shear-off function and for the determination of the biofilm shedding profile is presented. This profile can be used to provide information about the status of the distribution system in terms of shear-off from the biofilm on the pipe walls.

Monochloramine decay dynamics are investigated. The chlorine meter data is preprocessed with the help of titration data to correct meter drift. The data is then used in calibrating two different possible chlorine models: a model with a single decay coefficient and a model with bulk decay coefficient and wall demand (as used in Epanet). Important difficulties in identifying these parameters that come about because of the structure of the models are highlighted. Identified

decay coefficients are compared and tested for flow, inlet chlorine and temperature dependence.

The merits and limits of the approach to modelling taken in this work and a possible generalisation are discussed. The water industry perspective and an outlook are provided.

# Contribution to Knowledge

The accompanying thesis is based on work carried out by the author at Brunel University between October 1995 and December 1998.

All work and ideas in this thesis are original, unless otherwise acknowledged in the text by references. The work has not been submitted for another degree in this university, nor for the award of a degree or diploma at any other institution.

In the following, a list of the contributions of this thesis to knowledge in the fields of water quality modelling for water distribution systems and system identification is provided.

1. A qualitative characterisation of data collected by the author shows the structure of the particle counts data and highlights relationships between particle counts and bacteriological data.

2. The preprocessing of pipe rig data, in particular the chlorine meter data, is addressed in some detail. It gives novel insight into the degree of uncertainty associated with chlorine data and presents an original procedure for the correction of these errors.

3. The approach to the development of the system structure from data that is taken in this thesis is novel. The modelling work of this thesis is based on data and is obtained with the help of specifications and assumptions and validated by fitting and physical or biological interpretation.

4. The particle counts model, resulting from the approach taken in this thesis, is another important new contribution. The concept of a local shear-off

function allows the development of a linear model that describes shear-off from biofilms that comes about due to a flow increase.

5. The particle counts model describes dynamic transient biofilm detachment in terms of particle counts, a process that previously found little attention and no mathematical description in the literature.

6. The determination of the biofilm shedding profile opens a new way for testing distribution systems for critical areas in terms of particle shear-off. Thus, the state of the system can be investigated.

7. Finally, through the comparison of the parameter estimation of two possible monochloramine decay models, novel insights in the limitations and the usefulness of these models are presented.

Parts of chapter 1, chapter 3, work related to section 8.2 and results from previous experiments were published at the Doctoral Research Conference, Department of Manufacturing and Engineering Systems, Brunel University [96]. Parts of chapter 4 were included in the Proceedings of the International Conference on Biofilms in Aquatic Systems [98]. Earlier results of the work presented in section 5.3 and chapter 7 were published at the International Conference on Computing and Control for the Water Industry [97].

# Contents


**I Background** 1

**1 Introduction** 2
- 1.1 Overview . . . 2
- 1.2 Water Quality in Water Distribution Systems . . . 3
- 1.3 Processes in Water Pipes . . . 5
  - 1.3.1 Suspended Biomass . . . 5
  - 1.3.2 Biofilm . . . 6
  - 1.3.3 Nutrients . . . 6
  - 1.3.4 Disinfectant . . . 6
  - 1.3.5 Particles . . . 7
- 1.4 A Systems View . . . 7
- 1.5 Thesis Organisation . . . 8

**2 Literature Review** 9
- 2.1 Introduction . . . 9
- 2.2 Water Distribution Systems . . . 10
- 2.3 Water Quality for Distribution Systems . . . 12
- 2.4 Biofilms in Water Distribution Systems . . . 14
  - 2.4.1 Definition and Structure . . . 14
  - 2.4.2 Biofilm Processes . . . 15
  - 2.4.3 Detachment from Biofilms . . . 17
  - 2.4.4 Disinfection of Biofilms . . . 19
  - 2.4.5 Measuring Biofilms . . . 23
  - 2.4.6 Biofilm Kinetics and Models . . . 24
- 2.5 Suspended Material . . . 27
  - 2.5.1 Suspended Biomass . . . 27
  - 2.5.2 Kinetics of Suspended Bacteria . . . 28
  - 2.5.3 Inanimate Particles and Particle Counters . . . 29
  - 2.5.4 Propagation of Conservative Substances . . . 30
- 2.6 Chlorine as Disinfectant . . . 32
  - 2.6.1 Chlorine Chemistry and Simple Chlorine Kinetics . . . 32
  - 2.6.2 Modelling of Reactive Substances . . . 34
    - 2.6.2.1 Models . . . 34
    - 2.6.2.2 Case Studies . . . 37
    - 2.6.2.3 Variability of Decay Coefficients . . . 40
- 2.7 Temperature . . . 42

2.8 Multi-Quality Models . . . 42
2.9 Algorithms and Simulation . . . 44
2.10 System Identification and Physical Modelling . . . 45
2.11 The Approach of This Thesis . . . 47
2.12 Conclusions . . . 49

**II Data** **50**

**3 Experimental Work** **51**
3.1 Experimental Set-Up . . . 51
3.1.1 The Pipe Rig . . . 51
3.1.2 The Pipe Rig as Input-Output System . . . 53
3.2 Measurement Method . . . 54
3.2.1 Heterotrophic Plate Counts . . . 55
3.2.2 Bottled Samples for Heterotrophic Plate Counts . . . 55
3.2.3 Epifuorescence Microscopy . . . 56
3.2.4 Particle Counters . . . 56
3.2.5 Chlorine Meters . . . 57
3.2.6 Chlorine Titrations . . . 58
3.2.7 Bottled Samples for Chlorine Titrations . . . 58
3.2.8 Volumetric Flow Meter . . . 59
3.2.9 Temperature, pH and RedOx Potential . . . 59
3.3 Experiments . . . 60
3.3.1 Pipe Rig Experiments During 1996 . . . 60
3.3.2 Bottle Experiments During 1996 . . . 62
3.4 Problems Encountered . . . 63
3.5 Summary . . . 64

**4 Qualitative Characterisation of the Data** **66**
4.1 Total Particle Counts . . . 67
4.1.1 Observations . . . 68
4.1.2 Discussion and Hypotheses . . . 70
4.1.2.1 Peaks . . . 70
4.1.2.2 Occasional Particle Step . . . 72
4.1.2.3 Slow Signal . . . 72
4.1.2.4 Inlet Particle Counter Signal . . . 73
4.1.2.5 Particle Counts after Decrease of Flow . . . 74
4.2 Particle Counter Size Distributions . . . 74
4.2.1 Observations . . . 75
4.2.2 Discussion and Hypotheses . . . 76
4.3 Disinfection . . . 77
4.3.1 Observations in the Pipe Rig . . . 77
4.3.2 Observations in Bottled Samples . . . 79
4.4 Temperature . . . 81
4.5 Bacteriological Data . . . 81

4.5.1 Heterotrophic Plate Counts . . . 81
4.5.1.1 Observations in the Pipe Rig During SFTs . . . 82
4.5.1.2 Long-Term Observations in the Pipe Rig . . . 84
4.5.1.3 Observations in Bottled Samples . . . 85
4.5.2 Epifluorescence Microscopy Counts . . . 88
4.5.3 Discussion . . . 90
4.5.3.1 Heterotrophic Plate Counts . . . 90
4.5.3.2 Epifluorescence Microscopy Counts . . . 91
4.5.3.3 Summary . . . 92
4.6 Long-Term Effects . . . 93
4.7 Conclusions . . . 93

**III Model** **95**

**5 Preprocessing of Data** **96**
5.1 Introduction . . . 96
5.2 Switching the Particle Counters . . . 97
5.2.1 Ratios of Particle Counters . . . 97
5.2.2 Original Order of Particle Counters . . . 100
5.3 Chlorine Meter Data . . . 101
5.3.1 Correction of Chlorine Meter Errors . . . 101
5.3.2 Alternative Correction Procedures . . . 106
5.3.3 Summary . . . 109
5.4 Travel Times (Delay Times) . . . 109
5.4.1 Calculation of the Travel Time . . . 110
5.4.2 Possible Errors in Calculating the Travel Time . . . 111
5.4.3 Error Correction . . . 113
5.4.3.1 Length Correction . . . 114
5.4.3.2 Adjustment of the Meter Extraction Flows . . . 115
5.4.3.3 Final Correction . . . 116
5.5 Implementation . . . 120
5.6 Conclusions . . . 121

**6 Modelling of Particle Counter Data** **123**
6.1 Introduction . . . 123
6.1.1 Purpose . . . 123
6.1.2 Particle Counters in the Test System . . . 123
6.1.3 Results . . . 124
6.2 Model Specifications . . . 124
6.3 Numerical Statistical Models . . . 127
6.3.1 Total Particle Counts . . . 127
6.3.1.1 All attached biomass in a cell is sheared-off . . . 129
6.3.1.2 Clumps of random size are sheared-off . . . 130
6.3.1.3 A constant fraction of the remaining biofilm is sheared-off . . . 132

6.3.1.4 A decreasing fraction of the remaining biofilm is sheared-off . . . 133
6.3.2 Particle Counter Size Distributions . . . 134
6.3.3 Conclusions . . . 137
6.4 Parametric Model of the Total Particle Response . . . 137
6.4.1 Assumptions . . . 138
6.4.1.1 Peaks . . . 138
6.4.1.2 Occasional Particle Step . . . 139
6.4.1.3 Basic Model of the Slow Signal . . . 139
6.4.1.4 Extended Model of the Slow Signal . . . 142
6.4.1.5 Inlet Particle Counter Data . . . 144
6.4.1.6 Model for Particle Counts After Flow Decrease . 144
6.4.1.7 Discussion of Assumptions . . . 145
6.4.2 Development of the Positive Input Slope Model . . . 146
6.4.3 Development of a Negative Input Slope Model . . . 149
6.4.4 Examples . . . 151
6.5 Parameter Identification . . . 155
6.5.1 Data Preparation (Peak Erase) . . . 156
6.5.1.1 Peak Erase by Hand . . . 156
6.5.1.2 Automatic Peak Detect and Erase . . . 157
6.5.1.3 Inclusion of Peak Models . . . 158
6.5.2 Time Constant $T_a = \frac{1}{a}$ . . . 159
6.5.3 Parameters $k_1(f)$ and $k_2(f)$ . . . 160
6.5.4 Issues in Parameter Determination . . . 164
6.5.4.1 Impact of Peak Erase . . . 164
6.5.4.2 Normalisation of Data for Simulation . . . 165
6.6 The Initial Biofilm Shedding Profile . . . 166
6.7 Results . . . 168
6.7.1 Parameters . . . 169
6.7.2 Biofilm Shedding Profile . . . 172
6.8 Discussion . . . 177
6.9 Validation and Limitations . . . 182
6.10 Implementation . . . 183
6.11 Conclusions . . . 184

**7 Comparison of Models of Monochloramine Decay 185**
7.1 Introduction . . . 185
7.2 Review of Chlorine Kinetics . . . 186
7.3 Total Chlorine Kinetics . . . 188
7.4 Determination of Decay Coefficients . . . 190
7.4.1 Parameter Estimation for the Single Decay Coefficient Model 190
7.4.2 Parameter Estimation for the Model With Two Decay Coefficients . . . 193
7.4.3 Issues in Estimation . . . 194
7.5 Bottled Samples . . . 195
7.6 Analysis of Pipe Rig Data . . . 197

7.6.1 Single Decay Coefficient . . . . . 197
7.6.2 Combined Decay Coefficients . . . . . 204
7.7 Discussion . . . . . 206
7.8 Implementation . . . . . 207
7.9 Conclusions . . . . . 208

**IV Conclusion** **210**

**8 Discussion and Conclusions** **211**
8.1 Merits of this Approach to Modelling . . . . . 211
8.2 Generalisation . . . . . 212
8.3 Water Industry Perspective . . . . . 213
8.4 Future Perspective . . . . . 214
8.5 Conclusions . . . . . 216

**Bibliography** **218**

**Appendix** **231**

**A Model-Relevant Data** **232**
A.1 Total Particle Counts . . . . . 232
A.2 Size Distributions of Particle Counts . . . . . 245

**B Calculations for the Determination of $k_1(f), k_2(f)$** **258**
B.1 Introduction . . . . . 258
B.2 Calculation of the Laplace Back-Transform . . . . . 259
B.3 Calculation of the Full Integral . . . . . 261
B.4 A Test of Validity . . . . . 263

**C Implementation in Matlab** **265**
C.1 Overview . . . . . 265
C.2 Using the Water Quality Toolbox . . . . . 266
C.2.1 Reading Data and Time Formats . . . . . 266
C.2.2 Processing of Raw Data, Visualisation and Graphical Input 266
C.2.3 Data Analysis . . . . . 267
C.2.4 Starting a Session . . . . . 268
C.3 Summary . . . . . 268

**D Reynolds Numbers** **269**

# List of Figures


1.1 Criteria for water quality in water distribution systems . . . . . 4
1.2 Processes in water pipes . . . . . 5

3.1 Schematic drawing of the "TORUS" pipe test rig at Kempton Park. 52
3.2 The pipe rig as an input–output system . . . . . 54
3.3 Experimental Schedule showing flow and total chlorine at the pipe rig inlet, three baseline regimes of Experiment 1 are indicated . . 60

4.1 First example of total particle counts: SFT 5 . . . . . 68
4.2 Second example of total particle counts: SFT 8 . . . . . 69
4.3 Particle Counter Size Distribution of sample point 1. . . . . 75
4.4 Total chlorine vs. travel time and time at the inlet, 15.10.1996 (step flow trial 7). . . . . 77
4.5 Total chlorine vs. travel time and time at the inlet, 26.11-29.11.1996 (step chlorine trial 1). . . . . 78
4.6 Total chlorine in free chlorine bottles . . . . . 80
4.7 Total chlorine in monochloramine bottles . . . . . 80
4.8 Temperature on the left y-axis over the full experimental time period with inlet flow on the right y-axis for comparison with the schedule of the experiments . . . . . 82
4.9 Heterotrophic plate counts of inlet tank (INLET) and three sample points along the rig (SP 1, SP 2, SP 3) and inlet flow. . . . . 83
4.10 Heterotrophic plate counts of sample point 2, inlet tank and flow . 84
4.11 HPC of bottles without chlorine . . . . . 85
4.12 HPC of free chlorine bottles . . . . . 86
4.13 HPC of monochloramine bottles . . . . . 87
4.14 SFT 7: Epifluorescence microscopy counts of 'clumps' of 10 or more bacteria . . . . . 89
4.15 SFT 8: Epifluorescence microscopy counts of 'clumps' of 10 or more bacteria . . . . . 90
4.16 Simplified pattern in heterotrophic plate counts; inlet flow values are given on the right y-axis. . . . . 91
4.17 Comparison of patterns in epifluorescence counts of 'clumps' of 10 or more bacteria and the particle counter size distribution; inlet flow values are given on the right y-axis. . . . . 92

5.1 Physical quantities and measured data . . . . . 96

5.2 Discrete Fourier transform of the multiplicative error function $\epsilon_M^{IR}(t)$. 102
5.3 Corrected and uncorrected chlorine data of sample point 1. . . . . 104
5.4 Corrected and uncorrected chlorine data of sample point 3. . . . . 105
5.5 Alignment of particle counts with original parameters. . . . . 113
5.6 Alignment of particle counts of SFT 1 with final correction. . . . . 115
5.7 Alignment of particle counts of SFT 4 with final correction. . . . . 116
5.8 Alignment of particle counts of 14.12.96 (baseline flow) with final correction. . . . . 117
5.9 Alignment of particle counts of SFT 6 with final correction. . . . . 118
5.10 Alignment of particle counts of SFT 8 with final correction. . . . . 119
5.11 Alignment of total chlorine with final correction. . . . . 120

6.1 Qualitative Simulink model of particle counter response to a step increase in flow . . . . . 126
6.2 Schematic showing the discretisation of the pipe rig into $n$ cells . 128
6.3 Particle counts response to an increase in flow if all attached biomass in a cell is sheared-off. Probability of shedding is 0.01. . . . . 129
6.4 Particle counts response to an increase in flow if all attached biomass in a cell is sheared-off. Probability of shedding is 0.5. . . . . 130
6.5 Particle counts response to an increase in flow if clumps of random sizes are sheared-off. Probability of shedding is 0.5. . . . . 131
6.6 Particle counts response to an increase in flow if 1% of the remaining biofilm is sheared-off. Probability of shedding is 0.5. . . . . 132
6.7 Illustration for the subsequent remaining amounts of biofilm with a decreasing fraction (double-exponential) shear-off. Always 50 % of the remaining fraction is sheared-off. . . . . 133
6.8 Particle counts response to an increase in flow if a decreasing fraction of the remaining biofilm is sheared-off. Probability of shedding is 0.5. . . . . 134
6.9 Particle counter size distributions. . . . . 135
6.10 Particle counter size distributions. . . . . 136
6.11 Linear system with input flow $f(t)$ and output total particle counts $p(t)$ . . . . . 148
6.12 Linear system with apparent initial shedding profile $b^*(\vartheta)$ as input and output total particle counts $p(t)$, positive input slope model. . 149
6.13 Linear shear-off function and corresponding particle counter response for a flat Biofilm Shedding Profile. . . . . 151
6.14 Exponential shear-off function and corresponding particle counter response for a flat Biofilm Shedding Profile. . . . . 152
6.15 Sum of two exponential shear-off functions (second order system) and corresponding particle counter response for a flat Biofilm Shedding Profile. . . . . 152
6.16 Decreasing Biofilm Shedding Profile and corresponding particle counter response for an exponential shear-off function. . . . . 153
6.17 Increasing Biofilm Shedding Profile and corresponding particle counter response for an exponential shear-off function. . . . . 153

6.18 Quadratic Biofilm Shedding Profile and corresponding particle counter response for an exponential shear-off function. . . . . 154
6.19 Effect of reduction of negative edge threshold in peak detect for apparent initial biofilm shedding profile of SFT 6 . . . . . 164
6.20 Unfiltered and filtered apparent initial biofilm shedding profile of SFT 2 . . . . . 167
6.21 Apparent initial biofilm shedding profile of SFT 1 . . . . . 173
6.22 Apparent initial biofilm shedding profile of SFT 2 . . . . . 174
6.23 Apparent initial biofilm shedding profile of SFT 3 . . . . . 175
6.24 Apparent initial biofilm shedding profile of SFT 4 . . . . . 176
6.25 Apparent initial biofilm shedding profile of SFT 5 . . . . . 177
6.26 Apparent initial biofilm shedding profile of SFT 6 . . . . . 178
6.27 Apparent initial biofilm shedding profile of SFT 7 . . . . . 179
6.28 Apparent initial biofilm shedding profile of SFT 8 . . . . . 180
6.29 Apparent initial biofilm shedding profile of SFT 9 . . . . . 181

7.1 Simple first order decay of total chlorine. . . . . 189
7.2 Monochloramine in glass bottles and an exponential function is fitted to all data. . . . . 196
7.3 Free chlorine in glass bottles and an exponential function is fitted to all data. . . . . 197
7.4 Decay Coefficients in period 12, as example of estimated single monochloramine decay coefficients $K$ of data with low standard deviation. . . . . 199
7.5 Decay Coefficients in period 30, as example of estimated single monochloramine decay coefficients $K$ of data with high standard deviation. . . . . 200
7.6 The combined decay coefficient $K$ as used in Epanet versus the wall demand $k_w$. . . . . 204

A.1 SFT 1: Total particle counts during high flow . . . . . 233
A.2 SFT 2: Total particle counts during high flow . . . . . 234
A.3 SFT 3: Total particle counts during high flow . . . . . 235
A.4 SFT 4: Total particle counts during high flow . . . . . 236
A.5 SFT 5: Total particle counts during high flow . . . . . 237
A.6 SFT 6: Total particle counts during high flow . . . . . 238
A.7 SFT 7: Total particle counts during high flow . . . . . 239
A.8 SFT 8: Total particle counts during high flow . . . . . 240
A.9 SFT 9: Total particle counts during high flow . . . . . 241
A.10 SFT 10: Total particle counts during high flow . . . . . 242
A.11 SFT 11: Total particle counts during high flow . . . . . 243
A.12 SFT 12: Total particle counts during high flow . . . . . 244
A.13 SFT 1: Particle counter size distributions. . . . . 246
A.14 SFT 2: Particle counter size distributions. . . . . 247
A.15 SFT 3: Particle counter size distributions. . . . . 248
A.16 SFT 4: Particle counter size distributions. . . . . 249

A.17 SFT 5: Particle counter size distributions. . . . . 250
A.18 SFT 6: Particle counter size distributions. . . . . 251
A.19 SFT 7: Particle counter size distributions. . . . . 252
A.20 SFT 8: Particle counter size distributions. . . . . 253
A.21 SFT 9: Particle counter size distributions. . . . . 254
A.22 SFT 10: Particle counter size distributions. . . . . 255
A.23 SFT 11: Particle counter size distributions. . . . . 256
A.24 SFT 12: Particle counter size distributions. . . . . 257

D.1 Reynolds numbers versus volumetric flow . . . . . 270

# List of Tables


2.1 $c \times t$ values . . . . . 21
2.2 Monochloramine Decay Constants and Flow Rate . . . . . 41
2.3 Comparison between physical modelling, system identification and "hybrid" approaches. . . . . 46

3.1 Bottles taken for bacteriological analysis . . . . . 63
3.2 Bottles taken for chlorine titrations . . . . . 64

5.1 The ratios of the particle counters before and after switching . . . 98
5.2 Percentage $p_{FT0.3}$ of the maximal value of the Fourier transform at $f = 0.3\frac{1}{\text{day}}$. . . . . 107
5.3 Additive error residuals in mg/l. . . . . 108
5.4 Errors on abscissa after alignment of particle counts. . . . . 114

6.1 Thresholds for peak erase and filter window sizes. . . . . 168
6.2 Investigated time periods of SFTs. . . . . 169
6.3 Data of model parameters $a$ and $k_1(f)$ for step flow trials 1 to 9. . 169
6.4 Statistical analysis of data concerning time constants $T_a$. . . . . 170
6.5 Approximation constants $c'$ and $c''$ during step flow trials 1 to 9. . 171
6.6 Final values of total particle counts at high flow during step flow trials 1 to 9. . . . . 172

7.1 Decay coefficients and other fitted parameters of monochloramine and free chlorine bottled samples. . . . . 196
7.2 Monochloramine decay coefficient data. . . . . 198
7.3 Pairs of time periods with average decay coefficients that are not significantly different. . . . . 202
7.4 Results of the estimation of combined decay coefficients . . . . . 206

# Principal Symbols and Abbreviations

| | |
|---|---|
| $1(t)$ | unit step function |
| $A$ | cross-sectional flow area of pipe |
| AOC | Assimilable Organic Carbon |
| ATP | adenosine triphosphate |
| $a$ | decay coefficient in particle counts model |
| BSP | Initial Biofilm Shedding Profile |
| $B(s)$ | Laplace transform of $b(x)$ |
| $B^*(s)$ | Laplace transform of $b^*(\vartheta)$ |
| BDOC | Biodegradable Dissolved Organic Carbon |
| $b(x)$ | initial biofilm shedding profile, part of particle counts model |
| $b^*(\vartheta)$ | initial biofilm shedding profile as function of modified variable |
| $b_1(x)$, $b_2(x)$ | initial biofilm shedding profiles for extended specifications |
| $b_a(i)$, $b_s(i)$ | attached and suspended biomass in cell $i$, respectively |
| $b_5(\cdot)$ | fifth order Butterworth filter with zero-phase distortion |
| $c(x,t)$ | total chlorine concentration |
| $c_\infty$ | non-reactive fraction of total chlorine ($c_\infty = 0$ for free chlorine) |
| $c_m(x,t)$, $c_m(t)$ | chlorine meter reading |
| $c_b(x,t)$, $c_b(t)$ | result of bench titrations of chlorine |
| $c_c(x,t)$, $c_c(t)$ | corrected chlorine reading (after preprocessing) |
| $c$, $c'$, $c''$ | validation constants in particle counts model |
| $c_1(T)$, $c_2(T)$ | parameters of the exponential tail of the particle counts model |
| $D$ | molecular diffusivity of substance in fluid, $D = \frac{\nu}{Sc}$ |
| DOC | Dissolved Organic Carbon |
| $d$ | pipe diameter |
| $\delta$ | small positive pertubation |
| $\delta(t)$ | Dirac's delta impulse |
| $\delta'(t)$ | derivative of $\delta(t)$ |
| e.g. | for example |
| EPS | Extracellular Polymeric Substances |
| $\epsilon_M(t_i)$ | multiplicative error function, for chlorine preprocessing |
| $\epsilon_A(t_i)$ | additive error function, for chlorine preprocessing |
| $\epsilon_M^R(t)$ | $\epsilon_M(t_i)$ reverse-calibrated |
| $\epsilon_M^{IR}(t)$ | $\epsilon_M(t_i)$ reverse-calibrated and interpolated |
| $\epsilon_A^{IR}(t)$ | $\epsilon_A(t_i)$ reverse-calibrated and interpolated |

| | |
|---|---|
| $\epsilon_M^{IR,0}(t)$ | $\epsilon_M^{IR}(t)$ with the zero-frequency value set to zero |
| $\epsilon_M^{IRF}(t)$ | filtered error function $\epsilon_M^{IR}(t)$ |
| $\epsilon_M^{IW}(t)$ | $\epsilon_M(t_i)$ interpolated within recalibration windows |
| $\epsilon_A^{IW}(t)$ | $\epsilon_A(t_i)$ interpolated within recalibration windows |
| $\epsilon_M^{IW,0}(t)$ | $\epsilon_M^{IW}(t)$ with the zero-frequency value set to zero |
| $\epsilon_M^{IWF}(t)$ | filtered error function $\epsilon_M^{IW}(t)$ |
| $f(t)$ | flow rate |
| $H$ | total static head |
| HPC | Heterotrophic Plate Counts |
| i.e. | that is |
| $K$ | chlorine decay coefficient |
| $k_b$ | bulk demand, part of the chlorine decay coefficient |
| $k_w$ | wall demand, part of the chlorine decay coefficient |
| $k_f$ | flow dependent mass transfer coefficient |
| $k_1$, $k_2$ | parameters in particle counts model |
| $k = \frac{k_1}{k_2}$ | ratio of parameters in particle counts model |
| $k_d$ | biofilm detachment coeficient in 1/second |
| $L$ | pipe length |
| $L_f$ | biofilm thickness for biofilm detachment kinetics |
| $\ell_i(t)$ | polynomial for linear interpolation in the interval $[t_i, t_{i+1}]$ |
| MDPE | medium density polyethylene |
| M.V. | Maximum Value (in particle counts signal) |
| $\nu$ | kinematic viscosity of fluid |
| $p(t)$ | particle counter signal at a fixed point $x = x_0$ |
| $p_d(x,t)$ | local particle shear-off density |
| $Q$ | pump discharge |
| $R_H$ | hydraulic radius |
| SFT | Step Flow Trial |
| SP | Sample Point |
| Sc | Schmidt number |
| $Sh$ | Sherwood number or Nusselt number for mass transfer |
| $S(s)$ | Laplace transform of $s(t)$ |
| $s(t)$ | local shear-off function, part of particle counts model |
| $s_{inv}(t)$ | inverse Laplace transform of $S^{-1}(s) = \frac{1}{S(s)}$ |
| $s_1(t)$, $s_2(t)$ | local shear-off functions for extended specifications |
| $\sigma$ | standard deviation |
| $\mathcal{T}$ | temperature |
| $T$ | travel time to a fixed point $x_0$, $T = \tau(x_0)$ |
| $T_a$ | time constant in particle counts model, $T_a = \frac{1}{a}$ |
| $T_K$ | time constant in chlorine decay models, $T_K = \frac{1}{K}$ |
| TOC | Total Organic Carbon |
| $t$, $t_0$, $t_1$, $t_2$ | time |
| $t_j^r$ | $j$th recalibration time |

| | |
|---|---|
| $\tau(x)$, $\tau(x,t)$, $\tau(i,j)$ | travel time |
| $\vartheta$ | modified variable of biofilm shedding profile. $\vartheta = T - \tau$ |
| $\theta$ | threshold in peak erase algorithm |
| $\Delta t$, $\Delta\tau$ | hydraulic time step; sampling time |
| $Re$ | Reynolds number |
| $r(t_i)$ | reverse-calibration factor at time $t_i$ |
| $r_d$ | biofilm detachment rate in kg/(m$^2$ s) |
| $\rho$ | biofilm density for biofilm detachment kinetics |
| $V$ | volume |
| $V_{01}$, $V_{12}$, $V_{23}$ | pipe rig volume between two sample points |
| $v$, $v(t)$ | velocity of water |
| $\mathcal{W}$ | set of recalibration windows |
| $W_j$ | $j$th element (recalibration window) of $\mathcal{W}$ |
| $w$ | number of windows in $\mathcal{W}$ |
| $x$, $x_0$, $x_1$, $x_2$ | distance along the pipe rig |

# Glossary

Biofilm: A collection of microorganisms and their extracellular products bound to a solid surface. Biofilms are generally organic although there might be entrained inorganic debris.

Epifluorescence Microscopy: Measurement method for counting individual or clumps of live, injured and dead bacteria using fluorescent staines.

Heterotrophic Plate Counts: Measurement method for counting bacteria colonies (injured or dead bacteria are not counted, 'clumps' cannot be distinguished from single bacteria).

Initial Biofilm Shedding Profile: Snapshot of the initial amount of particles coming off the pipe walls as a function of location (i.e. distance or length); only particles that exhibit some attachment to the walls are included thus implying that they are part of the biofilm.

Local Particle Shear-off Density $p_d(x,t)$: The density per unit length of particles that are sheared-off the pipe walls given as a function of time and distance.

Local Shear-off Function $s(t)$: Particles that are sheared-off the pipe walls as a function of time only.

Shear-off: Continuous removal of biofilm due to shear forces (also known as erosion).

Sloughing: Detachment of large amounts of biofilm, aided by shear forces.

Step Flow Trial: Step increase of flow rate and subsequent step decrease (after between 14 hours and several days); frequently used as input signal for the pipe rig.

Titration: Chemical bench analysis, used for the determination of chlorine content (in terms of free chlorine, monochloramine and dichloramine) in water samples.

# Part I

# Background

# Chapter 1

# Introduction

## 1.1 Overview

This work is concerned with water as distributed in potable water supply systems. Elements of these large-scale systems are pipes, valves, pumps, reservoirs etc. The hydraulics of these systems are governed by non-linear equations involving the flow and head loss in each element.

In recent years there has been an increasing awareness of the importance of maintaining water quality in water distribution systems [35, 33]. This has given rise to the need to utilise computer models to simulate changes in water quality in order to predict and control water quality throughout distribution networks [59].

It is the aim of this work to quantify some important aspects of water quality in water distribution systems. In the long run, this should lead to the possible use of water quality in a similar way as the other states of the system (like flow or head), e.g. for estimation, control or as part of a cost function for the purpose of optimisation.

To achieve this, state variables that describe water quality (i.e. describe it to an extend considered sufficient for the purposes of this work) are defined and the underlying equations or mathematical system structure which describes there relationships is found. In this work, the methodologies of system identification

are used for that end. The water quality variables investigated in this thesis are foremost particle counts and monochloramine, but bacteriological counts (like heterotrophic plate counts or epifluorescence microscopy) are discussed as well.

A model of the response of the particle counts to an increase of flow is developed and this model is used to determine parameters and a biofilm shedding profile that give information about the condition of the pipe system in terms of biofilm (or other) shear-off. In addition, two published models of chlorine decay are adopted for monochloramine, the decay coefficients are estimated and compared, and they are investigated for dependence with other water quality variables.

## 1.2 Water Quality in Water Distribution Systems

The definition of water quality as such is by no means straightforward. Generally, it is perceived to be a collection of upper or lower limits on selected possible contaminants of water [143, 31]. Thus, a wide range of substances and physical parameters could be considered, however, the models presented in the literature frequently concentrate on water age, the propagation of conservative substances (e.g. particulate matter) or reactive chemical substances, such as disinfectants, as in [59, 123, 154] among others.

Other relevant substances include heavy metals, various toxins, dissolved oxygen, chlorides, total chlorine, and bacterial counts (e.g. heterotrophic plate count, HPC), among others. Turbidity or pH are generally also considered. Since this work is concerned with treated water, bacteria are considered to be crucial in determining the quality of water. These possible water quality criteria are illustrated in fig. 1.1.

Obviously, the treatment process is an important determinant of further water quality, however, even under the most advanced treatment small numbers of bacteria enter the distribution system. These bacteria have a potential of growth

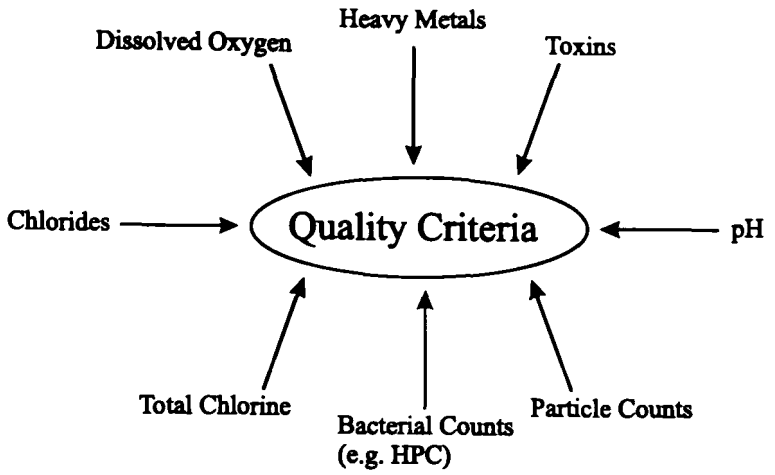


**Figure 1.1:** *Criteria for water quality in water distribution systems*

and multiplication, especially since the water is otherwise quite "clean". Thus important limiting factors for bacterial growth and multiplication, and therefore for water quality, are the amount of nutrients available and the possible presence of a disinfectant.

This thesis is concerned with the quality of the water between the outlet of the treatment plant and the consumer's tap. In this context, the disinfectant concentration is of paramount importance (rather than the nutrient content, which normally cannot be influenced after treatment). The most frequently used disinfectants in the U.K. are free chlorine ($Cl_2$) and monochloramine ($NH_2Cl$). Since the disinfectant reacts with a number of substances in water, its residual is decaying.

Another important factor is the bacteria concentration in the system. Because of the difficulties in taking pipe cutouts, water utilities generally use plate counts or epifluorescence microscopy counts as indication of biofilm growth and detachment. This seems to be justified if the system is exposed to high flow rates since it has been reported in the literature that increased biofilm detachment may be due to increased shear stress (among other things) [20, 122, 26, 144]. In this work different methods of measuring biofilm detachment under high shear stress conditions are investigated (heterotrophic plate counts, epifluorescence counts and particle counts). Shear stress is introduced by an experiment consisting of a series of flow increases.

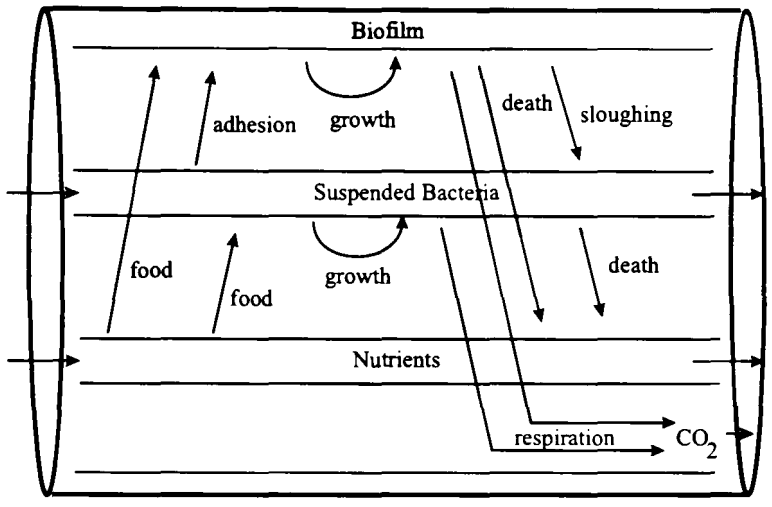


**Figure 1.2:** *Processes in water pipes*

## 1.3 Processes in Water Pipes

There are numerous chemical and biological processes taking place in any section of pipe in a water distribution system, which have an effect on water quality parameters. In Fig. 1.2, a schematic drawing of these processes is given.

### 1.3.1 Suspended Biomass

Bacteria or, more generally, biomass entering a distribution system may undergo any of the following processes:

- Growth and multiplication of living, non-injured bacteria. For this purpose, they utilise nutrients and respire.
- Respiration. On this level of organisms this can by viewed as a direct loss of mass (since $O_2$ is inhaled and $CO_2$ is exhaled).
- Death, which makes the dead bacteria part of the pool of nutrients.
- Adhesion. Some of the bacteria entering a pipe section will settle and adhere to the pipe walls and thus form a layer of biofilm.
- The number of suspended bacteria will be increased by sloughing parts of biofilm due to shear stress.

### 1.3.2 Biofilm

The bacteria settling on pipe walls form a layer of biofilm. A possible definition of "biofilm" is given in [20] (after [100]): "a biofilm is a collection of micro-organisms and their extracellular products bound to a solid (living or inanimate) surface (termed a substratum)" (p.57). Biofilm bacteria are involved in the same processes as suspended bacteria, i.e. growth and multiplication, respiration, death, adhesion (increase of amount of biofilm bacteria) and sloughing (or shear-off). In particular the decrease of biofilm bacteria due to sloughing (i.e. due to shear stress) is flow dependent.

### 1.3.3 Nutrients

Nutrients are depleted by all living biomass present. Dead biomass, however, adds nutrients to those already present.

### 1.3.4 Disinfectant

Disinfectants are generally highly reactive substances. Thus, their pure form declines in number over time to form new chemical species. This chemical reaction can kill bacteria, however the disinfectant will also react with many other substances.

The more highly reactive a disinfectant, the faster it decays, and generally the better it disinfects (while there is something left). Free Chlorine ($Cl_2$) is highly reactive and therefore decays quickly, whilst monochloramine ($NH_2Cl$) decays more slowly.

In the system under consideration, monochloramine is chosen as disinfectant since a residual of this substance is present longer than a free chlorine residual. However, this implies a slower rate of reaction with all water constituents including bacteria. The combination of all chlorine species (free chlorine, monochloramine, dichloramine, etc.) is generally termed total chlorine. There is normally no free chlorine in the considered test system.

It is suggested by some authors that monochloramine reacts better with

biofilm than free chlorine since it penetrates deeper layers of the film due to its slower reaction rate [85].

### 1.3.5 Particles

Suspended particles in the bulk liquid of more than 2 $\mu$m in diameter can be counted through on-line particle counters or may be measured through microscopic techniques. They may be inanimate or animate, conservative or reactive. Animate (i.e. reactive) particles are chiefly the suspended bacteria mentioned above, but inanimate particles are mainly debris like pieces of pipe material or entrained dirt. In the case discussed in this work it appears that animate particles form the predominate portion of counted particles.

## 1.4 A Systems View

The approach taken in this paper is inspired by systems science, viewing the test rig as a system of independent variables (flow rate, initial disinfectant concentration), dependent variables (disinfectant residual, biofilm, particles, bacteriological counts), parameters (e.g. temperature, pipe material, source water quality, initial biofilm present) and their relationships.

For the purpose of this project, a system is considered to be a theoretical object rather than e.g. the existing pipe rig. A system can be viewed as a set of variables and parameters together with their relationships. A suitable definition is e.g. given by Forrester [53]: "As used here a 'system' means a grouping of parts that operate together for a common purpose" (p.1-1). In the case considered in this work, this common purpose exists in a quite abstract way as being water quality or effecting water quality.

The associated model is the transformation of the system into the abstract domain of mathematics.

To make this transformation easier and to enhance the understanding of the system, only a simplified version of the system is transformed. This simplification

must preserve, however, all relevant variables, parameters. and relationships of the system for the specified purpose, i.e. explanation or prediction.

## 1.5 Thesis Organisation

Chapter 1 gives an introduction to the problem of water quality modelling, chapter 2 reviews the available literature in the field. The experimental work, as described in chapter 3, was undertaken at Thames Water Utilities Ltd. During the period of June 1996 to December 1996 the author was almost full-time at the experimental facility to take care of the required work. Chapter 4 describes the results obtained from these experiments. This characterisation of the data is used as a basis for the analysis of the experimental results in part III of this work. In this part, the preprocessing of chlorine meter and particle counts data is covered in chapter 5, the particle counts model in chapter 6 and the comparison of two monochloramine models in chapter 7. The thesis finishes with a discussion and conclusions in chapter 8. Appendices provide a comprehensive collection of data plots (appendix A), mathematical derivations for some of the particle counts model (appendix B) and an overview of the implementation of this work in Matlab (appendix C).

# Chapter 2

# Literature Review

## 2.1 Introduction

The literature in the fields of water distribution systems, water quality and mathematical modelling is very extensive and only a representative sample can be presented here. Naturally, the focus lies on those publications which are most relevant to this work, but also some work of more marginal significance for this thesis has been include, especially in the sections concerning water quality.

Grayman and Clark [59] give an overview of water quality modelling for distribution systems. They distinguish three different types of models of water distribution systems:

- hydraulic models "which simulate the flow quantity, flow direction, and pressure in the system"(p.81),
- steady state water quality models "which determine the movement of contaminants, their flow paths and travel times through the network under steady state operational and demand conditions"(p.81), and
- dynamic water quality models "which simulate the movement and transformation of substances in the water under time varying conditions"(p.81), i.e. demand, pressure or flow vary e.g. diurnally (or in other words: transient phenomena are also modelled).

Besides a brief explanation of these types of models, an example of a model of the propagation of a conservative (i.e. non-reactive) substance is given. In this case example the usefulness of a model for prediction purposes and analysis of a distribution system is demonstrated. The source of pollution (two leaks) could be found and validated in this investigation.

The publication by Shamir and Howard [131] gives also an overview of water quality modelling, some general thoughts and a "system's approach." The overview covers water quality as used in simulation models, methods of analysis, global network analysis and an approach to the optimisation of a hydraulic or a combined hydraulic/water quality model.

In addition to the types of models discussed in the above publications, other models which focus more on biological processes were developed recently [62, 49], see sections 2.4.6 and 2.5.2.

## 2.2 Water Distribution Systems

All the work of this thesis is aimed at potable water distribution systems. These systems are governed by hydraulic equations (flow and head) and are normally large-scale and non-linear.

A comprehensive introduction into water distribution systems is given in the book "Operational Control of Water Systems: Structures, Algorithms and Applications" by Brdys and Ulanicki [17]. It uses a systems view in investigating water systems and covers in depth, among other things, modelling, simulation, scheduling and operational control of water distribution systems, together with several case studies.

From the rich literature on hydraulic modelling only few titles are selected for this review.

Shamir and Howard's [130] publication contains an introduction to the processes involved in obtaining hydraulic models. It describes the Hardy-Cross method, which is, however, in the meantime hardly used due to poor numerical efficiency on computers.

The article by Alexander *et al.* [2] contains some basic considerations concerning the hydraulic modelling of water distribution systems and presents some of the features of their simulation program.

Several possible uses of hydraulic modelling are given: (1) analyse problems, (2) develop emergency operating procedures, (3) find water system development plans, (4) determine priorities of improvement in a capital improvement programme, (5) find out the capabilities of the existing system for different demands, (6) compare different scenarios, (7) evaluate effects of major customers, (8) consider benefits or operational problems of several water systems, (9) evaluate effects of proposed major changes, and (10) develop a real-time operational control system.

For the development of such a model it is necessary to have a schematic diagram of the system which defines sources of supply, pumping, storage, a distribution pipeline grid, etc. This could be obtained from physical features (topography, supply, reservoirs, pipelines) and operational records (source pumpage, reservoir levels, booster pumps, demand).

The underlying theory are basically "Kirchhoff's Laws" for water systems:

(1) Continuity: the rate of flow into each junction (node) must be equal to the rate of flow out of that node (including demands),

(2) Loop: total head loss around a loop is zero.

The head loss–flow relationship is for most compounds nonlinear. Thus, either Newton's method or the Hardy-Cross method are used for linearisation and numerical solution.

The hydraulic simulation program utilises Hardy-Cross and Hazen-Williams formulae for the head loss vs. flow calculations. It can simulate source pumps ($H = a - bQ^c$, with $a, b, c$=constants, $H$=total static head, and $Q$=pump discharge), booster pumps, altitude valves, check valves, and pressure reducing valves among other things.

Cohen [38] develops a dynamic hydraulic model for Amsterdam's distribution system. Advantages of dynamic models over static ones include (1) the possibility

to test the exploitation of the system, i.e. pumps, reservoirs, and controlling components, (2) the possibility to compare different solutions in the design stage, (3) the availability of travel times, (4) diagnosis capabilities, and (5) the possibility to simulate calamities.

Controlled valves, pumps or boosters are necessary to be able to control the flows in the network. In this case the dynamic simulation can be used to optimise the system performance, even in terms of quality.

Appropriate laws of hydraulics, diagrams of the network, and statistical estimates of the drinking water consumption are used to build the model. Quite an extensive derivation of the equations is given. A model of linear partial differential equations is constructed.

A example of a simple network is given and solution methods for large-scale systems are sketched. Finally a brief description of the DYNA software package is included.

The publication by Males [99] is concerned with a graph-theoretic approach to hydraulic modelling. Definitions of graphs are given briefly.

Water distribution systems are viewed as directed graphs (node-link networks) or digraphs. Indices describing the complexity of these graphs are possible (e.g. cyclomatic number, accessibility index, dispersion index). Specific indices for water systems are possible.

A public domain program WADSTAT can calculate these measures.

The paper by Andersen and Powell [3] highlights the problems associated with the controlling elements that are generally present in water systems (like non-return valves, pressure reduction valves or pressure sustaining valves).

## 2.3 Water Quality for Distribution Systems

As indicated in the introduction, water quality is generally defined in terms of criteria which concern certain contaminants of water.

Train's book "Quality Criteria for Water" [143] contains a definition of water quality criteria:

> "A specific concentration of water constituents which, if not exceeded, are expected to result in an aquatic ecosystem suitable for the higher uses of water."

Train gives a list of a number of water quality parameters, e.g. chemical elements or physical parameters like pH or temperature, and states the significance of each parameter on one to ten pages each.

The book "Water Quality Surveys" [73] published by the UNESCO and the World Health Organisation (WHO) wants to be "a guide to the collection and interpretation of water quality data" (subtitle). It includes the treatment of many practical matters and technical aspects concerning the collection and interpretation of water quality data. This book is, however, not restricted to distribution systems.

Dojlido and Best [47] in their book "Chemistry of Water and Water Pollution" give an extensive account of the chemistry involved in systems concerned with water quality. In the last chapter, a water quality index is defined. This index incorporates unit indices for each water quality parameter (range of 0 to 100) and weightings of each parameter found through questionaires.

Sinha *et al.* [133] present a "Combined Water Quality Index" to evaluate the water quality in distribution systems. This water quality index takes into account dissolved oxygen, pH, chloride concentration, turbidity, residual chlorine, conductivity, and MPN counts[1], and weights the normalised values of these parameters at each node with the flow through that node.

Adam and Kott [1] focus on the maximum growth rate of suspended bacteria and conclude "it seems that the maximum growth rate technique could serve as an additional parameter needed in the evaluation of water quality in the distribution system" (p.1412).

[1] MPN counts are not defined in this paper.

## 2.4 Biofilms in Water Distribution Systems

### 2.4.1 Definition and Structure

Wimpenny [157] states that "[there] is no simple definition of biofilms since these vary so dramatically in geometry and composition"(p.1), however, he still attempts to define a biofilm as "a predominantly two-dimensional microbial community which forms at a solid/liquid interface and which may become spatially heterogeneous by virtue of physico-chemical gradients that develop within it"(p.1).

Bryers [20] gives a slightly different definition of biofilm (according to the 1984 Dahlem Konferenz [100]): "a biofilm is a collection of microorganisms and their extracellular products bound to a solid (living or inanimate) surface (termed a substratum)"(p.57).

Van der Wende and Characklis [151] define biofilm as "a layer of microorganisms in an aquatic environment held together in a polymeric matrix attached to a substratum [...]. The matrix consists of organic polymers that are produced and excreted by the biofilm microorganisms and are referred to as extracellular polymeric substances (EPS)"(p.250).

According to this paper, biofilms are sometimes continuous, evenly distributed layers, but "often quite patchy in appearance"(p.250). A maximum thickness of a few hundred micrometres is said to be possibly reached by distribution system biofilms. Biofilms are further described as generally heterogeneous (i.e. containing different distinct microenvironments of bacterias). In addition, the film "often contains organic or inorganic debris"(p.250).

The paper of Murga *et al.* [105] gives microscopic evidence for the thickness variability of biofilm. Thickness profiles of several frozen single species biofilms are presented. Depending on the species of bacteria in the biofilm, different profiles are observed, ranging from a fairly homogeneous layer (for *Pseudomonas aeruginosa*) to a very patchy biofilm (*Klebsiella pneumoniae*).

Stoodley *et al.* [138] found that biofilm after long periods (17 days) of either laminar or turbulent flow exhibited different structures, either it contained cell clusters intersected by channels (low flow) or it had developed streamers from

the trailing edges of the clusters (high flow). Keevil [80] distinguishes between a basal layer of concentrated biofilm (thickness of ca. 5 $\mu$m) and a raised layer of up to 100 $\mu$m consisting mainly of microcolonies (a group of identical cells) that form streamers (a string of cells, attached at the base and otherwise floating in suspension).

The book "Biofilms" by Characklis and Marshall [27] gives a comprehensive overview of many aspects of biofilms, like their structure, rates of transfer processes, models and applications in technology.

### 2.4.2 Biofilm Processes

In his paper "Biologically Active Surfaces: Processes Governing the Formation and Persistence of Biofilms" [20] Bryers gives a well structured account of the processes involved in the formation of biofilms:

- Deposition-related processes, i.e. the substratum preconditioning, the cellular particle transport, and adhesion.

- Metabolic processes, i.e. growth and replication, substrate conversion (e.g. in wastewater treatment), and extracellular polymer production.

- Removal processes, i.e. predator harvesting, shear-related removal, abrasion, and sloughing.

Van der Wende and Characklis [151] focus on examples of biofilm occurrences in water distribution systems (i.e. case examples, however almost no quantitative data are included), its relevance for these systems, and possible disinfectant methods.

They define breakthrough as "the increase in bacterial numbers in the distribution system resulting from viable bacteria passing through the disinfection process" (p.249) and growth as "the increase in viable bacterial numbers in the distribution system resulting from bacterial growth downstream of the disinfection process" (p.249/250). Mentioned as main risks to water quality due to biofilms are bad taste, odour, and a high number of bacteria.

Quantitative results concerning possible disinfection of biofilms due to free chlorine in a test reactor system are provided. Monochloramine is said to be more effective in biofilm disinfection without data being given in this paper.

LeChevallier *et al.* [84] investigate which particular bacteria are part of biofilms. Biofilm samples were taken through scraping and pipe coupons. The samples were analysed with heterotrophic plate count (HPC) on $R_2A$ agar and "five-tube most-probable-number procedure" (p.2716) to enumerate coliforms. Total organic carbon (TOC) and assimilable organic carbon (AOC) were also analysed.

Results include that chlorine had little impact on the occurrence of coliforms; a free chlorine residual of 1.0 mg/litre was insufficient for full disinfection; and flushing did not necessarily reduce the amount of bacteria present.

In the introduction, Nagy and Olson [106] are cited as stating that "HPC bacteria levels increase 1 log[2] for every 10 years of service" (p.2714).

Donlan and Pipes [48] use a specifically developed "corporation sampling device (CSD)" to monitor biofilm in water supply systems. The CSD inserts sampling cylinders in water mains which can be removed for lab assays. The investigated parameters were temperature, total chlorine, HPC, solution composition, pH, alkalinity, TOC, and other chemical parameters. Some strong relationships between the following were found:

- water temperature and HPC of bulk water,
- water temperature and chlorine concentration,
- flow velocity and HPC of sampling cylinders,
- cylinder HPC and season,
- HPC of attached bacteria (cylinders) and HPC of bulk water.

No strong relationships between individual nutrient parameters and attached microbial density could be found.

[2] by a factor of 10

Martin *et al.* [101] use two glass plates, 33 × 24 cm, exposed to a flow of tap water, to measure biofilm. Steady state was reached after only two days.

Servais *et al.* [129] compare bacterial data of several French distribution systems. According to them, bacterial growth can be controlled by both, chlorine and the absence of nutrients. They establish the biodegradable dissolved organic carbon (BDOC) as a good measure for available nutrients in water and therefore a good source for the estimation of the amount of bacteria present in the absence of chlorine. The biofilm was evaluated from cast-iron coupons by an original method based on exoproteolytic activity [136], "which has been shown to be proportional to bacteria biomass"(p.12) [8].

The data from the distribution systems is evaluated in several tables and graphs. Only very little bacterial activity was found in water with chlorine residuals of 0.1–0.3 mg/litre.

### 2.4.3 Detachment from Biofilms

Detachment is a biofilm process like the ones discussed in the previous section. However, since the detachment from biofilms is the main consideration in our particle counts model of chapter 6, a separate section is devoted to it.

Bryers, in the above mentioned paper [20], distinguishes between four different types of biofilm removal processes. Predator harvesting can be quite common, it is the grazing of microbial biofilm by protozoa. Shear-related removal (or erosion) is a continuous process. Bryers sees a connection between shear, biofilm thickness and flow velocity. Abrasion is not very important in potable water distribution, but features in some biological reactors. It is the removal of biofilm due to the collision with particles. Sloughing, finally, is an event where large amounts of biofilm are detached. It is an apparently random, discrete process.

Peyton and Characklis [113, 114, 115] utilise the same equipment as used in [151]. They focus on the relationships between glucose concentration or rotational speed and biofilm thickness or detachment. In the investigated test reactor system glucose concentration is proportional to both biofilm thickness and detachment

whereas rotational speed has no influence on both. In addition they correlate various published models of biofilm detachment with their experimental results.

Stewart [137] provides a short summery of the previously published models of biofilm detachment that are also used in [115]. All models describe the detachment rate $r_d$ and contain the following:

$r_{di}$ = detachment rate of component $i$, in kg/(m$^2$ sec),
$k_d$ = detachment rate coefficient, in varying units,
$\rho_i$ = density of component $i$ in the biofilm, in kg/m$^3$,
$L_f$ = biofilm thickness, in m,
$\tau$ = fluid shear stress, in N/m$^2$.

Various equations for the detachment rate have been put forward, Stewart gives the following examples:

$$r_{di} = k_d \rho_i L_f \tag{2.1}$$

$$r_{di} = k_d (\rho_i L_f)^2 \tag{2.2}$$

$$r_{di} = k_d \rho_i L_f^2 \tag{2.3}$$

$$r_{di} = k_d \rho_i L_f \tau^{0.58} \tag{2.4}$$

$$r_{di} = k_d \tau \rho_i \tag{2.5}$$

Rittman proposed eq. (2.1) and the shear stress dependence of eq. (2.4) [122]. He reviews this and other models in [122] which stands for a number of contributions to the field by him.

Characklis *et al.* [28] proposed eq. (2.2), Gujer and Wanner [61] proposed equation (2.3) as part of their model of biofilm processes (cf. section 2.4.6), and Bakke *et al.* [6] suggested the first-order (linear) dependence on shear stress in eq. (2.5).

Both, Peyton and Characklis [115] and Stewart [137], propose more complicated detachment models. Peyton and Characklis suggest a dependence on the product of the nutrients utilisation rate, yield coefficient of biomass on substrate, flow velocity and biofilm thickness. Stewart includes the (local) growth rate of

bacteria (which also depends on nutrients and yield) and a variable depth of shear-off.

Dukan *et al.* [49] investigate three different detachment models (cf. section 2.5.2): (1) detachment is proportional to the number of fixed bacteria (2) detachment takes place only over a certain thickness proportionally to the number of fixed bacteria and their growth rate, or (3) detachment takes place throughout the thickness of the biofilm, otherwise like (2). They choose model (1) for the detachment from the chlorinated layer of the biofilm and model (3) for the non-chlorinated layer.

All of the publications discussed in this section are chiefly concerned with medium- or long-term variability of biofilm thickness due to shedding (or shear-off). Thus, the time dependence is generally assumed to be linear (i.e. a rate per time unit is found) or slowly varying. Only Peyton and Characklis [115] and Bakke and Olsson [7] mention that it was observed that shear-off briefly increases during a change of shear force, however, with an return to original values after five retention times in the experimental apparatus (a chemostat reactor). They do not investigate the transient dynamics any further.

In the work of the present thesis it is found that transient (i.e. short-term) phenomena can have a decisive impact on the amount of biomass or inanimate particles in the distribution system over periods of several days. In addition, transient detachment may account for the removal of significant amounts of biofilm. Therefore, the transient phenomena are investigated in detail to obtain information about the amount of biofilm present in the system (cf. chapter 6).

### 2.4.4 Disinfection of Biofilms

LeChevallier *et al.* [85] examine the potential of several biocides (in particular free chlorine and monochloramine) for the inactivation of biofilm bacteria. They show experimentally that monochloramine is a more efficient disinfectant of biofilms. While for free chlorine the resistance of biofilm bacteria is 150 to 3000 times higher than the resistance of suspended bacteria, resistance to monochloramine

was found to be only 2 to 100 times higher for attached as opposed to unattached bacteria.

In LeChevallier *et al.* [86] it is investigated what happens with biofilm in distribution systems if a disinfectant residual is applied.

A small (21.95 m or 72 ft) pipe system with controlled pH, temperature and flow rate consisting of different pipe materials is investigated. Chlorine and monochloramine are the independent variables and ammonia, phosphate, turbidity, water conductivity, TOC, glucose, and biofilm are measured. Biofilm is measured by

- 25 mm × 25 mm glass coverslips placed into pipes at quick-disconnect couplings; thickness is measured microscopically,
- permanently mounted electrodes monitoring the increase in electrical resistance (however reported results "did not appear to be related to biofilm thickness or plate count density", p. 15),
- scraping the interior of pipes and measuring the amount of viable bacteria through heterotrophic plate count (HPC).

Results include the following:

- The effectivity of disinfectants depends heavily on the pipe material.
- Monochloramine is (if higher than a certain threshold of roughly 2 mg/l) more effective against biofilm (especially on cast iron).
- Corrosion has a major impact.
- $c \times t$ values (concentration of disinfectant × time for the inactivation of 99% of the biofilm) do not differ much between attached and dissolved bacteria, see table 2.1.

  The "attached" bacteria were scraped from the pipe wall and than put in suspension.
- Biofilm thickness is between 60 and 110$\mu$m.

**Table 2.1:** *$c \times t$ values*

| | attached | unattached |
|---|---|---|
| Free Chlorine | $0.1 \frac{\text{mg min}}{l}$ | $0.08 \frac{\text{mg min}}{l}$ |
| Monochloramine | $95 \frac{\text{mg min}}{l}$ | $145 \frac{\text{mg min}}{l}$ |

- There is no linear relationship between disinfectant concentration and disinfectant efficiency (i.e. doubling disinfectant concentration does not result in twice the inactivation).

Clark *et al.* [36] present a study of the effects of various disinfectants ($O_3$, free $Cl_2$, $NH_2Cl$) on biofilm.

A pilot facility at Nancy is used to investigate biofilm. It consists of two sets of three loops with an average retention time of 24 hours per loop. The biofilm is evaluated from coupons consisting of pipe materials with a wetted surface of $2cm^2$ placed at the end of a sampling device probe which was inserted flush with the pipe wall. The bacterias on the surface of the sampling device are removed through sonication.

It is assumed that the biofilm reaches steady state after three to five weeks (depending on disinfectant residual). In lab assays the following was analysed:

- free and total chlorine,
- dissolved organic carbon (DOC),
- biodegradable dissolved organic carbon (BDOC),
- bacterial density
  - from water samples (bulk water),
  - from coupons (biofilm),

  HPC were used to enumerate viable bacteria and microscopic counting to find total bacteria.
- disinfection by-products.

It is observed that "the biofilm build-up increased with residence time in the loop, and increased dramatically after disinfectant residuals disappeared" (p.274).

In Block *et al.* [13] the same experimental set-up as in [36] is used.

Biofilm accumulation seems to be not prevented by chlorine. An equation for the biofilm growth rate (from [152]) is given and the relationship between the amount of total attached cells and DOC is provided (found through linear regression).

Block *et al.* [12] use again a very similar test apparatus to the one used in the previous papers [36, 13]. Results include the following

- chlorine slows down the formation of biofilm but does not prevent it,
- there exist log linear relationships of attached cells vs. chlorine concentration, planktonic cells vs. chlorine concentration, and planktonic HPC vs. chlorine concentration,
- chlorine was more effective than monochloramine (on suspended bacteria and biofilm),
- a model was made but only graphs are presented,
- BDOC increases the amount of cells even if chlorine is present.

In the report by Packer [112] of the Centre for Applied Microbiology and Research (CAMR) a test apparatus consisting of a seed vessel and a test chemostat is used to investigate the water quality of the water treated by the Advanced Water Treatment Centre (AWTC) of Thames Water Utilities at Kempton. The AWTC was also used as a source for the experiments described in this thesis.

This report investigates which particular bacteria form part of the biofilm in the test chemostat for both with and without monochloramine disinfection. Some results are that coliforms disappear after three days of high monochloramine residual; coliforms live in biofilm longer than suspended; and the AWTC water does not have a significantly changed nutrient content compared to water from previous treatment.

### 2.4.5 Measuring Biofilms

Frequently, biofilm samples were taken through scraping and pipe coupons [45, 84, 86, 36, 12, 129]. Others use devices which are inserted into water pipes for a period of time and then evaluated [48, 101, 86].

Jass *et al.* [75] use a modified Robbins device coupled to a chemostat. The Robbins device is a turbular flow system filled with a microbiologically controlled feed water, containing circular test pieces (coupons) for the evaluation of biofilm on different surfaces in a reproducible manner. The modified Robbins device includes retractable pistons from the inside of a rectangular section pipe [19].

Van der Kooij and Veenendaal [149, 150] use a special biofilm monitor developed by the Dutch company KIWA NV Research and Consultancy to measure biofilm. This biofilm monitor consists of a glass column (diameter 2.5 cm; length 60 cm) containing glass cylinders on top of each other. The column is supplied with the water to be investigated with a constant velocity (0.2 $\frac{m}{s}$). Periodically one or two cylinders are taken from the column. Subsequently, biomass density according to adenosine triphosphate (ATP) analysis and heterotrophic plate counts is obtained.

In [149] a large amount of data (in graphs) on biofilm formation with no chlorine present is given. Generally, the growth of a biofilm starts after 10 days and is normally monitored for 75 to 150 days. This paper claims that the analyses of AOC and BDOC is not enough to determine biofilm growth, instead the biofilm is evaluated with the ATP method and the biofilm formation rate (BFR) and the biofilm formation potential (BFP) are evaluated. (BFR and BFP are defined by the authors in [149].)

In [150] again the biofilm formation characteristics BFR and BFP are evaluated (using the biofilm monitor). Other methods used to determine "the rate and extent of bacterial multiplication in samples of the water to be investigated" (p. SS1-2) are:

- colony counts,
- turbidity measurements,

- ATP analysis,
- microscopic techniques,
- assessing the degree of removal of dissolved organic carbon (DOC), i.e. the biodegradable dissolved organic carbon (BDOC), or
- assessing the concentration of easily assimilable organic carbon (AOC).

The experimental set-up used for the experiments discussed in this thesis, the Kempton Park "TORUS" pipe rig of Thames Water [69] contains coupons flush with the pipe wall. Due to the difference between pipe wall and coupons in surface structure if investigated under the microscope, the small size of the coupons (1 $cm^2$) and the limited number of coupons (for continuous sampling), it was decided to consider only indirect measures of biofilm in this study (i.e. particle counts, suspended bacteria).

### 2.4.6 Biofilm Kinetics and Models

Kinetics are the first step towards a full model. Investigations in biofilm kinetics imply that the data is collected with the intention to produce a rigorous description of the underlying processes, generally in mathematical terms, possibly at a later stage or by somebody else. A model is normally a set of many one-equation kinetic descriptions, each of a process that interacts heavily with the others.

The paper by LeChevallier [83] is concerned with the major factors of microbial water quality, i.e. breakthrough, growth and disinfection. According to the author "[there] is no unified model to describe microbial processes in distribution systems, although almost all of the parameters have been studied and could be modeled"(p.365). However only an outline of a possible model is presented. A number of useful references are given.

Breakthrough consists of bacteria passing through the treatment process into the distribution system. Typical amounts of bacteria getting into the system "may range between 10 and 100 cfu/ml"(p.365) (plate counts on $R_2A$ agar). Although injured bacteria may comprise a significant portion of the total cell

population they are not normally found with standard heterotrophic plate counts (HPC). These bacteria may survive due to attachment to organic or inorganic particles.

The growth rate of biofilms depends on

- the physiochemical (i.e. chemical, thermodynamical) properties of the interface,
- the physical roughness of the surface,
- the physiological factors of the attached microorganisms,
- shear forces, and
- the possible reactions of disinfectants with extracellular polymer substances (EPS).

Factors influencing bacterial growth are

- temperature and rainfall,
- nutrients availability,
- ineffectiveness of disinfectant residual,
- corrosion and sediment accumulation, and
- hydraulic effects.

The most important nutrients required for bacterial growth are carbon, nitrogen and phosphorous in the ratio 100:10:1 (C:N:P), thus assimilable organic carbon (AOC) is growth limiting. Therefore, the author suggests combining a hydraulic model with AOC levels, bacterial growth rates and disinfectant kinetics.

Finally, disinfection does not totally prevent bacteria from proliferating. Some factors that have an effect on bacterial survival in chlorinated waters are

- attachment to surfaces,

- bacterial aggregation,
- age of biofilm,
- encapsulation,
- previous growth conditions,
- alterations in bacterial cell wall and
- the choice of disinfectant.

Again a number of useful references are given.

In Trulear and Characklis [145] an annular reactor is used as the test equipment (at 30°C ± 0.5°C). The thickness of the biofilm on a removable slide is determined microscopically. Again glucose is the source of nutrients for the bacteria.

A typical experiment progression normally includes three phases: induction, accumulation and plateau.

This paper includes a number of equations of e.g. the mass balance across the reactor of glucose accumulation or the accumulation of attached biomass among others. Data is given for the net biofilm accumulation and several other dependent variables changed through the independent variables rotational speed and glucose concentration. In their discussion the authors try to explain some of the observed effects. An interesting concept in this context is the active biofilm thickness which represents a maximum depth of penetration of glucose into the biofilm (dependent on glucose concentration).

Block *et al.* [12] present some results of a model differential equations which also includes biofilm, however, without presenting the model.

The papers of Gujer and Wanner [62, 61] develop a model for a mixed population biofilm. They develop a model of biofilm processes from physical (or biological) principles, in particular mass transfer relations. Numerous equations are provided.

Gujer and Wanner discuss briefly the merits of deductive modelling (as is done by them) over inductive modelling, which they see as using a "black box." One

of the chief advantages of their approach is that "the underlying mathematical derivations are consistent" (p.398) and "that each assumption must be clearly identified and its significance discussed" (p.398). The approach taken forward in this thesis aims at a "grey box" (thus it is basically inductive, i.e. it starts from data) rather than a system with no explanatory power, which implies that the given advantages of deductive (consistency, clear assumptions) are still aimed at (cf. section 2.11).

Dukan *et al.* [49] also include the biofilm in their model of water quality, see section 2.5.2.

## 2.5 Suspended Material

The following papers are concerned with material that is suspended in water distribution systems, which may include both biomass and inanimate material.

### 2.5.1 Suspended Biomass

Some papers mentioned in section 2.4 are partially concerned with bulk fluid bacteria, e.g. Nagy and Olson [106], Servais *et al.* [129], Block *et al.* [12] or LeChevallier *et al.* [85].

Huck [71] gives a review on measurement methods of suspended organic matter. There are a number of different methods discussed and also examples (mainly in water treatment processes) given.

On a conceptual level, Huck distinguishes between measurements aimed at bacterial regrowth and measurements aimed at the effects on chlorine demand. In the former case, AOC should be investigated, in the latter BDOC.

Also the paper of Maier *et al.* [93] discusses many measurement principles for different parameters. In particular the following parameters are dealt with: turbidity, colour, UV-absorption, nitrate, fluor carbohydrates, mangan, fluor, aluminium, ammonia, phosphate, temperature, conductivity, pH, oxygen, redox-potential, chlorine, and ozone.

The main result of the paper by Haas *et al.* [63] is that "[the] results of the statistical analyses did not support the hypothesis that the physiochemical measurements would suffice to produce reliable predictions of microbial water quality" (p. 475).

In the article by Goshko *et al.* [57] no strong relationships between plate counts and other parameters like chlorine residual or turbidity could be established. Samples were obtained from real distribution systems.

### 2.5.2 Kinetics of Suspended Bacteria

The model used by Block *et al.* [12] also includes suspended biomass, however, the model equations are not presented.

Dukan *et al.* [49] present a model that incorporates biodegradable dissolved organic carbon (BDOC), temperature, residual free chlorine, pH, hydraulic conditions (flow, diameters), free (i.e. suspended) bacteria and biofilm bacteria. For simplicity, the biofilm is modelled as a uniformly distributed over the pipe surface, however, they distinguish a chlorinated and unchlorinated layer within the biofilm. Equations of bacterial growth and its temperature dependence are given with source, the action of chlorine on bacteria is also presented mathematically (its source is not entirely clear from the paper). The model of bacteria mortality takes into account protozoa grazing which implies that the temperature dependence of bacteria mortality does not follow an Arrhenius law.

A number of equations are provided, e.g. chlorine disappearance kinetics, the concentrations of BDOC, free bacteria and active free bacteria, mass balance equations, both for chlorinated and non-chlorinated biofilm, for BDOC, fixed bacteria and active fixed bacteria and the mortality of fixed and free bacteria.

Detachment of bacteria from biofilm is identified as an important factor for the amount of free bacteria. Three different detachment models are presented and two of them are chosen for the chlorinated and unchlorinated biofilm layer, respectively.

Finally some initial results are given. They find steady state thresholds for

BDOC (0.2–0.25 ppm) and temperature ($16^0$C $\pm$ $1^0$C) below of which no significant multiplication of free bacteria takes place. They also simulated the response to a step in BDOC from 0.5 ppm to 0.4 ppm. The BDOC changes rapidly in a system with a maximum retention time of 60 hours (change within tens of hours). The active fraction of fixed bacteria not attained by free chlorine and the quantity of fixed biomass change within 10–25 days. The concentrations of active free bacteria and total free bacteria settle down to a nearly stable value after about 5 days but still exhibit some slow trend until about 30 days.

The publication of Piriou *et al.* [117] gives some more information on the model introduced in [49]. It gives a short description of the mathematical model and of the software package Piccobio. Model validation experiments, both on a experimental pipe rig and real distribution systems, are presented together with some simulation results. Apart from the thresholds already discussed in [49] they also find the water quality problems and the location of a booster chlorination station through simulation. Piriou *et al.* [118] give another overview of the functionality of Piccobio, however, without mentioning the name.

### 2.5.3 Inanimate Particles and Particle Counters

Apart from bacteria, inanimate particles may be present in the bulk liquid of water pipes. They (together with the biomass) can be measured by particle counters, provided their size falls into an appropriate size range.

The paper by O'Shaughnessy *et al.* [110] evaluates the performance of particle counters in comparison with counts made by microscopic processes. In particular a forward-angle light scattering (FALS) particle counter sensor was compared to scanning electron and optical microscope counts, and the FALS sensor was compared to a light obscuration sensor (as used in the experimental set-up used for this work, the "TORUS" pipe rig). It was found that particle counters undercount in comparison to both microscopic counts, with the degree of undercounting increasing as size range increases. Furthermore, the comparison of particle counters showed that light scattering sensors were more accurate than light obstruction

sensors when measuring latex spheres. However, when counting microorganisms, light obstruction sensors were better than light scattering counters. Since counters are calibrated for latex spheres, sizing particles, in particular if the particles are not spherical, is frequently inaccurate and therefore, "total counts made by a particle counter within a particular size range should be viewed relative to previous counts and not as an absolute indication of the number of particles with diameter associated with that size range" (p.69). A number of references are included.

The American Water Works Association Research Foundation report "A Practical Guide to On-Line Counting" by Hargesheimer and Lewis [65] gives an extensive account of the practicalities involved in using particle counters. They discuss the use of particle counters (they have been used most frequently for the evaluation of filter efficiency in water treatment), state the different types of counters (light obstruction or scattering), elaborate on how the sensors work, show different ways of looking at counts (e.g. total counts or size distributions), give a wealth of information on how to achieve best results when using particle counters and talk about quality assurance during operation. Both, batch (i.e. one-off) particle counters and continuously on-line counters are discussed.

Hatukai *et al.* [66] use particle counters to monitor water treatment. They find (among other things) that particle counters are more sensitive to changes of water quality as result of modification of operating conditions than turbidity meters.

In the next section, the publications by Woodward *et al.* [159] and Ta [140] will be discussed (among others) which are both investigating particle counts in the "TORUS" pipe rig, which was also used for the experimental work presented in chapter 3 of this thesis.

### 2.5.4 Propagation of Conservative Substances

The first work on water quality was concerned with the age of water. This, however, gives naturally rise to the investigation of conservative (i.e. non-reactive)

substances since the methodology is the same. the difference is simply the use of a 'substance' instead of just water.

The U.S. Environmental Protection Agency (EPA) report written by Clark *et al.* [35] gives the most extensive account of the example for the propagation of conservative substances in a actual water distribution system also used in [59, 32, 30, 60]. The results of the steady state model and the development of the dynamic model are presented.

It is remarked that already "hydraulic analysis and verification of flows in a system is an art in itself"(p.2).

Grayman *et al.* [60] introduce the concept of "dynamic water quality models" as opposed to steady state models. They focus on conservative substances, however mention how non-conservative substances could be dealt with (first order kinetics).

This paper gives a rather detailed account of the practicalities involved in developing dynamic models, e.g. the trade-off between simulation time and model accuracy involved in the choice of the discretisation time step. The concept of a dynamic model is described in words.

In addition, the same example as in [59, 35, 32, 30] is given.

Clark and Goodrich [32] includes a brief overview of modelling very similar to that in [59] and a short discussion of trihalomethanes (TTHMs) simulation (which is more extensively given in [37]). In addition, it states some ideas on how the actual human exposure to water contaminants could be modelled.

Clark [30] gives an extensive case study of the application of both a steady state and a dynamical model for the prediction of various water quality parameters (like amount of disinfectant by-products present or substance propagation). A fluoride tracer experiment in an actual distribution system is described (same example as in [59, 32, 60, 35]).

To model the system, EPANET [124, 123], a public domain hydraulic and water quality modelling package provided by the US Environmental Protection Agency is used.

The paper of Biswas *et al.* [10] gives a number of interesting references. The

authors apply methods of fluid dynamics to develop a model of deposition, to calculate velocity fields or to investigate cavities and bends. A lead accumulation and transport model is presented consisting of partial differential equations. In addition, results from modelling chlorine are presented.

Kennedy *et al.* [81] did fluoride and chlorine tracer studies to determine travel times. Results of these experiments are given graphically.

Woodward *et al.* [159] investigate the behaviour of particles in the Kempton test rig of Thames Water. Results from a step flow trial validate the generally made assumption of plug flow (for turbulent flow conditions), since the particle profile is propagated through the rig without dispersion.

The number of particles increases for a short period of time sharply with flow step increase. The explanation for this phenomenon is the existence of "hot spots", in which loose deposits accumulate preferably. These deposits are lifted into suspension with a step increase of the flow rate.

The internal report of Thames Water Utilities Ltd. "Analysis of the Particle Counts and the Chlorine Decay in PIPE RIG During the Step Flow Trials" by Tuan Ta [140] deals with the same experiments as [159, 160]. As additional information it contains the way in which the travel times were calculated. The average of two appropriate subsequent flow data points was used to calculate the volume covered in a given time interval.

## 2.6 Chlorine as Disinfectant

### 2.6.1 Chlorine Chemistry and Simple Chlorine Kinetics

An extensive treatment of chlorine chemistry and other issues involved in chlorinating potable water, wastewater, cooling water, industrial processes, and swimming pools is given in White's "Handbook of Chlorination and Alternative Disinfectants" [156].

A good, broad and concise overview on chlorination is given in the Blue Pages of the International Water Supply Association on "The Practice of Chlorination:

Application, Efficacy, Problems and Alternatives" [74]. This booklet gives a biological and chemical view on chlorine in distribution systems without including quantitative kinetics (e.g. decay coefficients). In addition, brief mention is made of the use of organic chloramines and monochloramine as disinfectant.

The report of Thomas [141] gives a summary of what was going on in chloramination in Australian Water Authorities at that time. The information provided in this report includes that

- the aim of most water authorities is to obtain 0.2 to 0.5 mg/l at the extremity of their system, however sometimes only the monochloramine residual decreases to 0.05 mg/l;
- the ammonia injection point can be clogged with calcium carbonate;
- in laboratory tests monochloramine is 25-100 times less effective than free chlorine, however field results are better, possibly due to an initial reaction of free chlorine as disinfectant before it forms monochloramine;
- microbial results (in particular concerning coliforms) differ substantially for the systems considered;
- the amount of disinfection by-products (THMs) is far smaller with chloramination compared to free chlorination; and
- false free chlorine residuals in the presence of ammonia and false monochloramine residuals due to indistinguishable organic chloramines are observed.

Norton and LeChevallier [109] investigate the effect of chloramination on water quality in distribution systems. Monochloramine doses in excess of 2 mg/litre were used with the result that in general, chloramination seemed to be more effective against coliforms and live bacteria as measured with HPC than free chlorine. For evaluation, they consider HPC, coliforms, corrosion, disinfection by-products and nitrification among other things. Many references are included.

The article of Ram and Malley [120] states also the possibility of a false free chlorine reading for various tests. In tests performed under laboratory conditions

the apparent chlorine residual was sufficient to determine that bacteria will not grow (with actual chlorine doses of 0.5 to 1 mg/l).

Feng [52] discusses the behaviour of organic chloramines in some detail. It is found that organic chloramines have no or little disinfecting power, in particular the lethal activities of organic chloramines are lowest at pH near neutral (pH 7). Water distribution systems generally hold a pH of about 8.

Gotoh [58] assumes an approximate first order decay of free chlorine. As possible reasons for chlorine decay he gives "(1) degradation of free chlorine, (2) reaction with contacting pipe material, and (3) reaction with oxidising substances in water"(p. SS 21-18). The first order decay factor is determined for cast iron pipes with no lining, epoxy resin-lined cast iron pipes and mortar-lined ductile cast iron pipework. Other materials were investigated but results are given only for these materials . In addition, a field survey procedure is provided.

In an experiment carried out by Nic Proux and reported by Rory Todd [142] it was established that nitrite can not exist together with free chlorine in the same sample, i.e. nitrite will react with free chlorine to form other chlorine species.

### 2.6.2 Modelling of Reactive Substances

Modelling reactive substances is the natural next step from modelling conservative substances as discussed in section 2.5.4. In this section, model equations for chlorine decay and case studies of their application will be discussed together with a more detailed focus on the issue of decay coefficient variability.

#### 2.6.2.1 Models

Rossman [123] describes EPANET, a public domain program package for hydraulic and water quality modelling developed by the U.S. Environmental Protection Agency. EPANET is described in detail in [124].

Rossman gives the equations of the hydraulic model (possible utilisation of Hazen-Williams, Darcy-Weisbach or Chezy-Manning formulas) and the water quality model equations together with a short introduction to the computer im-

plementation.

EPANET can model the propagation of conservative and reactive substances (i.e. free chlorine). The chlorine decay coefficient $K$ for first order chlorine decay depends on both bulk water demand $k_b$ and wall demand $k_w$. Thus,

$$K = k_b + \frac{k_w k_f}{R_H(k_w + k_f)} \tag{2.6}$$

(with $k_f$=mass transfer coefficient between bulk flow and pipe wall and $R_H$=hydraulic radius). The mass transfer coefficient $k_f$ depends among other things on the Reynolds number and therefore on the flow.

The chlorine dynamics are

$$\frac{\partial c(x,t)}{\partial t} = -\frac{f}{A}\frac{\partial c(x,t)}{\partial x} - Kc(x,t) \tag{2.7}$$

(with $c$=chlorine concentration, $t$=time, $x$=axial distance, $f$=flow, $A$=area) and the solution is

$$c(x_2,t_2) = c(x_1,t_1) \cdot \mathrm{e}^{-K(t_2-t_1)} \tag{2.8}$$

with

$$x_2 - x_1 = v \cdot (t_2 - t_1), \tag{2.9}$$

where $t_1$, $t_2$ represent time, $x_1$, $x_2$ represent upstream and downstream distance along the pipe, respectively, and $v = \frac{f}{A}$ is the constant velocity of water in the pipe.

Colin and Grapin [40] combine their own hydraulic model (AREMAN) with a water quality model of the form

$$\frac{\partial c_i}{\partial t} = E_x\frac{\partial^2 c_i}{\partial x^2} - v\frac{\partial c_i}{\partial x} + \Phi_i \tag{2.10}$$

with $c_i$=chlorine concentration, $E_z$=axial dispersion coefficient, $v$=water velocity

in the pipe, $c_i$=tracer concentration, $x$=space variable, $\Phi_i$=production term and index $i$=$i$th pipe.

They use highly parallel hardware and thus can solve systems with upto 10000 of these partial differential equations (PDE).

In Biswas *et al.* [11] a more complicated model of chlorine decay, incorporating the biofilm demand, is given. The model equations are derived by methods of fluid dynamics and are valid only for steady state, i.e.

$$\frac{\partial c}{\partial t} = 0 \tag{2.11}$$

(with c=chlorine concentration).

As the model of chlorine decay the following equation is found:

$$g(r)\frac{\partial c}{\partial x} = \frac{1}{\mathrm{Pe_a}}\frac{\partial^2 c}{\partial x^2} + \frac{A_0}{r}\frac{\partial}{\partial r}\left(r\frac{\partial c}{\partial r}\right) - A_1 c \tag{2.12}$$

(with $g(r) = 1$ for plug flow, $r$=radius, $\mathrm{Pe_a} = \frac{lv}{d}$, $l$=pipe length, $v$=flow velocity, $d$=diffusion constant).

If axial diffusion is neglected and plug flow is assumed, the following equation is obtained.

$$\frac{\partial c}{\partial x} = \frac{A_0}{r}\frac{\partial}{\partial r}\left(r\frac{\partial c}{\partial r}\right) - A_1 c. \tag{2.13}$$

The wall demand of the biofilm is one boundary condition of this partial differential equation.

Taking into account all boundary conditions the radial average of the chlorine concentration is obtained to be:

$$c_{average}(x) = \sum_{n=1}^{\infty} \frac{4A_2^2}{\lambda_n^2(\lambda_n^2 + A_2^2)} \times e^{-(A_1+\lambda_n^2 A_0)x}. \tag{2.14}$$

"Thus, three dimensionless parameters, $A_0$, $A_1$, and $A_2$, govern the chlorine decay in the distribution system. $A_0$ accounts for the radial diffusion and depends on the pipe length, on the effective diffusivity of chlorine and on the flow rate

throughout the system. $A_1$ depends on the reactivity of chlorine with species such as viable cells or chemical compounds in the bulk liquid phase and on the residence time in the system. $A_2$ is a wall consumption parameter depending on the wall consumption rate, on the pipe radius and on the effective diffusivity of chlorine"(p.1718). The $\lambda_n$ are the solution of $\lambda_n J_1(\lambda_n) = A_2 J_0(\lambda_n)$ where $J_0$ and $J_1$ are the Bessel functions of the first kind of order zero and one.

In addition, an algorithm to solve this equation numerically is provided.

The paper by Lu *et al.* [91] is following-up [11]. It gives an extensive model of dynamics in water systems for conservative substances, chlorine and biofilm, in particular biofilm thickness. It encompasses 13 partial differential equations and is based on fluid dynamics and mass balance equations. The wall demand is taken into account and within the bulk fluid first order kinetics of chlorine species are assumed.

A number of simulation results are graphically depicted.

Chen and Brdys [29] develop a frame work for the estimation of parameters and states of a system including both quantity and quality with known measurement bounds. Quality is defined through the concentrations of reactive substances as used in EPANET [123]. Brdys *et al.* [16] take this one step further by developing an operational control scheme for quantity and quality (again as a possibly reactive concentration).

#### 2.6.2.2 Case Studies

Wable *et al.* [154] use Piccolo to model chlorine concentrations in water distribution systems.

First order kinetics for chlorine decay are derived from the chemical equations. The network model is based on a hydraulic model and plug flow, no radial or axial diffusion, perfect mixing at node, and conservation of fluxes are assumed. After the hydraulic regime is known they find the residence time, the concentration of any compound, and the origin of the considered water volumes. The procedure to achieve this requires the integration of the kinetics over the residence time for each pipe, and for each node the mean of the concentration is averaged by the

flow rate.

They consider single pipes in an actual distribution system (Paris) to determine the free chlorine demand and show that a log-linear relationship between the decay coefficient and temperature exists. Similarly, TOC is related to free chlorine decay.

The paper of Sharp *et al.* [132] attempts to measure free chlorine decay through measuring flow (i.e. travel time) and chlorine concentrations. An uncertainty analysis was done and results from experiments in an actual system are given.

Liou and Kroon [88] give another example of the application of a dynamic model of the propagation of conservative substances to an actual distribution system and outline the theory used for non-conservative substances.

LIQVARS by Stoner Associates is used to develop the steady state hydraulic model. The additional dynamic model divides the pipes in volume elements and propagates them with every time step.

Hunt and Kroon [72] tune first order free chlorine decay coefficients to actual data.

Chambers and Joy [25], in a Water Research Centre (WRc) report prepared for Thames Water, aim to validate first-order kinetics for free chlorine decay. They did an extensive sampling programme, but less extensive statistical analyses. Problems occurring during the project are discussed (e.g. some of the measurements were discarded because the sampling locations were not representative for what they theoretically should stand for). The precision of the chlorine measurements could be significantly improved through the adoption of an accurate sampling procedure.

It is noted that the chlorine decay in bulk water samples (bottle tests) is very different from the actual chlorine decay in the system (for which the author of the current work assumes the biofilm to be responsible).

Clark *et al.* [34] present a case example of modelling chlorine decay in an actual distribution system. In this system there is a high wall demand.

It is remarked that storage tanks, due to long retention times, may cause

serious water quality problems. In addition, it is mentioned that a "simulated distribution system or a pipe loop"(p.885) was at the time of submisson under construction.

Heraud *et al.* [67] present results from sampling in a real system in France together with the application of chlorine models incorporated into Piccolo (cf. [49]). Sampling in a real distribution system brings the draw-back of fluctuations in inlet chlorine (0.28–0.97 mg/l) and temperature (11.6–24.1$^0$C).

Sampling was performed at hydrants at a flow rate of about 1.4 l/s. No velocity is given (or sample tube diameter). A transient response of the sampling process (due to hydrant deposits?) was observed and for this reason the sampler waited 5 min for bacterial counts to level off before the sample was taken.

The analytical programme contained analyses of temperature, dissolved oxygen, redox potential, turbidity, iron, particle counts (method or results not further specified), TOC, BDOC, $UV_{254nm}$ absorbance, free chlorine ('Chlorscan' microsensors are discussed in the paper, including measurement principle and further literature; their limit of detection is 0.02 mg/l), trihalomethanes (THM), HPC on PCA medium at 22$^0$C and 37 $^0$C, HPC on R2A at 22$^0$C, total coliforms, fecal streptococceae, *Aeromonas hydrophilia* and *Pseudomonas aeruginosa.*

A microbial evolution over time and location was observed. There is a small decrease in bacterial counts over a period of 50 min (fast decay of chlorine) and significant changes happened over a period of several months (influenced by both chlorine and temperature).

The free chlorine model is based on first order exponential decay with decay coefficients dependent on the pipe material (old grey cast iron, cement-lined grey cast iron, and other) and pipe diameter. From representative data for two diameters the decay coefficients for other diameters were calculated using a equation given in the paper (p.69). Neither derivation nor source are provided, but it is mentioned that Piccolo is used for calculating the coefficients (i.e. this equation might be built into Piccolo, or it could be otherwise empirical).

Chlorine model and measurements agree reasonably well. According to the authors the differences are due to the shortcomings in hydraulic modelling (e.g.

inaccurate demand patterns). The model identified regions with no chlorine and thus it found effective places for booster chlorinations.

Piriou *et al.* [118] includes some more information on the chlorine meters that were also used in [67].

Clark *et al.* [37] present the propagation of a conservative substance (trihalomethane, TTHM) and a first order decay of free chlorine.

The chlorine decay constant incorporates in this paper the wall demand $k_w$ as used in EPANET (found through trial and error). It is demonstrated that TTHMs are closely related to UV absorption.

#### 2.6.2.3 Variability of Decay Coefficients

One important issue in chlorine decay modelling is the question if the decay coefficient is a constant parameter (i.e. first order decay) or varies with flow, biomass, pipe material or other factors. EPANET [124] uses a decay coefficient which includes a flow and biofilm dependence through the wall demand. Heraud *et al.* [67] use decay coefficients dependent on the pipe material. Other relationships are possible.

Some researchers validate the assumption of first order free and total chlorine decay, like Chambers *et al.* [24] of the WRc. Only little statistical analysis is included. The simulation packages WATNET and WATQUAL are used for hydraulic and water quality modelling, respectively.

Burgess *et al.* [21] give an outline of an experiment procedure to develop dynamic water quality models incorporating first order chlorine decay with wall demand. The results of this project are presented in Burgess *et al.* [22]. It is observed that first-order kinetics seem to fit the data, however the decay factor is system dependent. A temporal variation of typically about 40 % of the mean decay coefficient is generally observed. No explicit expression for the wall demand is provided.

Lungwitz *et al.* [92] investigate chlorine decay in an actual distribution system. The relevant equations, as given in Rossman's paper on EPANET [123, 124], are provided. It is observed that the chlorine decay coefficient assumes different

values depending on whether chlorine is increased or decreased at a pipe inlet (booster chlorination). This phenomenon is explained with axial diffusion due to a concentration gradient.

Elton *et al.* [51] are concerned with both the propagation of conservative substances (including source blending) and the propagation and reaction of non-conservative substances, i.e. free chlorine. For chlorine decay first order kinetics are assumed.

Four different real-world water distribution systems were investigated, however only few results of models are given. It was found "that chlorine decay rates depend on initial concentration, pipe diameter, pipe material, pipe condition, water temperature, and pH. These are in addition to the influence of source water characteristics"(p.49). The authors work for Severn Trent Water and used the Stoner Workstation Service to model these distribution systems.

Schneider *et al.* [128] find that the free chlorine decay coefficient depends on flow and other parameters like pH and temperature. They use methods of continuous time system identification, the Poisson Moment Functions [148], and a least squares estimator for decay coefficient determination. First and second order chlorine decay models are investigated. Woodward *et al.* [160] found evidence that the monochloramine decay constant is flow dependent. Results as given in table 2.2 are presented. The same set-up as for the work of this thesis (the "TORUS" pipe rig) is used.

**Table 2.2:** *Monochloramine Decay Constants and Flow Rate*

| Flow rate (l/s) | Decay constant ($h^{-1}$) |
|---|---|
| 0.07 | $0.051 \pm 0.007$ |
| 0.25 | $0.095 \pm 0.008$ |
| 0.9 | $0.173 \pm 0.008$ |

In addition, a relationship between monochloramine concentration found through titration and chlorine concentration measured on-line is graphically depicted in [160].

## 2.7 Temperature

Fransolet *et al.* [54] establish a strong relationship between bacterial growth in distribution systems and temperature. A number of data are presented, however, without developing a mathematical model.

In Chambers [23], a WRc report following up [25], the long term variability of the chlorine decay rate is investigated.

A temperature dependence of the form

$$K = A \cdot \exp\left(\frac{-B}{\mathcal{T}}\right)$$

is established ($K$=decay coefficient, $\mathcal{T}$=temperature, $A, B$=constants). However, only few data could be provided to validate this equation and even within this data rather large long-term changes, which do not fit the model, are observed (thus only part of the data are used to validate the model).

A similar temperature dependence is used in Piccolo. The Piccolo Reference Manual [127] includes a brief description of the Quality Module of Piccolo.

It is possible to use a chlorine decay coefficient $K_{H20}$ which depends on total organic carbon (TOC) and temperature $\mathcal{T}$ according to

$$K_{H20} = \text{TOC} \times \exp(14.4) \times \exp(-6050/\mathcal{T}) \tag{2.15}$$

(TOC in mg/l, $\mathcal{T}$ in K, $K_{H20}$ in $\text{min}^{-1}$) and to use diameter dependent decay constants within the distribution system.

## 2.8 Multi-Quality Models

Multi-quality models are concerned with distribution systems that mix water of different quality.

The article by Reike *et al.* [121] is geared towards the use of poor quality water (salty water) in irrigation systems in Israel. This is only possible if it is sufficiently diluted with high quality fresh water. Water quality is considered in

terms of salinity.

Hierarchical two-level control is suggested to achieve sufficiently good water for irrigation. The upper control level is concerned with finding an optimal steady state distribution of flow rates, pressures and quality within the network. Parts of this algorithm can be performed off-line before hand, as e.g. a path finding algorithm based on graph theory. The flow rates between each source and each consumer are chosen as the state variables of the system for the optimisation problem.

The lower control level is concerned with maintaining the optimal values of flow, pressure and quality. Special emphasis is given to a method of predictive control which takes account of dead-times in the system.

In this paper no explicit quality model or values of any parameters are given. However, an objective function (cost function) is provided. This work is based on simulation, no experiments are recorded.

Ostfeld and Shamir [111] deal with the design of multi-quality distribution system models in steady state. In addition, they give an outline of the optimisation problem with a possible solution.

The optimal design is done concerning discharge (Which source and what is its relative contribution of each source to total supply? Is there a source node where supply reaches its bound?), quality (Is there a node at which a threshold concentration is reached? To what degree is water being treated (removal ratio) at treatment source nodes, and is there a treatment source node at which treatment reaches its bound?), and head (Is there a node at which the head reaches its bound? Are dummy valves being used within pumping stations?).

The paper of Coulbeck *et al.* [43] use a cost function incorporating pumping and treatment costs (i.e. How much of each tank are you using?). Quadratic programming is used to obtain optimal results. where costs in terms of money are minimised. For inclusion in the optimisation, a monetary value was assigned to water quality after treatment.

## 2.9 Algorithms and Simulation

Rossman and Boulos [125] compare different numerical methods for water quality modelling. They investigate the Eulerian finite-difference method (FDM), the Eulerian discrete volume element method (DVM), the Lagrangian time-driven method (TDM) and Lagrangian event-driven method (EDM). It is concluded, among other things, that TDM is the most versatile of the tested methods. Currently, DVM is used in EPANET. That method is discussed in some more detail in Rossman *et al.* [126].

Boulos *et al.* [14] and Boulos *et al.* [15] introduce the event-driven algorithm (EDM, see above) to model contaminant propagation in distribution systems. The paper [15] is a more mathematical description of this algorithm with an abstract example included, whereas [14] elaborates more on background, method, and ideas without giving many equations.

The advantage of the event-driven method is that the discretisation of the continuous model, which is always needed in computer applications, is now event-oriented rather than uniform. Thus, the discretisation is now inherent to the system and therefore exhibits better characteristics.

Chen and Brdys [16] use an approach employing bounds on variables for the solution of a joint parameter and state estimation problem. Brdys *et al.* [29] combine mixed integer programming and genetic algorithms to obtain an optimal control schedule for a water distribution system, taking into account both the hydraulic conditions (quantity) and quality in terms of propagation of substances (normally free chlorine).

The EPANET User's guide [124] by Rossman includes an introduction to the relevant theory. The most important equations are also given by Rossman in [123]. In addition, the manual includes a short derivation of the relationship of the decay constant with the bulk water and wall chlorine demands as given in eq. (2.6).

GINAS [42] is a hydraulic simulator for water systems. A suite of software is available from Water Software Systems which includes network simulation,

operational scheduling, demand prediction, network model simplification and a water quality simulator.

The description of WASMACS (Water Systems Monitoring and Control Software) by R. S. Powell [119] contains an overview of the suite of software developed by Brunel University. It includes among other things a graphical user interface, a relational database, a quasi-dynamic and a static network simulator, a state estimator using weighted least squares, the possibility to detect and locate leaks and predict demands, a pump optimiser, and an optimised pressure controller.

Piccolo [127] is another hydraulic simualtion package. It contains also a Quality Module that covers chlorine kinetics. Recently, an extension of Piccolo for bacteriological water quality, Piccobio, was presented [117].

A paper by Cohen [39] describes QUALI, a sub program to DYNASIM. DYNA is described in [38]. Both are developed in Fortran 77 on VMS.

## 2.10 System Identification and Physical Modelling

Probably one of the most influential textbooks in system identification is Ljung's "System Identification: Theory for the User" [89]. Other important textbooks in the field are Söderström and Stoica [135], Unbehauen [146] (in German), or more recently Johansson [77], Ljung and Glad [90], and Walter and Pronzato [155].

All these books are written by authors belonging to, what could be termed, the control community. Within this community system identification is differentiated from 'mathematical modeling' [135] or 'physical modeling' [90]. Gold [55], working on modelling in biological systems, argues along similar lines, when he distinguishes between 'correlative' models and 'explanatory' models. To follow Söderström and Stoica [135, p.4], 'mathematical modeling' is an analytical approach to find a model from basic laws of physics (or biology etc.), whereas system identification is an experimental approach, where a model is fitted to recorded

**Table 2.3:** *Comparison between physical modelling, system identification and "hybrid" approaches.*

| **name** | "Physical Modelling" | "Hybrid" Methods, e.g. "Empirical Modelling" | System Identification |
|---|---|---|---|
| **based on** | physical insight | both | data |
| **structure** | Tailor-Made | "Grey-Box" | Black-Box |
| **interpretation of parameters** | yes | partially | no |

data by assigning suitable numerical values to its parameters.

The standard linear model structures that are used in system identification contain generally an autoregressive and a moving average part of a suitable order with an exogenous input (ARMAX models). In particular, differences in the model of the influence of the noise on the output signal gives rise to variations of that model, see [89, 155, 77].

In table 2.3 these "pure" approaches, system identification and physical modelling, are compared with "hybrid" methods, e.g. "empirical modelling" as used by Johansen and Foss [76] or semi-physical modelling as discussed by Lindskog and Ljung [87]. Lindskog and Ljung write that "[by] semi-physical modeling we will mean the process to take physical insight about the behavior of the system into account, to use that insight to find adequate nonlinear transformations of the raw measurements so that the new variables — the new inputs and outputs — stand a better chance to describe the true system when they are subjected to standard model structures (typically linear in the new variables)" (p. 1199 of [87]). Similarly, Johansen and Foss [76] combine four linear models to one nonlinear model based on operating regimes. Thus, standard model structures are combined based on physical insight. A similar approach is taken by Nelles *et al.* [108] or Babuška and Verbruggen [5], where Fuzzy weighing functions are used for the interpolation of local linear models. Other "hybrid" approaches of modelling

are possible.

Table 2.3 indicates the basis, type of structure and interpretability of parameters for physical modelling, system identification and "hybrid" approaches. Whereas a physical model is based on physical insight with a structure that is tailored to the particular problem, system identification models are based on experimental data and a standard model structure (Black Box) is assumed. "Hybrid" approaches include some physical insight and some conclusions from data and therefore the model structures are frequently termed "Grey-Box" models. This reflects also on the physical meaningfulness of the model parameters. While a physical model contains only meaningful parameters, it is generally impossible to interpret the parameters of a Black-Box model as obtained through system identification. Semi-physical or empirical modelling is again a mixture of the two extremes, because some of the parameters may carry a physical interpretation, but not all of them.

The most critical issue in system identification and "hybrid" approaches is the determination of a nonlinear model structure. Several methods for selecting between several possible structures have been published, e.g. Billings [9], Haber and Unbehauen [64] or Unbehauen [147]. Standard nonlinear model structure include Volterra series, Wiener and Hammerstein models. Sjöberg *et al.* [134] discuss feed-forward neural networks as possible nonlinear black-box models.

## 2.11 The Approach of This Thesis

In this thesis, the dynamics of suspended particles, the impact of biofilm on particles and monochloramine as disinfectant in the system are considered. Two different types of published chlorine models are compared and a new particle counts model is developed.

The chlorine decay models contain either a single decay coefficient [22, 24, 51, 123, 154] or a combined decay coefficient as proposed by Rossman [123, 124, 92] (section 2.6.2.1). In particular, the variablity of decay coefficients as discussed in section 2.6.2.3 is investigated in chapter 7 [67, 92, 123, 128, 160].

Chapter 6 of this thesis investigates particle counts (section 2.5.3) as an in-

dication of suspended biomass (section 2.5.1). The relationship between them is discussed in [110, 98] and [65, 140, 159] elaborate on the use of particle counters for similar purposes.

This thesis focuses on the contribution of biofilm to the suspended biomass (after a flow increase). Therefore, different biofilm structures [151, 105, 138, 80] (section 2.4.1) are discussed briefly and the effect of a disinfectant in the system [85, 112] (section 2.4.4) is shown. The dynamics involved in biofilm detachment are generally reduced to a linear time dependency in the literature [137, 115, 122, 28, 61, 6] (section 2.4.3). However, in the case considered in this thesis the transient shear-off did have an important impact on the biofilm in the pipe rig and therefore a new model is developed. This model allows a shedding profile which is related to biofilm thickness to be obtained. The biofilm thickness is difficult to measure [149, 150] (section 2.4.5).

The approach taken in this thesis to the development of the particle counter model structure from data is novel. It was initiated by the author with simpler experimental data in the work for his Master of Science [94, 95], but it was never used for such a complicated system. To date, there is (to the author's knowledge) no procedure available for finding a nonlinear system structure directly from data, however, methods for selecting between several possible structures have been published [9, 64, 147].

In the case discussed in [94, 95], some prior knowledge (i.e. a physically meaningful parameterisation and the model for the limits of one of the parameters) was available. This knowledge of a non-trivial model for a partially vanishing parameterisation implies knowledge of system structure. The full model incorporates that knowledge together with specifications derived from the data.

For the particle counts model presented in this thesis there is less prior knowledge available. Again specifications derived from data are developed. These specifications have to be fulfilled if a model is to fit the data. Due to little prior knowledge, assumptions about the system structure have to be made, which in turn are investigated for their meaningfulness by numerical modelling and parameter identification. Results and the interpretation of them form, as in the

earlier work [94, 95], an important part of the model validation.

## 2.12 Conclusions

This review covered literature in the field of water quality modelling for water distribution systems. The focus of this review lay on biofilms, suspended bacteria and inanimate particles and various species of chlorine as disinfectant.

This chapter is not intended as an exhaustive review of the literature in the field of water quality modelling, but it attempted to present a representative selection of important publications. It gives an overview of the state of the art in water quality modelling for distribution networks and of some relevant literature not directly in that field.

# Part II

# Data

# Chapter 3

# Experimental Work

## 3.1 Experimental Set-Up

### 3.1.1 The Pipe Rig

Between January 1993 and January 1994 Thames Water Utilities Ltd. designed and commissioned the "TORUS" pipe test distribution system at Kempton Park Water Treatment Works. It was intended to mimic as closely as possible the conditions found in a real distribution system.

The first large-scale pilot distribution system was built in 1986 by the International Water Research Centre at Nancy, France (NAN.C.I.E.) [41, 36]. It consists of two sets of three pipe loops in series. The individual loops provide mixed reactor conditions (as opposed to a once-through system). Both Lyonnaise des Eaux [116] and the U.S. Environmental Protection Agency [34] built facilities based on a similar layout (i.e. looped systems).

The "TORUS" pipe rig, however, is the only once-through large-scale pilot facility. A schematic drawing of this pipe rig is provided in figure 3.1. The pipe rig consists of a 1.3 km, 110 mm inside diameter pipe distribution system built of approved construction materials. It is mainly made of medium density polyethylene (MDPE), but contains about 1–2 % exposed or coated iron pipes. It is divided into three sections of approximate length 500 m, 400 m and 400 m, respectively, which are buried 0.5–1.0 m underground. After each buried section

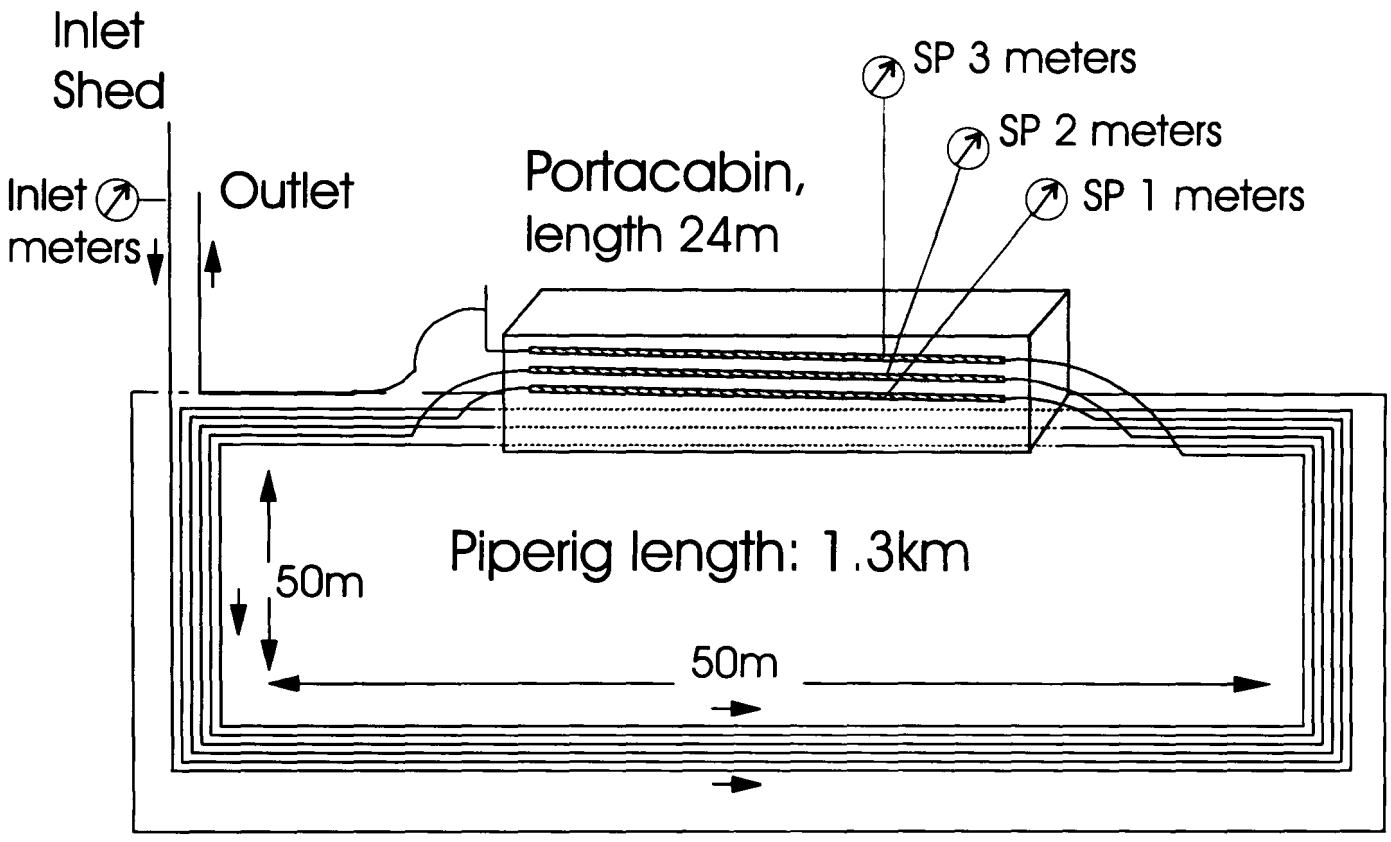


**Figure 3.1:** *Schematic drawing of the "TORUS" pipe test rig at Kempton Park. The rig has a total length of 1.3 km, most of it buried under ground apart from the initial and final parts and three sections of 24 m in the portacabin. Four meter locations at the inlet ('Inlet meters') and sample points 1 ('SP 1 meters'), 2 ('SP 2 meters') and 3 ('SP 3 meters') are shown. This figure is reproduced with permission after a drawing by A. Delanoue.*

the water passes through a 24 m experimental testing station with facilities for on-line monitoring, water sampling and for studying the performance of pipe materials. In addition, there is a sampling station with on-line meters at the pipe rig inlet. Measurements were taken at the inlet (i.e. at the balancing tank situated there or shortly thereafter) and at the three sample points along the rig. Both grab samples and on-line meters were employed. The design and construction of the "TORUS" test distribution system are described in [69, 44].

During the time of the 1996 experiments, the rig was fed with water from the Advanced Water Treatment Centre (AWTC) at Kempton Park. Thus the treatment of the lowland surface water used as a source to the rig consisted of pre-ozonation, coagulation and mixing, flocculation, rapid gravity filtration, main ozonation, granular activated carbon filtration, slow sand filtration and disinfection. Before the water enters the rig, bisulphite ($SO_2$) is used to reduce

the disinfectant residual to (generally) 0.25 mg/l of free chlorine. Subsequently ammonia is added to transform, in this case, all free chlorine ($Cl_2$ or HOCl) into monochloramine ($NHCl_2$). Therefore, after a balancing tank situated just in front of the pipe rig inlet, a total chlorine residual of about 0.35–0.4 mg/l is obtained. The inlet chlorine concentration was changed to higher values for short periods within the experiments.

In later experiments (in 1997) a different feed of water was used: the main treatment works at Kempton Park (rather than the AWTC). The treatment process is basically the same as that of the AWTC, however the monochloramine dose was less stable and generally varied around the higher value of about 0.5 mg/l.

Measurements and instrumentation include the following.

- Heterotrophic plate counts
- Epifluorescence microscopy counts
- Particle counters
- Total chlorine meters and bench titrations
- Volumetric flow meter
- pH and temperature meters

They are described in some detail in the following section (section 3.2).

Results of experiments done with the "TORUS" pipe rig, which are only indirectly related to this work, are published in [159, 160, 45], some initial results of these experiments can be found in [98, 104].

### 3.1.2 The Pipe Rig as Input-Output System

If a "systems view" as introduced in section 1.4 is applied, the "Torus" pipe rig is considered to be an input-output system, i.e. through complete knowledge of the input-output behaviour the system is completely described. In the present case this approach has to be taken cautiously since the output depends on past

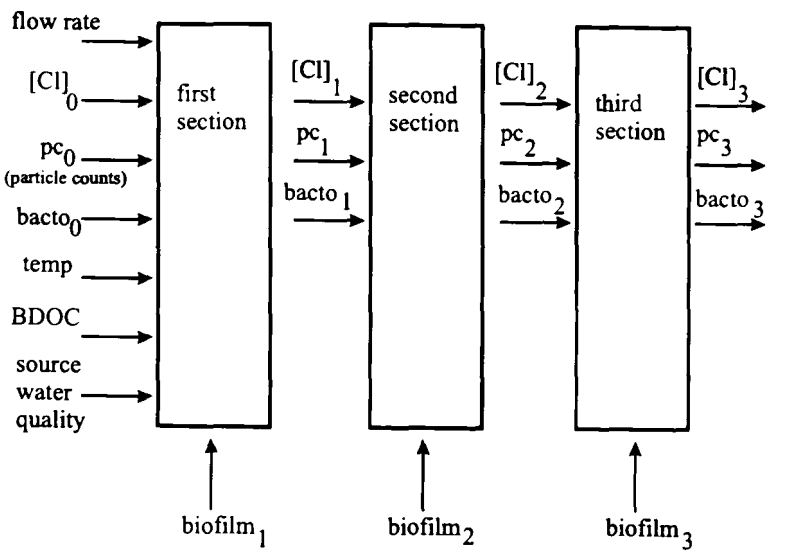


**Figure 3.2:** *The pipe rig as an input–output system*

input (because of the biofilm) and since metabolic processes (growth, death, and respiration) are to some extent independent of the input. This way of viewing the pipe rig is illustrated in fig. 3.2.

The inputs of the investigated system are flow, monochloramine concentration at the pipe inlet, amount of bacteria entering the pipe rig (found through culture assays), initial amount of biofilm present, amount of particles counted by the particle counter at the pipe inlet, amount of nutrients entering the rig (often measured in terms of Biodegradable Dissolved Organic Carbon, BDOC) and source water quality. The outputs of the system are monochloramine (or total chlorine) concentration along the rig, particle counts, amounts of suspended bacteria (again found through culture assays), and amount of biofilm present. One of the most important parameters which has to be taken into account is temperature. Most of these input variables cannot be chosen, only the monochloramine concentration and the flow are independent variables.

## 3.2 Measurement Method

In what follows, both grab samples and on-line meters which were used during the experiments, are described briefly. All meters were connected to a SCADA system via 4–20 mA cables. Data include readings in time intervals (sampling

times) of 5 min or 2 min from particle counters, chlorine meters, temperature meters and pH meters. Grab samples of heterotrophic plate counts, epifluorescence microscopy counts and chlorine titrations were taken at irregular intervals (the majority during step flow trials).

### 3.2.1 Heterotrophic Plate Counts

Since water utilities generally use plate counts or epifluorescence microscopy counts as indications of biofilm growth and detachment both these methods were used in this study. Grab samples for heterotrophic plate counts (HPC) were taken three times a week and at a higher frequency during step flow trials. Counts of colony forming units (cfu) were performed on $R_2A$ agar after 7 days of incubation at $22^0$C by the Thames Water labs. Standard procedures were applied when taking samples, which include flaming the sample taps and using the standard lab bottles with bisulphite tablets for the neutralisation of chlorine.

Note that HPC count only the number of bacteria or bacteria accumulations capable of proliferation (e.g. forming a colony), not injured or dead bacteria. In addition an accumulation ('clump') of bacteria will be counted as only one cfu.

### 3.2.2 Bottled Samples for Heterotrophic Plate Counts

During September and October 1996 fourteen sets of between 12 and 18 bottles were taken at 10 time instants. Bottles were made either of plastic or glass. On four occasions plastic and glass sets were taken simultaneously. Three replicate bottles were evaluated immediately and after time intervals of 1 to 10 days (using a different set of three bottles at each time).

Plastic bottles used were the standard Thames Water grab sample bottles, which are, however, not tested for as long periods of time as were necessary here. The glass bottles were burnt at $555^0$C and sealed by the Thames Water labs. When taking the bottles, first the tap was flamed, then they were half filled, rinsed, and subsequently filled completely. At the time of sending them off for evaluation, bisulphite tablets were added to chlorinated water. Thus, before the

evaluation of bottles any disinfectant present was uninhibited in its action.

Water samples of unchlorinated water and water containing monochloramine were taken at the inlet tank tap (during the corresponding disinfection regimes in the rig). Water after disinfection with free chlorine was obtained from the tap before ammonia dosing within the disinfection stage of the treatment process. Disinfection is the last stage of water treatment. In it, the treated water is brought into contact with a high free chlorine residual (in this case about 0.8–0.9 mg/l after 5 min contact) for about 30 min. Afterwards the free chlorine residual is reduced by dosing bisulphite (to about 0.25 mg/l). Ammonia dosing (to turn free chlorine into monochloramine) is the next (and last) step of this stage. At the pipe rig inlet tank total chlorine residuals of about 0.4 mg/l were measured.

For the duration of the bottle experiment the samples were kept in cardboard boxes, inside the pipe rig portacabin. This ensured that the temperature of the bottles was similar to the temperature in the pipe rig.

### 3.2.3 Epifuorescence Microscopy

Epifuorescence microscopy counts using acridine orange as staining agent were performed on grab samples throughout the experiments and especially during step flow trials. The method was adopted by S.M. McMath and A. Delanoue for this particular application [103, 104]. This method makes it possible to count all bacteria, even if injured or dead, and allows the investigation of bacteria sizes and accumulations. This implies that if they occur in 'clumps' each bacterium can be counted separately, which is impossible with heterotrophic plate counts.

### 3.2.4 Particle Counters

Particle Counters ("Versacount" from Hiac/Royco) were installed at four locations along the pipe rig, i.e. close to the start of the rig, named 'Inlet', and at the before mentioned three sample locations, termed 'Sample Point (SP) 1, 2, and 3'. The inlet particle counter was not present at the start of the experiments (see

section 3.3).

Each of these counters extracts 60 ml/min of water from the pipe rig and measures particles by leading this sample through a sensor. The sensor obtained a reading for each particle proportional to the size of the shadow cast by it in a laser beam. The number which is referred to as 'particle count' is the number of particles which pass through the sensor divided by the volume of water that passed through the counter averaged over one minute, thus, it is the number of particles within one ml of sample water. Particle counts that are not divided by the volume of sample are generally referred to as 'cumulative' particle counts (i.e. particles per time unit). They are not used in this thesis.

The size of each particle is information additional to the (plain) particle count. Particles were sorted in different bins according to the size of their shadow (diameters between 2 $\mu$m and 5 $\mu$m, 5 $\mu$m and 10 $\mu$m, 10 $\mu$m and 15 $\mu$m, 15 $\mu$m and 20 $\mu$m, 20 $\mu$m and 25 $\mu$m, 25 $\mu$m and 50 $\mu$m, 50 $\mu$m and 100 $\mu$m, and 100 $\mu$m and 150 $\mu$m). The counters were calibrated in six monthly intervals with latex spheres for recognition of these sizes. Therefore, particle counts can be distinguished according to the size range they cover. The total counts of all particles $> 2\mu$m are referred to as 'total particle counts', any reference to counts within one bin (e.g. counts of particles with diameter between 2 $\mu$m and 5 $\mu$m) are generally termed difference counts. In this work size distributions of particle counts are also used. The size distribution contains the amount of particles in each size range (bin) divided by the total particle count. In other words, it contains the percentage of all particles which fall into a certain size range (or bin).

The fact that the counters were calibrated with latex spheres introduces discrepancies between the readings of different counters for not-spherical particles. This issue is addressed in section 5.2.

### 3.2.5 Chlorine Meters

Chlorine meters ("Medway" from Portacel) were installed at the three sample points and the inlet of the pipe rig. They are capable of measuring either free

chlorine of total chlorine. All meters extract a flow of less than 200 ml/min. The water sample passes through a cell containing two electrodes of dissimilar metals, i.e. one of gold, the other of copper. This sets up an electrolytic action, generating an electric current that is proportional to the concentration of free or total chlorine in the water. Addition of Potassium Iodide to the normal buffer solution, which is circulated in the cell in addition to the sample, changes the obtained measurement from free to total chlorine. A range of 0 to 2 mg/l of free or total chlorine was used during the experiments. The manufacturer's manual gives the accuracy of the meters as $\pm 0.05$ mg/l at full scale deflection.

Chlorine meters have to be recalibrated, both in zero position and span, in regular intervals, since they drift slowly out of calibration. If they are allowed to drift too far from the actual value, the meter may leave the linear region of its scale, which would introduce errors that are very difficult to correct. The problem of meter drift is addressed in section 5.3.

### 3.2.6 Chlorine Titrations

Chlorine titrations allow readings for free chlorine, monochloramine and dichloramine to be obtained. The combination of all these is known as total chlorine. Titrations are a bench analysis performed on a bottled sample of water. They were done on site by members of the pipe rig team (including the author of this thesis). The method employed during this work uses diethyl-p-phenylene diamine (DPD) as an indicator to produce pink/red colour in a sample prepared with an appropriate buffer and Potassium Iodide (for monochloramine and dichloramine). This solution is titrated against Ferrous Ammonium Sulphate. Some samples were double-checked with the Dr. Lange analysis system, which is based on a spectrophotometric method.

### 3.2.7 Bottled Samples for Chlorine Titrations

During September to November 1996 eight sets of between 3 and 10 bottles were taken at eight time instants. All bottles were made of glass except for those

used for the immediate titrations. Five of the eight bottles for the immediate titrations were made of plastic, the others were glass bottles. Three or more replicate titrations were done per bottle. They were done immediately and after time intervals of 0.5 hours to 7 days (using a different bottle at each time).

The glass bottles were cleaned by filling them with nitric acid for at least twelve hours. Subsequently they were rinsed with sample water. Samples of water containing monochloramine were taken at the inlet tank tap (at the time when monochloramine was in the rig). Water after disinfection with free chlorine was obtained from the tap before ammonia dosing within the last stage of the treatment process. The bottles were kept, like the bacteriological ones, in cardbord boxes in the pipe rig portacabin.

### 3.2.8 Volumetric Flow Meter

An electromagnetic flow meter (Krohne) at the inlet (i.e. before all meter stations) obtained volumetric flow readings in litre/second by measuring the voltage induced by the water flow in a magnetic field.

### 3.2.9 Temperature, pH and RedOx Potential

Temperature, pH and Reduction–Oxidation Potential, 'ReDox', were all measured with the same meter ("Meredian" from Leeds & Northrup, with three probes). Meters were installed at the three sample points along the rig and extract about 200 ml/min. For the present investigation RedOx was disregarded, and pH was only monitored (the pH value is generally stable at around 8) but not taken further into account. The pH measurement is temperature compensated. Temperature is measured by an electronic temperature sensor. Only temperature was considered in the further analysis.

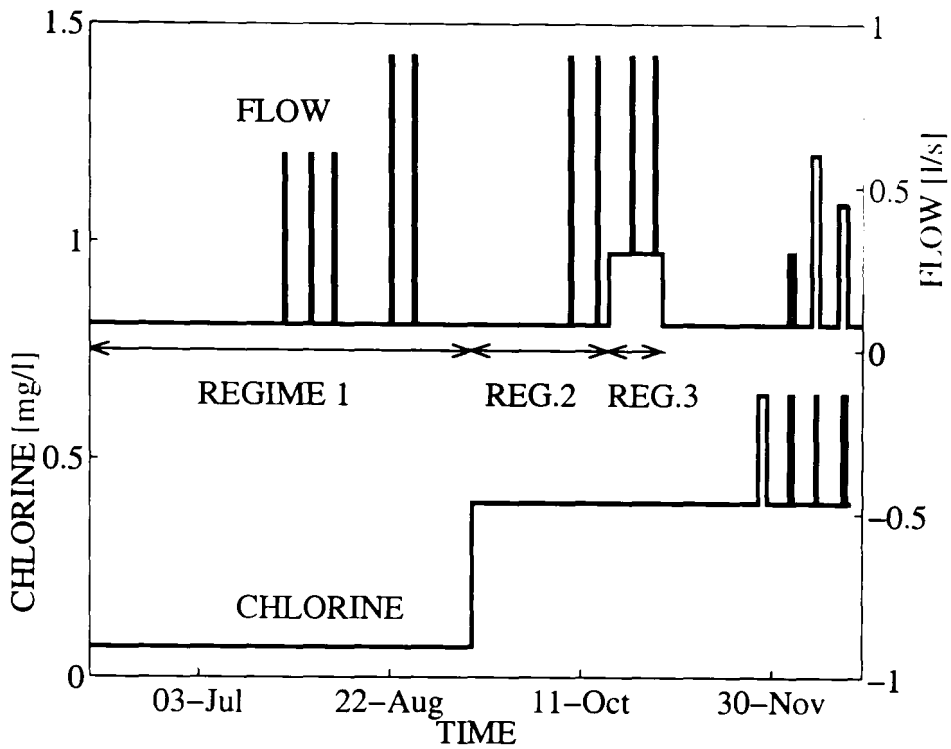


**Figure 3.3:** *Experimental Schedule showing flow and total chlorine at the pipe rig inlet, three baseline regimes of Experiment 1 are indicated*

## 3.3 Experiments

### 3.3.1 Pipe Rig Experiments During 1996

The 1996 experiments took about five months of preparation and seven months of actual data gathering. They consisted of 12 sharp flow increases lasting 12 hours to three days and subsequent decreases to previous flow values (termed 'step flow trial', as opposed to changes in baseline flow) and four step chlorine trials. The experimental schedule is depicted in fig. 3.3.

The experiments can be divided into two parts, Experiment 1 consisting of the step flow trials 1 to 9 and Experiment 2 consisting of the remaining three step flow trials and four step chlorine trials. Experiment 1 is aimed at obtaining some information about the effect of biofilm on water quality, Experiment 2 was designed to result in some information about changes in chlorine decay due to changes in flow or inlet chlorine concentration.

Three main baseline regimes in terms of flow and disinfectant regime can be distinguished in Experiment 1 (as marked in fig. 3.3).

regime 1: laminar baseline flow (0.08 l/s, 0.0084 m/s, Reynolds number 920),

no disinfectant residual in the rig

regime 2: laminar baseline flow (0.08 l/s, 0.0084 m/s, Reynolds number 920), disinfection of about 0.35-0.4 mg/l total chlorine at the inlet of the rig

regime 3: turbulent baseline flow (0.3 l/s, 0.032 m/s, Reynolds number 3500), disinfection of about 0.35-0.4 mg/l total chlorine at the inlet of the rig

Within each of the considered regimes, at least two step flow trials took place to provide an indirect measurement of the biofilm present. Evidence for increased biofilm detachment due to a flow increase within the "TORUS" pipe rig has been found previously [159]. The higher flow rates during step flow trials were 0.6 l/s (0.063 m/s, Reynolds number 6900), 0.9 l/s (0.095 m/s, Reynolds number 10400) and 0.45 l/s (0.047 m/s, Reynolds number 5200). Since the transition from laminar to turbulent flow occurs generally between Reynolds numbers of 2000 and 4000 [102], all high flow rates are turbulent. For a graph of Reynolds numbers versus flow rate see Appendix D.

In particular, Experiment 1 aims at identifying the relationships between the amount of biofilm present and flow rate or total chlorine concentration. The first part of this experiment aims to establish the relationship between biofilm accumulation and flow rate, without any chlorine present (i.e. only one independent variable). In the second part it was anticipated to establish a relationship between biofilm detachment and chlorine concentration for two baseline flow rates.

Throughout the different regimes of this experiment several step flow trials took place. The idea behind these trials is that the increased shear off from the biofilm might give some indication about how much biofilm is present without removing all of it (due to the short duration). The baseline flow period between step flow trials may help to establish if conditions are still similar.

Experiment 2 is concerned with the relationship between chlorine concentration within the pipe and initial chlorine concentration or flow rate. To obtain a maximal amount of chlorine decay data, both of spatial and temporal decay, the transient response to step input changes (step in inlet total chlorine or step in flow rate) is considered and not only the (short-term) steady state. Furthermore,

for each pair of independent variables a step flow trial with incorporated step chlorine trial of roughly 2–3 days duration was made.

The time scale in Experiment 2 is much shorter compared to the first part of the experiments, thus it was anticipated that each step trial is long enough to establish changes in the monochloramine decay rate. This short duration of these step flow trials gives the possibility to assume that the effect of biofilm is the same throughout the step flow trial and the usage of a reference flow (and chlorine concentration) in between each step trial allows to calculate possible long-term changes in chlorine decay. These long-term changes are to date merely side effects of this experiment, however, they may be considered in future work.

### 3.3.2 Bottle Experiments During 1996

During September and October 1996 fourteen sets of between 12 and 18 bottles for bacteriological analysis were taken at 10 time instants as already described in section 3.2.2, which focuses on the measurement method. Three replicate bottles were evaluated immediately and after time intervals of 1 to 10 days (using a different set of three bottles at each time).

The schedule for this experiment is given in table 3.1. There the date and time when each set was taken, the material of the bottles, the type of disinfection present in the bottles, the number of bottles in a set and the time until they were send for evaluation are given. The material of the first three bottles of all sets was plastic, since these samples were within the limits of the standard procedures which use bottles made of that material.

During the period of September, October and November 1996 eight sets of between 3 and 10 chlorine bottles were taken at eight time instants as already described in section 3.2.7 (again chiefly dealing with the measurement method). Three or more replicate titrations were done per bottle. They were done immediately and after time intervals of 0.5 hours to 7 days (using one new bottle for all replicas each time).

The schedule for this experiment is given in table 3.2. There the date and

**Table 3.1:** *Bottles taken for bacteriological analysis (heterotrophic plate counts) as part of the bottles experiment of September/October 1996*

| Set number | Taken at | Material | Disinfection regime | Number of bottles | Evaluation after [days] |
|---|---|---|---|---|---|
| 1 | 3-9-96 14:15 | plastic | no chlorine | 15 | 0,1,2,3,7 |
| 2 | 4-9-96 16:00 | plastic | no chlorine | 15 | 0,1,2,4,7 |
| 3 | 4-9-96 16:00 | glass | no chlorine | 12 | 0,1,2,7 |
| 4 | 5-9-96 15:00 | plastic | no chlorine | 15 | 0,1,2,4,7 |
| 5 | 5-9-96 15:00 | glass | no chlorine | 14 | 0,1,2,4,7 |
| 6 | 12-9-96 14:45 | plastic | monochloramine | 15 | 0,1,3,4,7 |
| 7 | 12-9-96 14:45 | glass | monochloramine | 14 | 0,1,3,4,7 |
| 8 | 13-9-96 13:00 | plastic | monochloramine | 15 | 0,1,3,4,7 |
| 9 | 13-9-96 13:00 | glass | monochloramine | 14 | 0,1,3,4,7 |
| 10 | 17-9-96 15:00 | glass | monochloramine | 18 | 0,1,2,3,4,7 |
| 11 | 23-9-96 16:00 | glass | free chlorine | 15 | 0,1,2,3,7 |
| 12 | 24-9-96 14:00 | glass | free chlorine | 14 | 0,1,2,5,7 |
| 13 | 30-9-96 | glass | free chlorine | 18 | 0,1,3,7,10 |
| 14 | 4-10-96 | glass | free chlorine | 11 | 0,3,4,7 |

time, disinfection regime and number of bottles in the respective set are given. In addition the time in days that elapsed until the last bottle was titrated is provided. Intermediate bottles were evaluated at various times, roughly after 0 hrs, 0.5 hrs, 1 hr, 4 hrs, 6 hrs, 24 hrs, 30 hrs, 48 hrs, 72 hrs, 5–7 days. One or more of these times were generally omitted to allow for long time investigation (i.e more than 3 days).

## 3.4 Problems Encountered

There are a number of problems which did occur during the data collection period of 1996. Some are given in the following.

- meter drift (in particular chlorine meters)
- limits of accuracy of meters
- equipment failures (e.g. one of the circuit boards on the inlet chlorine meter) and delivery delays (inlet particle counter)

**Table 3.2:** *Bottles taken for chlorine titrations as part of the bottles experiment of September/November 1996*

| Set number | Taken at | Disinfection regime | Number of bottles | Last evaluation [days] |
|---|---|---|---|---|
| 1 | 12-9-96 15:30 | monochloramine | 9 | 5 |
| 2 | 13-9-96 15:20 | monochloramine | 9 | 6 |
| 3 | 17-9-96 15:50 | monochloramine | 9 | 7 |
| 4 | 18-9-96 16:00 | monochloramine | 7 | 7 |
| 5 | 25-9-96 13:00 | free chlorine | 9 | 12 |
| 6 | 2-10-96 17:50 | free chlorine | 3 | 1 |
| 7 | 4-11-96 11:20 | free chlorine | 10 | 2 |
| 8 | 5-11-96 11:40 | free chlorine | 10 | 6 |

- source water quality changes and treatment plant failures
- particle numbers entering the rig vary significantly
- temperature is uncontrolled and will have some effect on bacteria
- time scale of some effects could be several months
- no meter to measure the amount of biofilm in the rig is available
- heterogeneity of biofilm may cause effects of biofilm to change over time

For some of these problems remedies can be found, e.g. frequent titrations are used to check on chlorine meters and thus adjust for meter drifts. Other possible problems, like the influence of temperature and source water quality have to be taken into account in the model. The heterogeneity of the biofilm and its possible effects are neglected.

## 3.5 Summary

This chapter introduced the experimental set-up used for the work of this thesis and gave an outline of the experiments performed to obtain the data.

The "TORUS" pipe rig provided by Thames Water Utilities Ltd. was used as set-up. It is a large scale once-through experimental distribution system. A

number of meters and grab samples were employed for these experiments, including a flow meter, particle counters, total chlorine meters, titrations, heterotrophic plate counts and epifluorescence microscopy.

The main element of almost all pipe rig experiments is the step flow trial (SFT). Chiefly two sets of experiments were performed in 1996, the first aiming mainly at biofilm and particle counts, the second at total chlorine. Bottle experiments, for bacteriological analysis and for evaluation of chlorine, were also performed using the same water as in the pipe rig. Schedules of all experiments are provided in this chapter.

The following chapters give an overview of the collected data and an in-depth analysis of them.

# Chapter 4

# Qualitative Characterisation of the Data

The first step towards obtaining a model from the experiment results is to clarify what can be learnt from the data. In the experiment described in this work heterotrophic plate counts (HPC) and epifluorescence microscopy counts are considered, which are frequently used within the water industry as indications of biofilm growth and detachment. In addition particle counters were used for the same purpose. Furthermore, monochloramine, which is used by various water utilities to control bacterial populations, is investigated. For a description of the measurement methods used to obtain readings of these variables see section 3.2.

Since the goal of this work is to obtain information about the behaviour of the investigated aspects of water quality, amongst the total duration of the experiments of seven months, the focus of attention lies on periods of input variable (i.e. flow) changes. These were known as the step flow trials (SFTs).

Together with examples, a characterisation of the data will be given in this chapter. In addition, hypotheses for the underlying phenomena or relationships with other aspects of water quality are included. Modelling will be used in the following chapters to decide on the best hypothesis. The aim of this chapter is to set out the basis of the models developed or investigated in part III of this thesis.

Particle counts and monochloramine decay will be the subject of the subsequent chapters 6 and 7, respectively. Only the bacteriological data (including the HPC bottles) feature little in further chapters of this thesis, since the inaccura-

cies arising from this type of analysis is too great for analytical modelling them. Therefore, some emphasis is put on these results in this chapter. In particular, section 4.5.3 summarises the results obtained from heterotrophic plate counts and epifluorescence microscopy data. Due to the relationships of particle counts with bacteriological results (cf. section 4.5.3), the models of particle counts are an indication of processes involving bacteria.

## 4.1 Total Particle Counts

A full description of the particle counters used for these experiments is provided in section 3.2.4 on page 56. Briefly, these counters measure the number of particles per volume of water (i.e. per ml) and the size of the respective particles. This section is concerned with the total particle counts, which are the number of all measured particles per ml (i.e. all particles with diameter $> 2\mu$m). The observations of this section are, however, in principle equally valid for counts of larger particles (e.g. $> 5\mu$m, $> 10\mu$m etc.) or even difference counts. Size distributions of particles are the object of section 4.2.

Two typical examples of total particle behaviour during a SFT are given in figs. 4.1 and 4.2. The first figure depicts the total particle counts during step flow trial 5 which took place on 28 August 1996, the second figure depicts the same data during SFT 8 of 24 October 1996. Volumetric flow rate, measured at the inlet, and total particle counts for three sample points along the rig (SP 1, SP 2, SP 3) are given on the same y-axis on a logarithmic scale. In fig. 4.2 inlet particle data is also included. Note, for comparison, that fig. 4.1 is the same SFT as the example of heterotrophic plate counts given in fig. 4.9.

Since the observations of this section are based on all data, additional relevant portions of the total particle counts data are provided in appendix A.1. There the particle counts of all twelve step flow trials of the 1996 experiment can be found (figs. A.1 to A.12 on pages 233–244). Within this appendix only one sample point is given per graph, which is a different way of presentation compared to the examples provided in this chapter.

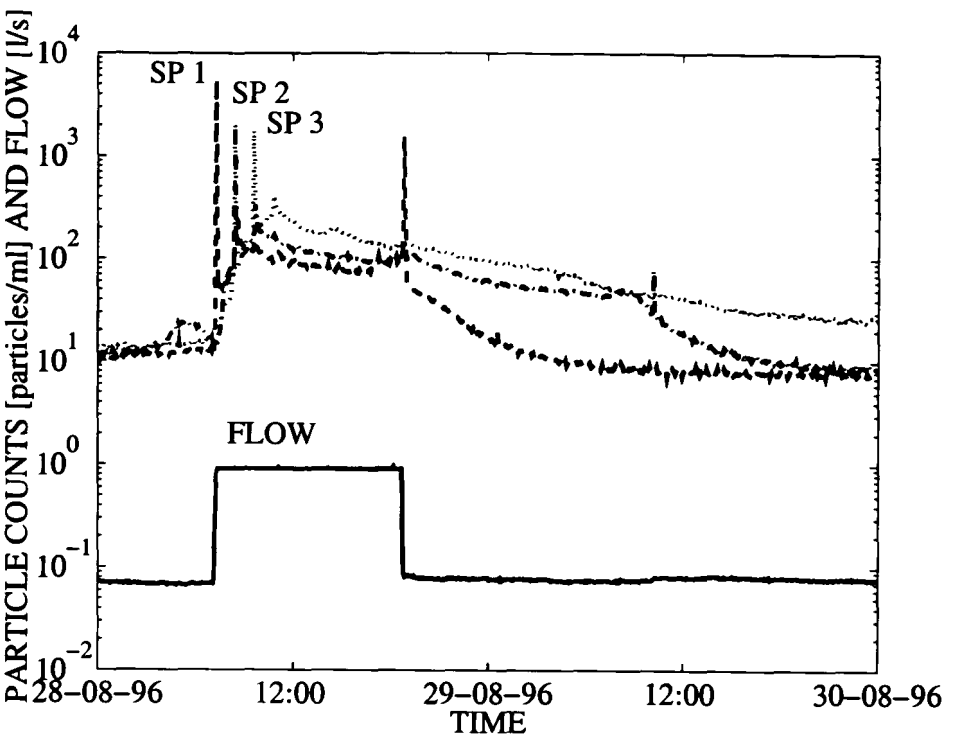


**Figure 4.1:** *Step flow trial 5 as first example of total particle counts. Depicted are three sample points along the rig (SP 1, SP 2, SP 3) and inlet flow.*

### 4.1.1 Observations

From the examples given in figs. 4.1 and 4.2 some observations which are typical for the complete data can be made.

- The particles move through the rig, i.e. a behaviour of particles similar to the one observed upstream is measured downstream after a time interval. This time interval agrees approximately with the predicted travel time between the respective points (cf. section 5.4).

- Sharp peaks occur with flow increase. These peaks propagate almost intact through the rig. They occur only within less than about one travel time to the respective sample point.

- A pattern of behaviour which occurs simultaneously throughout the rig is observed: particle counts increase slowly at high flow, reaching a maximum after about one full travel time to that particular sample point and decline subsequently. The counter signal settles after a short period at high flow

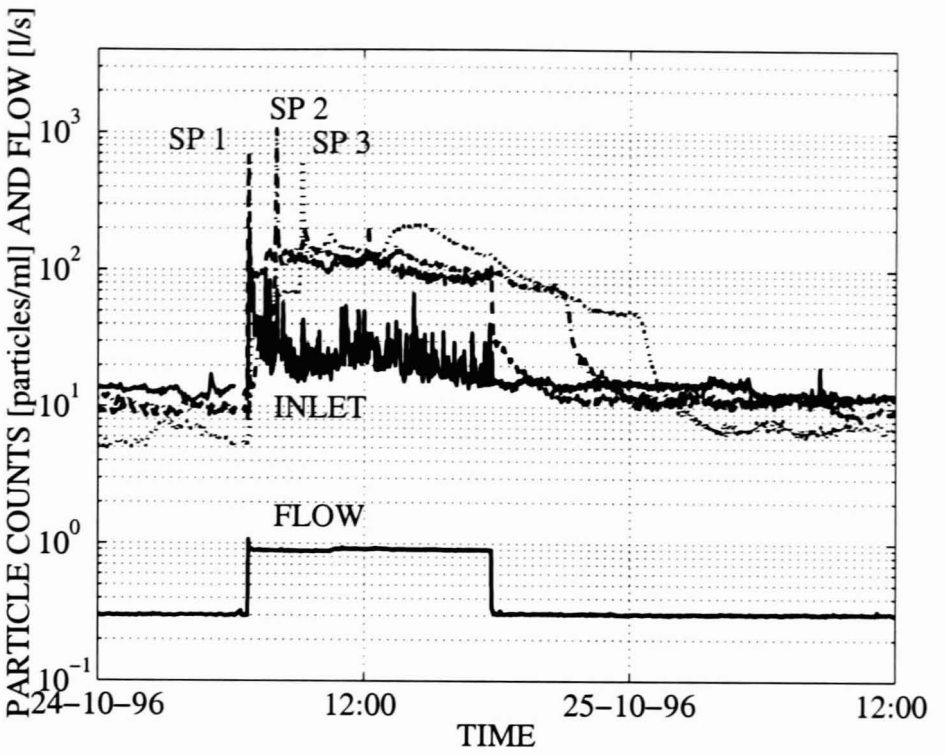


**Figure 4.2:** *Step flow trial 8 as second example of total particle counts. Depicted are inlet particle counts, counts at all sample points (SP 1, SP 2 and SP 3), and flow measured at the pipe rig inlet.*

to a value that is generally higher than the low flow (baseline) value. This will be referred to as the 'slow signal'.

The decline is generally strictly monotonic, however, if all the relevant data provided in this work (figs. A.1 to A.12 on pages 233–244) is considered, notable exceptions emerge. In particular, "humps" sometimes occur within the decline, e.g. in all sample points at SFT 3 (fig. A.3 on page 235) and only sample point 3 of SFT 8 (fig. 4.2 or fig. A.8). Also, as the experiment progresses this signal becomes less prominent. E.g. in SFTs 8 and 9 (figs. 4.2 and A.9) the decline almost degenerates into a straight line.

- Occasionally particles increase at sample point 1 with flow and stay at the higher value until flow decrease (e.g. in SFT 8, fig. 4.2).

- On a few occasions a sharp peak occurs at sample point 1 with flow decrease (e.g. in SFT 5, fig. 4.1).

- After step down in flow the total particle counts decrease slowly. They settle

down to a potentially different value than before the SFT within about one (low flow) travel time.

- The inlet particle counter data as given in fig. 4.2 exhibits a large number of apparently random peaks throughout the high flow period. These peaks do not propagate through the pipe rig. A decaying signal is additively underlying the random peaks.

### 4.1.2 Discussion and Hypotheses

As indicated by the bullet points above, the particle counter data is split into several parts, which might be quite independent of each other. This hypothesis is expanded further in this section, and, if appropriate and possible, underlying explanations are put forward. Based on the observations established in the previous section, three different particle counter signals originating from the step increase in flow will be considered: peaks (mainly at increase of flow), a step in particles and a slow signal.

From the point of view of usefulness of the data for the construction of a model, signals that have only 'face value' have to be distinguished from those with observable underlying effects. Only the latter are suitable as a starting point for a model. Both types of signals occur in the data described above.

#### 4.1.2.1 Peaks

Peaks occur either directly with increase of flow or (but only in section 1) with flow decrease. They occur only at well defined points along the rig which are identical to the sample points (and the inlet) or, considering the limited accuracy of the data, in close proximity to them. The accuracy of data is limited by the sampling time, which was initially 5 min (that corresponds, at a flow rate of 0.6 l/s, to a distance of about 19 m in a 110 mm diameter pipe, at 0.9 l/s to 28.4 m) and later 2 min (equivalent to 7.6 m at 0.6 l/s and 11.4 m at 0.9 l/s).

These observations indicate that the peaks originate from valves or bends which are situated close to the sampling points. There are two main valves which

have to be opened or closed for a flow increase or decrease: on the one hand there is the pipe rig inlet valve, which marks the beginning of the rig, and on the other hand there is a gate valve for fine adjustments just in front of sample point 1. Peaks sometimes occur at sample points 2 and 3, in particular only in SFTs 1 and 7. The fact that there are, however, always initial peaks originating from close to the inlet and sample point 1 is very strong evidence for the hypothesis that the valves are the origin of these particles. Very seldom there is a peak at step down, but again when that does occur it is only observed at sample point 1. Thus, this leades to the hypothesis: closing the valve near sample point 1 may sometimes lead to a release of particles.

The narrow width of the peaks indicates that the release of particles is not only narrowly localised but also that it happens quickly. If particles were released over a longer period of time, broader peaks would be observed, the same would be true if the point of release covered a large length of pipe. The short release period indicates that these particle do not have a strong adherence to the pipe wall. All material which has the potential of becoming entrained is lifted into suspension (almost) at once. This behaviour is different from the supposed phenomena underlying the slow part of the particle counter signal as discussed in section 4.1.2.3. Thus, it is proposed that these particles are loose deposits which are collected mainly in the valves.

The hypothesis, that in the particles in peaks are loose deposits entrained into suspension form localised 'hot spots' due to a sudden flow increase, was already put forward in [159].

Within this work, peaks are considered to be 'face value' signals. Not because no relevant underlying effects are expected, but because the exact shape of the peaks is unobservable since the sampling time is too large for a detailed picture of their structure. However, because the main interest of this work is in the biofilm coating of the distribution system and it is assumed that the origin of these particles is unrelated to it, there is no need to gain a deeper understanding of the behaviour of the particles in peaks.

Finally, since the peaks propagate with about the theoretical travel time

through the pipe rig, they can be used to improve the estimate of the travel time, cf. section 5.4.

#### 4.1.2.2 Occasional Particle Step

A second 'face-value' signal is the occasional particle step as described in section 4.1.1. It occurs only in some SFTs and, similar to some of the peaks described in section 4.1.2.1, this signal originates always from sample point 1. In particular, its origin is not further than 12 m upstream of particle counter 1, since it was observed at a flow of 0.9 l/s only. This indicates that the origin of this signal is again the valve situated in front of sample point 1. The shape of this signal suggests a near constant release of particles into suspension, which are propagated through the rig. A certain size of the opening of the valve could cause this effect, for instance by inducing eddies which lift an almost constant amount of loose particles into suspension whilst the flow is high.

#### 4.1.2.3 Slow Signal

The most interesting part of the particle counter response to a step increase of flow rate, from the modelling point of view, is the slow signal as described in section 4.1.1. Although the maximum values of this part of the particle counter response are reached after the travel times to the respective sample points, this signal is not merely propagating through the rig: at all sample point a simultaneous increase of counts that starts with the increase of flow is seen. The fact that the counts are first increasing and then decreasing rules out the hypothesis of a mere artefact produced in the counters due to the variation in flow, since this would result in fairly constant higher counts for a higher flow in the pipe rig. Thus, this is a generic effect occurring over the whole length of the pipe rig simultaneously.

Possible explanations of the underlying processes include an increased number of patches of biofilm (e.g. a biofilm consisting mainly of streamers) which are sheared off the pipe walls with a certain probability at high flow or repeated, random sloughing (a continued supply of particles) due to a thick, rich layer of

biofilm. Simulation results presented in section 6.3.1 on page 127 imply that the latter hypothesis better matches the observed data. The hypothesis of the particle counter response being due to a continuous shear-off which is decreasing in size was mentioned earlier by the author *et al.* in [98].

Since this signal is slow, the particles considered here adhere better to the wall than those particles that form the peaks, for the material is not coming off the wall at once. Therefore, it is conclude that these particles were attached particles.

The concept of a local shear-off density (with units $\frac{\text{particles}}{\text{ml}}$ per metre) will be introduced in section 6.4.1.3. This concept allows the development of an equation (i.e. a parametric model) that describes the slow signal. It follows the hypothesis of repeated shear-off given above. Again, the magnitude of the shear-off has to decrease over time.

If assumption 1 of section 6.4.1.3 is followed, then the shape of the decline of the slow signal reflects the shape of the local shear-off function. If, in addition, assumption 2 of section 6.4.1.3 is considered to be valid, then a major influence on the increase of the slow signal is the biofilm shedding profile, which is related to the biofilm thickness.

#### 4.1.2.4 Inlet Particle Counter Signal

The inlet particle counter exhibits a large number of apparently random peaks or spikes during high flow. These peaks do not appear after the flow is decreased and do not propagate through the pipe rig (i.e. they do not appear at the other sample points). In particular the latter argument gives rise to the conclusion that these are artefacts, in this case generated by, or in the line to, the particle counter. It therefore does not reproduce the conditions in the pipe rig. The inlet particle counter is the same type of counter as the others, however, it was installed only during the experiments of 1996 and might be slightly different because of its later manufacturing date. In addition, it does not use a pump to maintain the flow at a constant level but an overflow mechanism. However, this does not imply that the flow through the counter changed during high flow, since the counter flow was

monitored and found to be within a few ml/min of the target flow of 60 ml/min. In summary, it is assumed that the spikes or peaks in the inlet particle counter signal are artefacts but the reason for their appearance is not known.

Underlying these spikes is a decaying function. Since the inlet particle counter is very close to the inlet (within 5 m downstream of the inlet valve) this signal corresponds reasonably well to the hypothesis of a local shear-off function as discussed above.

#### 4.1.2.5 Particle Counts after Decrease of Flow

Particle counts decrease at the end of a step flow trial. An immediate end of the additional shear-off introduced by the increase of flow is proposed to explain this observation. Following that assumption the particle counts should decrease within one travel time. This coincides with the data. The counts do not necessarily settle down to the same level as before the step flow trial, however, a definite decrease occurs. Given the low accuracy of particle counts in terms of absolute numbers, the trend towards lower numbers is considered more conclusive than the actual final value.

## 4.2 Particle Counter Size Distributions

In this section, the size distributions of particle counts as introduced in section 3.2.4 on page 56 are investigated. Briefly, a size distribution contains the percentages of total particles which fall into the available size ranges.

Fig. 4.3 depicts, on the left y-axis, the percentages of all counted particles which fall within the size ranges 2–5 $\mu$m diameter, 5–10 $\mu$m and 10–15 $\mu$m (for the same step flow trial as the epifluorescence data in fig. 4.14). Only sample point 1 is depicted. Inlet flow is given on the right y-axis.

The size distributions of sample points 2 and 3 are similar to each other, and the shape of the size distribution of the particle counter at the inlet (downstream of the tank) is also similar but here the signal amplitudes are reduced to very small values.

The size distributions of all sample points and the inlet and of all step flow trials of 1996 are given in appendix A.2.

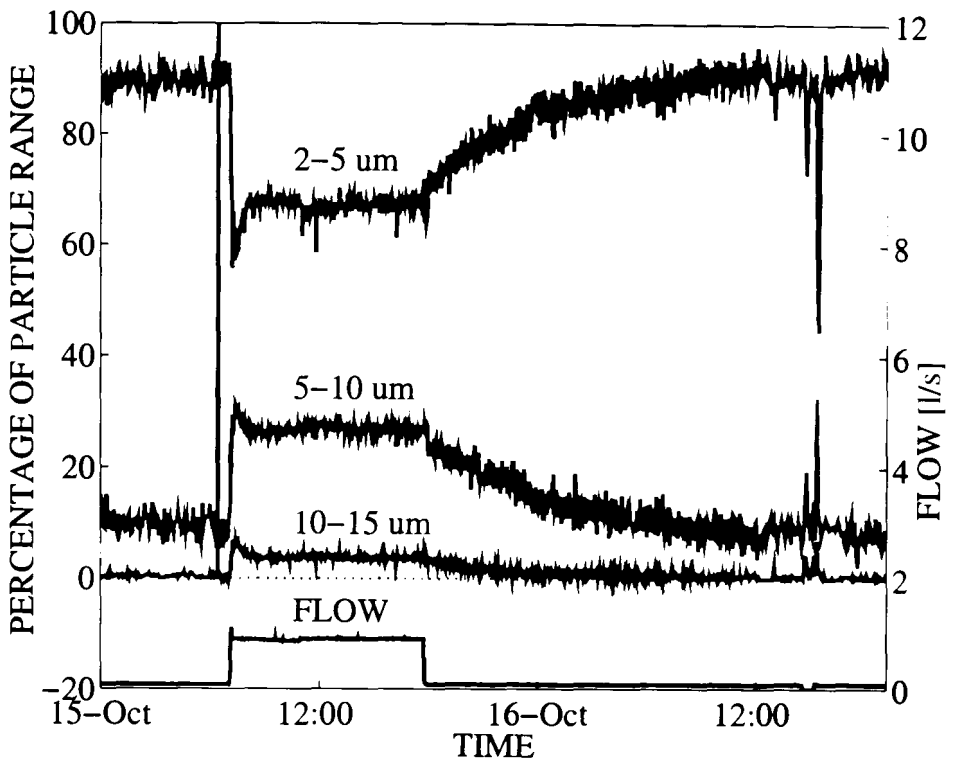


**Figure 4.3:** *Particle Counter Size Distribution of sample point 1 (as percentages), particle diameters are within 2–5 μm, 5–10 μm, and 10–15 μm; Inlet flow values are given on the right y-axis.*

### 4.2.1 Observations

It is useful to distinguish between small particles (2–5 $\mu$m) and large particles (5–10 $\mu$m, 10–15 $\mu$m etc.), since these groups of size ranges exhibit a very different behaviour. From fig. 4.3 several patterns of behaviour can be observed.

- There are peaks within the initial period of the step flow trial. They are negative for small particles and positive for large particles. A comparison with total particle counts shows that the peaks coincide.

- Within the initial period of the SFT something like a dip in small particles and a hump in large particles takes place. This pattern does not always contain a clear minimum/maximum value; it consists, during some SFTs (e.g. SFTs 5 and 9), purely of an overall decrease/increase. It finishes shortly after one travel time.

- If a step in particles occurs (cf. section 4.1.2.2), the percentage of large particles is significantly higher. This can be seen particularly well in SFT 8, when the propagation of particles released at sample point 1 by this phenomenon during high flow is observed in sample points 2 and 3 after decrease of flow.

- At a little more than one travel time past the start of the SFT the percentages settle to a fairly constant level. For SFTs to 0.9 l/s, this level is different from the values before the flow increase: the percentages of large particles are larger, the percentage of small particles is smaller than at low flow. Thus, the relative amount of large particles increases significantly during high flow. For SFTs to 0.6 l/s (SFT 1, 2 and 3) the percentage levels settle down to similar values as before the flow increase.

- After the decrease of flow, the percentages return slowly to values that are close to those observed before the SFT. This occurs within about one (low flow) travel time.

### 4.2.2 Discussion and Hypotheses

The particle counter size distributions (fig. 4.3) show a similar phenomenon as the epifluorescence counts given in fig. 4.14: there increased numbers of particles ('clumps') with flow increase are observed, in the size distributions an increase of the percentage of large particles within the total number of particles is seen.

This could be due to a different size distribution of attached as opposed to suspended bacteria. The attached bacteria are predominately larger. With a step increase of flow, attached bacteria are sheared-off from the biofilm and, thus, change the size distribution of suspended particles. This hypothesis is investigated in some more detail in section 6.3.2.

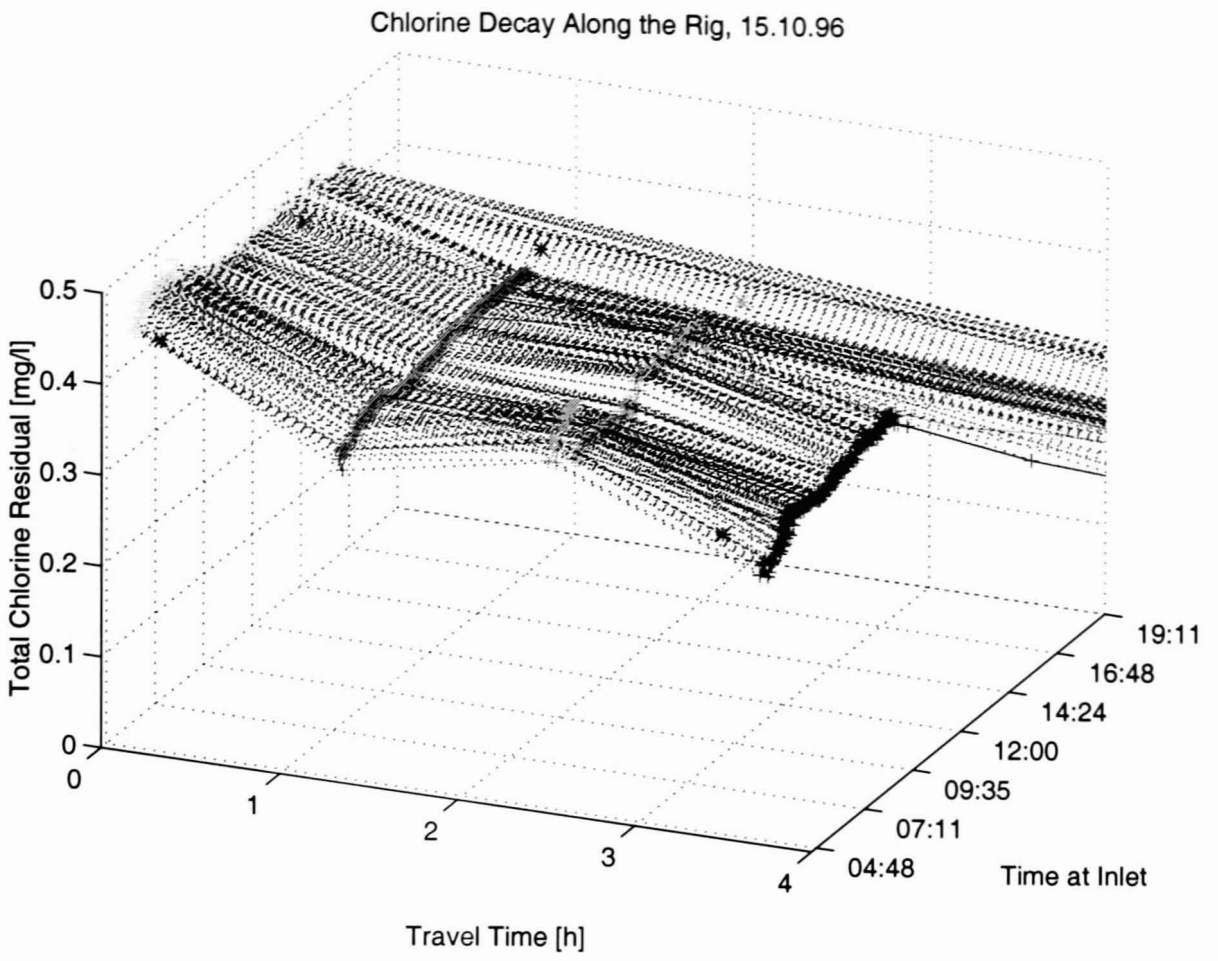


**Figure 4.4:** *Total chlorine vs. travel time and time at the inlet, 15.10.1996 (step flow trial 7). The asterisks ('*') are titration data (see text).*

## 4.3 Disinfection

During the experimental campaign of 1996, after four months of no chlorine, monochloramine was used as disinfectant in the pipe rig. In this section some examples of chlorine data, obtained from the pipe rig and from bottled samples, are provided. A quantitative treatment of these data can be found in section 5.3 and chapter 7.

### 4.3.1 Observations in the Pipe Rig

Figs. 4.4 and 4.5 show plots of total chlorine versus both time and travel time. The data for step flow trial 7 and the step chlorine trial are depicted. The travel time is the time it will take for a small volume of water (an aliquot) to reach a respective sample tap from the inlet shed, whereas the time at Inlet is the actual clock time when a considered aliquot of water started at the inlet.

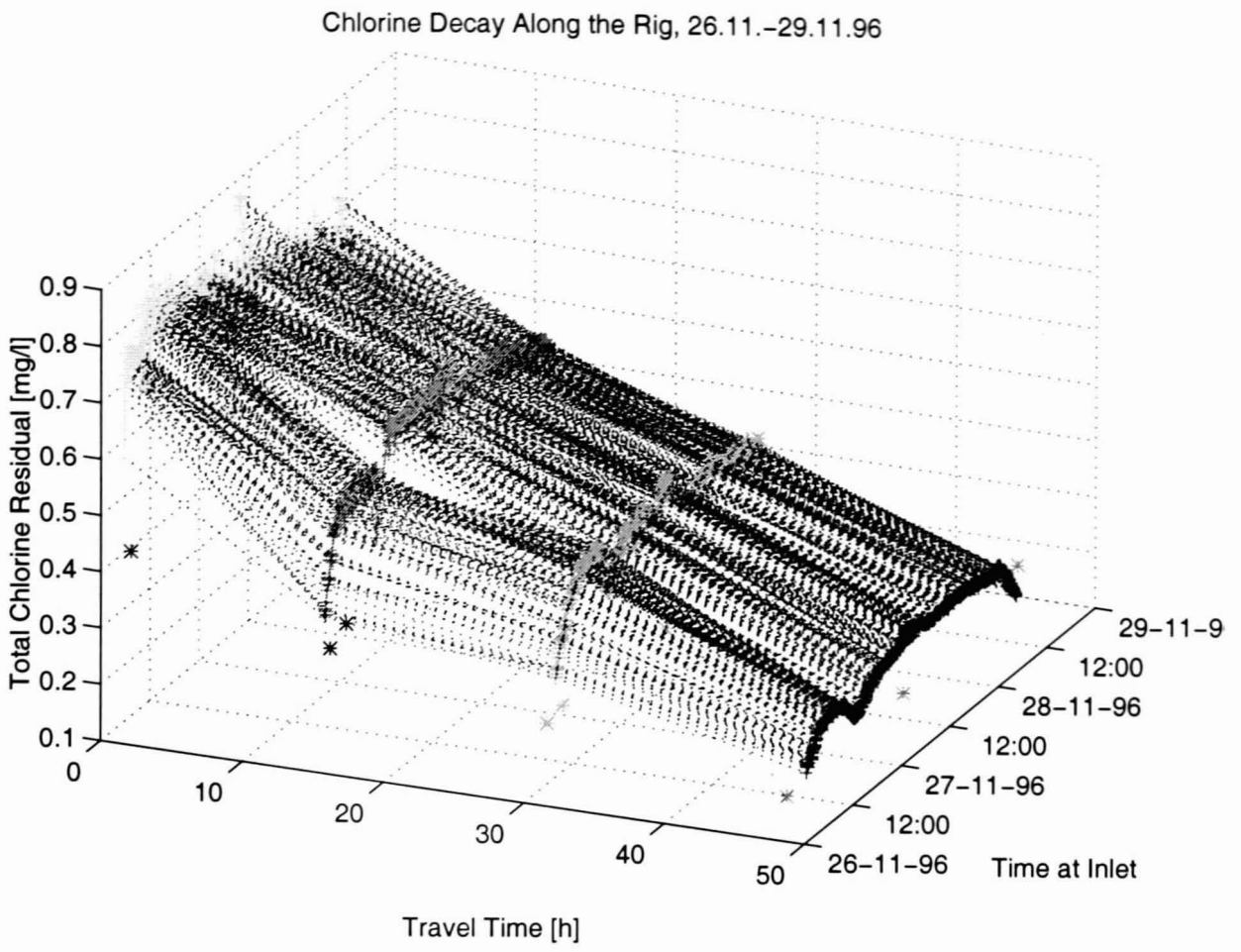


**Figure 4.5:** *Total chlorine vs. travel time and time at the inlet, 26.11-29.11.1996 (step chlorine trial 1). The asterisks ('*') are titration data (see text).*

On the figures, total chlorine is given on the y-axis (vertical), the travel time is given on the x-axis (horizontal) and the inlet clock time for the start of this aliquot is depicted on the z-axis (into the plane of the paper). The sample taps are represented by the travel time. The travel times are calculated for the three sample points along the rig and the plots along the x-axis are formed by connecting these calculated values through straight lines. Three lines along the z-axis (into the plane of the paper) show when the sample points 1, 2 and 3 were reached by the aliquots that started at the time given on the z-axis.

It is seen from these graphs, how total chlorine decreases over the length of the rig by following the lines of data along the x-axis (the travel time-axis). Each such line shows how the chlorine residual in one aliquot of water decreased over time and distance while travelling through the pipe rig. Going along the z-axis it is seen in fig. 4.4 that the time for the water aliquots suddenly becomes much larger towards the end of the shown portion of data. The reason for this is that

the SFT also comes to an end towards that point and thus the aliquots which are shown travel only part of there way at high flow, which increases the overall travel time.

Note that there is almost certainly a problem with the meter at sample point 2 in fig. 4.4. It shows a higher chlorine residual as the meter at sample point 1. This is quite obviously impossible, since it would imply that in some aliquots of water the chlorine residual while travelling down the pipe rig. This problem is addressed in section 5.3.

In fig. 4.5 the travel time does not change over the span of the depicted data, since this graphs shows a pure step chlorine trial with no change of flow. It is seen that the chlorine residual increases at the beginning of the data set, forming something like a 'hill' in the third dimension. However, the decay of chlorine along the rig (along the travel time axis) is still observed.

On both figures, figs. 4.4 and 4.5, mainly meter data is given. Due to problems with meters (as discussed in section 5.3) titrations are more accurate. They are also included in these graphs, as single stars or asterisks ('*'), however, it is difficult to discern the titration data within these graphs. Figs. 5.3 and 5.4 on page 104 and page 105 show the difference between meter data and titration.

### 4.3.2 Observations in Bottled Samples

In figs. 4.6 and 4.7 results of total chlorine titrations of bottled samples are presented. Three or more replicate titrations were done per sampling instant. These replicates are shown as crosses '+', their average as connected squares. For the detail on the measurement method see sections 3.2.7 and 3.3.2.

In fig. 4.6, four sets of bottles with free chlorine as disinfectant are depicted. The four sets shown in fig. 4.7 show bottles with monochloramine. Since both figures have the same axis ranges, visual comparison of the two graphs shows that free chlorine decays faster than monochloramine, as expected. Decay coefficients for these data will be calculated in section 7.5 on page 195. The aim of this part of the experiments is to compare the decay coefficients obtained from bottled

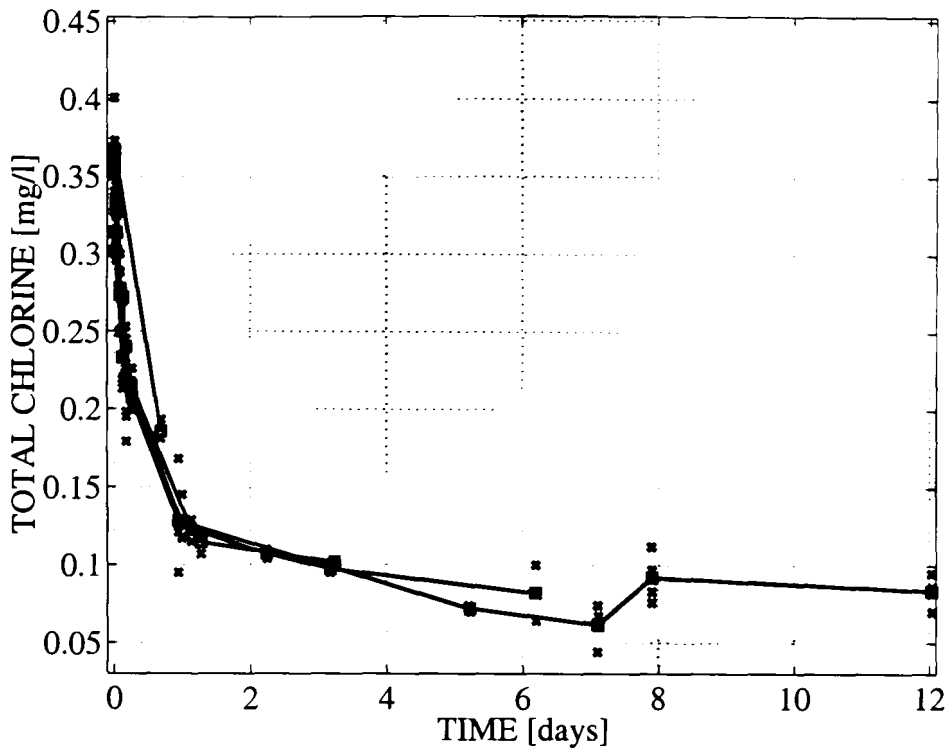


**Figure 4.6:** *Bottle samples with free chlorine: titrations of total chlorine of glass bottles. Lines with squares show average titration results, results of replicas are given as unconnected crosses '+'*

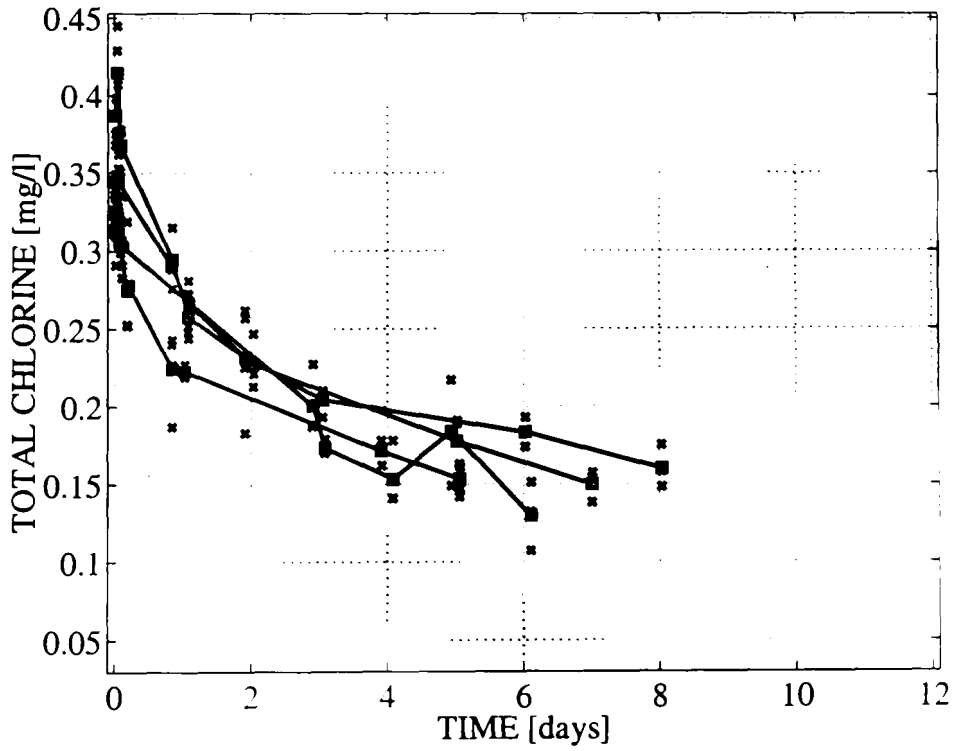


**Figure 4.7:** *Bottle samples with monochloramine: titrations of total chlorine of glass bottles. Lines with squares show average titration results, results of replicas are given as unconnected crosses '+'*

samples with those obtained in the pipe rig. The difference of the two is expected to be chiefly due to the biofilm in the rig. This question is addressed in chapter 7.

Note that in fig. 4.6 the total chlorine residual reduces to a near constant value which remains even after 12 days. As well as free chlorine, total chlorine generally contains also monochloramine and dichloramine. In these bottles no monochloramine was introduced, but due to interaction with organic substances in the treatment process, organic chloramines are expected to be present in the sample water [52]. In titrations they generally show up as dichloramine. Since organic chloramines are almost non-reactive, they stay close to constant over a period of 12 days (cf. section 7.2).

## 4.4 Temperature

Fig. 4.8 shows the change in temperature during the whole seven months of experiments. Temperature is given on the left y-axis, inlet flow is provided as reference on the right y-axis. The short spells of zero temperature in the measurements depicted in fig. 4.8 are artefacts which originate generally from periods of zero flow into the pipe rig. The flow values show short spikes at the beginning of several step flow trials. These are the initial overshoot which occurred occasionally at flow increase. From fig. 4.8 it is seen that the temperature changed from about $22^0$C to roughly $8^0$C within the duration of the experiments. This correlates quite well with the heterotrophic plate counts given in fig. 4.10 (see section 4.5.1.2).

## 4.5 Bacteriological Data

### 4.5.1 Heterotrophic Plate Counts

In fig. 4.9 typical results of heterotrophic plate counts, in this case for step flow trial 5, are given. A logarithmic scale is used for better overview. In this particular example no chlorine was present in the rig and the flow increase was 0.08 l/s to 0.9 l/s (regime 1). Flow at inlet and plate counts for the pipe-rig inlet tank and

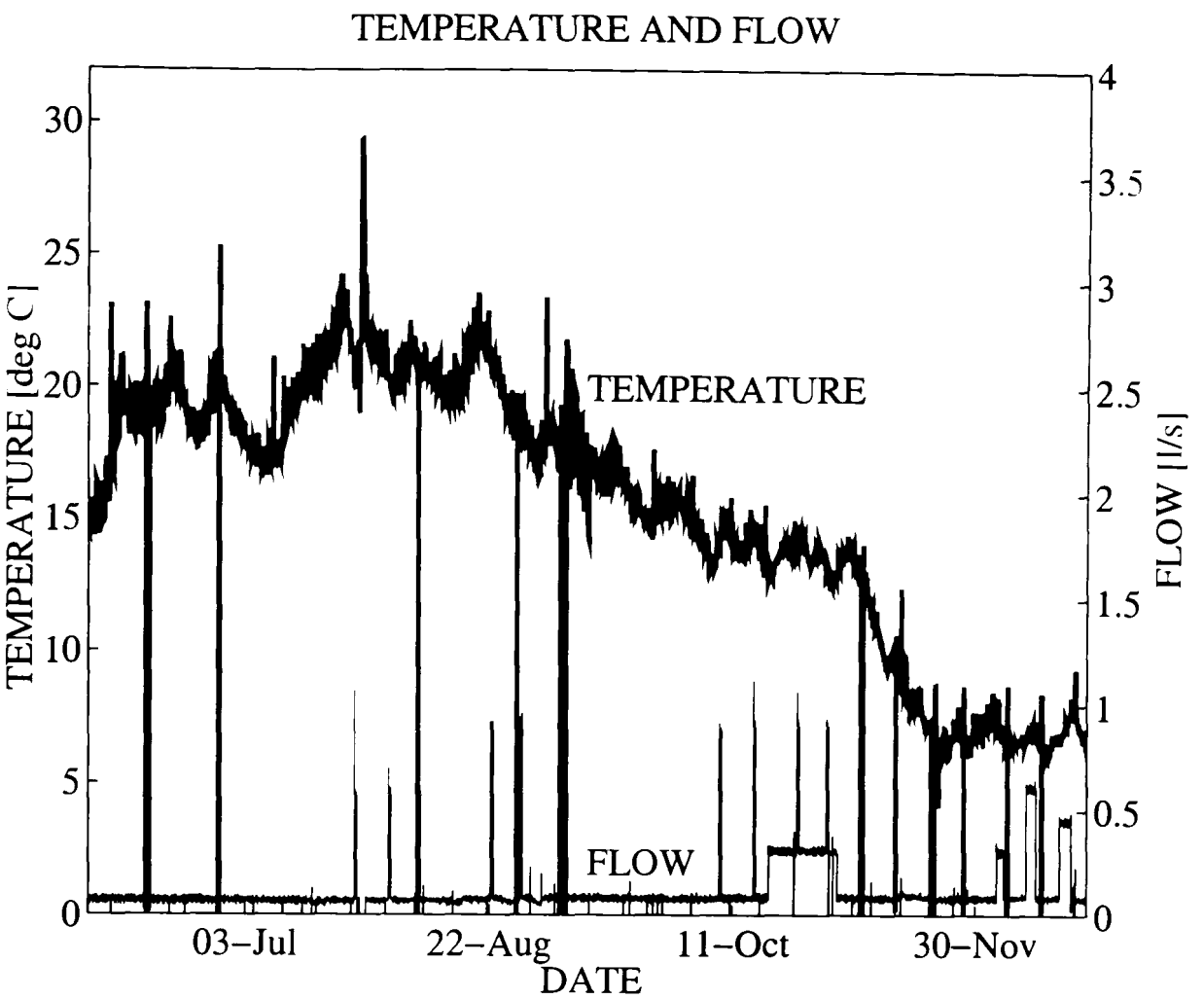


**Figure 4.8:** *Temperature on the left y-axis over the full experimental time period with inlet flow on the right y-axis for comparison with the schedule of the experiments*

the three sample points along the rig (INLET, SP 1, SP 2, SP 3) are given on the same y-axis on a logarithmic scale. Total particle counts for the same step flow trial are given in fig. 4.1 on page 68.

#### 4.5.1.1 Observations in the Pipe Rig During SFTs

The following observations can be made.

- Plate counts at the inlet of the pipe rig (tank) are significantly lower than the counts elsewhere in the rig.
- Plate counts are in general before the start of the step flow trial higher at the three sample points than at the inlet.
- Plate counts increase at the very start of the step flow trial; the magnitude

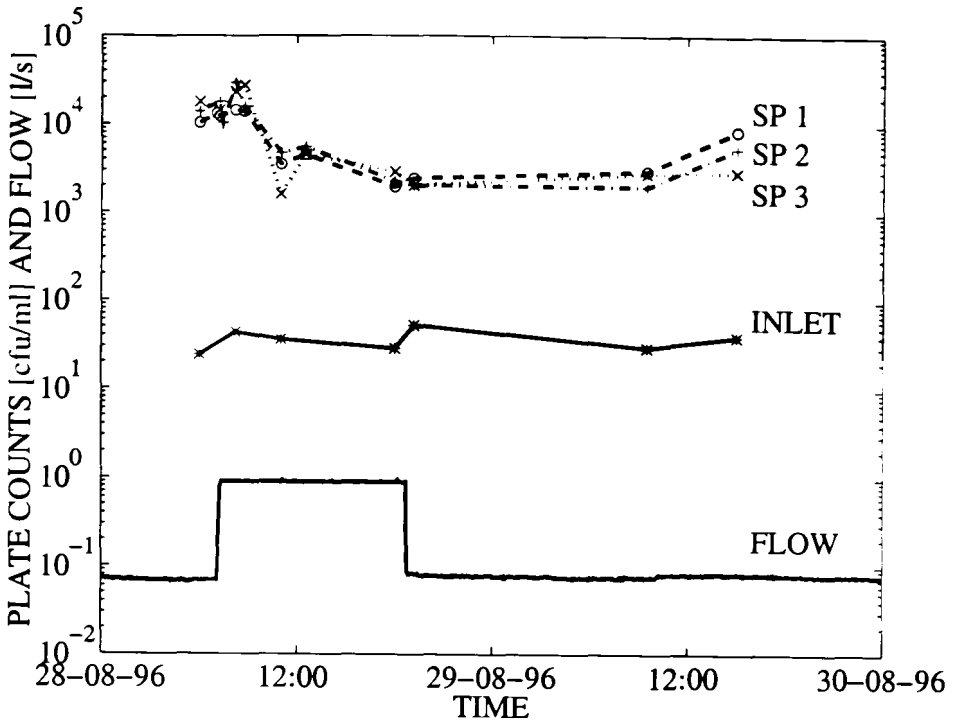


**Figure 4.9:** *Heterotrophic plate counts of inlet tank (INLET) and three sample points along the rig (SP 1, SP 2, SP 3) and inlet flow.*

of this increase varies for different trials.

- Plate counts decrease generally within roughly one travel time, i.e. the time it takes for the aliquot of water which was first to pass through the rig at the higher flow rate to go all the way through the rig. Due to the fairly low sampling frequency of grab samples (compared to on-line instruments), it can not be said for certain, exactly how long it takes until the HPC settle down.

- Counts generally stabilise within the final stages of the step flow trial. Again, the time of settling down varies from step trial to step trial and occasionally the decrease occurs throughout the high flow period.

- After the step flow trial there is initially no change in plate counts.

- Plate counts increase slowly at baseline flow. This can be seen from the fact that immediately before the flow increase counts are always higher than directly after the previous SFT.

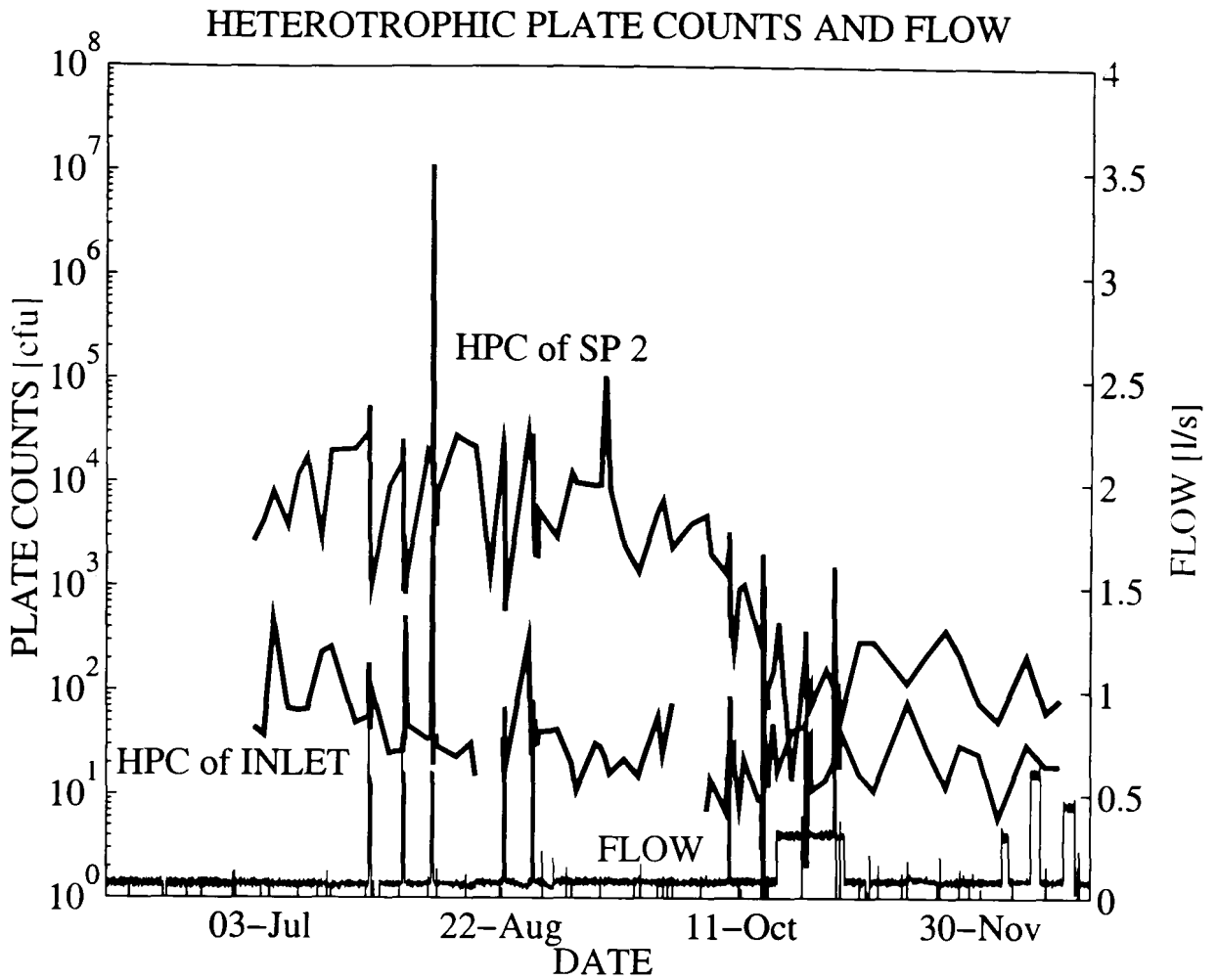


**Figure 4.10:** *Heterotrophic plate counts of sample point 2 (HPC of SP 2), inlet tank (HPC of INLET) and inlet flow. Plate counts are given on left y-axis, flow on right y-axis.*

#### 4.5.1.2 Long-Term Observations in the Pipe Rig

In fig. 4.10 HPC of sample point 2 and the inlet tank are presented. Plate counts are given on the left y-axis. The right y-axis shows the flow values which are included for reference. As can be seen from the time given on the x-axis this graph shows the HPC for the whole experimental period of 1996 (about seven months).

From these data it can be seen that the plate counts in the incoming water (inlet tank) stay low throughout the experimental period. However, the heterotrophs in the pipe rig decrease with successive increases of flow, the addition of monochloramine and the decrease of temperature. Note that the decrease of HPC in September 1996 coincides roughly with a decrease of temperature (cf. fig. 4.8). There is, however, no one-to-one match between temperature and HPC,

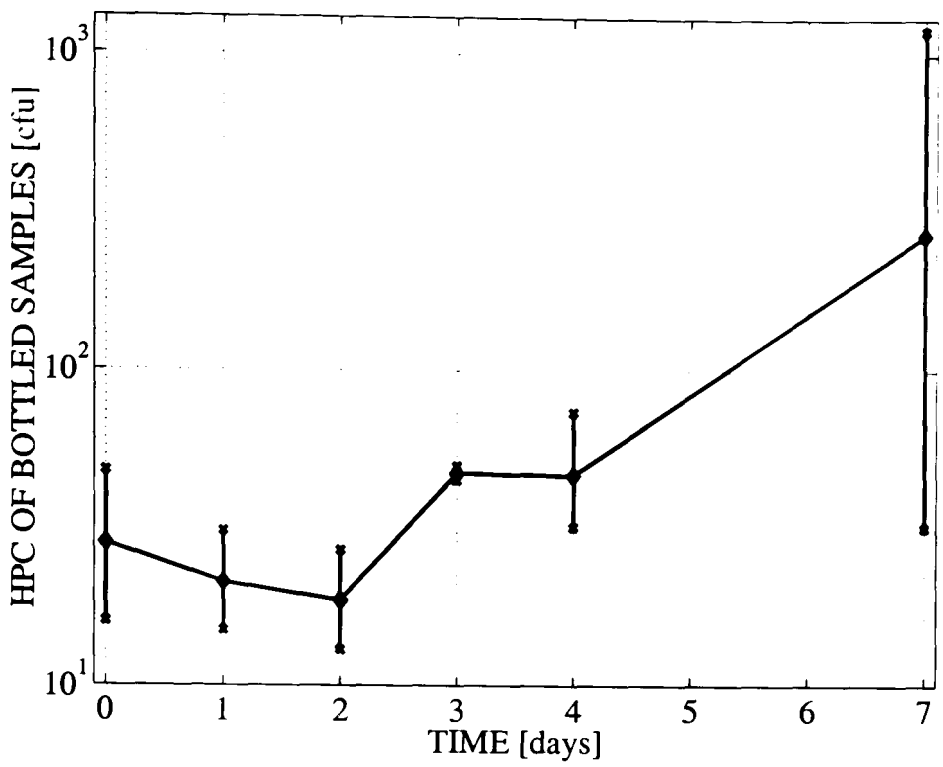


**Figure 4.11:** *Bottle samples without chlorine: logarithmic plot of two sets of heterotrophic plate counts of glass bottles. Lines with diamonds show average HPC, total range of replicate results is shown by bars terminated with* '`x`'.

which implies that the introduction of chlorine (also in September) and the flow changes (starting again in October) influenced the HPC.

#### 4.5.1.3 Observations in Bottled Samples

Some results of heterotrophic plate counts (HPC) of bottled samples are given in figs. 4.11–4.13. Depicted are the colony forming units (cfu) found after the time given on the abscissa. A logarithmic scale is used for the HPC. Several sets of three replicate bottles per time instant were averaged for the figures and are given as a connected line in the graphs. At each time instant a range bar shows in addition the spread of results (minimum and maximum HPC of all replicate bottles evaluated at that time). Due to the different number of sets, a maximum of six, twelve and nine replicate bottles are the basis of each data point (with range bar) in figs. 4.11, 4.12 and 4.13, respectively. (Note that not always all bottles could be evaluated.)

Depicted are all sets made with glass bottles, giving samples without chlorine

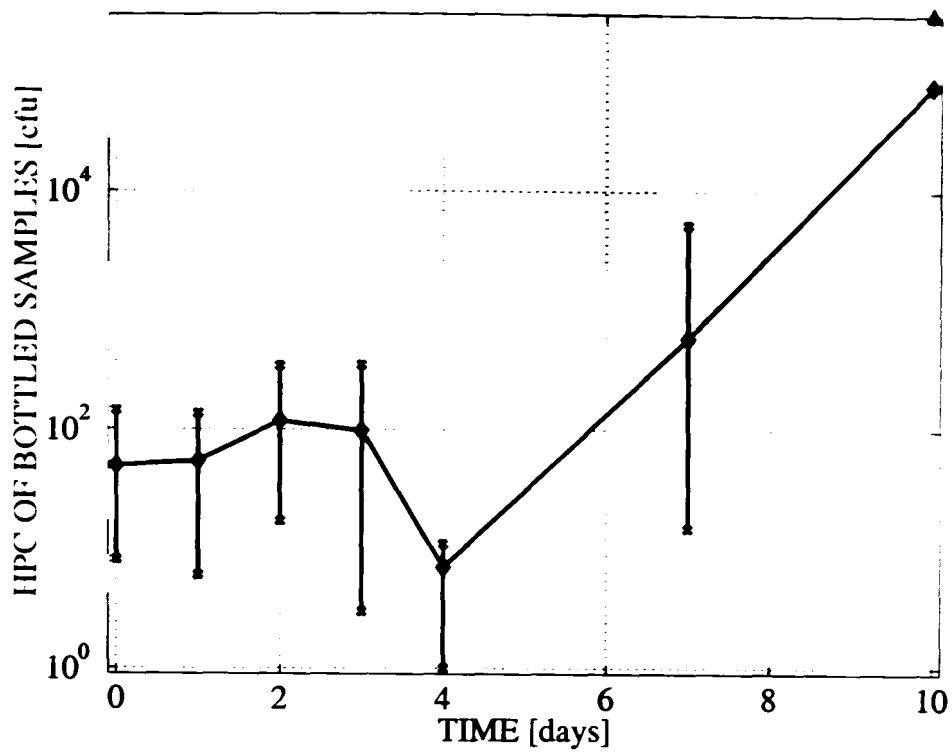


**Figure 4.12:** *Bottle samples with free chlorine: logarithmic plot of four sets of heterotrophic plate counts of glass bottles. Lines with diamonds show average HPC, total range of replicate results is shown by bars terminated with* '**x**'. *The triangle at the time 10 days indicates that the analysis of two bottles showed a HPC of more than 300000, without finding the exact number.*

(fig. 4.11), with free chlorine (fig. 4.12) and with monochloramine (fig. 4.13) as disinfectant in the bottles.

The aim of this part of the experiments was to establish the biological stability of the water as it would normally enter the distribution system, but in the absence of any influence of the system (in particular the biofilm). Note that the maximum retention time of the pipe rig (between inlet and sample point 3) is about 48 hours (i.e. an inlet flow of 0.07 l/s).

The obtained results of HPC in water without chlorine in fig. 4.11 show lower counts as expected. Counts increase within the first two days only little and after seven days the range of obtained values is very large, which implies that although in some bottles HPC rose sharply there are other bottles with very little increase of counts over the seven day period of investigation. Results of plastic bottles show a drastic increase already at the second day. Since it is, however, not clear if the material of the bottles is related to this observation, these results are not

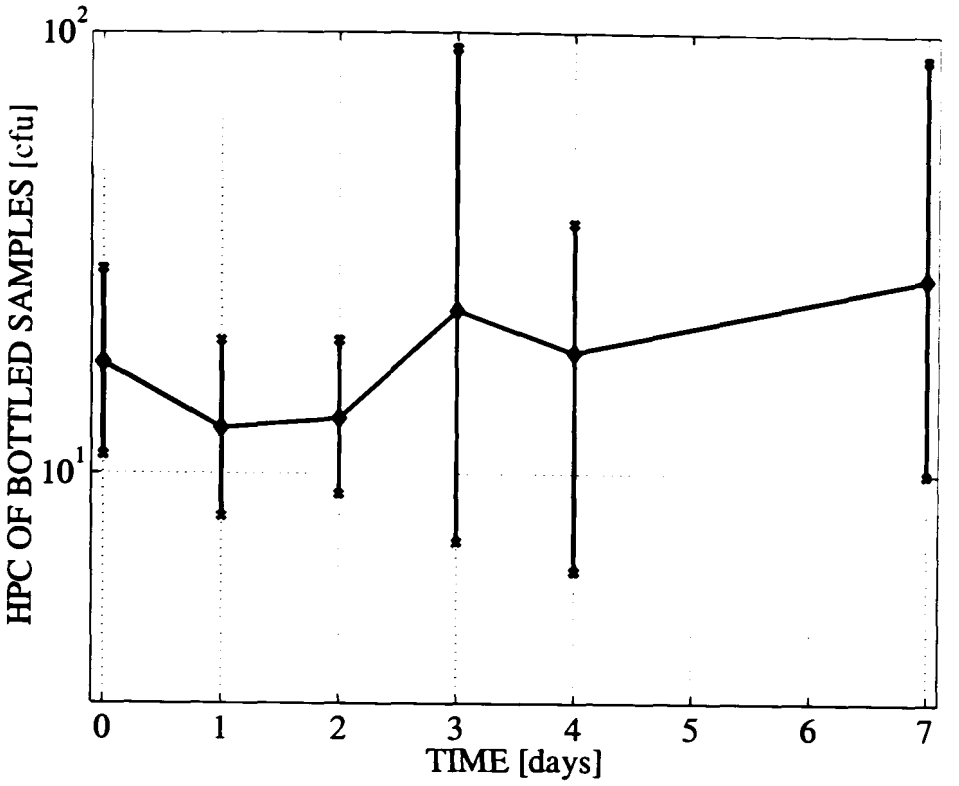


**Figure 4.13:** *Bottle samples with monochloramine: logartithmic plot of three sets of heterotrophic plate counts of glass bottles. Lines with diamonds show average HPC, total range of replicate results is shown by bars terminated with* `x`.

included.

Considering again the pipe rig retention time of two days, these results indicate that the water is biologically stable within the pipe rig, especially since the retention time is reduced to less then four hours during SFTs (at 0.9 l/s inlet flow).

The graph of HPC of bottles with free chlorine given in fig. 4.12 shows a more prominent increase of counts in the average. In one set the counts increase about 10 fold between day 3 and day 7, while other sets a fairly stable over 7 days. The three bottles evaluated after 10 days show very high counts with two bottles higher than the highest investigated count of 300000 (the exact HPC is unknown). An increase in counts was expected since free chlorine reacts with organic and inorganic particles in the water and thereby loses its disinfecting power. From fig. 4.6 on page 80 it is seen that after about three days total chlorine is reduced to about 0.1 mg/l, which represents the fraction of organic chloramines in the water (see section 4.3.2). Since they are non-reactive, the sample water is at that

stage disinfectant free and the same behaviour of heterotrophs as with no chlorine is observed, as would be expected. Again counts remain fairly low within a pipe rig retention time.

The graph of HPC in bottles with monochloramine is given in fig. 4.13. It shows that counts remain approximately stable and low throughout the seven day period. This reflects well the expected slower decay of monochloramine (see section 4.3.2).

In summary, it is seen that the disinfectants react as expected, i.e. free chlorine is used up after a few days and monochloramine lasts throughout a whole week. The feed water of the pipe rig is within the maximum retention time of the system biologically approximately stable. Any increase of bacteria in the pipe rig is likely to originate in shear-off from the pipe walls.

### 4.5.2 Epifluorescence Microscopy Counts

Epifluorescence microscopy counts (as adopted by S.M. McMath for this particular application [103, 104]) give the possibility to investigate in more detail if bacteria are present in 'clumps' or not. All the epifluorescence data used in this thesis were collected by S.M. McMath and A. Delanoue. In fig. 4.14 the number of large 'clumps' per ml (i.e. 'clumps' containing 10 or more bacteria) for step flow trial seven is depicted. Data for the four sample points along the rig (on the left y-axis) and the corresponding inlet flow values (on the right y-axis) are given. For this step flow trial the flow rate was increased from 0.08 l/s to 0.9 l/s with monochloramine present (regime 2). Fig. 4.15 depicts the same data for SFT 8. Note that in this figure the example with the largest variability of counts at high flow is given.

Fig. 4.14 is a typical example of epifluorescence results for large 'clumps'. A less typical result is presented in fig. 4.15. There the data for step flow trial 8 is depicted. It is the only step flow trial with such a marked variability at high flow and therefore it is considered to be the most variable epifluorescence data obtained during the 1996 experimental campaign. The other data also show variability at

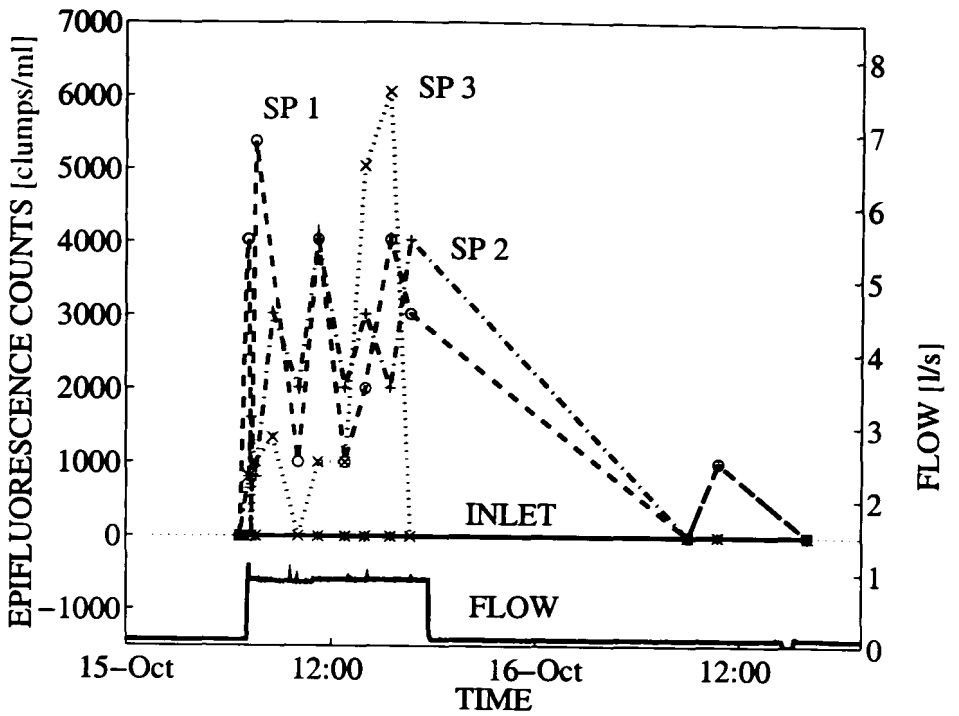


**Figure 4.14:** *Epifluorescence microscopy counts of 'clumps' of 10 or more bacteria of step flow trial 7; Inlet tank (INLET) and three sample points along the rig (SP 1, SP 2, SP 3) are shown; Inlet flow values are given on the right y-axis.*

high flow, but never to the degree as shown in fig. 4.15. It is obvious from the data of SFT 8 that the variance of bacteriological data can be very large.

In these examples, and the vast majority of the step flow trials, large 'clumps' were absent from the inlet tank samples. Prior to the step flow trial no large 'clumps' could be found in the entire rig, but as soon as the flow was increased, a significant increase in 'clumps' was observed. Only after the step down in flow was there a decline in the number of large 'clumps'. This comparison with particle counter size distributions is striking (see section 4.5.3).

The increase of 'clumps' is generally sustained throughout the high flow period. Fig. 4.15 is to some extend an exception to this rule, however, even in this case counts are on average throughout high flow significantly higher than at low flow.

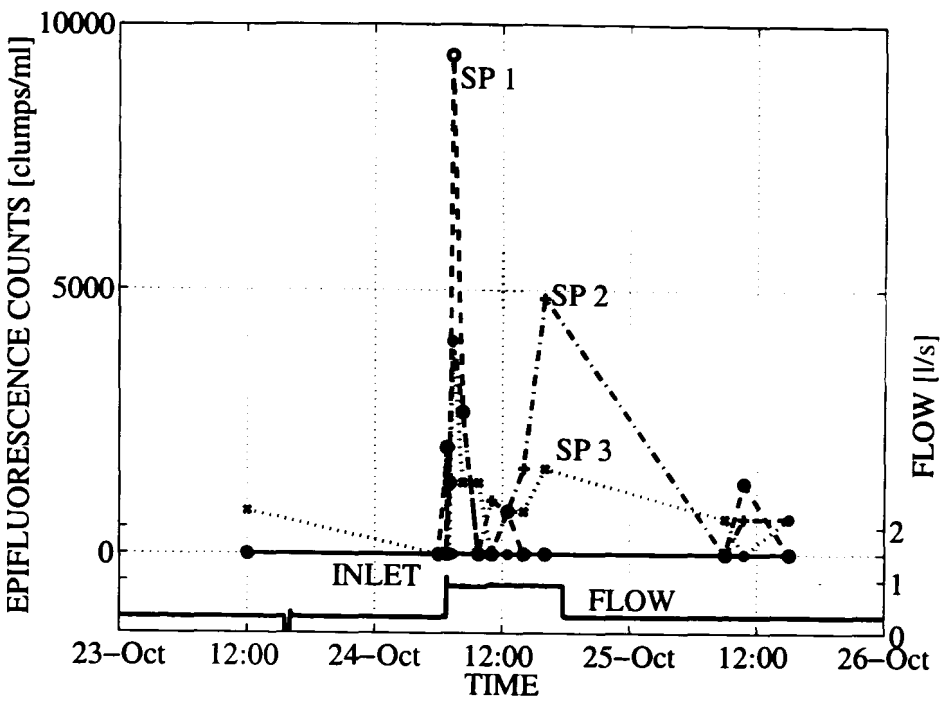


**Figure 4.15:** *Epifluorescence microscopy counts of 'clumps' of 10 or more bacteria of step flow trial 8; Inlet tank (INLET) and three sample points along the rig (SP 1, SP 2, SP 3) are shown; Inlet flow values are given on the right y-axis. This example shows the worst results of the 1996 experiments.*

## 4.5.3 Discussion

### 4.5.3.1 Heterotrophic Plate Counts

During baseline periods heterotrophs increase within, roughly, a week by about a factor of 5 to 10 (i.e. half a log to one log) at temperatures between $15^0$C and $22^0$C). Results from the bottled sample (fig. 4.11) do not sustain a hypothesis of regrowth of suspended bacteria. The results of the bottle experiments would indicate that the biofilm in the pipe rig is an important contributor to the increase of HPC in suspension at low flow.

The short peak in heterotrophs after flow increase is very likely due to a short and heavy shear off of biofilm and re-entrainment of settled deposits. Subsequently the heterotrophic counts settle down to a lower value within about one travel time. This indicates that a large amount of the suspended bacteria which are present at low flow is washed out of the pipe rig. The difference between inlet tank HPC and plate counts in the rig occurring subsequent to the initial wash-out must then originate from shear-off from the biofilm (note that the travel

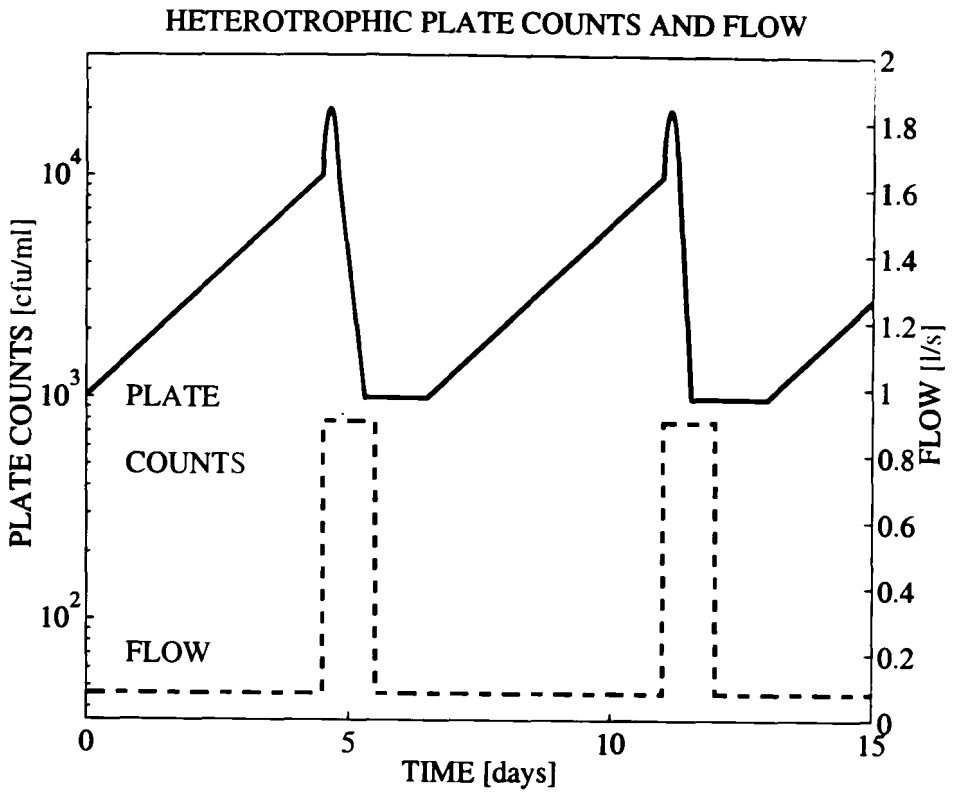


**Figure 4.16:** *Simplified pattern in heterotrophic plate counts; inlet flow values are given on the right y-axis.*

time through the rig is then only a few hours). After the return of the flow to the lower baseline values, the HPC recover.

The pattern of heterotrophic plate counts as discussed above is presented in a simplified form in fig. 4.16. Typical numbers of plate counts are given on the left y-axis, inlet flow values are shown on the right y-axis. This figure shows the expected "ideal" (and simplified) response of HPC to a SFT.

#### 4.5.3.2 Epifluorescence Microscopy Counts

Epifluorescence counts of 'clumps' with 10 or more bacteria show a sharp increase in number during high flow. Similarly, particle counter size distributions show a relative decrease in small particles and an increase in large ones. Thus, nothing conflicts with the hypothesis of a good comparison between these sets of data and a simplified pattern as depicted in fig. 4.17 is proposed. Similarly to fig. 4.16, typical numbers of epifluorescence counts and typical percentages of particle counter size distributions are shown on the left y-axes, while the right y-axes give corre-

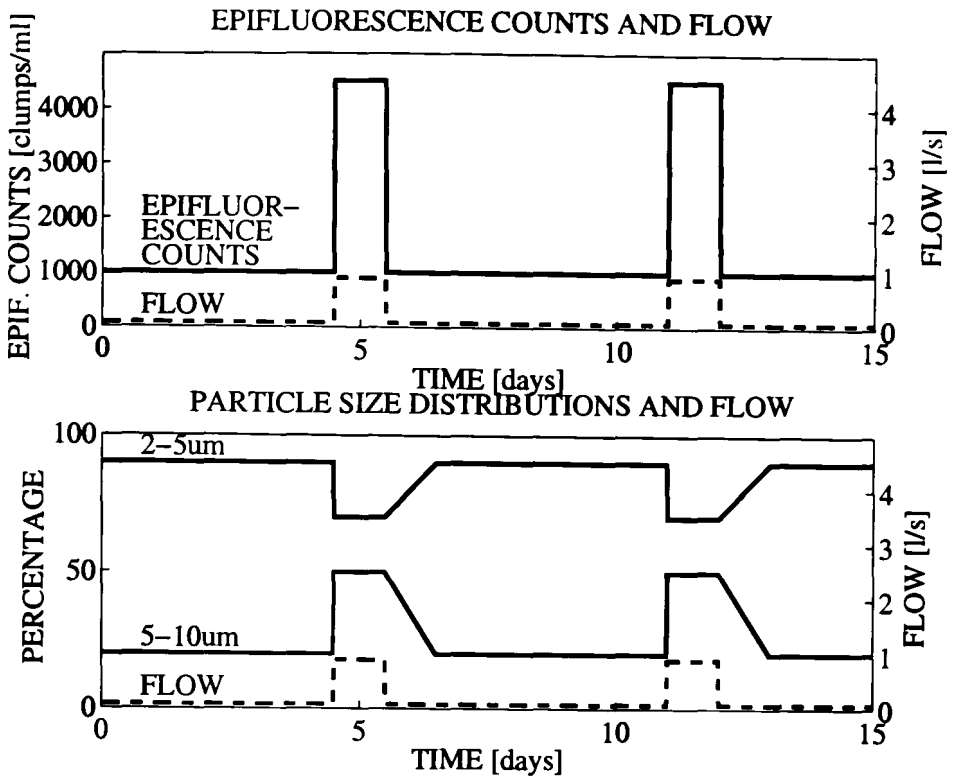


**Figure 4.17:** *Comparison of patterns in epifluorescence counts of 'clumps' of 10 or more bacteria and the particle counter size distribution; inlet flow values are given on the right y-axis.*

sponding flow readings. Both sets of data indicate a significant increase of sheared off material from the biofilm within the experimental distribution system.

The only major difference in shape between the curves shown in fig. 4.17 is that after the SFT it took about one travel time for the percentages in the particle counter size distribution to come back to normal (baseline flow) values. This is, however, most likely also the case in the epifluorescence data, since due to the less frequent sampling (this particular period was during the night), the slow decrease in large particles after flow decrease was probably not detected.

#### 4.5.3.3 Summary

The combination of step flow trials and particle counters provide a valuable technique of characterising biofilm detachment in water distribution systems.

Particle counter size distributions compare well to the simplified pattern of epifluorescence results of large 'clumps' . However, because of the much higher logging frequency (compared to grab sampling) and higher accuracy of measure-

ments, the particle counts give a more detailed time history if large 'clumps' of biofilm dominate (this condition has to be met since they do not count any particles smaller than 2 $\mu$m in diameter). Thus, particle counters will be of better use in a high shear stress environment (as e.g. during a step flow trial).

The results of this section provide evidence on the size distribution of the biofilm detached under a range of shear stress conditions.

## 4.6 Long-Term Effects

Throughout the twelve step flow trials the disinfectant and flow regime had little effect on the size distribution of particles and the epifluorescence microscopy results. However, successive increases of flow, the presence of monochloramine and the decrease of temperature caused an overall decrease of heterotrophs.

## 4.7 Conclusions

This chapter gave an overview of the data that will be used for modelling water quality in the following part III of this thesis.

Particle counts, both total and in size distributions, monochloramine, temperature, heterotrophic plate counts and epifluorescence microscopy counts of large 'clumps' were discussed. Especially the bacteriological counts will feature only marginally in the rest of this thesis, whereas the focus will be on total particle counts and monochloramine.

Important results from this chapter include the observations from total particle counts and their discussion in section 4.1.2. This section paves the way for the specifications of the particle counts model given in section 6.2. Similarly, the observations from the particle counter size distributions are instrumental for the numerical statistical models of the size distributions in section 6.3.2.

The discussion of the bacteriological results in section 4.5.3 provides further important conclusions. It was indicated that the biofilm in the pipe rig is an important contributor to the heterotrophic plate counts of suspended bacteria,

that the epifluorescence microscopy counts compare well with the particle counter size distributions and that particle counters will be of better use in a high shear stress environment. The relationship between epifluorescence counts and particle counter size distributions is especially relevant for the work of chapter 6 because it adds to the significance of a particle counts model that will be developed there.

# Part III

# Model

# Chapter 5

# Preprocessing of Data

## 5.1 Introduction

Preprocessing is concerned with the extraction of desired information about the measured physical quantities form meter output data. A meter transforms physical quantities into the available measured data, as illustrated in fig. 5.1.

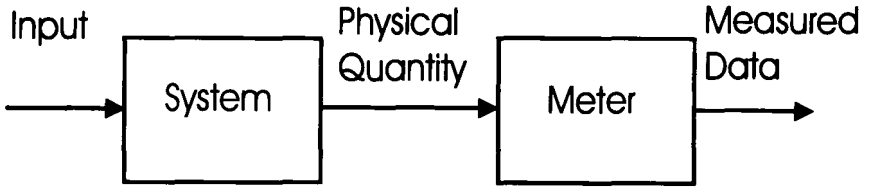


**Figure 5.1:** *Physical quantities and measured data*

The chlorine meters that are used in the experiments discussed in this thesis exhibit nonlinear dynamics of an order higher than one, i.e. a slow meter drift. Rather than attempting to model the transfer function of these meters, measured data are preprocessed with the help of additional, independent data, i.e. the chlorine titrations. The measurements of chlorine concentrations provided by titrations are considered to be more accurate than the meter readings and, therefore, the meter were recalibrated at irregular intervals (roughly every week or fortnight) using the titration data.

Different particle counters do not produce the same reading if fed with the same water (cf. "Switching the Particle Counters" below). Thus, additional in-

formation about particle counter accuracy was obtained through switching the water feed between the counters.

## 5.2 Switching the Particle Counters

The particle counters do not necessarily measure the same amount of particles even for exactly the same parcel (or aliquot) of water. These differences are attributed to differences in sensors, i.e. since sensors are calibrated to produce the same reading for spheres of a certain diameter they may react in a sensor specific fashion to particles of other shapes and thus produce a difference in counts.

To obtain some information about the difference between sensors, the particle counters 1, 2 and 3 (not 0 or inlet) were switched in a circular fashion (cf. below) once a week. Due to the physical distance between the inlet particle counter and the other counters it is impossible to incorporate counter 0 in the switching.

### 5.2.1 Ratios of Particle Counters

Columns 2 to 4 of table 5.1 contain the ratios of the average particle counts of the same water measured one hour before and after the switching by different particle counters (as indicated in the first row). Columns 5 to 7 of this table show the ratios of average particle counts of different water counted by, respectively, the same counter one hour before and after the switching of the counters. Sharp peaks or meter failures were excluded in both cases.

The last five rows give some statistics which describe the spread of data in the corresponding columns of data. Since ratios are considered in this context it would be inappropriate to calculate statistics based on the data as given. The aim of the linearisation is that the ratio of 0.5 should have the same distance from the target 1 as its inverse 2. Therefore, the data has to be normalised and linearised first. The intended mean is shifted from one to zero after a negation and inversion of all data points between zero and one. If the original stochastic variable as given in rows 2 to 18 of the table is referred to as $x$ and the new

**Table 5.1:** *The ratios of the particle counters (pc) before and after switching*

| | Same Sample Point | | | Same Particle Counter | | |
|---|---|---|---|---|---|---|
| | pc1/pc2 | pc1/pc3 | pc2/pc3 | pc1 | pc2 | pc3 |
| 15.07.96 | 1.509 | 0.908 | 0.931 | 2.200 | 0.583 | 1.208 |
| 22.07.96 | 1.703 | 1.710 | 1.229 | 0.769 | 1.427 | 1.115 |
| 29.07.96 | 1.337 | 0.988 | 0.977 | 1.283 | 1.283 | 0.804 |
| 05.08.96 | 2.333 | 1.578 | 0.756 | 1.059 | 1.116 | 0.946 |
| 12.08.96 | 2.150 | 1.530 | 0.761 | 0.978 | 1.089 | 1.004 |
| 19.08.96 | 1.615 | 1.279 | 0.707 | 1.218 | 0.873 | 0.839 |
| 27.08.96 | 1.700 | 1.162 | 0.784 | 1.016 | 1.021 | 1.106 |
| 03.09.96 | 1.712 | 1.135 | 0.696 | 1.024 | 0.845 | 1.214 |
| 09.09.96 | 2.046 | 1.244 | 0.525 | 1.145 | 0.817 | 0.924 |
| 17.09.96 | 1.768 | 1.251 | 0.561 | 1.291 | 0.621 | 0.989 |
| 30.09.96 | 2.259 | 15.246 | 7.008 | 1.016 | 1.027 | 0.995 |
| 07.10.96 | 5.777 | 23.057 | 2.400 | 1.154 | 2.350 | 0.222 |
| 14.10.96 | 2.089 | 13.487 | 6.830 | 0.669 | 0.714 | 2.213 |
| 22.10.96 | 1.275 | 1.157 | 0.745 | 0.926 | 1.068 | 0.831 |
| 28.10.96 | 1.734 | 1.130 | 0.589 | 1.093 | 0.640 | 1.290 |
| 07.11.96 | 1.295 | 17.789 | 13.300 | 1.733 | 0.842 | 0.663 |
| 08.11.96 | 1.417 | 12.719 | 9.025 | 0.611 | 1.707 | 0.954 |
| Statistical Analysis of linearised, normalised data | | | | | | |
| Mean | 0.957 | 4.728 | 1.718 | 0.1 | 0.004 | -0.16 |
| Median | 0.712 | 0.279 | -0.276 | 0.059 | 0.021 | -0.011 |
| Interquantile Range | 0.707 | 11.76 | 2.928 | 0.271 | 0.426 | 0.333 |
| Standard Deviation $\sigma$ | 1.048 | 7.442 | 3.875 | 0.42 | 0.507 | 0.933 |
| $\sigma_{min}$ for Normal Distr. | 0.818 | 5.805 | 3.023 | 0.328 | 0.396 | 0.727 |

variable is $y$, it is

$$y = \begin{cases} x - 1 & \text{for } x \geq 0 \\ -\frac{1}{x} + 1 & \text{for } x < 1 \end{cases} = \text{sign}(x-1) \cdot \left(x^{\text{sign}(x-1)} - 1\right). \qquad (5.1)$$

From eq. (5.1) it is obvious that $y = 0$ for $x = 1$ (normalisation) and that inverse ratios will feature with the same absolute value and different sign (linearisation). For a meaningful analysis, all statistics given in the last five rows are in $y$, and not in $x$.

Mean and median are provided in rows 19 and 20. The large difference of these two values in the case of columns 3 and 4 indicates data skew. Rows 21 and 22 give two measures of spread, interquantile range and sample standard deviation. The interquantile range is the difference between the 25th and the 75th percentile of the sample and has the advantage that it is not affected by outliers (like the standard deviation). From the table it is seen that the data spread is largest for columns 3 and 4, followed by column 2 and 7, while columns 5 and 6 exhibit small deviations. In column 7 only the standard deviation is large, while the interquantile range is comparatively low, this implies outliers, like the 0.222 in row 13. Without the transformation of eq. (5.1) this outlier would not have been recognised as such.

The last row gives the minimum standard deviation for which the respective column can be considered to be still normally distributed (with that standard deviation). It is

$$\sigma_{min} = \sqrt{\frac{(n-1)\sigma^2}{\chi^2_{0.05,n-1}}}. \tag{5.2}$$

The $\chi^2$ test statistic for an error probability of 0.05 and $n - 1 = 16$ degrees of freedom ($n$ is the sample size) is used to obtain that result. It is $\chi^2_{0.05,n-1} = 26.3$ (see [18, p.21]). This test statistic is routinely used for the test of variance (cf. [139, 78]). $\sigma_{min}$ has to be small if, as in this case, a small variation of data is required. For instance, if it is required to have a standard deviation not larger than 0.5, only columns 5 and 6 are normal distributions, while columns 2 to 4 and 7 are with 95 % probability (significance level of 0.05) not normally distributed.

The fact that the values in columns 5 to 7 are fairly constant and close to $y = 0$ ($x = 1$) could indicate one of two things: either the water quality throughout the rig is consistent (as far as the particle type is concerned) over the counter switching periods or the counters produce always the same measurements, no matter what water goes through them (specific only for the respective counter).

If the measurement of the counters were independent of the sensor and it is

assumed that the water before and after switching is roughly the same as far as the type of particles present is concerned, columns 2 to 4 would always contain values close to $x = 1$ (or $y = 0$). Alternatively, if the measurements were merely sensor specific, constant ratios should be found (which are not necessarily one) throughout each column. From the results discussed above it is seen that none of these assumptions is valid. The spread of data in columns 3 and 4 is large. This data can only be expressed in a normal distribution if standard deviations of more than 3.8 are assumed. Only column 2 is less spread out.

From this discussion it is concluded that

1. the particle counts depend on both the respective counter sensor and the type of particles going through them (possibly in terms of a predominance of shapes of particles);

2. the water in the whole of the pipe rig contains particles of roughly the same type at most times of counter switchings (apart from few exceptions like 7.10.96); and

3. the particle type varied significantly over time; even a period of only one day (rows 17 and 18) was enough to introduce noticeable variation.

### 5.2.2 Original Order of Particle Counters

For the purpose of analysis, especially concerning travel times, the data of the particle counters need to be switched back to its original particle counter sequence.

For this purpose a record of all the dates and times of switching the counters was kept. This data was imported into a file and used directly to modify the raw data such that the original order 1–2–3 of the particle counters is preserved within the entire data set. In the vicinity of the points of switching possible errors (i.e. wrong sequence) within a period of not more than one hour (generally much lower) may occur.

## 5.3 Chlorine Meter Data

The chlorine meters used during these experiments measure total chlorine by passing water through an electrolytic cell containing a gold and a copper electrode. The current produced by the electrolytic action is proportional to the concentration of chlorine in water. The manufacturer claims the accuracy of the meters as $\pm 0.05$ mg/l at a Full Scale Deflection of 2 mg/l. Analysis of data suggests that this performance is easily obtained in the short-term but that the instruments were subject to some long-term drift. The chlorine residual measured in the considered system is generally in the range 0.05 and 0.4 mg/l, i.e. fairly close to the limit of the meter range.

Potential errors associated with meter drift can be quite significant with respect to the measured signal. Therefore, it is important to correct this as far as possible before attempting to calculate the decay coefficient(s). This was done by comparing the meter readings against titrations, a bench analysis which yields values for free chlorine, monochloramine and dichloramine. The sum of these measurements is called total chlorine. Although there are errors associated with titrations, it is generally assumed that they are not systematic and may be considered to give the 'true' chlorine concentrations of the system. To minimise errors as much as possible replicate titrations were performed (i.e. 3 to 5 titrations of the same water sample). After discarding outliers the averages of the remaining titration values are used for the following considerations.

### 5.3.1 Correction of Chlorine Meter Errors

It is assumed that the (averaged) titration values give the 'true' total chlorine concentrations, whereas the meters are incorrect. It is further assumed that the error in the meter readings is due to a relatively slow meter drift. The aim of this correction procedure is to find this error signal by using titration results and then adjust the meter reading values as appropriate. Since a titration is a bench analysis, titration values are unequally spaced and relatively sparse (between one value a day to five values a day, no values on weekends). However, if the error

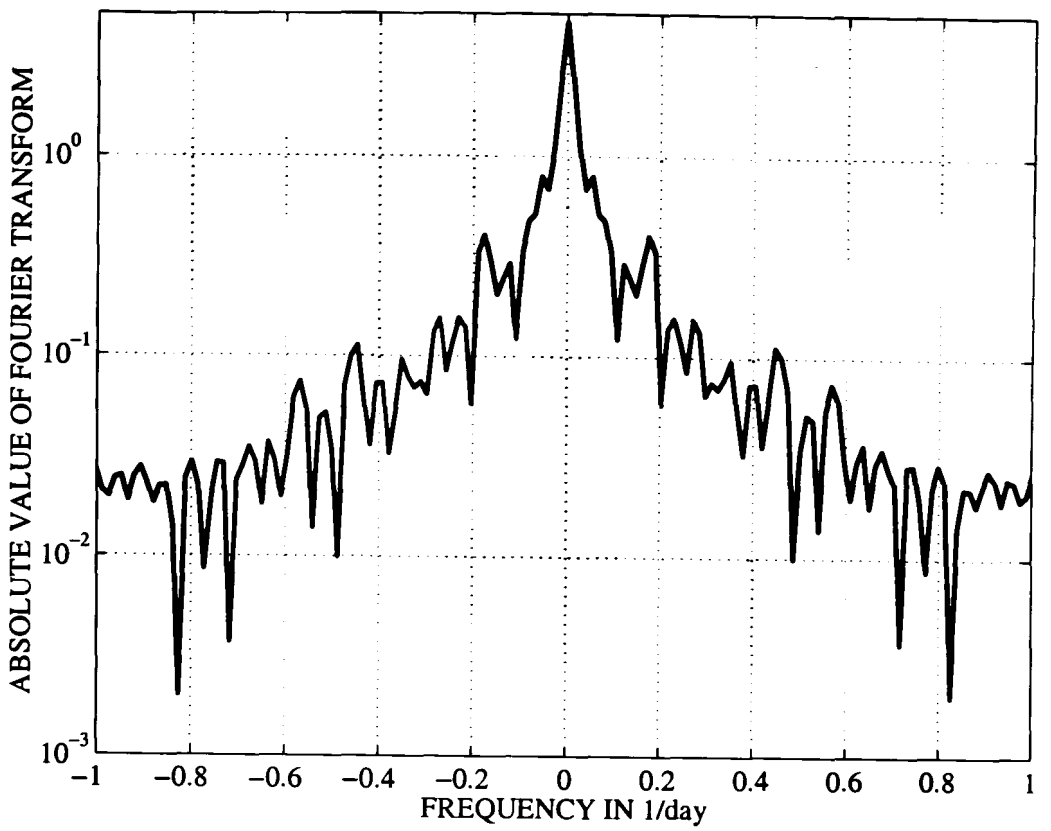


**Figure 5.2:** *Discrete Fourier transform of the multiplicative error function* $\epsilon_M^{IR}(t)$ *of sample point 3 before preprocessing (but after reverse-calibration) on a logarithmic scale.*

signal is only varying slowly the Nyquist theorem is still satisfied (i.e. there are at least two samples per period of the error signal).

Evidence for the validity of the assumption given above is indicated in the Fourier spectrum of a typical meter error function as depicted in fig. 5.2. In this graph an example of the absolute value of the Fourier spectrum of the equally spaced (interpolated) and reverse-calibrated signal $\epsilon_M^{IR}(t)$ — see eqs. (5.7) and (5.8) — is provided. The reverse-calibration removes the sharp changes that were introduced into the complete data by recalibrations. These changes may otherwise result in a high frequency error signal independent of meter drift. From this figure it is obvious that the spectrum decreases roughly exponentially with increasing frequency which shows a low high frequency content of the signal.

The multiplicative error function is calculated as the ratio between the titration data $c_b(x_0, t_i)$ and the chlorine meter data $c_m(x_0, t)$. Here $t_i$ denotes the unequally spaced time instants of the titrations, $t$ represents, for brevity, the equally and closely spaced time instants of the meter readings, and $x_0$ is the

distance of the point of investigation from the inlet. Since this section is only concerned with data specific to each sampling point, the dependence on the distance is irrelevant and will be omitted $x_0$ in this section. The multiplicative error function $\epsilon_M(t_i)$ (with the omission of the distance dependence) is obtainecd as

$$\epsilon_M(t_i) = \frac{c_b(t_i)}{c_m(t)\Big|_{t=t_i}}, \tag{5.3}$$

To reconstruct the error function between the time instants $t_i$, $\epsilon_M(t_i)$ is at first reverse-calibrated and then interpolated. For this, first the set $\mathcal{W}$ of recalibration windows is defined,

$$\mathcal{W} = \{W_1, W_2, W_3, \ldots, W_w\}. \tag{5.4}$$

The $w$ recalibration windows $W_j$ are of the form

$$W_j = \left[t_j^r + \delta, t_{j+1}^r - \delta\right], \tag{5.5}$$

where $t_j^r$ is the $j$th time of recalibration and $\delta$ is a small positive pertubation. From the above equation it is seen that these windows are rectangular and fixed. thus, they are not the moving windows frequently used in signal processing. Following eq. (5.5), the reverse-calibration factors are

$$r(t_i) = \prod_{k=1}^{j} \frac{c_m(t)\Big|_{t=t_k^r-\delta}}{c_m(t)\Big|_{t=t_k^r+\delta}} \text{ for } t_i \in W_j. \tag{5.6}$$

Thus, the reverse-calibrated error signal $\epsilon_M^R(t_i)$ is

$$\epsilon_M^R(t_i) = \epsilon_M(t_i) \cdot r(t_i) \tag{5.7}$$

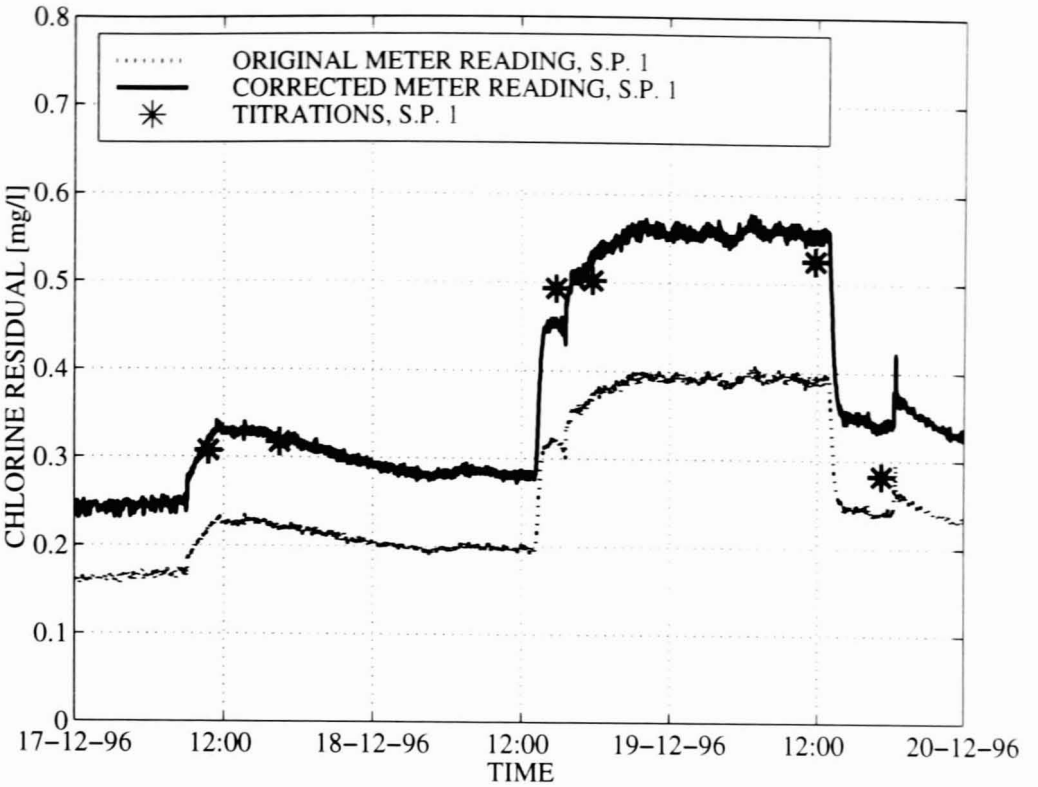


**Figure 5.3:** *Typical example of the correction attained by preprocessing. Corrected and uncorrected chlorine data of sample point 1.*

Finally, this error function is interpolated

$$\epsilon_M^{IR}(t) = \sum_{i=1}^{m-1} \epsilon_M^R(t_i) \cdot \ell_i(t), \tag{5.8}$$

where $\ell_i(t)$ denotes the linear interpolation function that is non-zero between $t_i$ and $t_{i+1}$ and $m$ is the number of titration times $t_i$ in the considered data. The superscript $I$ indicates that $\epsilon_M^{IR}(t)$ is an interpolated signal, the superscript $R$ refers to the reverse-calibration of eq. (5.7). The reverse-calibration is intended to inverse the effect of the recalibrations such that the chlorine reading directly after recalibration (at $t = t_k^r + \delta$) is the same as the reading just before recalibration (at $t = t_k^r - \delta$). Since the recalibrations guarantee that the meter is within the linear region of its scale the resulting error function $\epsilon_M^R(t_i)$ should adhere to the low frequency assumption made above.

Finally the error function $\epsilon_M^{IR}(t)$ is filtered, in accordance with the assumption of slow varying error, to remove any high frequency noise and smooth the signal.

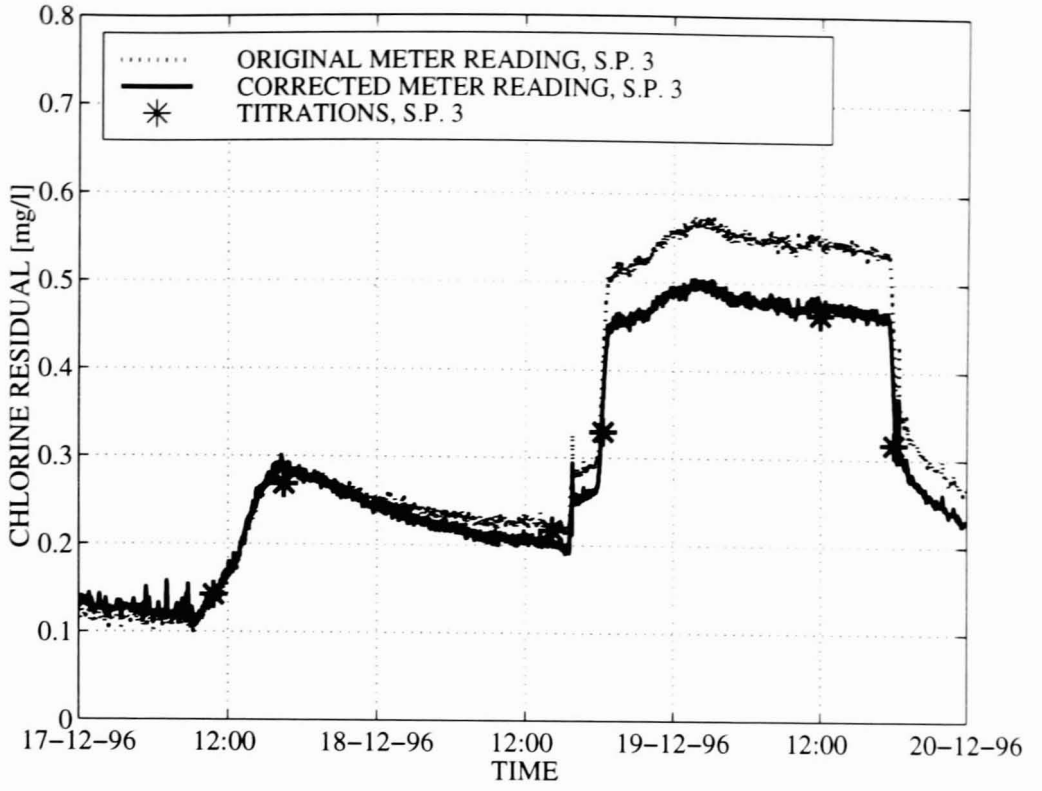


**Figure 5.4:** *Typical example of the correction attained by preprocessing. Corrected and uncorrected chlorine data of sample point 3.*

Thus,

$$\epsilon_M^{IRF}(t) = \epsilon_M^{IR}(t) * b_5(t), \tag{5.9}$$

where $*$ denotes the convolution sum of the discrete Fourier transform and $b_5(t)$ is the impulse response of a fifth order Butterworth filter. In this case, a zero-phase distortion Butterworth filter (no time shift between filtered and unfiltered signal)[1] was chosen. The cut-off frequency of 0.3 1/day was chosen for a remaining absolute value of the Fourier transform of approximately 1–2 % of its maximum value (cf. fig. 5.2).

Since the sampling frequency of the meters is adjustable, another interpolation step might be necessary at this point, such that the corrected chlorine data $c_c(t)$ can be obtained by multiplication of the meter data $c_m(t)$ with the final error

[1]Matlab function `filtfilt`.

function $\epsilon_M^{IRF}(t)$

$$c_c(t) = c_m(t) \cdot \epsilon_M^{IRF}(t) \tag{5.10}$$

Typical examples of the correction obtained with this procedure are given in figs. 5.3 and 5.4. These figures show original meter data (dashed line), corrected data (dotted line) and titration results (large asterisks). In fig. 5.3 data of sample point 1 of SFT 12 is shown. Here the titration results were much higher than the meter data. The corrected data contains accordingly larger values. Fig. 5.4 shows data of sample point 3 of the same SFT. In this case initial values of titrations and meter readings match well and in the second half of the SFT titrations are lower than the meter reading (the other way round in sample point 1). In the total investigated time period[2] the maximal absolute error is reduced from 0.28 mg/l to 0.13 mg/l, the maximal mean square error from 0.075 mg/l to 0.029 mg/l.

### 5.3.2 Alternative Correction Procedures

In the previous section, a procedure for the correction of chlorine meter data was demonstrated that utilises multiplicative error functions and reverse-calibration. Instead of these, additive error functions or windowed data could be used in the correction procedure.

The additive error function (or error residuals) $\epsilon_A(t_i)$ are the difference between the titration and the computer logged meter data, analogous to eq. (5.3). They are defined as

$$\epsilon_A(t_i) = c_b(t_i) - c_m(t)\Big|_{t=t_i}. \tag{5.11}$$

The main criteria for the decision between additive and multiplicative error functions is which of them better fulfills the low frequency assumption. Thus, the Fourier transform of the error function, as shown in figure 5.2, has to be small for

[2]In this thesis, titrations between 5.10.96 and 19.12.96 were considered with the exception of data between 5.11.96 21:00 hours and 7.11.96 midnight due to a treatment plant failure. Note that this time window is different from the one used in [97].

large frequencies. In this case, frequencies that have periods up to a few days are considered to be large. Keeping that in mind, the cut-off frequency for the filter was chosen to 0.3 1/day (period of 3 days). Accordingly, the percentage $p_{FT0.3}$ of the maximal value of the Fourier Transform at $f = 0.3$ 1/day is used as the most important indicator of a low frequency signal.

If $FT(f)$ is the discrete Fourier transform of a considered error function at the frequency $f$ in 1/day, then

$$p_{FT0.3} = \frac{FT(0.3)}{\max\limits_{f}(FT(f))} \cdot 100\%. \tag{5.12}$$

**Table 5.2:** *Percentage $p_{FT0.3}$ of the maximal value of the Fourier transform at $f = 0.3\frac{1}{\text{day}}$.*

| Sample Point | Percentages of Fourier transform of error function ... | | | | | |
|---|---|---|---|---|---|---|
| | $\epsilon_A^{IW}$ | $\epsilon_A^{IR}$ | $\epsilon_M^{IW}$ | $\epsilon_M^{IR}$ | $\epsilon_M^{IW,0}$ | $\epsilon_M^{IR,0}$ |
| Inlet | 49.86 % | 3.24 % | 0.81 % | 1.32 % | 43.68 % | 14.31 % |
| 1 | 10.11 % | 6.47 % | 0.35 % | 0.93 % | 3.11 % | 3.44 % |
| 2 | 20.88 % | 10.92 % | 1.20 % | 1.84 % | 22.35 % | 6.51 % |
| 3 | 8.96 % | 8.85 % | 1.46 % | 1.39 % | 9.22 % | 2.72 % |

Table 5.2 shows the percentage $p_{FT0.3}$ for several error functions. Note that only interpolated error signal are transformed, since the standard discrete Fourier transform requires equidistant data. Columns 2 and 3 show results for additive errors, columns 4 and 5 show multiplicative errors. In both cases, first data that was interpolated within the recalibration windows (columns 2 and 4) and then reverse-calibrated data (columns 3 and 5) are given. The windowed data preserves the recalibrations, which naturally introduces higher frequencies into the data as can be seen from comparison of $\epsilon_A^{IW}$ and $\epsilon_A^{IR}$. This is not apparent from comparison of $\epsilon_M^{IW}$ and $\epsilon_M^{IR}$ which is probably due to the shift of mean because of reverse-calibration which is significant in multiplicative errors but not in additive errors. The mean value (zero-frequency value or DC offset) is removed from the multiplicative error residuals in columns 6 and 7. Here, again, an overall larger percentage in windowed data is observed.

**Table 5.3:** *Additive error residuals in mg/l.*

| Type of error | Sample Point | Before preprocessing | Recalibration windows | Flow windows | Reverse-calibration |
|---|---|---|---|---|---|
| Maximal Error | Inlet | 0.2124 | 0.1911 | 0.2195 | 0.0860 |
| | 1 | 0.2848 | 0.1714 | 0.1969 | 0.0664 |
| | 2 | 0.2615 | 0.1406 | 0.2226 | 0.1307 |
| | 3 | 0.1010 | 0.1027 | 0.1755 | 0.0975 |
| Mean Square Error | Inlet | 0.0523 | 0.0481 | 0.0885 | 0.0258 |
| | 1 | 0.0754 | 0.0468 | 0.0712 | 0.0229 |
| | 2 | 0.0639 | 0.0392 | 0.0639 | 0.0286 |
| | 3 | 0.0404 | 0.0315 | 0.0667 | 0.0252 |

Thus, the most important columns in table 5.2 are the ones concerning reverse-calibrated data, i.e. columns 3, 5, and 7. Here a significantly higher reduction for multiplicative error functions $\epsilon_M^{IR}$ to 1–2 % is seen, but even if the zero frequency is not considered, i.e. if $\epsilon_M^{IR,0}$ is investigated, the overall reduction in the Fourier spectrum of the multiplicative errors is still better than with additive errors. Therefore, a multiplicative error is chosen for the correction procedure.

There are still several alternatives concerning the windowing of the data. In particular, recalibration windows, flow windows or pure reverse-calibration are investigated. Only the reverse-calibration does not need any windows, however, windowing does not interfere with the low frequency assumption as long as both the interpolation and the filtering is done separately in each window. In general, windows may help to contain problematic or erroneous data but the amount of data is smaller than for the non-windowed case. In particular, recalibration windows permit use of data in its raw form, and flow windows may allow us to take account of flow dependence of meter errors. But especially the last case does not give good results since some of the flow window contain only very few titrations (one or two). Note that for the use of flow windows a reverse-calibration is necessary (to remove the effect of recalibrations).

Table 5.3 shows maximum and mean square of additive errors $\epsilon_A$ before and after preprocessing. Note that this error alone is insufficient to judge the pre-

processing procedure; the preservation of the high frequency meter signal, as guranteed by the filtering and tested by the Fourier analysis above, is the other important criteria. It is therefore not appropriate to simply use a non-filtered linear interpolation of the titration signal, which would reduce all residuals to zero. Thus, a residual error which reflects problems in titrations, remains. However, this final error of the corrected data should be small.

The maximum error given in table 5.3 is the maximum $\epsilon_A$ in the investigated time period, the mean square error is the $l_2$-norm divided by the square root of the number of error values, i.e.

$$MSE = \sqrt{\frac{1}{m}\sum_{i=1}^{m}\epsilon_A^2(t_i)}. \tag{5.13}$$

From table 5.3 it is obvious that a pure reverse-calibration (column 6) leads to the best reduction in error compared to the data before preprocessing (column 3). Therefore this method was adopted.

### 5.3.3 Summary

Based on the assumptions that the chlorine titrations are more accurate than the meter data in the long term (low frequency) and that the meter data is more accurate in the short term dynamics (high frequency), a procedure for the correction of chlorine meter data was developed and tested in this section.

It uses multiplicative errors between titrations and meters, interpolates these errors after performing a reverse-calibration and filters the resulting signal before multiplication with the original (raw) data for correction.

## 5.4 Travel Times (Delay Times)

Travel time refers to the time the water will take or has taken to cover a certain part of the pipe rig starting at the inlet shed. Depending on which place along rig is to be reached and which (time dependent) flow is in the rig at that period

of time, the travel times will vary. In the rest of this thesis, the travel time variable will be referred to as $\tau$ and the travel time to a fixed point along the rig (normally one of the three sample points) as $T$, such that $T = \tau(x_0)$, if $x_0$ is that fixed point. Naturally, if the flow is constant, $T$ is constant.

The calculation of the travel time is not part of the preprocessing of data. The travel time is, however, a fundamental property of the investigated system and it appears in various guises throughout this thesis. The knowledge of this time is of particular importance for work related to chlorine decay (chapter 7), since there it is attempted to follow small aliquots of water on their journey through the pipe rig, but it also features in the particle counter work of chapter 6.

### 5.4.1 Calculation of the Travel Time

The travel time is calculated indirectly. It is

$$V = \int_0^T f(t)\,\mathrm{d}t \tag{5.14}$$

with $T$ = travel time, $V$ = total volume to be covered within $T$, $f(t)$ = time-dependent volumetric flow rate, $t$ = time. The zero value of time ($t = 0$) has to be normalised such that $t = 0$ when the considered aliquot of water starts at the inlet shed of the pipe rig.

In this case, the system is logged in discrete time and thus eq. (5.14) becomes

$$V = \sum_{i=1}^{n} f_i\,\Delta t_i \tag{5.15}$$

with

$$T = \sum_{i=1}^{n} \Delta t_i \tag{5.16}$$

The index $i$ of $f_i$ and $\Delta t_i$ indicates the time dependance of both variables. If the sampling time is uniform, eqs. (5.15) and (5.16) will be simplified by $\Delta t_i = \Delta t$ for all $0 \leq i \leq n$. The time dependence of $f_i$ (or $f(t)$) can normally not be simplified since step flow trials are considered, which implies that the aliquots of

water of which the travel time is desired may have started at low flow or may reach the considered sample point after the decrease of flow.

Equations (5.15) and (5.16) are used to calculate the travel time. Note that if $t = 0$ is chosen as suggested above, the travel time obtained in this way is the time it took the aliquot of water that is at the point of investigation at $t = T$ to reach that point from the inlet, starting at $t = 0$ from there. In other words, $T$ is the time it will take to reach the point of investigation if the parcel of water starts at the inlet at $t = 0$.

### 5.4.2 Possible Errors in Calculating the Travel Time

The calculation of the travel time in eq. (5.14) or (5.15) depends on the covered volume $V$ and the flow $f(t)$. The volume is calculated from length and diameters of the respective section of the pipe rig; the flow rate is the measured inlet flow minus extractions of meters and grab samples.

The basic (approximate) settings of these parameters as known from the construction of the pipe rig are given below.

- The pipe rig length is roughly 500 m between inlet and sample point 1, 400 m between sample points 1 and 2 and 400 m between sample points 2 and 3.

- The meter extraction flows are about 0.007 l/s at each sample point.

- The pipe rig consists mainly of 110 mm inside diameter pipe, but contains two sections of 3 m of 50 mm inside diameter pipes and two sections of 4 m of 25 mm inside diameter pipes (one section each between sample points 1 and 2 and sample points 2 and 3, respectively).

- The extraction of water due to grab sampling is not taken into account, it amounts to approximately 1.5 to 2 litre/day per sample point on routine days and can increase to a maximum of 10 litre/day per sample point on a day of extensive sampling (e.g. step flow trial day).

- The flow meter reading is directly logged and used as such without correction.

Since these data are frequently only approximately known (in particular the pipe rig length), they may cause errors in the calculation of the travel time. To check on the accuracy of the travel time calculation, the particle counter data as discussed in section 4.1.2.1 on page 70 is used. If we assume plug flow (turbulent flow conditions), peaks should be spaced in travel time intervals (travel time between sample points and inlet). Aligning these peaks will be used in the following as a means of fine tuning the parameters that effect travel time.

Errors in calculating the travel time may come about because of inaccuracies in any of the following:

- the pipe rig length,
- the flow rate of meter extractions,
- the inside diameter of pipes,
- taking into account the smaller diameter sections,
- the extraction of water due to sampling, or
- the meter reading of the flow meter.

Using the basic parameters, the travel time was calculated and the peaks of the particle counters were aligned. In doing so, however, significant errors in terms of the difference in time of the data peaks occurred. These errors lie in the range of approximately 20 minutes to 4 hours and 40 minutes. In column 3 of table 5.4 the alignment errors of several particle counter peaks are provided. These errors are the maximum distances between particle peaks of the sample points (including inlet, if appropriate). One example of particle counter data with the original parameter values is given in fig. 5.5. There one can see the particle counts of sample points 1, 2 and 3 aligned with the inlet counts for SFT 6. The alignment error in fig. 5.5 is 20 minutes. The same data are aligned perfectly using the final correction, see fig. 5.9.

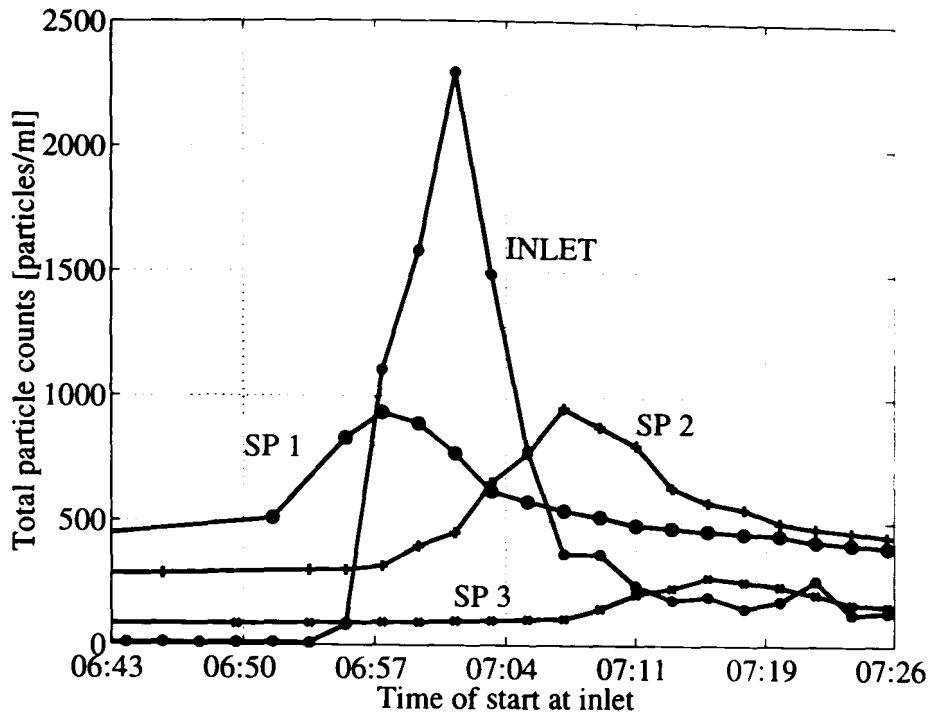


**Figure 5.5:** *Alignment of particle counts with original parameters for SFT 6 on 8.10.96. Inlet (INLET), sample point 1 (SP 1), sample point 2 (SP 2) and sample point 3 (SP 3) are shown. On the x-axis, the time of the start of the considered aliquot at the inlet is given. Same raw data as fig. 5.9.*

Note that due to the fact the flow rate is variable over the investigated time interval the difference between two data points (which is originally the sampling time) might expand or contract after alignment. For instance, an aliquot of water that has reached the point of investigation only a few minutes before the current time, may have started from the inlet an hour earlier than the aliquot that is currently at this point. Therefore, in this case of time extraction, the resolution of aligned data may become very coarse and a small error in the original data of, say, a few minutes can become several orders of magnitude larger.

### 5.4.3 Error Correction

Several avenues for correcting the error in the travel time were explored. The length of the pipe and the amount of extraction flow were varied initially, but the final correction was achieved with the help of the particle counter peaks. However, even the best correction procedure can not eradicate all errors. They may already be part of the original particle counter data which is used to corroborate the

**Table 5.4:** *Errors on abscissa after alignment of particle counts for original parameters, adjusted length and final correction.*

| Flow in l/s | Date | Alignment error, original parameters | Alignment error. adjusted length | Alignment error. final correction |
|---|---|---|---|---|
| 0.08 | 14.12.96 | not done | not done | 2 hr 15 min |
| 0.3 | 30.10.96 | 30-40 min | 0-15 min | not done |
| 0.45 | 17.12.96 | 2 hr 30 min | 1 hr 10 min | not done |
| 0.6 | 24.7.96 | 2 hr 40 min | 2 hr 20 min | 2 hr 20 min and 0 min |
| 0.6 | 1.8.96 | 30 min | 5 min | 0 min and 0 min |
| 0.6 | 6.8.96 | 2 hr 20 min | 10 min | 50 min and 0 min |
| 0.6 | 9.12.96 | 3 hr 10 min | not done | 15 min |
| 0.6 | 11.12.96 | not done | not done | 3 min |
| 0.9 | 21.8.96 | 4 hr 40 min | 1 hr 10 min | 1 hr 10 min and 5 min |
| 0.9 | 27.8.96 | 3 hr 30 min | 40 min | 5 min and 0 min |
| 0.9 | 8.10.96 | 4 hr 25 min and 20 min | 1 hr 15 min and 7 min | 45 min 0 min |
| 0.9 | 14.10.96 | 3 hr 30 min and 20 min | 50 min and 5 min | 25 min 0 min |
| 0.9 | 24.10.96 | not done | not done | 15 min |
| 0.9 | 30.10.96 | not done | not done | 2 min |

results and as is discussed above, already a small mistake of a few minutes may have a large impact on the alignment.

#### 5.4.3.1 Length Correction

Initially the length of the 110 mm diameter pipes were adjusted such that the distance between inlet and sample point 1 is reduced from 500 m to 450 m, and the distances between sample points 1 and 2, and sample points 2 and 3 are increased from 400 m to 450 m. Resulting alignment errors for a length corrected pipe rig are provided in column 4 of table 5.4.

With these corrections, the maximum error of approx. 4 hours 40 minutes was reduced to 1 hour 10 minutes. The worst alignment error found with this

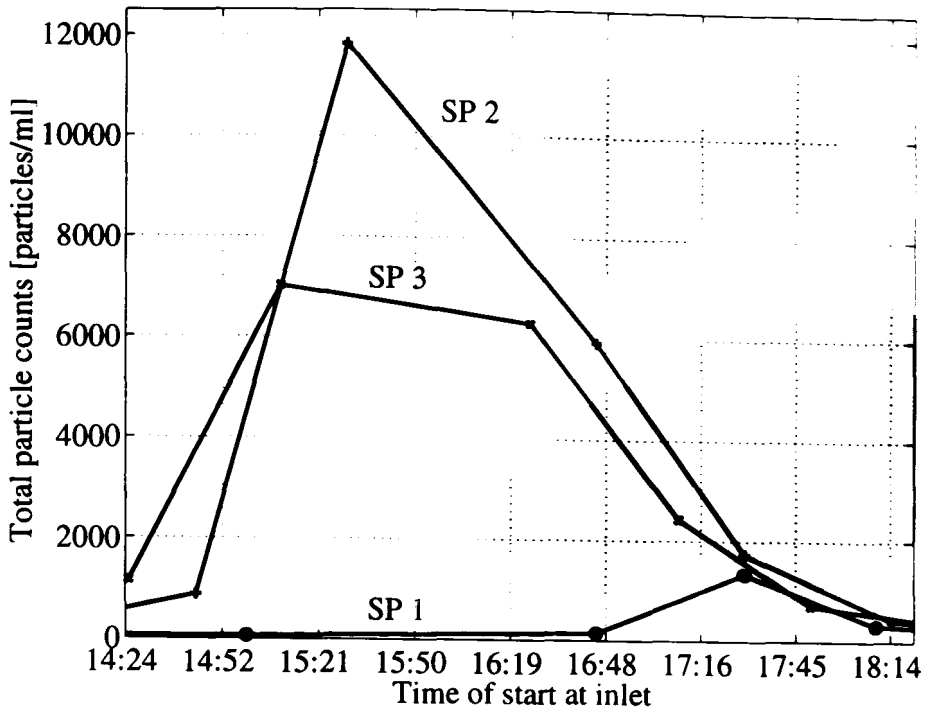


**Figure 5.6:** *Alignment of particle counts with final correction of parameters for SFT 1 on 25.7.96. Sample point 1 (SP 1), sample point 2 (SP 2) and sample point 3 (SP 3) are shown. On the x-axis, the time of the start of the considered aliquot at the inlet is given.*

procedure is 2 hours 20 minutes (from originally 2 hours 40 minutes). Frequently the error is reduced from errors between 30 minutes to 2 hours 20 minutes to below 15 minutes.

In summary, overall a significant improvement in alignment errors is found, however, with some remaining errors still rather large. As mentioned above, it is important to realise in this context, that a large time difference may not mean that there are many data points between the maxima, thus, the source of this error may be a small mistake in the original data (cf. section 5.4.3.3).

#### 5.4.3.2 Adjustment of the Meter Extraction Flows

An effect similar to the one described above could be obtained by changing the meter extraction flows. These meter extractions are measured manually with measuring cylinders. The measured meter extractions lie within the range 0.006 l/s to 0.009 l/s. Generally, it is assumed that the error on these measurements is below 10%. This was checked and validated by comparison with the flow meter

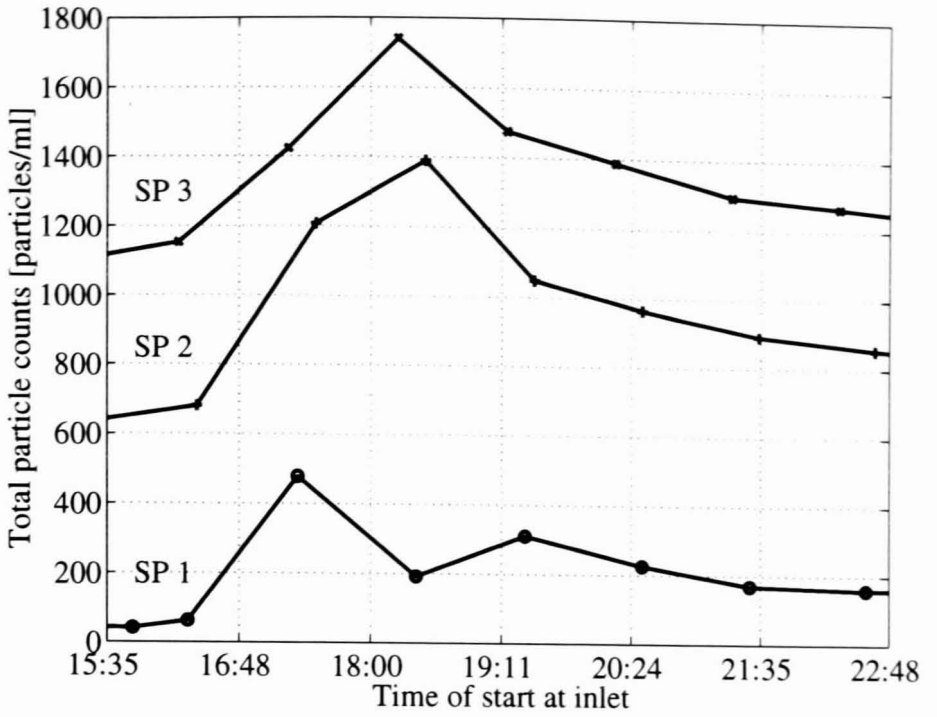


**Figure 5.7:** *Alignment of particle counts with final correction of parameters for SFT 4 on 22.8.96. Sample point 1 (SP 1), sample point 2 (SP 2) and sample point 3 (SP 3) are shown. On the x-axis, the time of the start of the considered aliquot at the inlet is given.*

readings. It is remarked that the low base line flow is 0.07 l/s.

Simulations were performed with meter extraction changes by 50%, 100% and 150%. However, only for significant changes in meter extraction flow (i.e. 100–150% of measured values, or from 0.007 l/s to 0.014 l/s or 0.0175 l/s, always per sample point) an alignment similarly good as in the case of length corrected results is achieved. For that reason it seems unlikely that the meter extraction flows have a big impact on the errors in the travel time.

#### 5.4.3.3 Final Correction

The final correction was achieved by taking the time distances between the peaks of particle counts at various step flow trials, calculating the required volume of pipe to fit such a time using eq. (5.15), and averaging the resulting volumes. The volume between the pipe rig inlet and sample point 1 is changed from $V_{01} = 4.09\ \mathrm{m}^3$ to $V_{01} = 3.9\ \mathrm{m}^3$, the volumes between sample points 1 and 2 or 2 and 3 from $V_{12} = V_{23} = 3.22\ \mathrm{m}^3$ to $V_{12} = V_{23} = 3.7\ \mathrm{m}^3$. This would reflect a change of

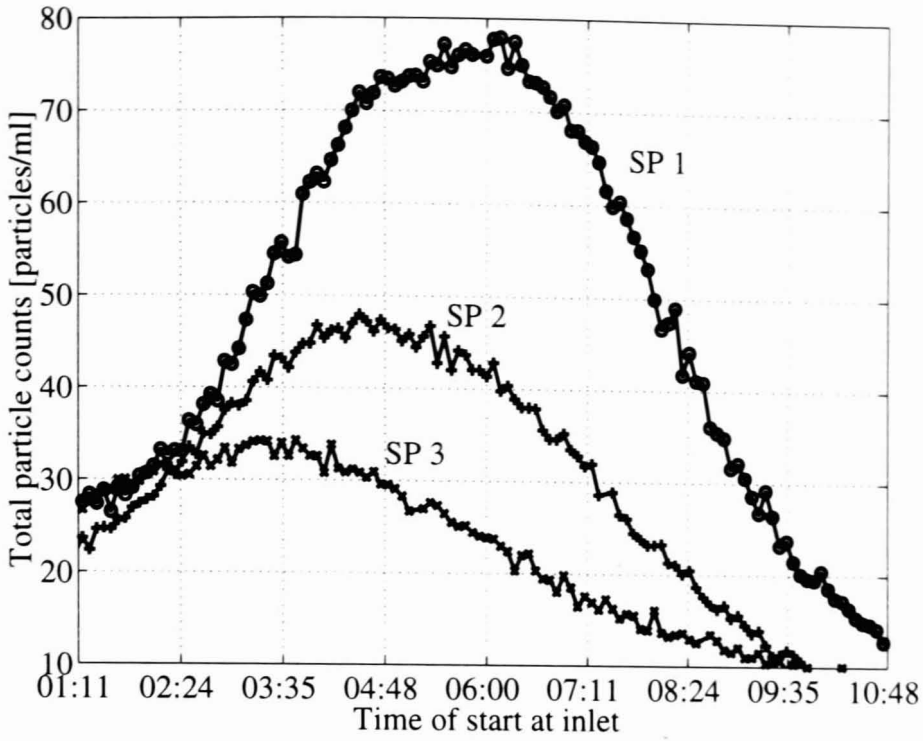


**Figure 5.8:** *Alignment of particle counts with final correction of parameters for 14.12.96 at the baseline flow of 0.08 l/s. Inlet (INLET), sample point 1 (SP 1), sample point 2 (SP 2) and sample point 3 (SP 3) are shown. On the x-axis, the time of the start of the considered aliquot at the inlet is given.*

length from 500 m to 410.36 m and from 400 m to 389.34 m, both for a uniform diameter of 110 mm throughout the whole rig. Note that the experimentally found travel times between peaks of the same sample points are necessarily not exactly equal (due to uncertainty in the data), however, if the travel times found through averaged volumes fit the data well, the considered volumes are likely to be close to the true ones.

Column 5 in table 5.4 provides error resulting from an alignment of particle counter data based on this final correction. Figures 5.6 to 5.10 show some of the particle counter after the final correction of the network parameters. Figure 5.11 depicts the same alignment for total chlorine meter data.

The alignment errors given in column 5 of table 5.4 are again the maximum distance between the peaks of sample points 1, 2 and 3 or inlet and sample point 1, 2 and 3. Since the calculation of the travel time is based on the distance between peaks it will not be surprising if a few of the alignment errors in column 5 of table 5.4 are zero. However, the fact that eleven of 21 alignment errors given in

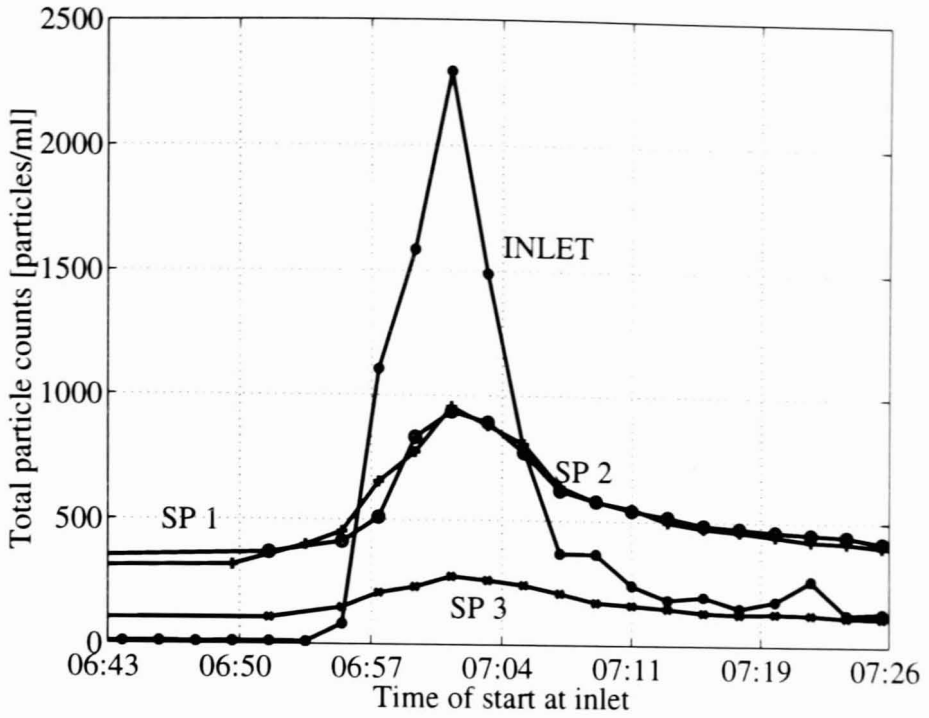


**Figure 5.9:** *Alignment of particle counts with final correction of parameters for SFT 6 on 8.10.96. Inlet (INLET), sample point 1 (SP 1), sample point 2 (SP 2) and sample point 3 (SP 3) are shown. On the x-axis, the time of the start of the considered aliquot at the inlet is given. Same raw data as fig. 5.5.*

the table are 5 min or less is very strong evidence that the considered volumes are correct.

Two of the worst cases in the table are presented in figures 5.6 and 5.7. These are peaks from SFT 1 on 24.7.96 and SFT 4 on 21.8.96, respectively. In both cases the alignment error corresponds to a distance of only one or two expanded sampling intervals. The expansion of the sampling time is due to the flow change. Some of the aliquots of water that reach the sample points will have started at the inlet before the start of the SFT. This results in a linearly changing travel time for a range of subsequent aliquots and therefore there are aliquots arriving at a sample point only 5 min after each other that started at the inlet with a time distance of more than an hour. This is exactly the case in figs. 5.6 and 5.7. Thus, an error in the data of only 5 to 10 min could be responsible for the alignment errors of these two cases. Such an error is likely if it is considered in addition that the slopes of the peaks of the counts align well, especially in fig. 5.6.

This explanation of the above discussed errors is adopted. However, the align-

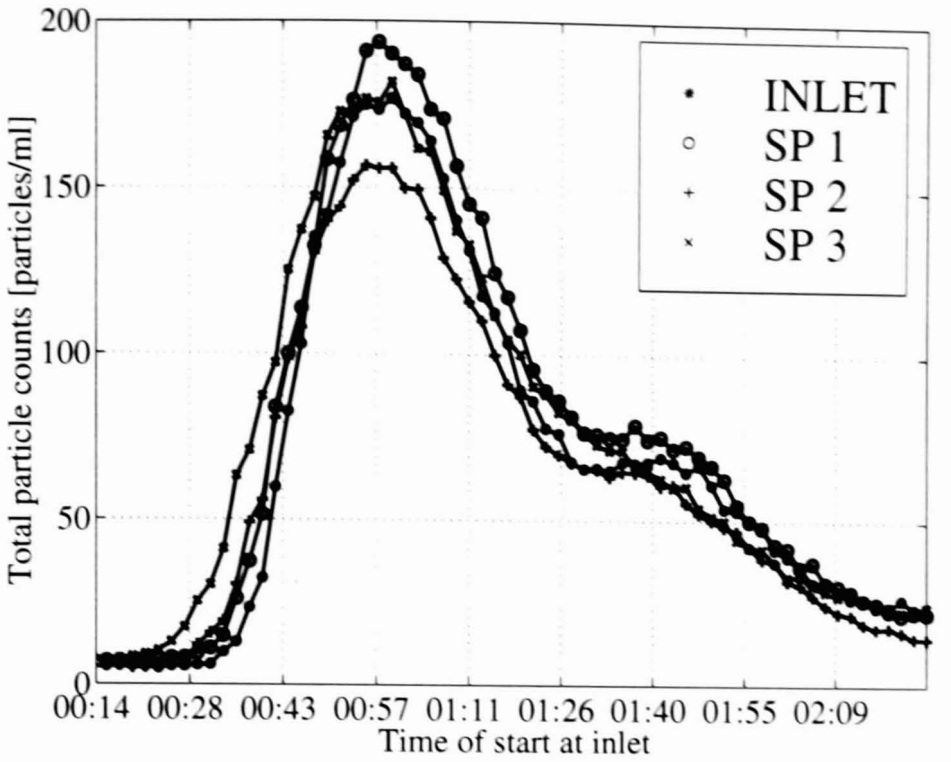


**Figure 5.10:** *Alignment of particle counts with final correction of parameters for part of SFT 8 on 11.12.96. Inlet (INLET), sample point 1 (SP 1), sample point 2 (SP 2) and sample point 3 (SP 3) are shown. On the x-axis, the time of the start of the considered aliquot at the inlet is given.*

ment error of 2 hours 15 minutes of the data of 14.12.96 given in fig. 5.8 must have a different reason. In this case many sampling points are within the interval of the alignment error and even the slopes do not align; there was, in addition, no flow change but a constant flow of 0.08 l/s. The total travel time between sample points 1 and 2 was approximately 27.5 hours, which means that the error in the calculation of the travel time is about 8.2 %. This is still an acceptable accuracy.

In the majority of cases the alignment is almost perfect, for instance in SFT 6 of 8.10.96 provided in fig. 5.9 and SFT 8 of 11.12.96 shown in fig. 5.10. The alignment errors are 0 minutes and 3 minutes, respectively. The raw data that is the basis of fig. 5.9 is the same as the raw data of fig. 5.5, where the original volume leads to an alignment error of 20 minutes.

The alignment error of total chlorine data is not included in the table. It is difficult to measure since the data contains no peaks but only edges, which are smoothed out due to chlorine decay. An example of total chlorine data is given in figure 5.11 that depicts the chlorine step trial of 26 November 1996 (the flow

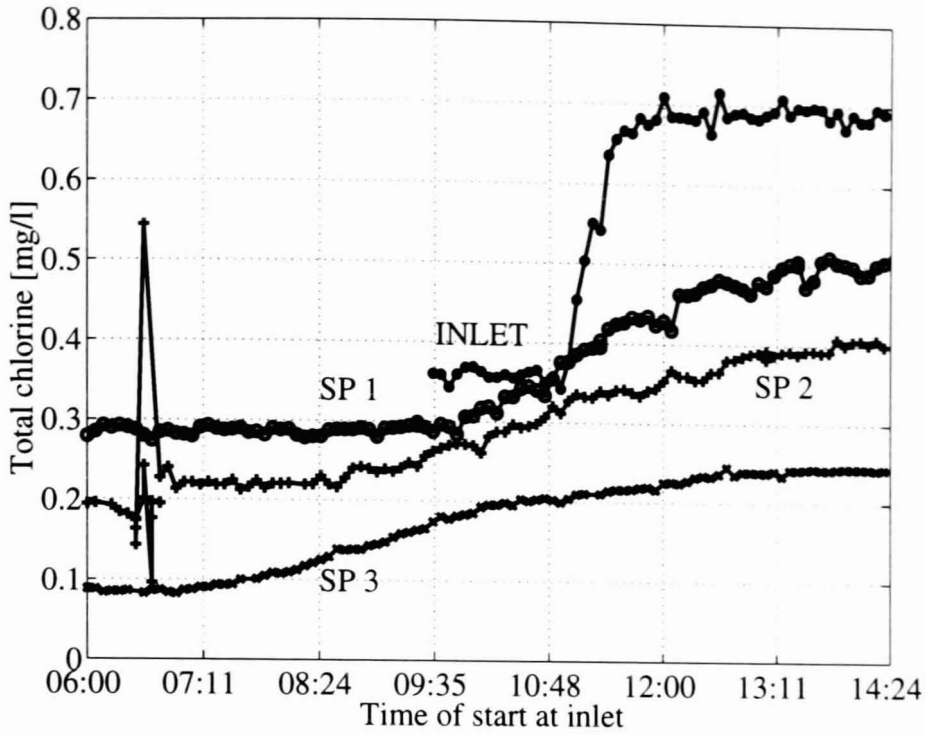


**Figure 5.11:** *Alignment of particle counts with final correction of parameters for the chlorine step trial on 26.11.96. Inlet (INLET), sample point 1 (SP 1), sample point 2 (SP 2) and sample point 3 (SP 3) are shown. On the x-axis, the time of the start of the considered aliquot at the inlet is given.*

regime is laminar with $f = 0.08$ l/s). It is seen from that graph that the edges agree reasonably well.

From the graphs provided in this section and table 5.4 it is concluded that the final correction of the volume of the pipe rig is very close to the actual volume of it. An error of up to 10 % or less than three sampling times is considered to be acceptable. Therefore, $V_{01} = 3.9$ m$^3$ and $V_{12} = V_{23} = 3.7$ m$^3$ are used for the calculation of the travel time.

## 5.5 Implementation

All calculations that are discussed in this chapter were implemented in Matlab as part of a Water Quality Toolbox (cf. appendix C).

The calculation of the particle ratios of section 5.2 is realised in `pcratio`. The switching of the particle counters into original order is realised in the Matlab files `wswitch` and `preproc`.

The chlorine related preprocessing of section 5.3 is realised in `clcalib`, which uses `residuals2`, `reverscal`, `resinterp`, `resfilter`, `wdezero`, `wtable1`, and `wxload` (all written by the author). The function `clcalib` is called in `preproc`.

The values for the appraisal of different chlorine preprocessing procedures as discussed in section 5.3.2 are calculated by `testclcalib`.

The calculation of the travel time as discussed above (section 5.4) is realised in `wttime` (using a conditional loop). An approximate travel time (for constant flow) is calculated by `wtraveltime`.

## 5.6 Conclusions

In this chapter various method for the preprocessing of water quality data of the pipe rig have been presented.

The ratios of particle counters that were switched (thus using the same water shortly after each other) were investigated. It was shown that the particle counts dependent on both, the respective counter sensor and the the predominat particle type in the sampled water. Furthermore, results indicated that the water in the whole of the pipe rig contained roughly the same particle type at most times of counter switchings and that the type of particles in water varied significantly over time. The counters could be switched back to their original order.

The correction of chlorine meter data was a significant part of the author's research work. A procedure based on the error between titrations and meter data was presented. The titrations are assumed to be more accurate, however, they are also sparse. Therefore a low frequency error function based on the ratios between these data sets was found, interpolated and filtered. This function was used to correct the meter data. Several ways of calculating the error function are possible, thus reasons for the choice made in this section were given.

Finally, the correct volume of the pipe rig was obtained such that the travel time can be calculated. Volumes of $V_{01} = 3.9\ \mathrm{m}^3$ between inlet and sample point 1 and $V_{12} = V_{23} = 3.7\ \mathrm{m}^3$ between sample points 1 and 2, and SP 2 and 3 were obtained.

The successful preprocessing of the data allows us now to investigate the data further for the modelling of particle counts (chapter 6) or the comparison of monochloramine models and the determination of decay coefficients (chapter 7).

# Chapter 6

# Modelling of Particle Counter Data

## 6.1 Introduction

### 6.1.1 Purpose

The purpose of this chapter is to develop a mathematical model which matches the particle counter data. This model should be able to predict such data under similar conditions and in addition, it should give some insight into the underlying phenomena that gave rise to it. In particular, since the step flow trials (SFTs) were intended to provide some information about the amount of biofilm present, it is desirable to try to obtain information on the biofilm thickness or the amount of material sheared off. In other words, one important question to be asked is "what can these data tell us about how the distribution system as a whole would behave in terms of suspended particles and shear-off potential of the biofilm?"

### 6.1.2 Particle Counters in the Test System

As described earlier, the system under investigation contains four particle counters located at the inlet and three sample points along the rig. The inlet particle counter was installed about half way through the 1996 experiment. Therefore, no inlet data are available for the first two SFTs (of 1996), and only sporadic hand-logged data for SFTs 3, 4 and 5. Beginning with SFT 6, the inlet particle counter was fully connected to the data acquisition system and thus the complete

data are available for processing.

All particle counters measure counts of particles per ml within certain size ranges, i.e. spheres of diameters 2–5 $\mu$m, 5–10 $\mu$m, 10–15 $\mu$m, 15–20 $\mu$m, 20–25 $\mu$m, 25–50 $\mu$m, 50–100 $\mu$m, and more than 100 $\mu$m. Therefore, two different types of particle counts can be considered, total counts (e.g. all particles with diameter $\geq$ 2 $\mu$m etc.), and difference counts (e.g. particles with 2 $\mu$m $\leq$ diameter $\leq$ 5 $\mu$m). In the following only total particle counts will be considered, mainly those of all particles (i.e. particles with diameter $\geq$ 2 $\mu$m).

### 6.1.3 Results

The main results of this work to date consist in a model that predicts the behaviour of total particle counts and provides the possibility to detect a profile of material sheared off from the biofilm over the rig and in terms of time. This profile will be termed apparent initial biofilm shedding profile (BSP). Obviously, after loss of biofilm material due to shedding the biofilm will not have the same magnitude anymore. Therefore, the profile will be a snapshot at the initial time instant.

## 6.2 Model Specifications

The behaviour of particle counts during step flow trials (SFTs) is described in detail in section 4.1. The observations of section 4.1.1 form the basis for and most important substance of what will be termed specifications in this section. These specifications are a set of requirements which any proposed particle counts model has to fulfil if it is to match the experimental results.

In the following, these specifications are presented.

1. The 'Slow Signal' — basic specifications.

   Type of signal:

   a) Particle counts increase slowly after a positive step change in flow ('Slow Increase').

b) This Slow Increase reaches a maximum value ('M.V.').

c) After reaching M.V. the particle counts decrease slowly to settle down at some value, generally higher than before step up ('Slow Decrease').

Shape of signal:

d) The shape of the Slow Increase varies considerably but on average counts increase.

e) The Slow Decrease decreases generally initially faster than later on.

Slow Increase, M.V. and Slow Decrease together form the 'Slow Signal'.

2. 'Slow Signal' — quantitatively:
   The M.V. is reached after approximately one travel time (the time it takes to reach the considered point from the inlet of the pipe rig).

3. 'Slow Signal' — extended specifications:

   a) At some step flow trials, the M.V. is reached after more than one travel time.

   b) Generally, specification 1e applies, however, occasionally the Slow Decrease degenerates to a straight line.

   c) The Slow Decrease is not always monotonic. Occasionally 'humps' appear within this part of the signal (cf. section 4.1.1).

4. There are extremely sharp and short lived peaks occurring during the Slow Increase period (specification 1). These peaks originate mainly from the inlet and Sample Point 1 (occasionally also from Sample Point 2 and 3) and propagate through the pipe rig ('Peaks').

5. Sometimes there occurs a sharp increase in particle counts at Sample Point 1 with step up and a sharp decrease at step down; this signal propagates through the rig ('Occasional Particle Step').

6. After step down in flow the total particle counts decrease slowly.

7. They settle down to a potentially different value than before SFT.

The nature of the data made it necessary to include several effects in these specifications that occur only occassionally (specifications 3 and 5). A basic model of particle counts during high flow will therefore include specifications 1, 2, and 5, while an extended model should take specifications 3 and 4 into account as well. Specification 2 and 3a have a special position in this context, since they already include some quantitative information. This is obtained from the data and thus is potentially inaccurate.

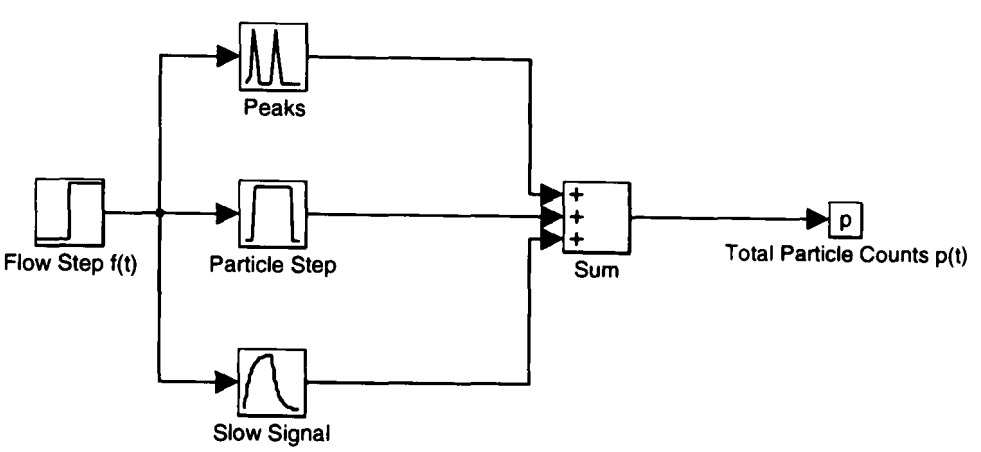


**Figure 6.1:** *Qualitative Simulink model of particle counter response to a step increase in flow*

Specifications 1–5 give rise to a qualitative model of the particle counter response to a step increase in flow as depicted in fig. 6.1. Thus, an input-output system with flow as input and (total) particle counts as output is considered here. Note that a different model is necessary for step down (which has to fit specifications 6 and 7). Thus, this is not a general model, it is only valid for this type of input signal (which is a nonlinear characteristic).

A quantitative model matching these specifications will be developed within this chapter.

## 6.3 Numerical Statistical Models

In a first attempt to generate a model for the particle counts response, a bottom-up approach is adopted. In this section, the randomised numerical implementation of several hypotheses of biofilm detachment will be explored. This model will be entirely numerical and based on statistical considerations. The starting point will be possible hypotheses to explain the total particle counter behaviour or the particle counter size distributions response to a SFT and show through simulation if these hypotheses match specifications 1 and 2 of total particle counts as given in section 6.2 or the observations of particle counter size distributions as described in section 4.2. The main aim of this section is, thus, to check the feasibility of suggested hypotheses for particle counts behaviour.

### 6.3.1 Total Particle Counts

As indicated above, this work will concentrate on the development of a basic total particle counts model covering the Slow Signal only (specifications 1 and 2 in section 6.2). Peaks are considered to be independent of the Slow Signal (cf. section 4.1.1). In addition, the focus lies on exploring the possibilities of basic models before the extended specifications (spec. 3) are incorporated.

To model the total particle counts the pipe rig is first simplified to a one-dimensional system, i.e the location along the pipe rig is characterised by only one variable: distance. This implies that only the net result of any one pipe circumference is considered and no variation according to the location on the circumference can be accounted for. This is a reasonable simplification since the current interest is into the behaviour of particles at a certain distance along the pipe rig and it is not attempted to distinguish according to position within a pipe cross-area. Furthermore, this simplification can be found frequently in the literature [115, 137, 122].

For this model the pipe rig is discretised into $n$ cells (for high accuracy, $n$ should be large) according to figure 6.2.

To each cell $i$ amounts of attached biomass $b_a(i)$ and suspended biomass $b_s(i)$

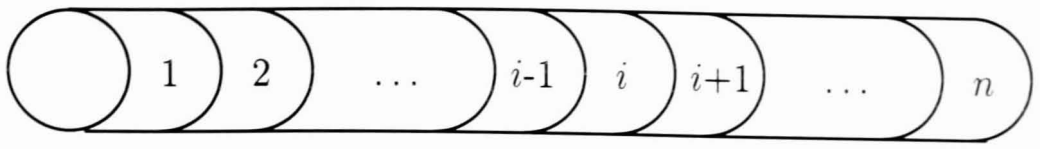


**Figure 6.2:** *Schematic showing the discretisation of the pipe rig into n cells*

are assigned. For the modelling of a particle counter response to a flow increase it is assumed, for simplicity, that initially (time $t = 0$) $b_s(i) = 0$ for all $i$.

To simulate what happens in the pipe rig the following algorithm was implemented. It includes different types of shear-off, which will be investigated in detail below.

Algorithm:

- decide randomly at each time instant if the biofilm in cell $i$, $b_a(i)$, is sheared off
- in case of shear-off, use one of the following types of shear-offs:

  1) all attached biomass in cell $i$ is entirely sheared-off

  2) a clump of predetermined or random size (smaller than $b_a(i)$) is sheared-off from $b_a(i)$

  3) a constant fraction (e.g. half) of the remaining biofilm $b_a(i)$ is sheared-off

  4) a decreasing fraction of the remaining biofilm $b_a(i)$ is sheared-off; the decrease of the fraction is proportional to the remaining biofilm $b_a(i)$

- propagate the suspended biomass $b_s(i)$ and add the sheared-off amount to it
- iterate the above procedure for all locations $i$ and for a number of time instants

In the following, simulation results of the different types of shear-off are discussed. In particular, biofilm might consist of 'streamers' [138, 80] which come off the wall as a whole. In this case the increased shear forces would then impact

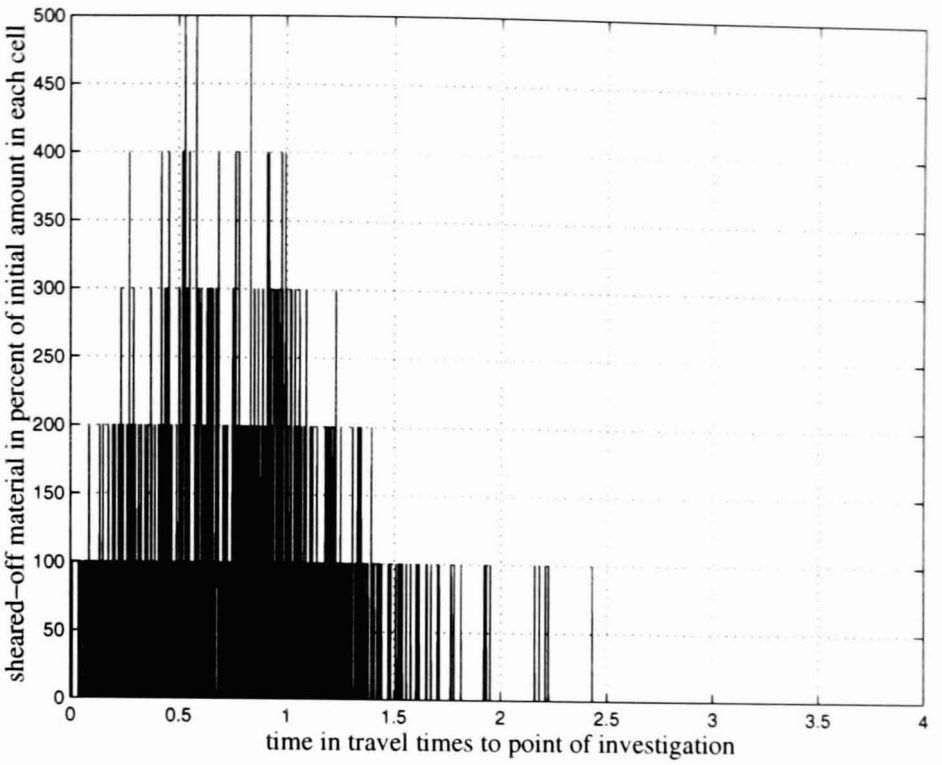


**Figure 6.3:** *Particle counts response to an increase in flow if all attached biomass in a cell is sheared-off. Probability of shedding is* 0.01.

in such a way that all the attached biofilm material at any point in the rig would come off at a random time during the high flow period (i.e. only once). Alternatively it could be thick biofilm of which particles of varying sizes are detached continuously.

#### 6.3.1.1 All attached biomass in a cell is sheared-off

The first assumption investigated in this section is a situation where only once during high flow do particles come off any given location along the pipe wall. Since a one-dimensional model is used this implies that on one whole circumference everything is shedded if shear-off occurs. This might be the case if the biofilm is patchy and consists merely of streamers.

Figs. 6.3 and 6.4 show simulation results with a probability of shedding of 1% (fig. 6.3) and 50% (fig. 6.4). On the y-axis the amount of sheared-off material is given, depicted as percentage of the material in each cell. The time given on the x-axis is normalised such that the travel time to the point along the rig which is under consideration is one. It is obvious that the case of 50% probability of

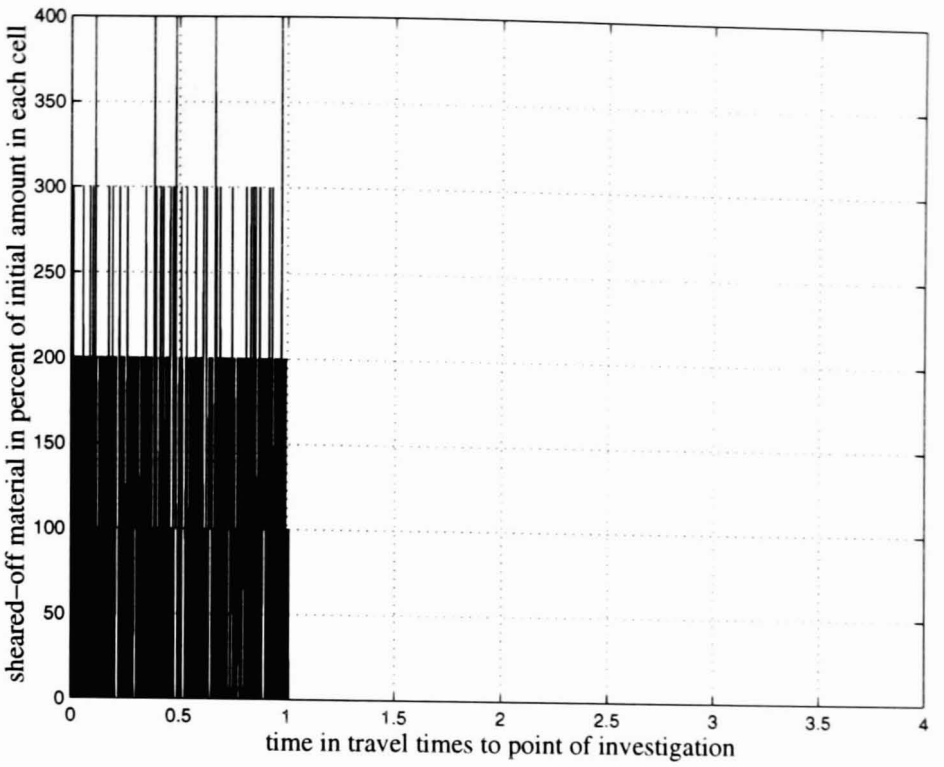


**Figure 6.4:** *Particle counts response to an increase in flow if all attached biomass in a cell is sheared-off. Probability of shedding is* 0.5.

shear-off does not fit specification 1, since simulation particle counts are high during one travel time and go to zero almost immediately after that. However, also fig. 6.3 does not match specifications 1a and 1d, since the simulation particle counts do not exhibit a clear trend. They fluctuate during one travel time, with values between zero and a few $b_a(i)$ occurring randomly throughout that period and slightly longer afterwards.

#### 6.3.1.2 Clumps of random size are sheared-off

The assumption that is investigated in this section is a situation where repetetive shedding of material (particles) is taking place. In the case considered here, the assumption of biofilm consisting predominately of streamers is still used, however, several streamers are possible along any given circumference of the pipe (i.e. any given location).

In fig. 6.5 results of a simulation with streamers of varying size are given. The random variation of streamer size has a constant mean. A simulation of multiple streamers of constant size equal to the mean of the randomly sized streamers

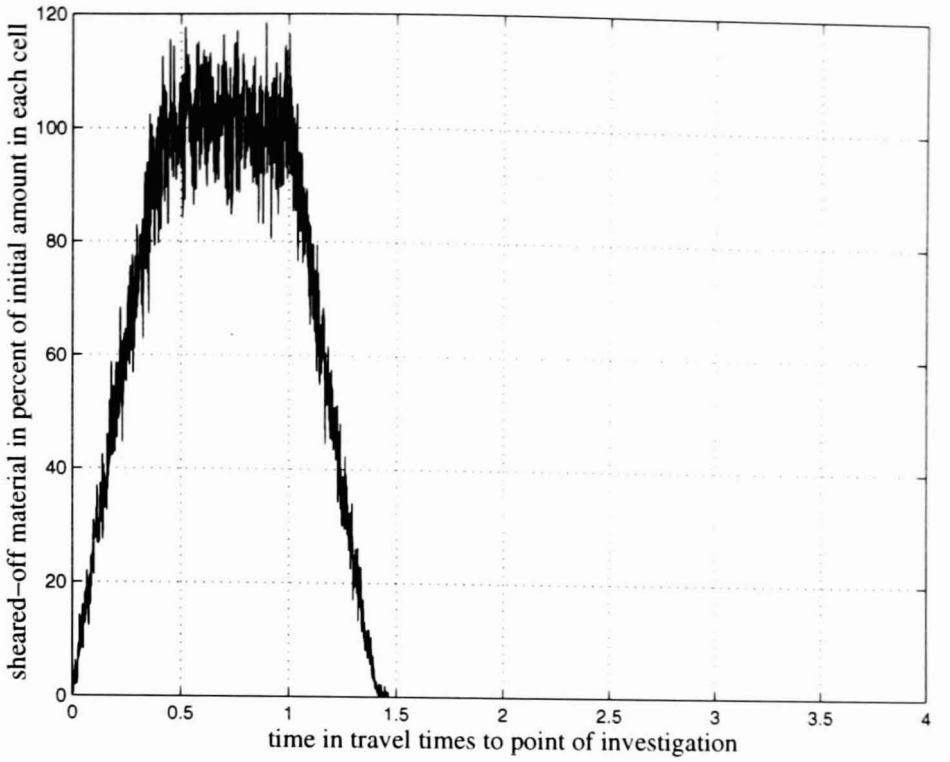


**Figure 6.5:** *Particle counts response to an increase in flow if clumps of random sizes are sheared-off. Probability of shedding is* 0.5.

gives the same trend. The figure shows (as above) the amount of sheared-off material on the y-axis (given as percentage of amount in each cell) and the time, normalised to one travel time, on the x-axis.

The results show, in principle, a linear increase of particle counts, a plateau and a linear decrease. The gradient of the increase and decrease depends on the average size of the streamers breaking off the wall. The shape of the response is very close to specifications 1a-1c, however, a plateau is not observed in the data. Still, if the parameters in the model are appropriate this plateau might be reduced to a single Maximum Value. However, specifications 1e, which requires a change of derivative through the decline, is not fulfilled given the straight line in the simulations and therefore this case can only be valid on the occasions when specification 3b (straight line decline) applies and does not qualify as a general model.

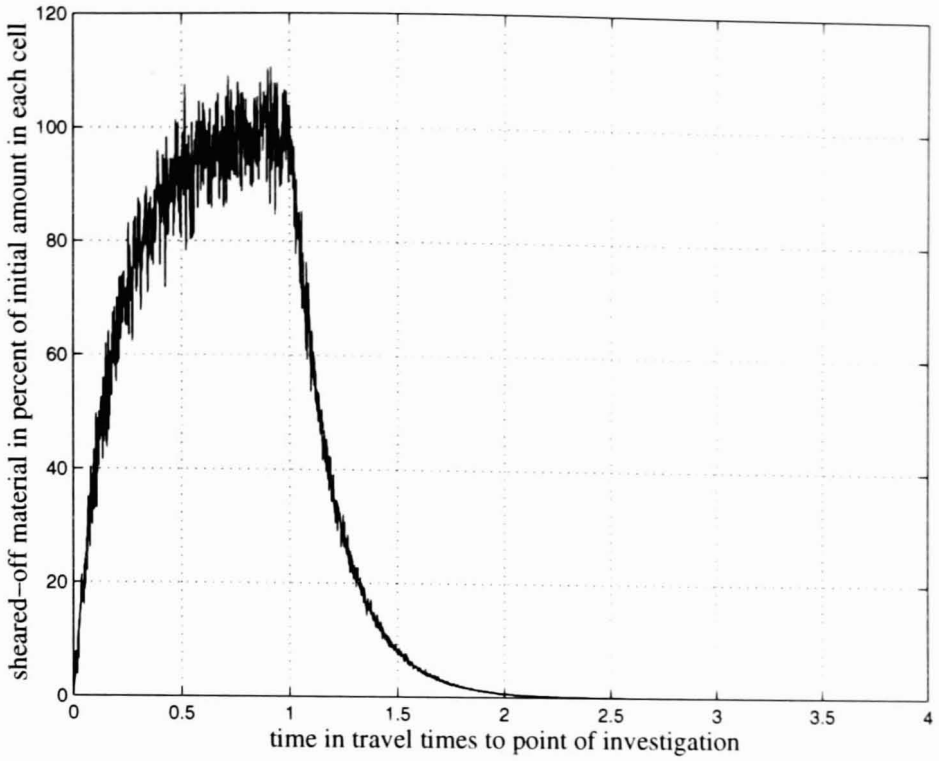


**Figure 6.6:** *Particle counts response to an increase in flow if 1% of the remaining biofilm is sheared-off. Probability of shedding is* 0.5.

#### 6.3.1.3 A constant fraction of the remaining biofilm is sheared-off

In this case a continuous shear-off is assumed. The amount of biofilm coming off the wall depends on the amount that is present on the wall. A constant fraction of biofilm is sheared-off if shedding takes place. This implies that the biofilm is 'rich', i.e. contains not just streamers but consists of a layer of cells with strong attachment to the wall and the capacity to supply the bulk water repeatedly with particles. In the example given in fig. 6.6 1% of the biofilm remaining on the wall is sheared-off if shedding takes place. Shear-off occurs in any one cell with a probability of 0.5. This figure shows the amount of sheared-off material on the y-axis (given as percentage of amount in each cell) and the time, normalised to one travel time, on the x-axis.

The simulation results presented in fig. 6.6 show a behaviour which follows an exponential function. An Increase, Maximum Value and Decrease is observed as required by specifications 1a–1c. In addition, specification 2 (Maximum Value after one travel time) is achieved, the changes in derivative as required in specification 1e are attained and the trend of specification 1d is present (the variability

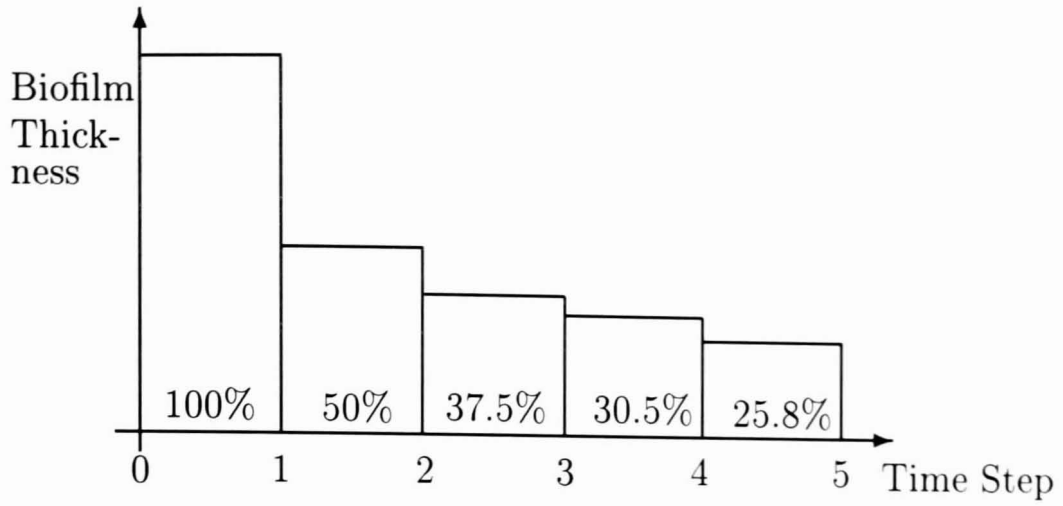


**Figure 6.7:** *Illustration for the subsequent remaining amounts of biofilm with a decreasing fraction (double-exponential) shear-off. Always 50 % of the remaining fraction is sheared-off.*

is readily introduced by assuming a variation over length of amount of biofilm present on the wall). Thus, this model fulfils all basic specifications of section 6.2.

#### 6.3.1.4 A decreasing fraction of the remaining biofilm is sheared-off

As opposed to section 6.3.1.3 in this case the amount of sheared-off material does not only depend on how much biofilm was left in a cell (just before shear-off) but also on the amount of biofilm that was in each cell before the process of shedding due to high flow started. In other words, the amount which is sheared-off is a fraction of a fraction, e.g. in the case of fig. 6.8, 50% of the percentage of initial biofilm which was left on the surface before shedding. I.e. if 50% of the initial biofilm remains, 25% of this remaining biofilm is sheared-off. This type of shear-off is illustrated in fig. 6.7.

Results of this simulation are given in fig. 6.8. Axes are the same as on the previous four figures, i.e. sheared-off material in the bulk liquid at the point of investigation is given on the y-axis and time on the x-axis. In fig. 6.8 it is seen that specifications 1 and 2 are fulfilled in much the same way as in the case given in section 6.3.1.3, however, due to the fact that a decreasing fraction of the remaining biofilm is sheared-off, the function involved here is of the type $f(t) = \exp(\exp(t))$.

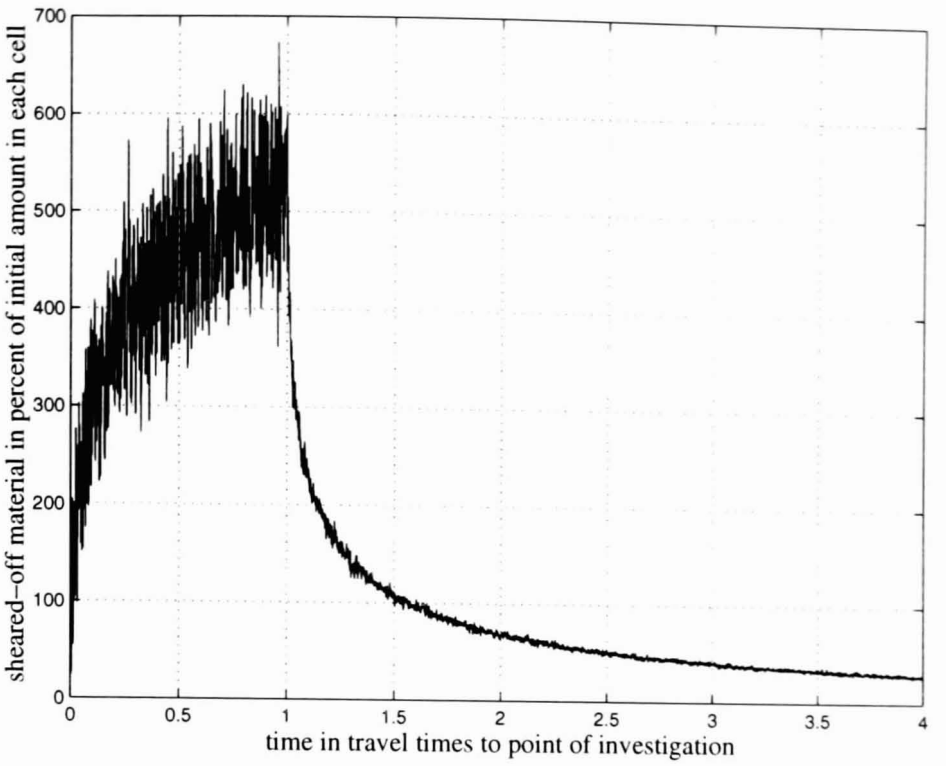


**Figure 6.8:** *Particle counts response to an increase in flow if a decreasing fraction of the remaining biofilm is sheared-off. Probability of shedding is* 0.5.

Thus, it is not possible to say for certain, what the exact shape of the increase/decrease is. It will be necessary to make sensible assumptions to obtain a usable model.

### 6.3.2 Particle Counter Size Distributions

The numerical statistical models of the particle counter size distributions presented in this section are based on the total particle counts simulation in which a constant fraction of the remaining biofilm is sheared-off (section 6.3.1.3). Three size ranges are simulated, they are labeled as 2–5 $\mu$m, 5–10 $\mu$m and 10–15 $\mu$m in figs. 6.9 and 6.10.

Percentages of total particle counts are assigned to these size ranges. Particles originating from the bulk liquid and attached particles are distinguished. The suspended particles occur in the percentages 85 % for 2–5 $\mu$m, 10 % for 5–10 $\mu$m and 2 % for 10–15 $\mu$m, the attached particles have a size distribution of 55 %, 27 % and 6 %. Thus, to match observations, a smaller fraction of small particles and a larger percentage of larger particles is assigned to attached particles. The

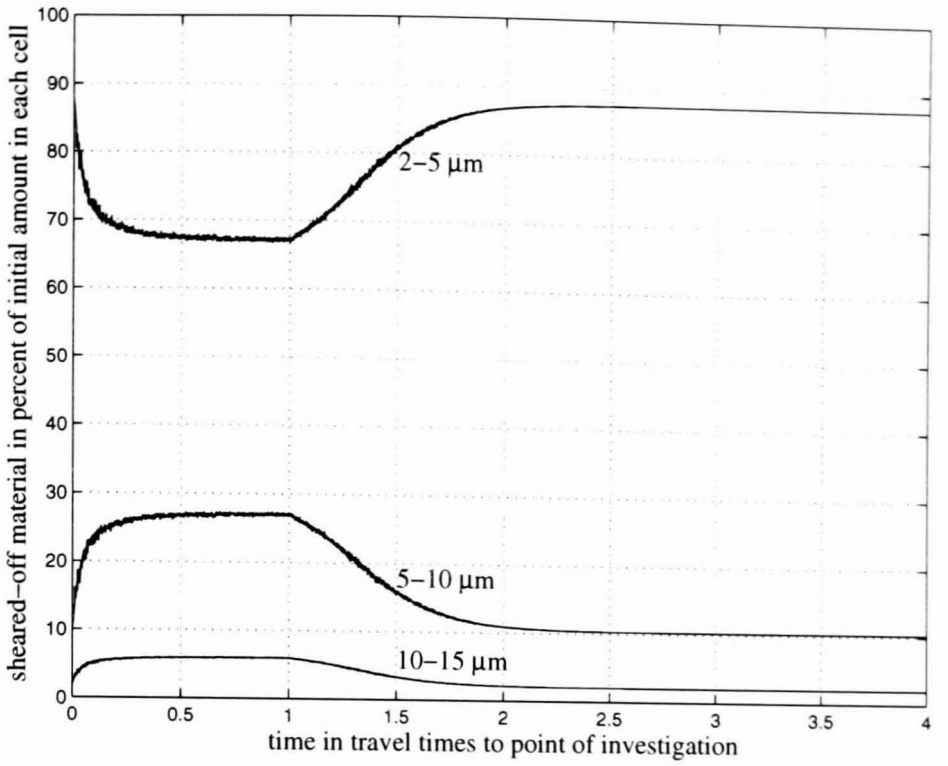


**Figure 6.9:** *Particle counter size distributions during high flow if only a constant fraction of the remaining biofilm is sheared-off. Three size ranges are marked as representing 2–5 µm, 5–10 µm and 10–15 µm. Probability of shedding is* 0.5.

ratio between material in a cell in the bulk liquid and attached material in a cell is chosen to be 1:5. Note that these numbers are not necessarily identical to actual percentages occuring in the investigated system.

The yield of material from the pipe walls behaves in the same way as the total particle counts of section 6.3.1.3, i.e. the shear-off from the whole of the biofilm is exponential. Simulation results for this case are given in fig. 6.9. This figure shows a very similar response to the total particle counts, i.e. the size ranges start off at the percentages for suspended bacteria and approach within one travel time the attached bacteria percentages via an exponetial function. After one travel time the percentages increase or decrease (as appropriate) with the suspended bacteria percentages as assymptotes. This is clearly not what is seen in the size distributions (see section 4.2 on page 74 or appendix A). It is not expected to see such a pronounced change of percentages towards suspended bacteria levels within the high flow period.

Therefore it is necessary to include the final value in the numerical statistical model of the particle counter size distribution. The final value (specification 1c)

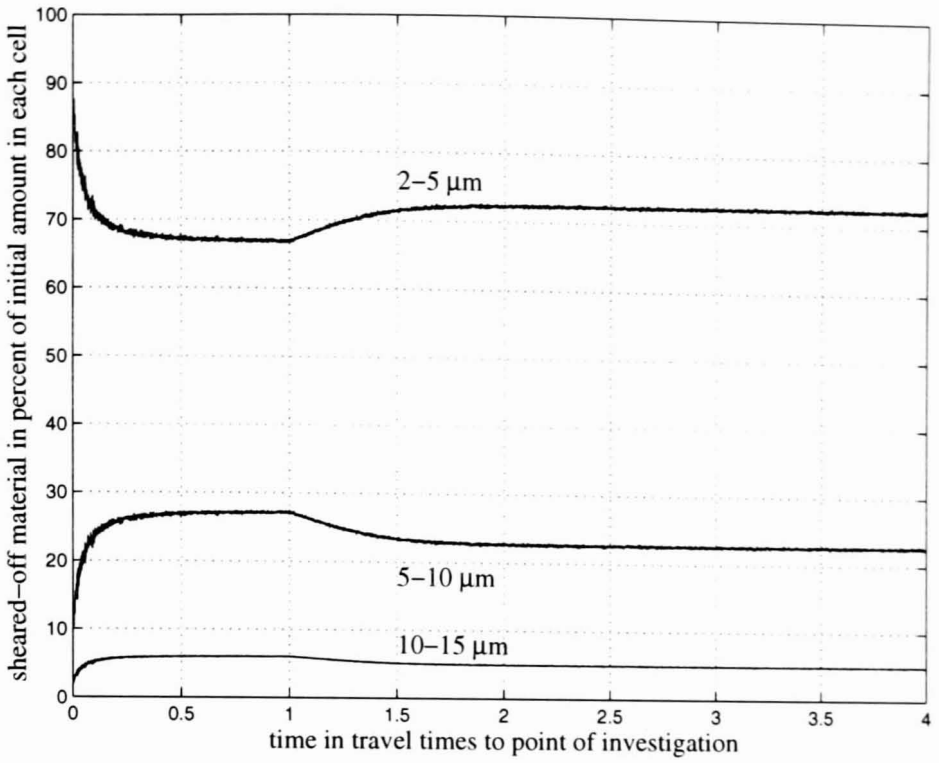


**Figure 6.10:** *Particle counter size distrbutions during high flow. Shear-off consists of a constant fraction of the remaining biofilm plus a constant shear-off. Three size ranges are marked as representing 2–5 µm, 5–10 µm and 10–15 µm. Probability of shedding is* 0.5.

implies a constant feed of particles from the pipe walls. This value is neglected in section 6.3.1, because there the focus was on mimicking the general shape of the signal for which the final value has limited significance. In this case, however, the constant feed of particles is relevant. For the simulation shown in fig. 6.10, a constant feed of particles from the pipe wall was introduced. To achieve this it is necessary to split the biofilm into two layers, one layer that experiences exponential shear-off, and a second layer that is a constant source of particles. This second layer has to be large compared to the amount of sheared-off material, otherwise it will be removed completely. In the case of fig. 6.10 it is chosen to be 10 times larger than the first layer of biofilm (the layer of exponetial shear-off).

The simulation results depicted in fig. 6.10 match specification 1c better than fig. 6.9. The percentages remain close to the values for attached biofilm. To achieve certainty about the underlying processes, it would be necessary to discuss more cases to obtain a better appreciation of what effects the particle counter size distributions. However, the focus of this work is on the total particle counts

and therefore only this brief discussion of size distributions is included.

### 6.3.3 Conclusions

The numerical simulation of statistical models for total particle counts and particle counter size distributions gives valuable insight into several possible underlying processes. This helps in the structure determination and the interpretation of the related parametric models.

## 6.4 Parametric Model of the Total Particle Response

The models of section 6.3.1 explored various hypotheses of how biofilm detachment may come about. These models are, however, difficult to fit to data. A parametric model is better suited for that purpose. In addition, the parametric approach allows the application of numerous mathematical methods for the development and usage of a model. The parametric model anticipated in this work will express the average amount of particles shedded from the pipe walls (i.e. no random variation as in section 6.3.1).

The standard approach to parametric modelling from data (system identification) requires the determination of the model structure before the parameters of the model can be fitted to any (noisy) data produced by the modelled system. From data alone, however, it is impossible to obtain the complete model structure. But it is possible to obtain some information about it, since the structure is reflected in the shape (e.g. exponential etc.) of the signal produced by the investigated system.

Possible approaches to obtain models of systems with unknown or partially known structure are on the one hand 'Black Box Models' and on the other hand semi-physical modelling or 'Grey Box Models'. In this work a novel flavour of 'Grey Box Models' will be used which combines information gained from data (the specifications of section 6.2) and assumptions based on physical or biolog-

ical knowledge of the system. Although there are many examples of 'Grey Box Models' in the literature, this particular approach is a contribution of the author. This idea was first applied to a far simpler system [95, 94], however, in most details it is used there in a way different from the work presented here.

The numerical statistical models of section 6.3.1 help to identify the mathematical structure of the parametric model (i.e. to come up with appropriate assumptions) because they explore mainly the shape of the data.

The model developed in this section is valid only for a specific input signal. The applicability of the structure is limited to step flow inputs and, in addition, the parameters depend on the magnitude of this step.

### 6.4.1 Assumptions

Assumptions complement the specifications of section 6.2 on page 124, they help to establish a mathematical structure of the model. As already discussed in section 6.2 and section 4.1.1 on page 68, three different particle counter signals originating from the step increase in flow will be considered (see fig. 6.1 on page 126). These three signals are assumed to be independent. Amongst those signals the ones described in specifications 4 and 5 are considered to have the least information about the state of the system. Therefore, they are termed 'face-value' signals in this work.

#### 6.4.1.1 Peaks

Since the Peaks (spec. 4) are very short lived and the lowest possible sampling time is 2 min, it is impossible to fit a model with any accuracy to them (not enough data points). In addition, they are assumed to be independent of (i.e. of different origin than) the Slow Signal. Therefore, in general the Peaks are removed from the particle counter response to a step increase of flow before any modelling takes place. The process of removing peaks (given in section 6.5.1.2) can be improved by assumptions on the shape (or structure) of these peaks. It is, thus, assumed in some of the work on automatic peak detect and erase (section 6.5.1.2) that peaks

have the same structure as the Slow Signal discussed in section 6.4.1.3. The only difference are the parameter values, in particular the value of the time constant governing the decline of the signal.

#### 6.4.1.2 Occasional Particle Step

The Occasional Particle Step (spec. 5) is assumed to be very close to a pure step signal occurring with flow increase at sample point 1 until the flow is decreased again. It has only face value since a pure step does not give any time information. This assumption implies that particles are released at a near constant rate at this location. It cannot be acertained from the data alone if this rate is constant, i.e. if this signal is a pure step. For, while it is straightforward to read the magnitude of step down in particles at the end of a SFT, it is difficult to determine for certain what magnitude the step increase at the start of the SFT has, since this signal is combined with a peak occurring at that point in time. However, the assumption of a pure step can be corroborated with the help of the input signal as is seen in the discussion, section 6.4.1.7.

#### 6.4.1.3 Basic Model of the Slow Signal

The most interesting part of the particle counter response to a flow step is the Slow Increase, Maximum Value and Decrease (the Slow Signal, specs. 1 and 2). It is the only part of the particle counter response to a step increase in flow that is included in the model which will be developed below. In other words, the 'face-value' signals will not be included in the model. This Slow Signal is believed to contain information about the biofilm on the pipe walls.

The most important hypothesis introduced in this section is the existence of a local particle shear-off density (i.e. in $\frac{\text{particles}}{\text{ml}}$ per metre) which is decreasing in magnitude over time as response to a flow increase. This concept is the cornerstone of the model developed in section 6.4.2 and, as can be seen from section 6.4.4, gives rise to a model which fulfils specifications 1 and 2. This concept was foreshadowed in section 6.3.1 where the pipe rig is split up into cells and the

shear-off behaviour is subsequently varied. This assumption was first mentioned by the author *et al.* in [98]. From this the first assumption is obtained.

**Assumption 1** *There exists a local particle shear-off density $p_d(x,t)$ for $t > 0$ with units $\frac{\text{particles}}{\text{ml}\cdot\text{m}}$ which is decreasing in magnitude over time. The distance along the rig is described by the variable $x$, time is given by $t$. The shear-off starts with the flow increase, thus $p_d(x,t) = 0$ for $t < 0$.*

Please note that it is possible to assume the existance of an arbitrary local particle shear-off density (not necessarily decreasing) without loss of generality. The only limitation is that the shear-off density gives the total shear-off of one complete circumference, however, any type of shedding can be expressed in that framework. Furthermore, if the data is normalised to a zero level before the step flow trial, the assumption $p_d(x,t) = 0$ for $t < 0$ will cover also a constant shear-off level before the biofilm.

In a next step, it is assumed that the impact of biofilm can be characterised in a meaningful way by one variable. The magnitude of this variable will depend on the location along the rig. It is hopefully closely related to the biofilm thickness, however, since only information about the suspended particles is available, the only direct information that can be derived from that is on shedding (rather than on what remains on the wall).

To take this assumption further, it is postulated that this biofilm shedding profile does not influence the dynamics of the shear-off, but only the start (and the end) of the particle density function. That makes it possible to separate time dependent and distance dependent effects. Then, the second assumption is obtained.

**Assumption 2** *The scalar valued function $b(x)$ is a meaningful parameter for the description of the amount of material initially sheared-off the biofilm and it does not influence the dynamics of subsequent shear-off. The shear-off function $s(t)$ is, thus, independent of the distance $x$ Therefore, the local particle density*

*function is now given by*

$$p_d(x,t) = b(x) \cdot s(t), \text{ for } t > 0. \tag{6.1}$$

Assuming the feasibility of a local shear-off density is still insufficient for a full model. An additional assumption on the shape of the local shear-off density $p_d(x,t)$ needs to be made. As will be shown in section 6.5 and 6.6, assuming the shape of the local time-dependent shear-off function $s(t)$ is sufficient to obtain a meaningful model. In the following, an exponential decay as investigated in section 6.3.1.3 is adopted. It is of the form

$$s(t) = k_1(f)\exp(-at) + k_2(f), \text{ for } t > 0. \tag{6.2}$$

A final value is included via $k_2(f)$ in this case. Eq. (6.2) is only one of the possible candidates for the local shear-off function $s(t)$. It fulfils, however, all of specifications 1 and 2 (in particular spec. 1e), as will be seen in section 6.4.4 or was already seen in section 6.3.1.3, and has some other arguments in its favour. This choice of $s(t)$ fits the specifications very well, occurs frequently in nature (e.g. capacitor discharge, biological growth processes) and offers distinctive advantages in mathematical handling over, e.g. the corresponding function in case 4 of the numerical statistical models (section 6.3.1.4). Note that, although the structure of eq. (6.2) is valid for any step flow input, the parameters $k_1(f)$, $k_2(f)$ depend on the magnitude of the flow step. Thus, the last assumption is obtained.

**Assumption 3** *The local time-dependent shear-off function $s(t)$ follows an exponential decay. Therefore, the local particle density $p_d(x,t)$ is of the form*

$$p_d(x,t) = b(x) \cdot \left(k_1(f)\exp(-at) + k_2(f)\right), \text{ for } t > 0. \tag{6.3}$$

*Here $a$, $k_1(f)$ and $k_2(f)$ are positive parameters, $t$ is the time variable, $x$ is distance and $b(x)$ is the function describing the amount of material that is initially sheared-off the biofilm, as introduced in assumption 2. The parameter $k_1(f)$ and*

*$k_2(f)$ depend on the magnitude of the input flow step.*

#### 6.4.1.4 Extended Model of the Slow Signal

The assumptions of the previous section cover the basic specifications, specs. 1 and 2 of section 6.2, but do not necessarily fulfil specification 3. An extended model is required for that purpose.

In what follows, possible extensions of the basic model are given. All the cases given above cover all requirements of specification 3, but not all of them lead to a usable model. Note that specification 3b, a straight line as the decreasing part of the slow signal, is possible even within the framework of all three assumptions of the previous section, since an exponential decay may look like a straight line in data if the time constant of the decay is large enough (and the collected data window covers only the beginning of the exponential signal).

1. If assumptions 2 and 3 are discarded only the general particle shear-off density $p_d(x,t)$ remains. This case can include all the extended specifications. However, without more information about this density this abstract expression is to general to obtain a usable model.

2. A feasible solution would be to replace the dynamic shear-off function $s(t)$ by a non-exponential or higher order exponential function. In fact, this function might take any form. The input particle data could be exploited to obtain it. This would imply that only assumption 3 has to be modified.

   If a shear-off function is used which reaches its maximum value at $t > 0$ (with $e^{-t}$ the maximum is reached at the initial time instant $t = 0$), the maximum is reached after more than one travel time, similar to the 'humps' observed in some of the data.

   This approach would essentially be within the framework of the basic model. in particular the independence of $s(t)$ from $x$ is maintained.

3. If the local shear-off function depends in general on the distance from the inlet, i.e. it is a function of both $x$ and $t$: $s^*(x,t)$, this case is essentially

the same as case 1 of this section. The distinction between $b(x)$ and $s^*(x,t)$ (both depend on $x$) is more or less philosophical and is not observable from the particle counter data.

This case is, however, applicable in model development if the shear-off function is uniform within each section of the pipe rig. Since there is one particle counter after each section, this would merely imply a loss of redundancy in the data. In this case there would be three local shear-off functions $s_{\text{sec.}1}(t)$, $s_{\text{sec.}2}(t)$ and $s_{\text{sec.}3}(t)$.

4. Another feasible approach is to view the 'humps' discussed in sections 4.1.1 and 6.2 as delayed shear-off. This would be seen in the data as an increase of particles after flow increase which follows the same pattern as the Slow Signal. The origin of this could be biofilm which resists the shear forces for some time and only late within the step trial is actually detached from the walls. This effect could cover both 'humps' or a maximum value after one travel time.

   The particle density changes to

$$p_d(x,t) = b_1(x) \cdot s_1(t) + b_2(x) \cdot s_2(t - t_d) \tag{6.4}$$

with $s_1(t) = 0$ for $t < 0$, $s_2(t) = 0$ for $t < 0$ and $t_d > 0$ an arbitrary delay time. Obviously, several delayed shear-off events are possible.

If both shear-off events in eq. (6.4) originate from the same "type" of biofilm, the two shear-off functions $s_1(t)$ and $s_2(t)$ should be the same or very similar. In particular, the time constant of the decay should be the same. This seems to be the case at SFT 8 (fig. 4.2 on page 69 or fig. A.8 on page 240), where the decay of the delayed effect at sample point 3 is within the same order of magnitude as the Slow Signal.

On the other hand, if loose deposits that are lifted into suspension substantially later than the start of the SFT are investigated, the time constant of $s_2(t)$ should be close to the decay time constant of the initial peaks.

This could be the case in SFT 3 (fig. A.3 on page 235), where the origin of the 'humps' in all sample points would be loose deposits at some point in section 1 (between inlet and sample point 1). This case is obviously not a true part of the Slow Signal anymore, thus the resulting 'humps' should be treated like the other peaks.

Although a number of feasible suggestions for an extended model of the Slow Signal were put forward in this section, none of them is easy to implement. Later on this thesis will be restricted to modelling the basic specification. The effects that are captured in the extended specifications do, however, generate problems during the process of parameter identification for the basic model. Therefore, a theory concerning the origin of these effects has to be adopted to be able to choose a sensible data window for parameter identification.

#### 6.4.1.5 Inlet Particle Counter Data

It is assumed that the spikes in the inlet particle counter signal described in section 4.1.2.4 on page 73 are an artefact generated by the counter aperture, since they do not propagate through to other sample points. The underlying (additive) signal is therefore the part of the inlet counter data which is relevant for this work. The inlet counter is located only a few metres downstream of the inlet valve and pump which mark the beginning of the pipe rig, $x = 0$. Due to the short length of pipe, the signal $p(t)$ that is observed by this counter is very close to the pure local particle density $p_d(x, t)$. Further down the pipe rig the signal $p(t)$ is convoluted and therefore significantly different to $p_d(x, t)$ (cf. section 6.4.2). This similarity is very useful for validation purposes, see the discussion in section 6.4.1.7.

#### 6.4.1.6 Model for Particle Counts After Flow Decrease

It is assumed that the local shear-off as described above ceases with decrease of flow and merely the propagation of already suspended particles is responsible for higher counts in the pipe rig (cf. section 4.1.2.5 on page 74). A negative slope model based on this assumption is developed in section 6.4.3.

#### 6.4.1.7 Discussion of Assumptions

The distinction between basic and extended model could be due to the "type" or quality of biofilm on the pipe walls. The first step flow trials of each regime (SFT 1, 4, 6) fit the basic model best, whereas the last step flow trials (SFT 10, 11, 12) fit it worst. Thus, it is possible to distinguish between times of thick and uniformly structured biofilm ("rich biofilm"), when the basic model fits well, and times of thin and patchy biofilm ("lean biofilm"), where the extended model is necessary. For a "lean biofilm" scenario it is expected that the material comes off in patches, which would explain the "humps" observed in the signal, while the shear-off function $s(t)$ is fairly flat. This difference in biofilm "type" may stem from the repeated flow increases and the introduction of monochloramine.

This shear-off function might be deduced from the inlet particle counter response. As mentioned earlier, the inlet particle counter is about 5 m downstream of the inlet valve, which marks the beginning of the pipe rig. Because this section is basically as small as a cell in section 6.3.1 the signal observed at the inlet counter is almost like a pure example of the shear-off function $s(t)$. The signal is, obviously, noisy and due to noise in the other counters it is advisable to retain as much redundancy as possible in the data. Therefore, the inlet particle counter signal is used to check results and not to modify the shear-off function $s(t)$.

The impact of the uncertainty about the exact shape of the Occasional Particle Step can be assessed in the light of the inlet particle counter response. It will be seen in section 6.4.4, that the shape of the shear-off function is similar to the shape of the particle counter response after one travel time. Therefore, if the shape of the rig counters corresponds well with the shape of the inlet counter (which is the case) it can be assumed that the Occasional Particle Step really is a pure step function.

Therefore in the following the assumptions for the basic model will be adopted and data which belongs to effects related to what is described in the extended specifications (i.e. the "humps") will be excluded. That implies that the assumption of belated shedding for anything related to the extended model is adopted

(case 4 in section 6.4.1.4), since the basic model and extended model are separable.

The task in the remaining part of this chapter is then to find a model from the assumptions in section 6.4.1.3 and to identify both the parameters of $s(t)$ and a numerical representation of the shape of $b(x)$.

### 6.4.2 Development of the Positive Input Slope Model

In this section, a basic model of the Slow Signal (specifications 1 and 2 of section 6.2) based on the assumptions of section 6.4.1.3 will be developed. This model captures the response of particle counts to a flow increase (positive slope of the input signal flow, i.e. start of a step flow trial).

The starting point is the particle count density $p_d(x,t)$ described in section 6.4.1.3. Its units are $\frac{\text{particles}}{\text{ml}\cdot\text{m}}$ and it depends on both the point $x$ along the rig, and the time $t$. Let $x = 0$ at the start of the rig and $x = x_0$ at the point under investigation. To obtain the total particle counts $p(t_0)$ at point $x_0$ and time $t_0$ from the particle count density $p_d(x,t)$, it is necessary to add the contributions of the particle density at $x = x_0, t = t_0$ to the contributions of the densities along the rig at previous times ($t < t_0$), which have been propagated with the velocity $v$ of the water to the point $x = x_0$. In the example of section 6.3.1 it would be necessary to sum up the appropriate contributions of each cell. In the case of a true density $p_d(x,t)$, however, it is required to take the limit of that sum and, therefore, an integral is obtained. Thus, the total particle counts $p(t)$ at $x = x_0$ are given by the integral over all particle count densities reaching $x = x_0$:

$$p(t) = \int_{x=x_0}^{0} p_d(x, t - \frac{1}{v}(x_0 - x))\,\mathrm{d}x, \tag{6.5}$$

where $v$ is the velocity of the water in the rig (in $\frac{m}{s}$). The limits of the integral could be reversed, which would make it necessary to replace $x$ by $x_0 - x$. Eq. (6.5) requires the velocity $v$ through the pipe rig to be constant for the entire time the water travelled from $x = 0$ (i.e. the inlet) to $x = x_0$. The argument of time, $t - \frac{1}{v}(x_0 - x)$, determines that the time instants of the particle density $p_d(\cdot,\cdot)$

which are considered in the integral at time $t$ correspond to the amounts of particles originating from the distances $0 < x < x_0$ that have reached $x_0$ at time $t$. If the time argument is written as given above, it is necessary to start integrating from the point of investigation $x = x_0$. Note that the fact that only one velocity $v$ is used implies that $p_d(x,t) = 0$ for $t < 0$ (no shear-off before the positive slope of flow occured, as assumed in section 6.4.1.3), since otherwise the argument $t - \frac{1}{v}(x_0 - x)$ would have to take into account the lower velocity before the flow increase (cf. section 6.4.3).

If travel time $\tau = \frac{x}{v}$ is considered instead of the distance $x$, it is necessary to deal with the integral

$$p(t) = v \cdot \int_{\tau=T}^{0} p_d(v\tau, t - T + \tau)\, \mathrm{d}\tau. \tag{6.6}$$

In the above equation, $T = \frac{x_0}{v}$ represents the travel time from the inlet to the point under investigation, $x = x_0$.

Incorporating the second assumption of section 6.4.1.3 means separating the dependencies on distance (or $v\tau$) and time $t$. Thus,

$$p(t) = v \cdot \int_{\tau=T}^{0} b(v\tau) \cdot s(t - T + \tau)\, \mathrm{d}\tau, \tag{6.7}$$

Here, $s(\cdot)$ represents the dynamic (i.e. time-dependent) function describing shear-off from the pipe walls, while $b(\cdot)$ represents the initial values of the dynamic shear-off, thus it is the wanted biofilm thickness or the initial biofilm shedding profile.

A substitution $\vartheta = T - \tau$ and a change of argument of the biofilm shedding profile to $b^*(\vartheta) = b(vT - v\vartheta) = b(v\tau)$ finally yields

$$p(t) = v \cdot \int_{\vartheta=0}^{T} b^*(\vartheta) \cdot s(t - \vartheta)\, \mathrm{d}\vartheta. \tag{6.8}$$

Eq. (6.8) is a standard convolution integral. To verify this, recall that $\int_{-\infty}^{\infty} b^*(\vartheta) \cdot s(t - \vartheta)\, \mathrm{d}\vartheta$ is the standard convolution integral; to obtain the limits as given in eq. (6.8) note that $b^*(\vartheta) = 0$ for $\vartheta < 0$, $b^*(\vartheta) = 0$ for $\vartheta > T$ and $s(t) = 0$ for $t < 0$.

Excluding all values of $\vartheta$ where $b^*(\vartheta) = 0$ leads to the limits given above. The fact that this is a standard convolution integral is extremely useful for obtaining a model, since the convolution describes a *linear system.*

Note that this equation describes only part of the water quality system. It considers only the response of particles to a particular input: a step in flow. Therefore this is a linear 'subsystem' of a larger, nonlinear system. The model of this 'subsystem' is depicted by a Simulink block diagram in fig. 6.11.

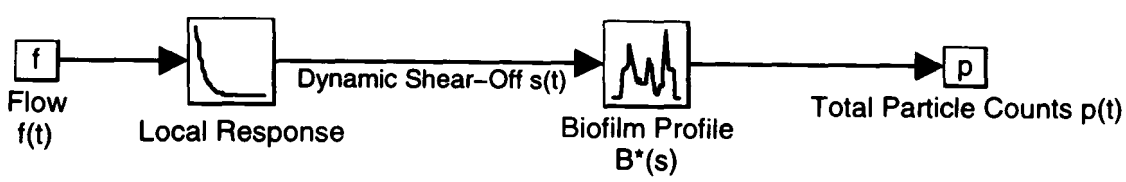


**Figure 6.11:** *Linear system with input flow $f(t)$ and output total particle counts $p(t)$*

Due to the commutative nature of the convolution the second half of fig. 6.11 is equivalent to fig. 6.12. This model allows us to determine the biofilm shedding profile $b^*(\vartheta)$ and from there $b(x)$ by using the inverse of the Laplace transform of the dynamic shear-off $S(s)$. Based on the assumptions of section 6.4.1.3 the equation which describes the dynamic shear-off $s(t)$ is known, however the adequate parameters are not. Normally these parameters would be found by using both the input and output data, however in this case the input is wanted and therefore unknown. On the other hand, some knowledge about the biofilm shedding profile is available. It has to start at the beginning of the pipe rig (the pump), i.e. at $x = 0$, $\tau = 0$ or $\vartheta = T$ and it has to finish (for the purpose of investigating the point $x = x_0$) at $x = x_0$, $\tau = T$ or $\vartheta = 0$, since it is impossible that the biofilm downstream from the considered point has any impact on the suspended particles. Thus, this knowledge about the biofilm shedding profile has to be used to obtain some information about the otherwise unknown parameters of the dynamic shear-off $S(s)$.

Incorporating the actual system $s(t)$

$$s(t) = k_1(f)\exp(-at) + k_2(f), \text{ for } t > 0$$

which was assumed in section 6.4.1.3, yields

$$p(t) = v \int_{\vartheta=0}^{T} b^*(\vartheta) \left(k_1(f)\mathrm{e}^{-a(t-\vartheta)} + k_2(f)\right) 1(t-\vartheta)\,\mathrm{d}\vartheta. \tag{6.9}$$

with

$$1(t) = \begin{cases} 1 & \text{if } t > 0 \\ 0 & \text{otherwise} \end{cases} \tag{6.10}$$

Using the Laplace transform $\mathcal{L}\{\cdot\}$, eq. (6.9) reads as

$$P(s) = v \cdot B^*(s) \cdot S(s) = vB^*(s)\left(\frac{k_1(f)}{s+a} + \frac{k_2(f)}{s}\right), \tag{6.11}$$

where $P(s) = \mathcal{L}\{p(t)\}$, $B^*(s) = \mathcal{L}\{b^*(t)\}$ and $S(s) = \mathcal{L}\{s(t)\}$.

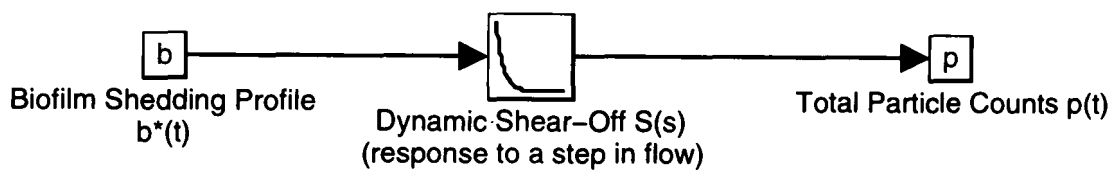


**Figure 6.12:** *Linear system with apparent initial shedding profile $b^*(\vartheta)$ as input and output total particle counts $p(t)$, positive input slope model.*

### 6.4.3 Development of a Negative Input Slope Model

A negative input slope model has to cover the particle counter response to the decrease of flow at the end of a step flow trial. This section follows the assumption of section 6.4.1.6, i.e. the local shear-off is reduced to zero with flow decrease at $t = T_E$. Therefore, it is $p_d(x,t) = 0$ for $t > T_E$ in addition to $p_d(x,t) = 0$ for $t < 0$. In contrast to the positive input slope model of section 6.4.2, different velocities need to be considered in this case.

The general fundamental equation is, in analogy to eq. (6.5),

$$p(t) = \int_{x=x_0}^{0} p_d\,(\,x, t - \tau(x_0, v(t)) + \tau(x, v(t))\,)\;\mathrm{d}x. \tag{6.12}$$

Note that in previous notation $T$ is used as travel time between $x = 0$ and $x = x_0$, thus $T = \tau(x_0)$. Recall that the time interval $\tau(x_0, v) - \tau(x, v)$ is the time it took the aliquot of water that is currently at $x_0$ to cover the distance from $x$.

If the step decrease of flow is assumed to be ideal, i.e. the time it takes to reach the lower flow is negligible, only two different velocities need to be taken into account, $v_H$ during high and $v_L$ during low flow. Thus, to obtain $p(t)$ it is necessary to find a distance $x_E(t)$ such that the aliquot of water which is presently at $x_0$ travelled the distance $0 < x < x_E(t)$ with the velocity $v_H$ and $x_E(t) < x < x_0$ with velocity $v_L$.

The integral of eq. (6.12) can be split to form

$$\begin{aligned} p(t) \;=\; & \int_{x=x_0}^{x_E(t)} p_d\,(\,x, t - \tau(x_0, v_L) + \tau(x, v_L)\,)\;\mathrm{d}x + \\ & + \int_{x=x_E(t)}^{0} p_d(\,x, t - (\tau(x_0, v_L) - \tau(x_E(t), v_L)) + \\ & -(\tau(x_E(t), v_H) - \tau(x, v_H))\,)\;\mathrm{d}x. \\ = \; & \int_{x=x_0}^{x_E(t)} p_d\left(\,x, t - \frac{x_0}{v_L} + \frac{x}{v_L}\,\right)\mathrm{d}x \\ & + \int_{x=x_E(t)}^{0} p_d\left(\,x, t - \frac{x_0}{v_L} + \frac{x_E(t)}{v_L} - \frac{x_E(t)}{v_H} + \frac{x}{v_H}\,\right)\mathrm{d}x. \end{aligned} \tag{6.13}$$

The correction $\tau(x_0, v_L) - \tau(x_E(t), v_L)$ of $t$ is necessary to adjust the time variable $t$ to the new origin $x_E(t)$.

Eq. (6.13) together with the condition $p_d(x, t) = 0$ for $t > T_E$ describes the particle counts model for a negative slope input completely. The decomposition $p_d(x, t) = b(x)s(t)$ is still valid with the restriction of $s(t) = 0$ for $t > T_E$. Note that the distance between the point of observation $x_0$ and $x_E(t)$ is the distance covered since the end of the step flow trial $T_E$ at the low velocity $v_L$, thus

$$x_0 - x_E(t) = (t - T_E)v_L. \tag{6.14}$$

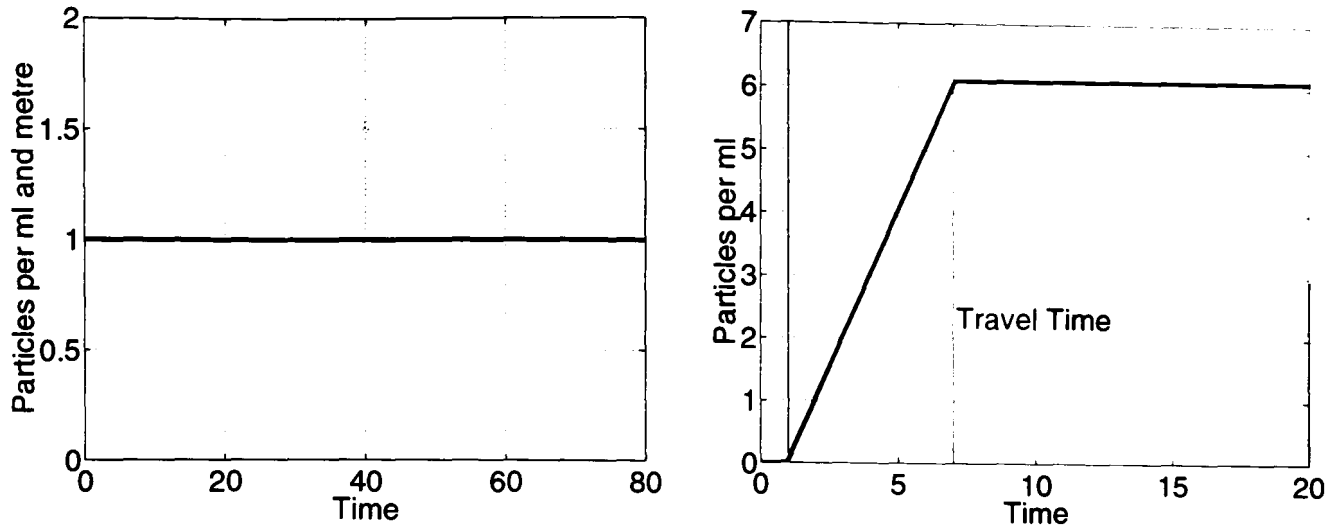


(a) Linear shear-off function

(b) Particle counter response

**Figure 6.13:** *Linear shear-off function and corresponding particle counter response for a flat Biofilm Shedding Profile.*

Due to the time dependence of the integral limit $x_E(t)$, it is not possible to transform eq. (6.13) into a convolution integral. However, if all parameters of $s(\cdot)$ and the biofilm shedding profile $b(\cdot)$ are known, it is possible to calculate an approximation of $p(t)$ from this equation by replacing the integrals through sums. Since the parameters and the biofilm shedding profile can be found by means of the positive slope model and the high flow data, this approach is feasible.

### 6.4.4 Examples

The aim of this section is to give some examples which illustrate the range of possible particle counter responses $p(t)$ for a given initial biofilm shedding profile (BSP) $b(\cdot)$ and a particle shear-off function $s(\cdot)$ as related in the basic model

$$p(t) = v \cdot \int_{\tau=T}^{0} b(v\tau) \cdot s(t - T + \tau)\, \mathrm{d}\tau, \tag{6.15}$$

given in eq. (6.7) of section 6.4.2. Within the framework of eq. (6.15) also examples which differ from assumption 3 of an exponentially decaying shear-off function are investigated.

Figs. 6.13–6.15 show the results of the variation of the shear-off function $s(t)$ on the particle counts $p(t)$. For these figures a flat biofilm shedding profile $b(x) =$

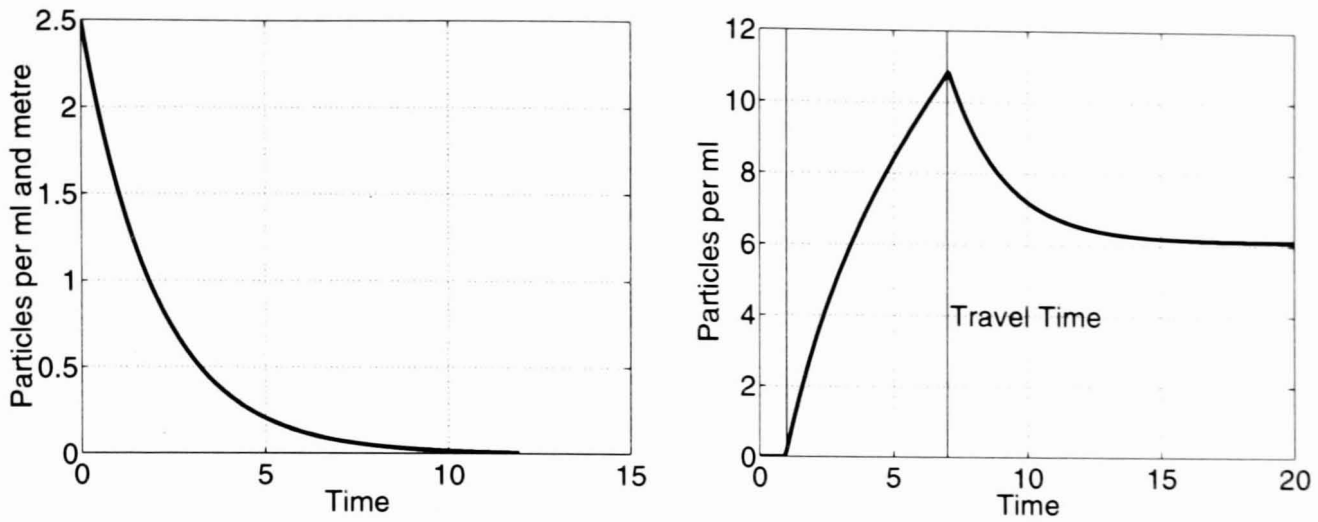


(a) Exponential shear-off function

(b) Particle counter response

**Figure 6.14:** *Exponential shear-off function and corresponding particle counter response for a flat Biofilm Shedding Profile.*

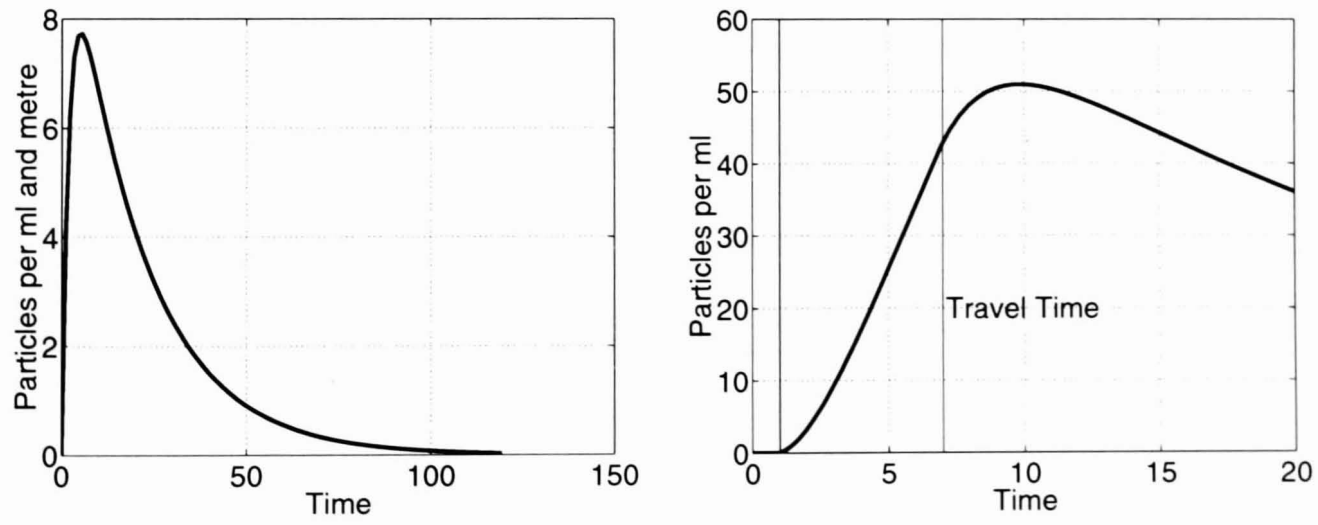


(a) Sum of two exponential shear-off functions (second order system)

(b) Particle counter response

**Figure 6.15:** *Sum of two exponential shear-off functions (second order system) and corresponding particle counter response for a flat Biofilm Shedding Profile.*

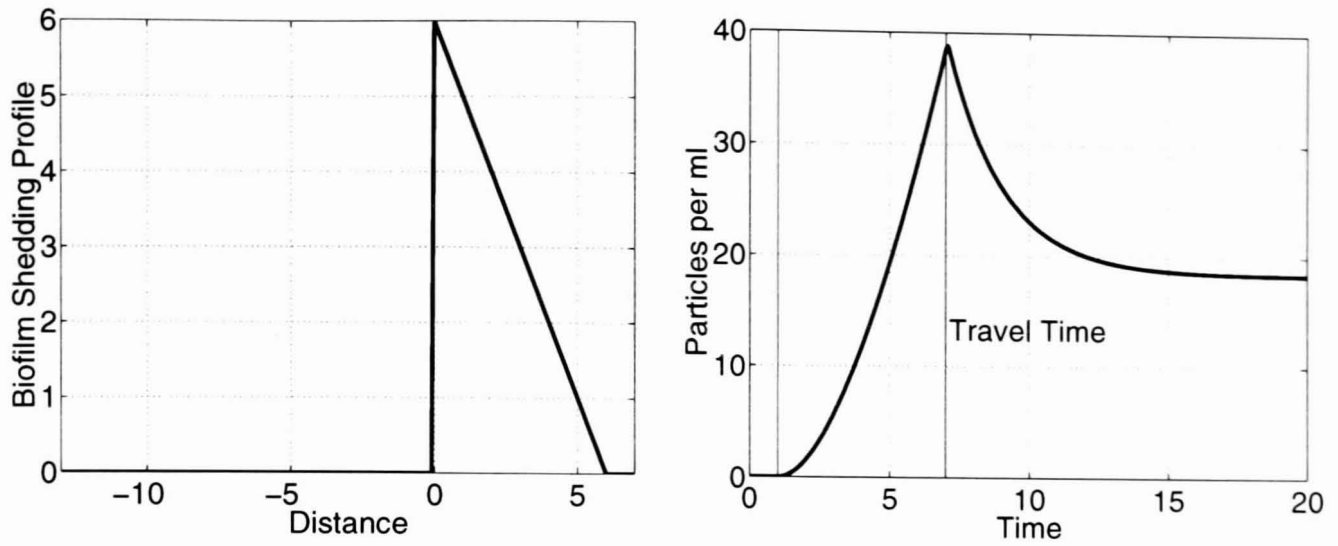


(a) Decreasing Biofilm Shedding Profile

(b) Particle counter response

**Figure 6.16:** *Decreasing Biofilm Shedding Profile and corresponding particle counter response for an exponential shear-off function.*

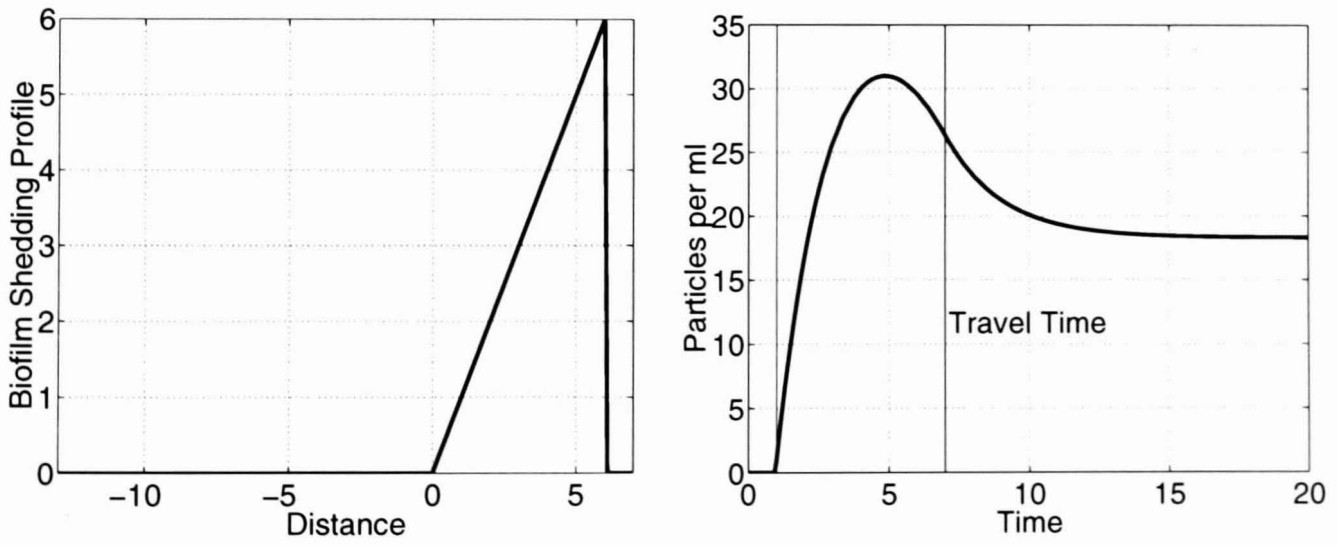


(a) Increasing Biofilm Shedding Profile

(b) Particle counter response

**Figure 6.17:** *Increasing Biofilm Shedding Profile and corresponding particle counter response for an exponential shear-off function.*

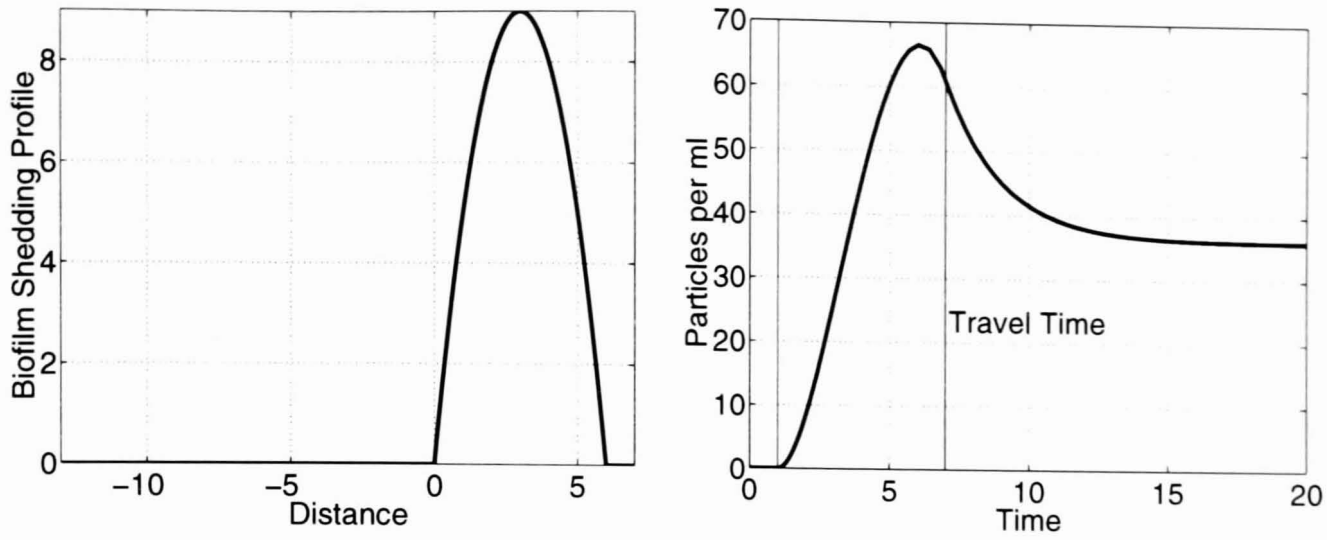


(a) Quadratic Biofilm Shedding Profile

(b) Particle counter response

**Figure 6.18:** *Quadratic Biofilm Shedding Profile and corresponding particle counter response for an exponential shear-off function.*

1 is assumed, i.e. the shear-off function $s(t)$ is the same as the shear-off density $p_d(x,t)$.

Fig. 6.13(a) provides the simplest example: after flow increase a constant shear-off occurs. Thus, the transfer function of the dynamic system $S(s)$ given in eq. (6.11) degenerates to a pure integrator ($k_1(f) = 0$). The response to a flow increase which started at the normalised time $t = 1$ in a system with travel time $t = 6$ is given in fig. 6.13(b). The start of the a SFT and the elapse of one travel time to the point of investigation are marked by vertical lines in this and all other figures of particle counter responses. The particle counts signal of fig. 6.13(b) is an underlying signal in all other particle counter responses $p(t)$ given in this section.

The case given in fig. 6.14 is assumed in section 6.4.1.3 (assumption 3 on page 141). There is an exponentially decreasing dynamic shear-off function $s(t)$ in fig. 6.14(a) which leads to a particle counter response $p(t)$ as given in fig. 6.14(b). This response is monotonicly decreasing after the elapse of one travel time.

The only possibility of a maximum value later than one travel time is given in fig. 6.15: a shear-off function $s(t)$ that is itself not monotonic and contains a maximum value. In this case $S(s) = \frac{5}{s^2+0.55s+0.025}$ or $s(t) = 11.11\mathrm{e}^{-0.05t} -$

$11.11e^{-0.5t}$.

Figs. 6.16–6.18 illustrate the impact of various initial biofilm shedding profiles (BSP) on a system with exponential shear-off function as given in fig. 6.14(a) (thus, assumption 3 is fulfilled). Investigated are a decreasing BSP (fig. 6.16), an increasing BSP (fig. 6.17) and a BSP with maximum value at half distance (fig. 6.18).

From the particle counter responses $p(t)$ given in figs. 6.16(b), 6.17(b) and 6.18(b), it is seen that the BSP has a significant impact on the particle counts until one travel time is over. However, it is has no influence on the shape of the particle counts response after the elapse of one travel time. Compare also fig. 6.14(b), where a flat biofilm profile with the same shear-off function as in figures 6.16–6.18 is used. From these four examples it is seen that a wide range of shapes of particle counts within the time less than one travel time may originate from the biofilm shedding profile, but that the shape of the particle counts after one travel time is determined by the shear-off function alone.

## 6.5 Parameter Identification

The problem to find the parameters of the system $S(s)$ is the standard problem of system identification. The standard solution would be to use a regressor composed of both input and output data to find the parameters. However, the present case is different, since there is hardly any knowledge of the input $b^*(\vartheta)$. The only known circumstance concerning the input is its start (at $\vartheta = 0$) and end (at $\vartheta = T$), i.e. it is known that a physically feasible input has to be zero for $\vartheta < 0$ and $\vartheta > T$.

Since the output signal $p(t)$ extends for a longer time (the step flow trials generally finish after 3 to 4 travel times $T$), this signal of $p(t)$ for $t > T$ can be used to gain information about the parameters of the system. The output response has for $t > T$ the *shape* of an impulse response (as will be shown in section 6.5.2) independent of the input signal. It is, however, not possible to read all parameters directly from $p(t)$ for $t > T$. An indirect method, which

involves the Laplace back-transform and a number of integrals, is employed in section 6.5.3 to find the remaining unknown parameters.

Since the magnitude of both parameters and input are unknown, they cannot be determined completely. There will be always an unknown factor possible that, if it is multiplied with the input and the system is divided by it, will leave the output unchanged. Therefore, the input will only show the shape of the biofilm shedding profile and not its absolute magnitude.

However, before the task of identifying the parameters of the Slow Signal $p(t)$ can be attempted, it is necessary to address the problem of the other signals given in section 6.2, the 'face-value' signals. The Occasional Particle Step (spec. 5) is readily removed by subtracting a constant value from all high flow values of the data of sample point 1 and the data of SP 2 and 3 in the corresponding time range. The magnitude of the particle step is determined by the step decrease of particle counts at the end of a SFT. This procedure will not be discussed further. The Peaks (spec. 4 in section 6.2), however, require additional analysis. They will be considered in the following section.

### 6.5.1 Data Preparation (Peak Erase)

The goal of this section is to show methods for the removal of peaks from the particle counter data. Two possible procedures for achieving a signal without peaks were implemented: one manual, the other automated, based on classical image processing. The procedures of this section are termed 'peak erase', since the peaks are supposed to be eliminated.

#### 6.5.1.1 Peak Erase by Hand

This fairly crude approach allows the user to identify the peaks-to-be-erased by hand (i.e. mouse click) in a graph. Only the final peak (originating from the inlet) is dealt with separately (cf. section 6.5.4.1).

#### 6.5.1.2 Automatic Peak Detect and Erase

This method is based on an approach of classical image processing (cf. e.g. section 7.1 in [56]). It investigates an approximation of the derivative to detect the presence of peaks. The algorithm for peak detection consists of two major steps:

a) Edge detect

b) Edge clustering

**a) Edge detection** investigates an approximation of the derivative of the total particle counts $p(t)$, i.e. $\frac{\mathrm{d}}{\mathrm{d}t}p(t)$. In this implementation the backward difference approximation is used. Thus,

$$\frac{\mathrm{d}}{\mathrm{d}t}p(t) \approx \frac{p(t) - p(t - \Delta t)}{\Delta t},$$

where $\Delta t$ is the sampling time (either 2 min or 5 min), cf. [4]. A different method (e.g. Tustin's method) could be used as well.

An edge is defined as a point were the derivative is higher than a certain, user defined, threshold $\theta$. Depending on the sign of the derivative, positive and negative edges are distinguished. Thus, an edge is identified via

$$\frac{p(t) - p(t - \Delta t)}{\Delta t} > \theta \quad \text{for a positive edge,} \tag{6.16}$$

$$\frac{p(t) - p(t - \Delta t)}{\Delta t} < -\theta \quad \text{for a negative edge.} \tag{6.17}$$

**b) Edge clustering.** It is more of an issue to find peaks (compared to edges), which on the one hand obviously consist of a positive and a negative edge and on the other hand may include some regions with smaller derivative or opposite derivative due to random errors.

Therefore, a procedure was included in the algorithm which clusters edges together to form peaks by starting with a positive edge and searching for the next negative edge. Another parameter which can be defined by the user, the

look-ahead, defines how many "false" derivatives are tolerated before the edge is discarded as not belonging to a peak.

The two design parameters, look-ahead and threshold, have to be chosen sensibly. Especially the threshold is very critical and some reality checks are incorporated in the Matlab implementation `bioprofi` to check if the threshold is too large or too small. In particular the peaks are tested for excessive peak width and the presence of the inlet peak is checked.

#### 6.5.1.3 Inclusion of Peak Models

Fundamentally, there are two possible way to deal with the shape of the peaks: to consider it completely unknown and thus only rely on the derivative (or the magnitude of the edge) or to assume that the peaks have basically the same shape as the Slow Signal but there are not enough samples to reconstruct it accurately (as discussed in section 6.4.1.1). The latter implies that the declining edge of the peak follows an exponential function. The time constant (or decay coefficient) of this exponential will be different to that of the Slow Signal. It will be a quicker decay (smaller time constant or higher decay coefficient). This difference in time constant can be attributed to the fact that these particles are loose deposits in this case which are lifted into suspension much quicker than attached material.

If this chain of thought is followed it becomes apparent that the M.V. can be dealt with in various ways. The peaks before the M.V. do not need to be considered here, since the fact that the Slow Signal is then increasing, gives a fairly clear picture of the end of the peaks. However, for the inlet peak (which falls together with the M.V.) it opens the possibility to fit a sum of two exponential functions (with fast and slow decay) to the Slow Signal after the M.V. (see section 6.5.4.1). Thus, in the Matlab implementation of this work, `bioprofi`, it is possible to opt for this way of fitting the parameters.

### 6.5.2 Time Constant $T_a = \frac{1}{a}$

The knowledge of the end of the biofilm shedding profile (together with $s(t) = 0$ for $t < 0$) allows us to investigate eq. (6.9) for $t > T$ without the step function $1(t - \vartheta)$. This is given as

$$\begin{aligned} p(t) &= v \int_{\vartheta=0}^{T} b^*(\vartheta) \left(k_1(f)\mathrm{e}^{-a(t-\vartheta)} + k_2(f)\right) \mathrm{d}\vartheta \\ &= v\mathrm{e}^{-at} \int_{\vartheta=0}^{T} b^*(\vartheta) k_1(f) \mathrm{e}^{a\vartheta} \mathrm{d}\vartheta + v \int_{\vartheta=0}^{T} b^*(\vartheta) k_2(f) \mathrm{d}\vartheta \qquad (6.18) \\ p(t) &= c_1(T)\mathrm{e}^{-at} + c_2(T), \text{ for } t > T, \qquad (6.19) \end{aligned}$$

or

$$p(t) = \overbrace{c_1(T)\mathrm{e}^{-aT}}^{c_1^*(T)} \mathrm{e}^{-a(t-T)} + c_2(T), \text{ for } t > T. \qquad (6.20)$$

Eq. (6.20) is the equation of an exponential function starting at $t - T = 0$. It is straightforward to fit this exponential function to the data $p(t)$ for $t > T$ in order to obtain the system parameter $a$ and two other parameters $c_1(T), c_2(T)$ which depend on $T$ and are related to the wanted parameters $k_1(f), k_2(f)$ in the following way:

$$\begin{aligned} c_1(T) &= v k_1(f) \int_{\vartheta=0}^{T} b^*(\vartheta) \mathrm{e}^{a\vartheta} \mathrm{d}\vartheta \qquad (6.21) \\ c_2(T) &= v k_2(f) \int_{\vartheta=0}^{T} b^*(\vartheta) \mathrm{d}\vartheta \qquad (6.22) \end{aligned}$$

Note that, rather than obtaining $c_1(T)$, the result of the fitting will be

$$c_1^*(T) = c_1(T)\mathrm{e}^{-aT}, \qquad (6.23)$$

as indicated in eq. (6.20). From this follows obviously $c_1(T) = c_1^*(T)\mathrm{e}^{aT}$.

The parameter $a$ is the inverse of the time constant $T_a = \frac{1}{a}$ which is frequently used as a measure of how quickly an exponential signal decays.

### 6.5.3 Parameters $k_1(f)$ and $k_2(f)$

The aim of finding $k_1(f), k_2(f)$ using eq. (6.21) and (6.22) is only partially achieved, since it is impossible to determine $k_1(f)$ and $k_2(f)$ from $c_1(T), c_2(T)$ without knowledge of the two integrals over $b^*(\vartheta)$.

For a flat biofilm shedding profile

$$b^*(\vartheta) = \begin{cases} c & \text{if } 0 \leq \vartheta \leq T \\ 0 & \text{otherwise} \end{cases} \tag{6.24}$$

$k_1(f)$ and $k_2(f)$ can be found up to an unknown constant $c$ according to the following equations (derived from eq. (6.21), (6.22) ).

$$\begin{aligned} k_{1flat} &= \frac{c_1(T)}{\frac{v \cdot c}{a}\left(\mathrm{e}^{aT} - 1\right)}, \\ k_{2flat} &= \frac{c_2(T)}{cvT}. \end{aligned}$$

However, it is unlikely that the biofilm shedding profile is flat. Therefore these values are only used for initial conditions and to check if the simulation results are theoretically correct. A model with parameters $k_{1flat}, k_{2flat}$ and $a$ will produce the same exponentially decaying signal for $t > T$ as is exhibited in the total particle counts data.

To allow for any shape of biofilm shedding profile $b^*(\vartheta)$, it is necessary to determine the integrals over the biofilm shedding profile through known signals. For this purpose the inverse of the Laplace transform $S(s)$ of the shear-off function $s(t)$, i.e. $S^{-1}(s)$, is used. The Laplace back-transform of $S^{-1}(s)$ is denoted by $s_{inv}(t)$.

Thus, the problem is to find (cf. eq. (6.21), (6.22) )

$$k_1(f) = \frac{c_1(T)}{v \int_0^T b^*(\vartheta)\mathrm{e}^{a\vartheta}\,\mathrm{d}\vartheta}, \tag{6.25}$$

$$k_2(f) = \frac{c_2(T)}{v \int_0^T b^*(\vartheta)\,\mathrm{d}\vartheta}. \tag{6.26}$$

with

$$b^*(\vartheta) = \frac{1}{v}\int_0^{\vartheta} p(t)s_{inv}(\vartheta - t)\,\mathrm{d}t. \tag{6.27}$$

Using the inverse of the Laplace transform $\mathcal{L}^{-1}\{\cdot\}$, $s_{inv}(t)$ is obtained to be

$$\begin{aligned} s_{inv}(t) &= \mathcal{L}^{-1}\left\{S^{-1}(s)\right\} \\ &= \mathcal{L}^{-1}\left\{\frac{s(s+a)}{s(k_1(f)+k_2(f))+ak_2(f)}\right\} \end{aligned} \tag{6.28}$$

In summary, it is necessary to find $k_1(f), k_2(f)$ from eq. (6.25), (6.26) given eq. (6.27) and (6.28). Since eq. (6.28) includes $k_1(f), k_2(f)$, non-linear optimisation methods will be used to solve this problem.

The calculation of the inverse Laplace transform is given in appendix B. The inverse shear-off function is obtained to be

$$\begin{aligned} s_{inv}(t) = &- \frac{a^2k_1(f)k_2(f)}{(k_1(f)+k_2(f))^3}\mathrm{e}^{\frac{-ak_2(f)}{k_1(f)+k_2(f)}t} + \frac{ak_1(f)}{(k_1(f)+k_2(f))^2}\delta(t) + \\ &+ \frac{1}{k_1(f)+k_2(f)}\delta'(t), \end{aligned} \tag{6.29}$$

where $\delta(t)$ is Dirac's delta impulse[1] and $\delta'(t)$ its derivative.

This result has to be incorporated in eq. (6.27), and then used in eqs. (6.25) and (6.26) (or eqs. (6.21) and (6.22) ). Thus, with the abbreviation

$$g_i(\vartheta) = \begin{cases} e^{a\vartheta}, & i = 1 \\ 1, & i = 2 \end{cases}$$

[1]The Dirac impulse is not a function in the normal sense. It is, however, a generalised function or distribution, cf. [70, 79]

eqs. (6.21) and (6.22) can be written as

$$\begin{aligned} c_i(T) =& k_i \int_{\vartheta=0}^{T} \int_{t=0}^{\vartheta} p(t) s_{inv}(\vartheta - t) g_i(\vartheta) \, \mathrm{d}t \, \mathrm{d}\vartheta \\ =& k_i \int_{\vartheta=0}^{T} \int_{t=0}^{\vartheta} p(t) \left( -\frac{a^2 k_1(f) k_2(f)}{(k_1(f) + k_2(f))^3} \mathrm{e}^{-\frac{a k_2(f)}{k_1(f)+k_2(f)}(\vartheta - t)} + \right. \\ & \left. + \frac{a k_1(f)}{(k_1(f) + k_2(f))^2} \delta(\vartheta - t) + \frac{1}{k_1(f) + k_2(f)} \delta'(\vartheta - t) \right) \times \\ & \times g_i(\vartheta) \, \mathrm{d}t \, \mathrm{d}\vartheta, \qquad i = 1, 2 \end{aligned} \tag{6.30}$$

A few steps of calculations (provided in appendix B) give the following result.

$$\begin{aligned} c_i(T) =& k_i \int_{\vartheta=0}^{T} \int_{t=0}^{\vartheta} -p(t) \frac{a^2 k_1(f) k_2(f)}{(k_1(f) + k_2(f))^3} \mathrm{e}^{-\frac{a k_2(f)}{k_1(f)+k_2(f)}(\vartheta - t)} g_i(\vartheta) \, \mathrm{d}t \, \mathrm{d}\vartheta + \\ & + k_i \int_{0}^{T} \left( p(\vartheta) \frac{a k_1(f)}{(k_1(f) + k_2(f))^2} + \frac{\mathrm{d}}{\mathrm{d}\vartheta} p(\vartheta) \frac{1}{k_1(f) + k_2(f)} \right) g_i(\vartheta) \, \mathrm{d}\vartheta \end{aligned} \tag{6.31}$$

By approximating the integrals numerically it is possible to obtain $k_1(f)$ and $k_2(f)$ from eq. (6.31) given $p(\cdot)$.

However, note that the given system of equations, eq. (6.31), is degenerate with respect to $k_1(f)$ and $k_2(f)$, i.e. it is only possible to find a solution for a ratio $k = \frac{k_1(f)}{k_2(f)}$, and not for each parameter $k_1(f)$, $k_2(f)$. To show this let $k_1(f) = k k_2(f)$ in eq. (6.31). Thus,

$$\begin{aligned} c_1(T) =& k \int_{\vartheta=0}^{T} \int_{t=0}^{\vartheta} -p(t) \frac{a^2 k}{(1+k)^3} \mathrm{e}^{-\frac{a}{1+k}(\vartheta - t)} \mathrm{e}^{a\vartheta} \, \mathrm{d}t \, \mathrm{d}\vartheta + \\ & + k \int_{0}^{T} \left( p(\vartheta) \frac{ak}{(1+k)^2} + \frac{\mathrm{d}}{\mathrm{d}\vartheta} p(\vartheta) \frac{1}{1+k} \right) \mathrm{e}^{a\vartheta} \, \mathrm{d}\vartheta, \end{aligned} \tag{6.32}$$

$$\begin{aligned} c_2(T) =& \int_{\vartheta=0}^{T} \int_{t=0}^{\vartheta} -p(t) \frac{a^2 k}{(1+k)^3} \mathrm{e}^{-\frac{a}{1+k}(\vartheta - t)} \, \mathrm{d}t \, \mathrm{d}\vartheta + \\ & + \int_{0}^{T} \left( p(\vartheta) \frac{ak}{(1+k)^2} + \frac{\mathrm{d}}{\mathrm{d}\vartheta} p(\vartheta) \frac{1}{1+k} \right) \mathrm{d}\vartheta. \end{aligned} \tag{6.33}$$

This shows again that it is impossible to fully determine both input and parameters of the system in fig. 6.12 from the output and the system structure. In the Matlab implementation, $k_2(f)$ is set to 1, which means effectively that $k_1(f)$ is

replaced with $\frac{k_1(f)}{k_2(f)}$ and $k_2(f)$ with $\frac{k_2(f)}{k_2(f)}$ in equations which feature the true values of $k_1(f)$ and $k_2(f)$. Therefore, the biofilm shedding profile is found only up to an unknown constant, say $c$. The algorithm used is provided by Matlab (i.e. `fmin`). It is a line search method based on golden section search and parabolic interpolation.

To check on the accuracy of the results for $k_1(f), k_2(f)$ the following values $c'$ and $c''$ can be calculated. For this test, $k_1(f)$ and $k_2(f)$ (obtained as given above) are used to first calculate the BSP $b^*(\vartheta)$.

$$c' = k_2(f) \cdot \frac{c_1(T)}{v \int_0^T b^*(\vartheta) k_1(f) \mathrm{e}^{a\vartheta} \, \mathrm{d}\vartheta}, \tag{6.34}$$

$$c'' = k_2(f) \cdot \frac{c_2(T)}{v \int_0^T b^*(\vartheta) k_2(f) \, \mathrm{d}\vartheta}, \tag{6.35}$$

Comparison of the above equations with eqs. (6.25), (6.26) shows that $k_1(f)$, $k_2(f)$ were replaced by $\frac{k_1(f)}{k_2(f)}$ and $\frac{k_2(f)}{k_2(f)}$. In the implementation, a sum approximation is used instead of the integral of eqs. (6.34) and (6.35).

Eqs. (6.34), (6.35) should lead to

$$c' \approx c'' \approx c, \tag{6.36}$$

as can be seen by comparison with eqs. (6.25) and (6.26). However, since data is generally noisy, eq. (6.36) will never be fully achieved. Therefore, the difference between $c'$ and $c''$ gives an indication on the "goodness" of the results.

Note that it seems possible to determine $k_2(f)$ from eqs. (6.34) and (6.35), since $c \approx k_2(f)$ should hold. However, it is not certain if the biofilm shedding profile $b^*(\vartheta)$ is not scaled and therefore it is meaningless to determine $k_2(f)$ this way. It is only correct if $b^*(\vartheta)$ is also correct in magnitude, and it is impossible to know that. Despite that, the relevance (or "goodness") of the results will not be altered as long as $c' \approx c''(\approx c)$ holds.

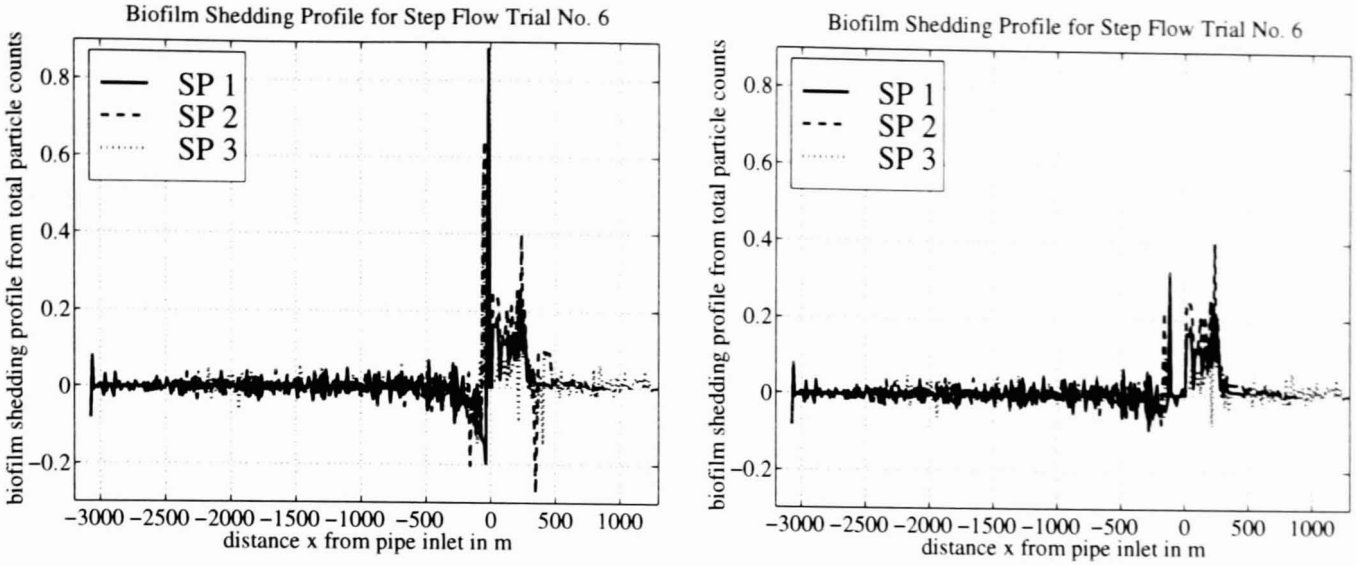


(a) Negative edge threshold is the same as the positive edge threshold.

(b) Negative edge threshold at 40% of positive edge threshold.

**Figure 6.19:** *Effect of the reduction of the threshold for the negative edge in the peak detect algorithm on the apparent initial biofilm shedding profile of step flow trial 6, 8 October 1996.*

## 6.5.4 Issues in Parameter Determination

### 6.5.4.1 Impact of Peak Erase

Accurate and effective erasing of the peaks is crucial for the parameter estimation process. In particular, if at any time the decrease in the signal is sharper than $e^{-at}$ the biofilm shedding profile (BSP) possibly becomes negative. This is especially relevant during the (erased) peaks, since the signal during these times is unknown and, for want of anything more accurate, replaced by a linear interpolation.

As already indicated in section 6.5.1.3 on page 158, there is a degree of freedom in dealing with the last peak in the data, which originates from the inlet (the peak at the M.V.). This peak is assumed to be of the same shape as the Slow Signal, however, with a greater decay coefficient in the exponential tail. To reduce the impact of the peak on the estimation of $a$, the current implementation fits a sum of two exponential functions and then discards the higher decay coefficient (shorter time constant). The merit of the higher decay coefficient as a number is questionable, since the sampling rate is not high enough to obtain an accurate picture of the peaks.

This has, however, the unfortunate side effect that the peak as found by fitting may be wider than the one found by peak erase based on the magnitude of edges. Therefore, the threshold $\theta$ in eq. 6.17 (i.e. for the negative edge) is modified to be less than the threshold for positive edges (as in eq. 6.16) to widen the detected peaks. Thus, the ratio of thresholds emerges as an additional design parameter.

The effect of this parameter is illustrated in figure 6.19. In that figure the BSP $b(x)$ of SFT 6 is depicted on the ordinate. On the abscissa the distance $x$ from the pipe rig inlet is shown. Particles at a negative distance (i.e. originating from the pipe work in front of the inlet) should make no contribution to the BSP; a zero-valued BSP for $x < 0$ indicates that the exponential tail of the Slow Signal matches the data perfectly. The variation of the BSP for $x < 0$ gives therefore an indication of the error associated with the fit of the model. However, the "drop off" towards negative values between -500 m and 0 m that can be seen in fig. 6.19(a) indicates a quite serious mismatch between data and model. It originates from the incomplete removal of the inlet peak when equal thresholds for positive and negative edges are used. The effect of a reduction of the threshold for negative edges to 40 % of the threshold for positive edges is shown in fig. 6.19(b): the negative "drop off" is almost entirely removed. In the implementation a negative edge threshold reduced to 80 % of the positive edge threshold is used as the default setting.

#### 6.5.4.2 Normalisation of Data for Simulation

All theoretical work assumes a start of the signal at $p(0) = 0$ for $t = 0$. However, the particle counts are not zero when an arbitrary increase of flow takes place (i.e at the start of the SFT). Therefore the data are normalised. This implies the assumption of a constant feed of particles going into the rig from the balancing tank, the same even after the increase of flow. The modelled particle counts response is independent of this constant input. For simplicity, the initial value of the particle counts at the start of the step flow trial is used as a reference for normalisation.

However, since the final value gives some information about the steady state

biofilm shedding for the respective regime, the final value is normalised not just with respect to the initial value but, for higher accuracy, with respect to a mean of particle counts during a period of 4.8 hrs before the start of the SFT.

## 6.6 The Initial Biofilm Shedding Profile

To obtain the initial biofilm shedding profile (BSP) the system as described in section 6.4.2 is considered. It has the following transfer function

$$\begin{aligned} \frac{P(s)}{B^*(s)} &= \left(\frac{k_1(f)}{s+a} + \frac{k_2(f)}{s}\right) \cdot v \\ &= \frac{s(k_1(f)+k_2(f)) + ak_2(f)}{s(s+a)} \cdot v. \end{aligned} \tag{6.37}$$

To obtain the initial biofilm shedding profile $b(t)$ from the total particle counts $p(t)$ it is necessary to simulate the inverse system

$$\frac{B^*(s)}{P(s)} = \frac{s(s+a)}{s(k_1(f)+k_2(f)) + ak_2(f)} \cdot \frac{1}{v}, \tag{6.38}$$

which is a non-causal (or improper) system (order of numerator greater than order of denominator). Systems of this type cannot be brought into standard state space form and thus are not readily simulated in common tools like Matlab. They also exhibit a strong susceptibility to noise since the derivative action reacts strongly to edges.

To address the problem of large variations in the BSP due to high frequency noise in the particle counts a running average filter is used to smooth the data. Such filters are frequently used for low pass filtering in applications of digital image processing [56]. Briefly, the data values are successively replaced by the average of the surrounding data. The number of data points to be included in the average is determined by an additional design parameter, the filter window size $n = 2i + 1$, where $i$ is the number of points before and, for symmetry, after the current data instant. In this implementation, the first $i$ points of the BSP, the final $i$ points of the BSP and the $2i$ points surrounding the Maximum Value

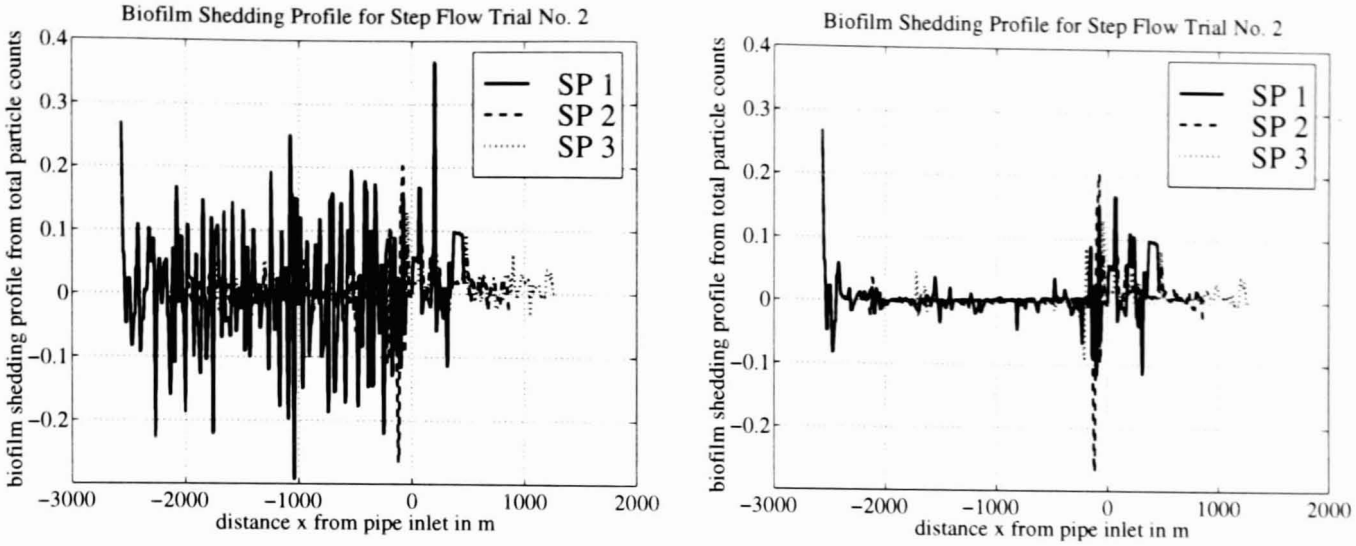


(a) Unfiltered biofilm shedding profile.

(b) Filtered biofilm shedding profile.

**Figure 6.20:** *Unfiltered and filtered apparent initial biofilm shedding profile of step flow trial 2, 1 August 1996. Filtered data uses a running average filter with window size 19.*

in the particle counts response (at $x = 0$ in the BSP) are not filtered.

The use of this filter is illustrated in fig. 6.20. There the BSP $b(x)$ of SFT 2 is depicted. In fig. 6.20(a) the unfiltered signal is presented, whereas fig. 6.20(b) shows the BSP after filtering with a running average filter of window size $n =$ 19. In this case a noise level in the unfiltered results that is of the same order of magnitude as the BSP is observed, however, filtering reduces the noise level significantly while the BSP signal remains intact.

The actual simulation of the improper system was performed by using an approximation of the derivative of $p(t)$ as input rather than the actual signal. Again (as in section 6.5.1.2) a backward difference approximation was used. With the introduction of this approximation, the order of the numerator is reduced by one compared to eq. (6.38) and the remaining system $\frac{B^*(s)}{sP(s)}$ is therefore proper.

For the simulation of the system $b^*(\vartheta)$ which depends on $\vartheta$ was used, as introduced in eq. (6.8), however, now $b(x)$ is of interest. The replacement of $\vartheta$ in $b^*(\vartheta)$ with $vT - v\vartheta$ finally yields the apparent initial biofilm shedding profile $b(-v\vartheta + vT) = b(v\tau) = b(x)$.

**Table 6.1:** *Thresholds for peak erase and filter window sizes.*

| SFT no | Thresholds in particles/(ml·day) Inlet | SP 1 | SP 2 | SP 3 | Filter window size |
|---|---|---|---|---|---|
| 1 | n/a | 200000 | 150000 | 100000 | 3 |
| 2 | n/a | 4000 | 4000 | 3000 | 19 |
| 3 | n/a | 8000 | 10000 | 10000 | 19 |
| 4 | n/a | 30000 | 30000 | 30000 | 15 |
| 5 | n/a | 10000 | 10000 | 10000 | 13 |
| 6 | 100 | 30000 | 30000 | 10000 | 11 |
| 7 | 100 | 30000 | 10000 | 10000 | 11 |
| 8 | 100 | 18000 | 10000 | 10000 | 15 |
| 9 | 100 | 12000 | 10000 | 7000 | 15 |

## 6.7 Results

In previous sections, various design parameters that introduce degrees of freedom into the identification process of the parameters of the particle counts model were defined. In particular, there are the look-ahead and the threshold $\theta$ of the peak erase (section 6.5.1.2), the reduction of this threshold for the negative edge as introduced in section 6.5.4.1 and the filter window size (cf. section 6.6). In addition there is the option to include a model of the inlet peak as discussed in section 6.5.1.3.

The thresholds used to obtain the results presented in this section are given in columns 2–5 of table 6.1, as look-ahead either 2 data points (for SFTs with sampling time 5 min) or 5 data points if the sampling time is 2 min were used. The reduction of the threshold for a negative edge is always 80% apart from SFTs 1 and 6, where it is 50% and 40%, respectively. The filter window sizes are also provided in table 6.1, in column 5. The peaks of SFTs 1–3 and 6 are modelled.

Finally, due to the difference between basic and extended specifications as discussed in section 6.4.1.4, not always all of the data at high flow of a SFT are consider, but the data used for identification is restricted to the range for which the basic specifications appear to be valid. These time ranges for SFTs 1–9 are presented in table 6.2.

**Table 6.2:** *Investigated time periods of high flow for SFTs 1–9.*

| SFT no | Date | Sample Point 1 | | Sample Point 2 | | Sample Point 3 | |
|---|---|---|---|---|---|---|---|
| | | Start | End | Start | End | Start | End |
| 1 | 25.7.96 | 6:55 | 20:20 | 6:55 | 20:20 | 6:55 | 20:20 |
| 2 | 1.8.96 | 6:40 | 20:10 | 6:40 | 20:10 | 6:40 | 20:10 |
| 3 | 7.8.96 | 7:30 | 15:35 | 7:25 | 17:30 | 7:25 | 19:10 |
| 4 | 22.8.96 | 6:55 | 18:40 | 6:55 | 18:40 | 6:55 | 18:40 |
| 5 | 28.8.96 | 7:10 | 16:45 | 7:05 | 18:10 | 7:05 | 13:50 |
| 6 | 8.10.96 | 6:50 | 17:40 | 6:50 | 17:40 | 6:50 | 17:40 |
| 7 | 15.10.96 | 7:05 | 10:50 | 7:05 | 12:00 | 7:05 | 13:10 |
| 8 | 24.10.96 | 6:40 | 10:30 | 6:45 | 11:45 | 6:40 | 12:50 |
| 9 | 30.10.96 | 7:15 | 10:45 | 6:45 | 12:10 | 6:45 | 13:15 |

**Table 6.3:** *Data of model parameters a and $k_1(f)$ for step flow trials 1 to 9, $k_2(f)$ is always set to 1 due to insufficient knowledge.*

| SFT no | $T_a = \frac{1}{a}$ in hours | | | | $k_1$ | | |
|---|---|---|---|---|---|---|---|
| | Inlet | SP 1 | SP 2 | SP 3 | SP 1 | SP 2 | SP 3 |
| 1 | no data | 1.69 | 2.00 | 1.87 | 104.48 | 60.20 | 32.31 |
| 2 | no data | 4.18 | 1.89 | 2.61 | 1.24 | 3.53 | 3.47 |
| 3 | no data | 2.63 | 2.31 | 2.16 | 2.29 | 5.96 | 11.88 |
| 4 | no data | 0.43 | 1.41 | 1.18 | 3.01 | 5.08 | 5.05 |
| 5 | no data | 2.84 | 2.73 | 1.50 | 11.05 | 4.59 | 3.17 |
| 6 | 0.73 | 2.10 | 2.12 | 2.54 | 13.03 | 7.77 | 4.22 |
| 7 | 0.36 | 1.48 | 0.84 | 3.90 | 1.33 | 1.57 | 3.60 |
| 8 | 0.18 | 1.42 | 0.54 | 0.66 | 2.60 | 2.70 | 1.94 |
| 9 | 0.33 | 0.29 | 0.64 | 0.62 | 1.86 | 2.18 | 2.60 |

### 6.7.1 Parameters

Table 6.3 gives the parameters of the particle shear-off models (as presented in section 6.6) obtained from step flow trials 1 to 9. Note that SFTs 1–3 are flow increases from 0.08 l/s to 0.6 l/s and SFTs 4+5 from 0.08 l/s to 0.9 l/s, all five with no chlorine going into the rig. SFTs 6+7 are with chlorine and step from 0.08 l/s to 0.9 l/s, whereas SFTs 8+9 (again with chlorine) are flow increases from 0.3 l/s to 0.9 l/s.

The time constants $T_a = \frac{1}{a}$ of the exponential decay give the time it took to decrease the amount of sheared-off material to about 37 % of its start value

**Table 6.4:** *Statistical analysis of data concerning time constants $T_a$. All means and standard deviations are given in hours.*

| SFT no | Sample Size | Sample Mean $T_a$ | Standard Deviation $\sigma$ | Minimum Standard Deviation $\sigma_{min}$ for Normal Distribution |
|---|---|---|---|---|
| 1 | 3 | 1.85 | 0.153 | 0.088 |
| 2 | 3 | 2.89 | 1.171 | 0.676 |
| 3 | 3 | 2.37 | 0.236 | 0.136 |
| 4 | 3 | 1.00 | 0.514 | 0.297 |
| 5 | 3 | 2.36 | 0.742 | 0.428 |
| 6 | 4 | 1.87 | 0.786 | 0.487 |
| 7 | 4 | 1.64 | 1.571 | 0.974 |
| 8 | 4 | 0.70 | 0.522 | 0.324 |
| 9 | 4 | 0.47 | 0.184 | 0.114 |

(both times added to the final value). Thus, a small $T_a$ indicates quick decrease in sheared-off material. This model is based on the assumption that $T_a$ (or $a$) is the same throughout the pipe rig. This implies that the variation in each row of $T_a$-data in table 6.3 is purely random.

The smallest time constant is $T_a = 0.29$ h, the largest is $T_a = 4.18$ h, both are found in sample point 1 data. The time constants found from inlet data are generally lower than the values found for SP 1 to 3. All values are within the same order of magnitude. Note that the small time constant of the data originating from SP 1 at SFT 4 may be due to an increase of inlet particle counts during SFT 4.

Some statistical analysis of the time constant data is provided in table 6.4. The mean of the time constants $T_a$ of the three or four sample points is given in column 3. The sample standard deviation $\sigma$ is provided in column 4 of that table, the minimum standard deviation for the data of $T_a$ to be normally distributed is given in column 5. These values are calculated via eq. (5.2) on page 99 using a sample size of $n$=3 for SFTs 1–5 and $n$=4 for SFTs 6–9 (see column 2). The used $\chi^2$ statistic is then either $\chi^2_{0.05,2} = 6.0$ or $\chi^2_{0.05,3} = 7.8$ (see [18, p.21]). These sample sizes are too small for any strong statistically founded statements, thus, the results have to be taken as an indication only. From these data it is seen that

**Table 6.5:** *Approximation constants $c'$ and $c''$ during step flow trials 1 to 9.*

| SFT | SP 1 | | SP 2 | | SP 3 | |
|---|---|---|---|---|---|---|
| no | $c'$ | $c''$ | $c'$ | $c''$ | $c'$ | $c''$ |
| 1 | 0.2752 | 0.3615 | 0.2757 | 0.2756 | 0.2755 | 0.2757 |
| 2 | 0.2669 | 0.2664 | 0.2693 | 0.2675 | 0.2655 | 0.2697 |
| 3 | 0.2743 | 0.2711 | 0.2727 | 0.2776 | 0.3830 | 0.3372 |
| 4 | 0.1828 | 0.1926 | 0.1735 | 0.1919 | 0.1782 | 0.1780 |
| 5 | 0.1684 | 0.2469 | 0.1732 | 0.1845 | 0.1713 | 0.1861 |
| 6 | 0.1846 | 0.1953 | 0.1843 | 0.1912 | 0.1830 | 0.1853 |
| 7 | 0.1644 | 0.1775 | 0.1657 | 0.1761 | 0.1759 | 0.1835 |
| 8 | 0.1789 | 0.1729 | 0.1564 | 0.1712 | 0.1595 | 0.1751 |
| 9 | 0.2022 | 0.1890 | 0.1664 | 0.1915 | 0.1682 | 0.1823 |

especially for SFTs 2 and 7 a high standard deviation would be needed for this data to be normally distributed, all other SFTs may be normally distributed with standard deviations of less than 0.5 hours. This indicates that the time constants generally agree, including the results from inlet data.

The other coefficients given in the previously mentioned table 6.3 are the $k_1(f)$ of section 6.6. It is impossible under in the given circumstances to determine all three $k_1(f)$, $k_2(f)$ and the biofilm shedding profile $b(x)$ completely, but it is possible to obtain them up to a common factor $c$. Therefore, $k_2(f)$ is chosen to be 1 for all step flow trials. The values of $k_1(f)$ may differ from sample point to sample point reflecting the different sensitivities of the particle counters, however, if all particle counters were counting the same numbers for the same sample of water, all $k_1(f)$ would have been the same.

Table 6.5 gives the coefficients $c'$ and $c''$ of section 6.5.3. These coefficients should be equal, i.e. $c' = c'' = c$ should hold. Thus, these values give an indication on the goodness of the identification procedure and the appropriateness of the model for a particular SFT. From the table it is seen that the values agree well.

Finally, table 6.6 gives the final values of total particle counts at high flow (during the step flow trial) together with information on the inlet flow and inlet total chlorine regime. The values presented in columns 4–6 of table 6.6 are the difference between the final value of the particle counts response (to an increase in

**Table 6.6:** *Final values of total particle counts at high flow during step flow trials 1 to 9.*

| SFT no | Flow in l/s | Total Chlorine in mg/l | Final Value of $p(t)$ SP 1 | SP 2 | SP 3 |
|---|---|---|---|---|---|
| 1 | 0.6 | none | 49.9 | 59.3 | 24.0 |
| 2 | 0.6 | none | 39.1 | 19.0 | 17.6 |
| 3 | 0.6 | none | 12.3 | 20.7 | 37.2 |
| 4 | 0.9 | none | 42.8 | 19.0 | 21.0 |
| 5 | 0.9 | none | 11.8 | 15.8 | 14.0 |
| 6 | 0.9 | 0.4 | 14.5 | 2.7 | 2.2 |
| 7 | 0.9 | 0.4 | 5.5 | 0.4 | 7.9 |
| 8 | 0.9 | 0.4 | 9.6 | 9.9 | 6.4 |
| 9 | 0.9 | 0.4 | 8.9 | 4.5 | 6.1 |

flow) and the average of the pre-SFT particle counts after any occasional particle step has been removed. These values are quite important, because they give an indication of the combined net effect of the shear-off function $s(t)$ and the biofilm shedding profile $b(x)$.

The results presented in table 6.6 indicate that the trend in final values is generally downwards; later SFTs have frequently lower final values. In particular, large final values are seen at the first SFT, values of more that 10 particles per ml at SFTs 2 to 5 and final values predominately below 10 particles at SFTs 6–9. There does not seem to be a relationship with flow rate, however, with the introduction of total chlorine as disinfectant into the rig, the final values become generally smaller. However, these variations are not very pronounced.

### 6.7.2 Biofilm Shedding Profile

The apparent initial biofilm shedding profiles (BSP) of step flow trials 1 to 9 are presented in figs. 6.21 to 6.29. If appropriate, the data was filtered with a running average filter of the window size given in the captions. All settings of the design parameters are provided earlier in this section (see tables 6.1 and 6.2). Each graph shows the BSP as found from particle counts measured at sample point 1 (SP 1), sample point 2 (SP 2) and sample point 3 (SP 3). These curves

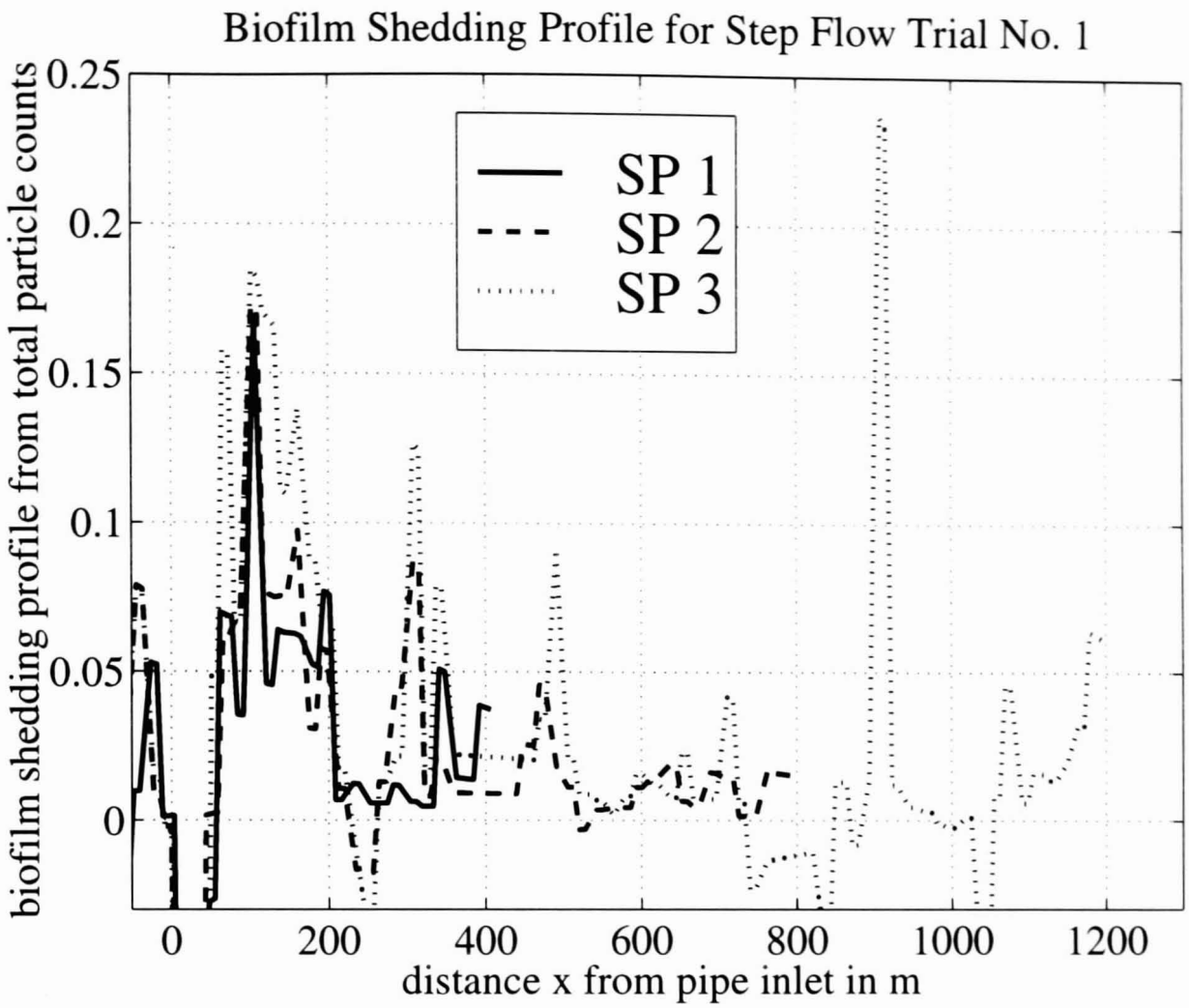


**Figure 6.21:** *Apparent initial biofilm shedding profile obtained from total particle counts of step flow trial 1, 25 July 1996. Filter window size is three, negative edge threshold is 50% of positive edge threshold.*

should ideally overlap. Negative distances as shown in figures 6.19 or 6.20 were excluded from the figures of this section, similarly negative BSP values (below -0.03) were cropped as well. Negative values of the BSP are physically impossible and, therefore, indicate data that does not fit the model. This may be due to noise in the particle counts or because of an incomplete peak erase. The latter will introduce negative or positive spikes in the vicinities of $x = 0$ m, $x \approx 450$ m, $x \approx 900$ m and at the end of the BSP.

The values of the BSP given on the ordinate have to be scaled to carry any direct physical meaning. This unknown scaling factor was already introduced at the end of section 6.5.3. Thus, the BSP magnitudes are meaningful in comparison with other values of the same BSP, but it is not possible to readily compare numerical values that originate from different SFTs. Note that the biofilm shed-

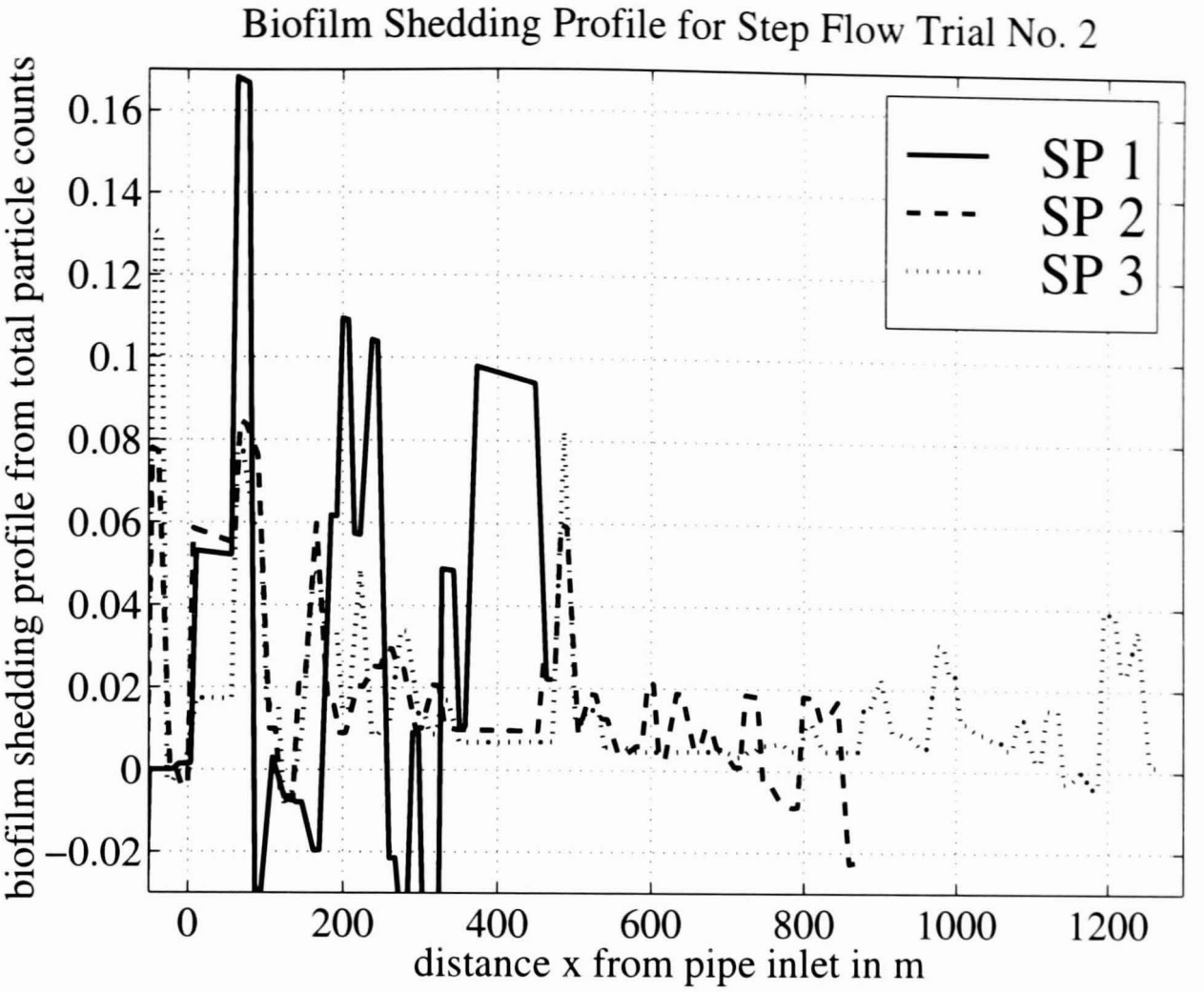


**Figure 6.22:** *Apparent initial biofilm shedding profile obtained from total particle counts of step flow trial 2, 1 August 1996. Filter window size is 19.*

ding profile is not a biofilm thickness profile. It is the amount of biofilm that is initially sheared-off from the pipe wall (up to an unknown factor) and as such shows the origins of high particle counts or the potential for shear-off over the distance of the rig.

The BSP as found from sample point 3 during SFT 3 (fig. 6.23) is not provided since particle counter 3 did not work properly during the first hours of that step flow trial. The high BSP values between 400 m and 750 m of SFT 4 in fig. 6.24 are not completely reliable since they might be partially due to the unusual increase of inlet particle counts during that SFT.

In the first three SFTs (figs. 6.21 to 6.23) the BSP is initially very high and decreases with a large gradient within the initial 400 m. In these three SFTs a high flow of 0.6 l/s was used and there was no chlorine present. SFTs 4 and 5

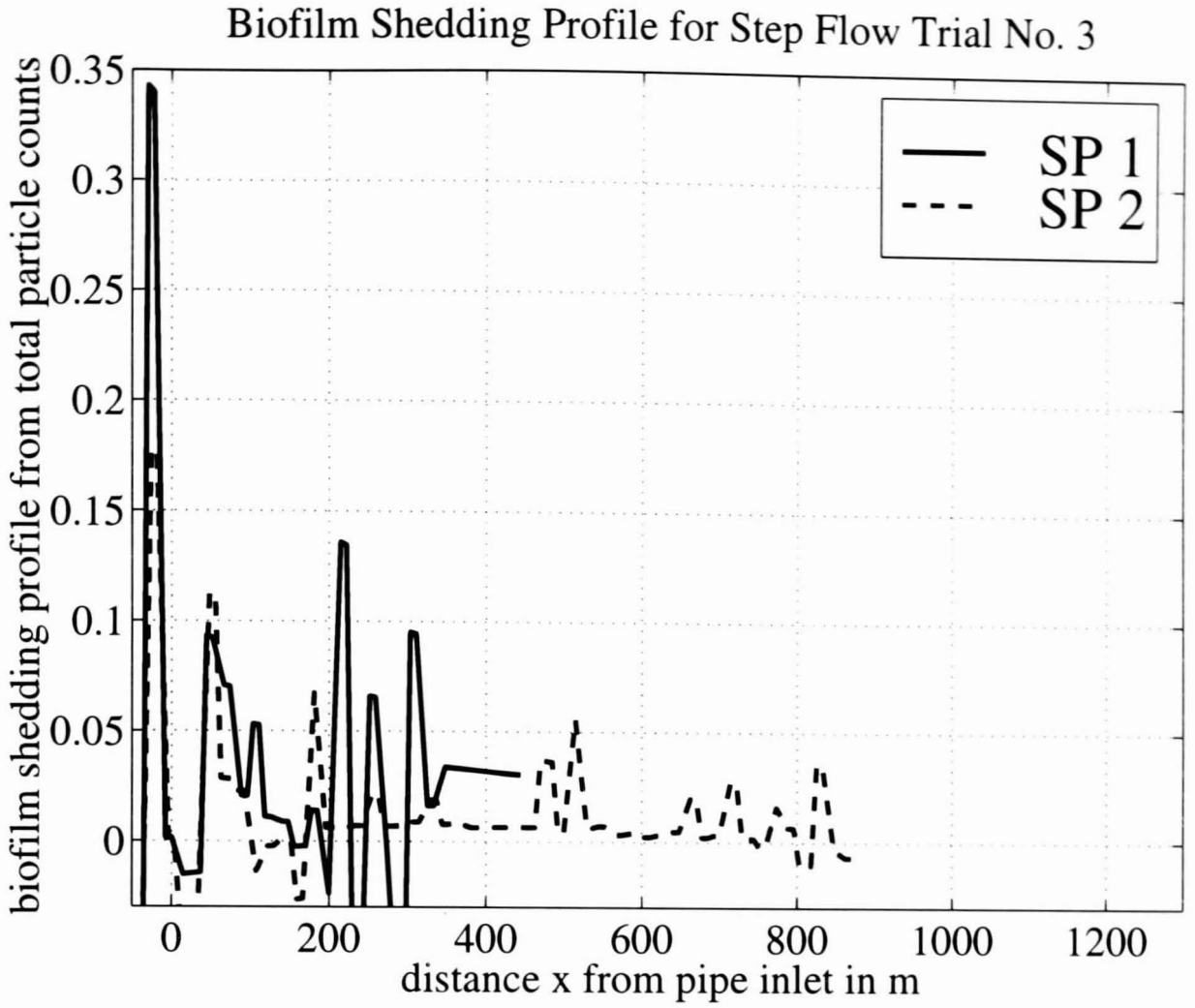


**Figure 6.23:** *Apparent initial biofilm shedding profile obtained from total particle counts of step flow trial 3, 7 August 1996. Filter window size is 19.*

are the last SFTs with no chlorine, however, the higher flow rate was 0.9 l/s. From figs. 6.24 and 6.25 it is seen that the BSPs of these SFTs exhibit relatively large magnitudes also for larger distances from the pipe rig inlet ($x > 500$ m). However, as mentioned above, the large counts of fig. 6.24 (SFT 4) might be spurious. Note that this increase in BSP for larger distances does not necessarily imply that more particles originate from these locations compared to SFTs 1–3, but it indicates that *relative to* the biofilm shedding in the first 400 m of each BSP, more particles are sheared-off in the later sections of the pipe rig.

Step flow trial 6 (fig. 6.26) is the first step flow trial after chlorine is re-introduced into the pipe rig. The high flow rate was 0.9 l/s. This SFT exhibits a close to constant BSP for the first 300–350 m and then a sharp decline to small values.

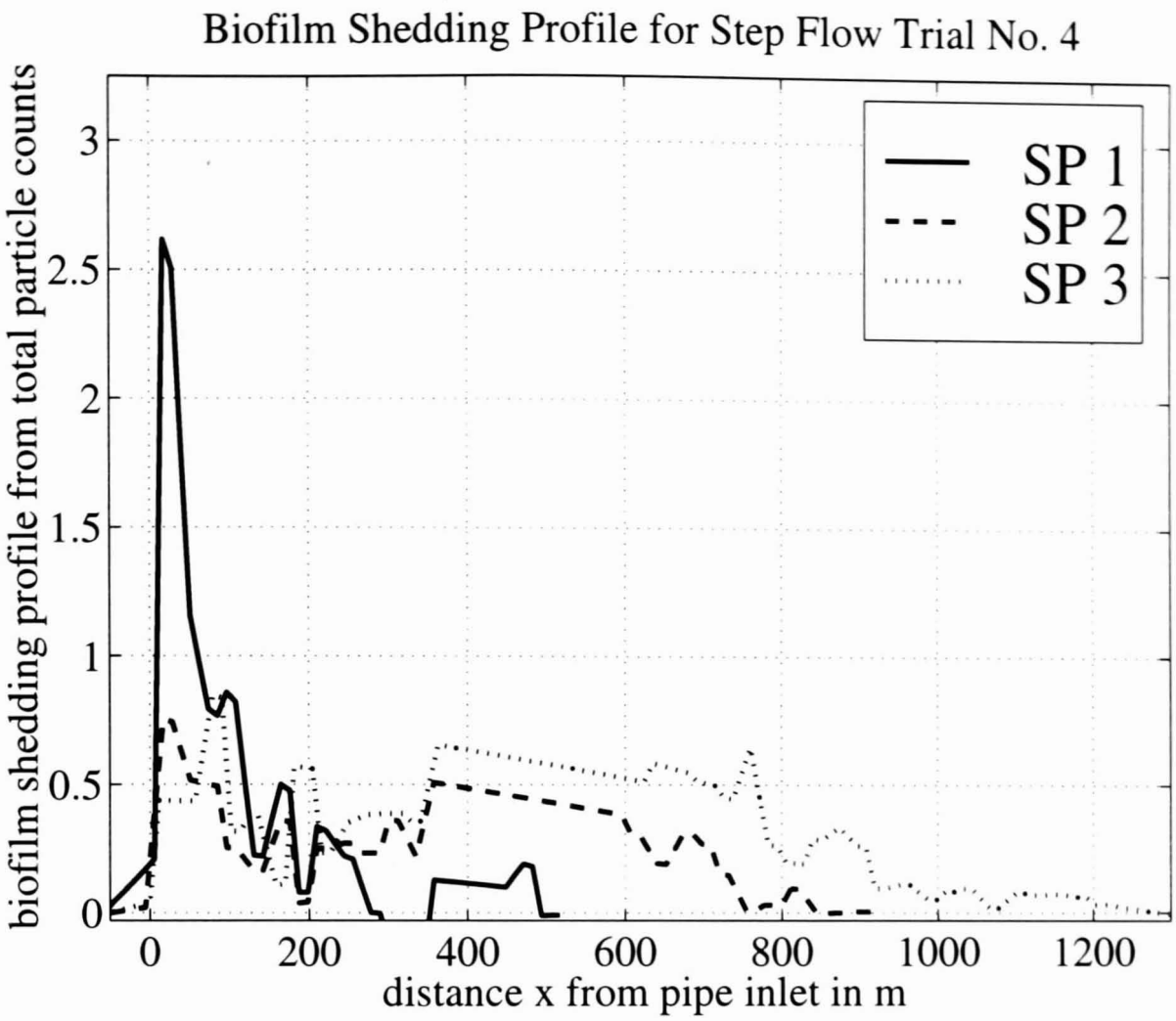


**Figure 6.24:** *Apparent initial biofilm shedding profile obtained from total particle counts of step flow trial 4, 22 August 1996. Filter window size is 15.*

SFTs 7–9 (figs. 6.27–6.29) all had a high flow rate of 0.9 l/s with total chlorine present in the pipe rig. The BSPs shown in figs. 6.27–6.29 are distributed over the whole pipe rig with similar magnitude, however they are very patchy. Note that these SFTs exhibit many traits of the extended model (cf. section 6.4.1.4) and therefore the application of the basic model, as done in this work, is more critical than in other SFTs. The data range was restricted to a time span were the basic model seems appropriate (cf. table 6.2), which should alleviate that problem.

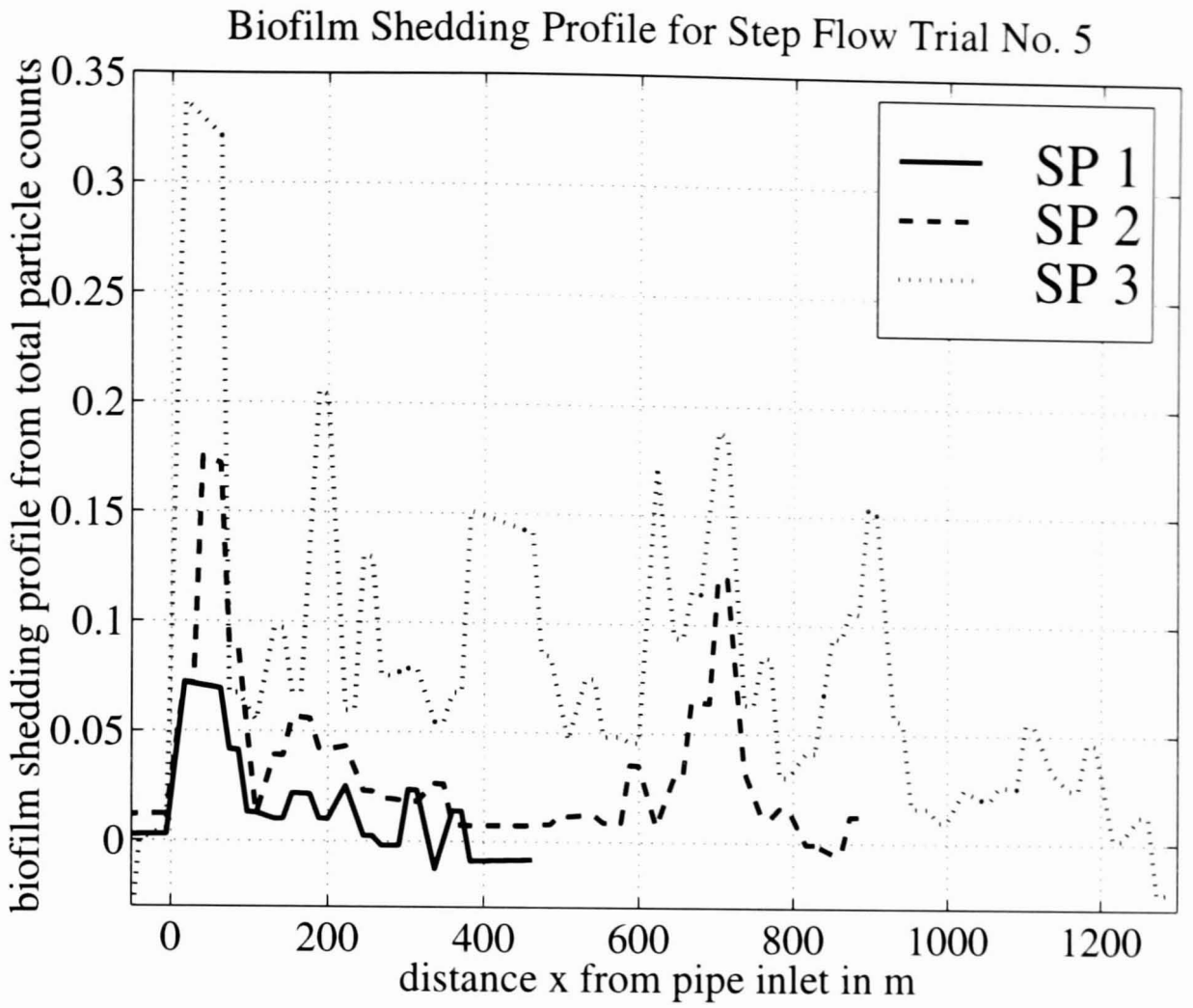


**Figure 6.25:** *Apparent initial biofilm shedding profile obtained from total particle counts of step flow trial 5, 28 August 1996. Filter window size is 13.*

## 6.8 Discussion

The initial biofilm shedding profile gives some indication about the state of the system before the step flow trial. It is a snapshot of sheared-off material at the start of the SFT. Thus, locations of the detachment of large numbers of particles are identified. The relationship to biofilm thickness or consistency is in principle unknown. Possibilities include a linear relationship to biofilm thickness, a linear relationship to the thickness of one layer of biofilm (perhaps related to the impact of the turbulent flow) or a dependence on the structure of biofilm, e.g. a lower shear-off for biofilm with many filaments.

A change in biofilm thickness would be expected with the introduction of chlorine. Without any disinfectant in the system it is likely that the depletion of nutrients is the overriding reason for a reduction of biofilm thickness over the

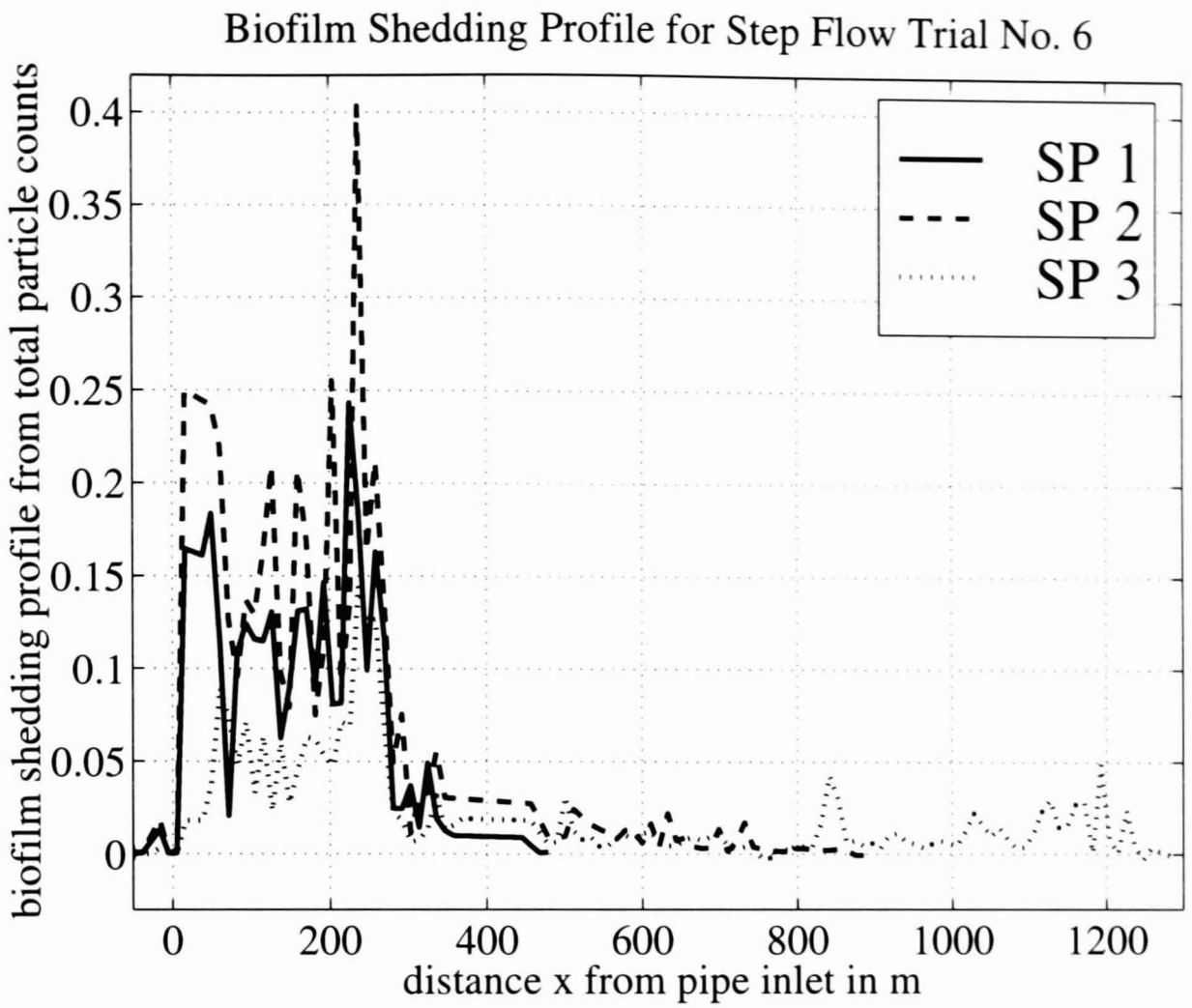


**Figure 6.26:** *Apparent initial biofilm shedding profile obtained from total particle counts of step flow trial 6, 8 October 1996. Filter window size is 11, negative edge threshold is 40% of positive edge threshold.*

length of the rig, however, with the introduction of monochloramine it is expected to see some destruction of biofilm in the part of the pipe rig that is reached by the disinfectant. SFT 6 holds a special position in this context, since it was performed soon after the re-introduction of monochloramine and, therefore, it may show a pipe rig condition in between these two cases.

These changes of biofilm thickness should effect the BSP. As presented in the previous section, a variation of the shape of the biofilm shedding profile is seen for different SFTs. The first three SFTs provide a good match with the expectations of a decreasing amount of biofilm with distance. SFTs 4 and 5 show the same behaviour, however the gradient is smaller. As mentioned above, SFT 6 holds a special position, since it is likely that the biofilm had not yet reached a steady state after the introduction of monochloramine. The initial plateau that

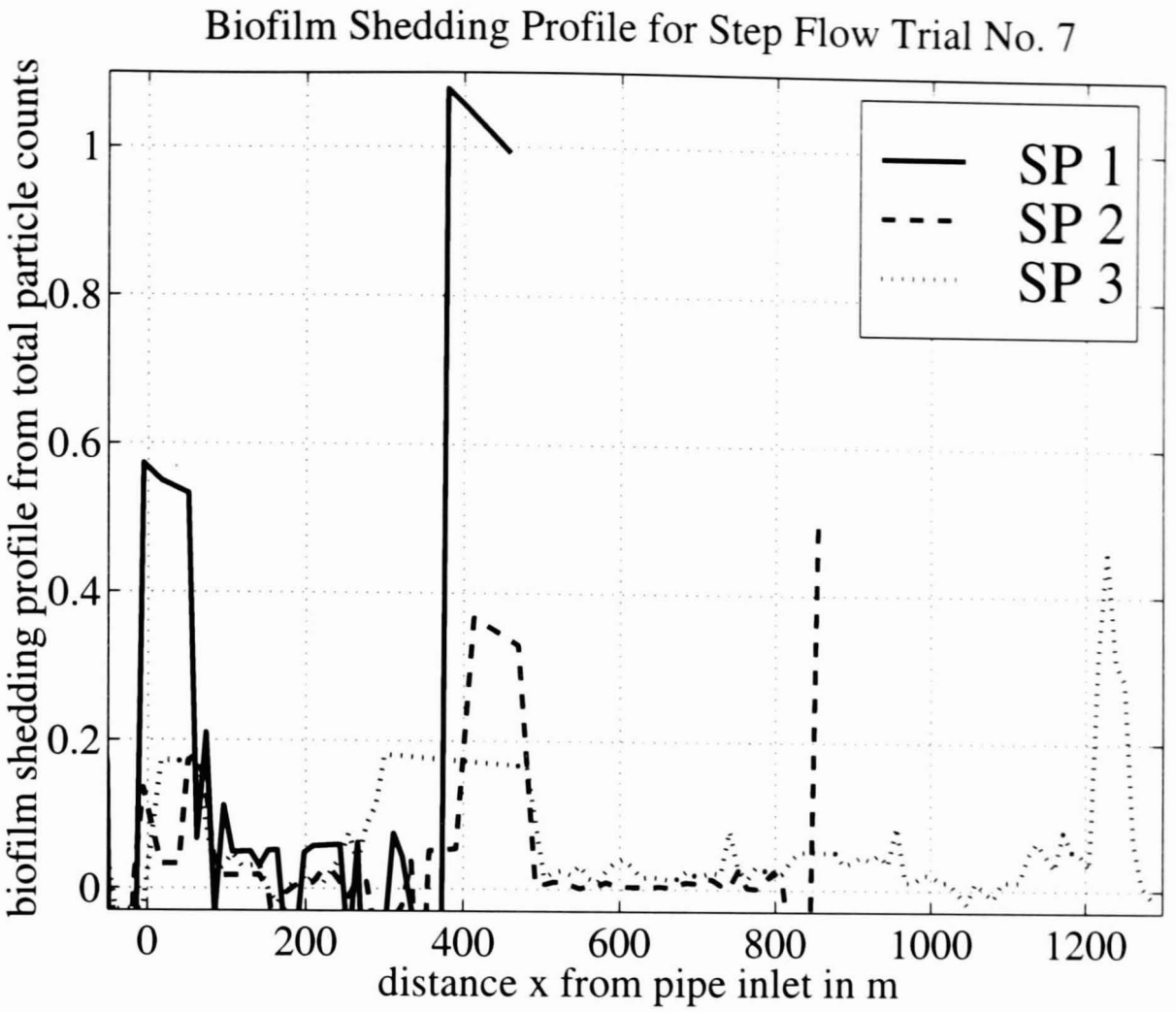


**Figure 6.27:** *Apparent initial biofilm shedding profile obtained from total particle counts of step flow trial 7, 15 October 1996. Filter window size is 11.*

is apparent in fig. 6.26 matches that interpretation. However, the following BSPs (SFTs 7–9) should start with smaller values (where monochloramine disinfected the rig), reach a maximum and then decline with declining availability of nutrients (like SFTs 1–5). But they exhibit fairly large counts at several places through the pipe rig and do not show any clear pattern, neither decreasing nor with maximum value. The reason for this is likely to be that the amount of biofilm that is left on the pipe surface is significantly less than during the first SFTs due to the combined effect of the previous SFTs, the introduction of monochloramine and the reduction of temperature.

The final values of $p(t)$ (table 6.6) support this conclusion. These values, which represent a net result of shedding, become much smaller towards later SFTs. It is important to note that the numerical values obtained from parti-

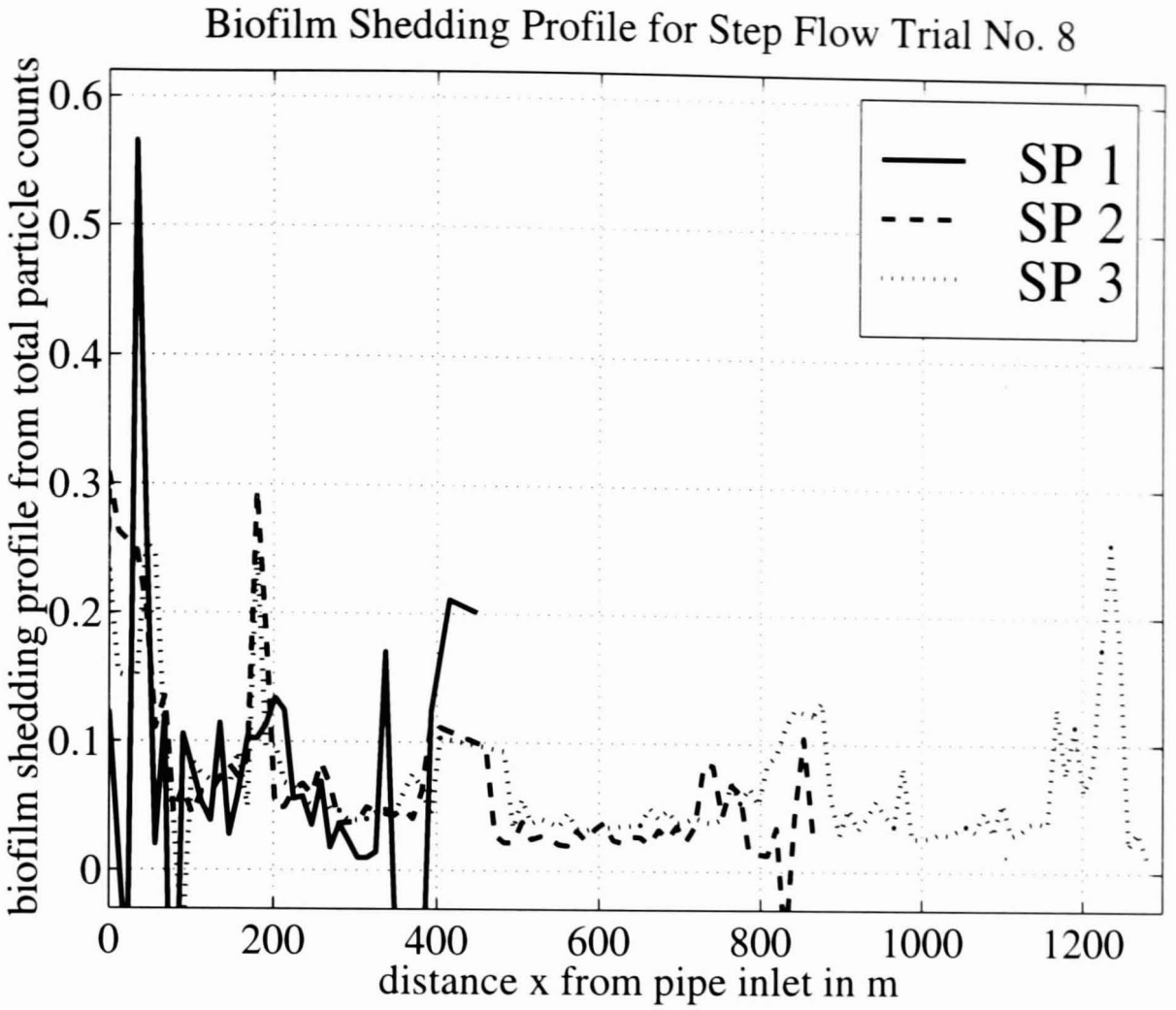


**Figure 6.28:** *Apparent initial biofilm shedding profile obtained from total particle counts of step flow trial 8, 24 October 1996. Filter window size is 15.*

cle counts are subject to measurement errors arising from variations in particle shapes, as discussed in section 5.2. The time constant is not effected by this problem. This parameter describes the transient time behaviour of particles after a flow increase whereas the final value describes the steady state. The transient behaviour describes the strength of the attachment of the biofilm. Both, steady state and transient parameters provide information on the effect of the conditions (or regime) in the pipe rig on the amount of sheared-off material. Since the investigation discussed here was dominated by relatively short SFTs (3–4 travel times, approximately 14–48 hours), it is possible that the final value describes a short-term steady state and that it is modified in the long-term.

These long-term dynamics are, however, not part of the particle counts model presented in this chapter. This model is predominately concerned with the tran-

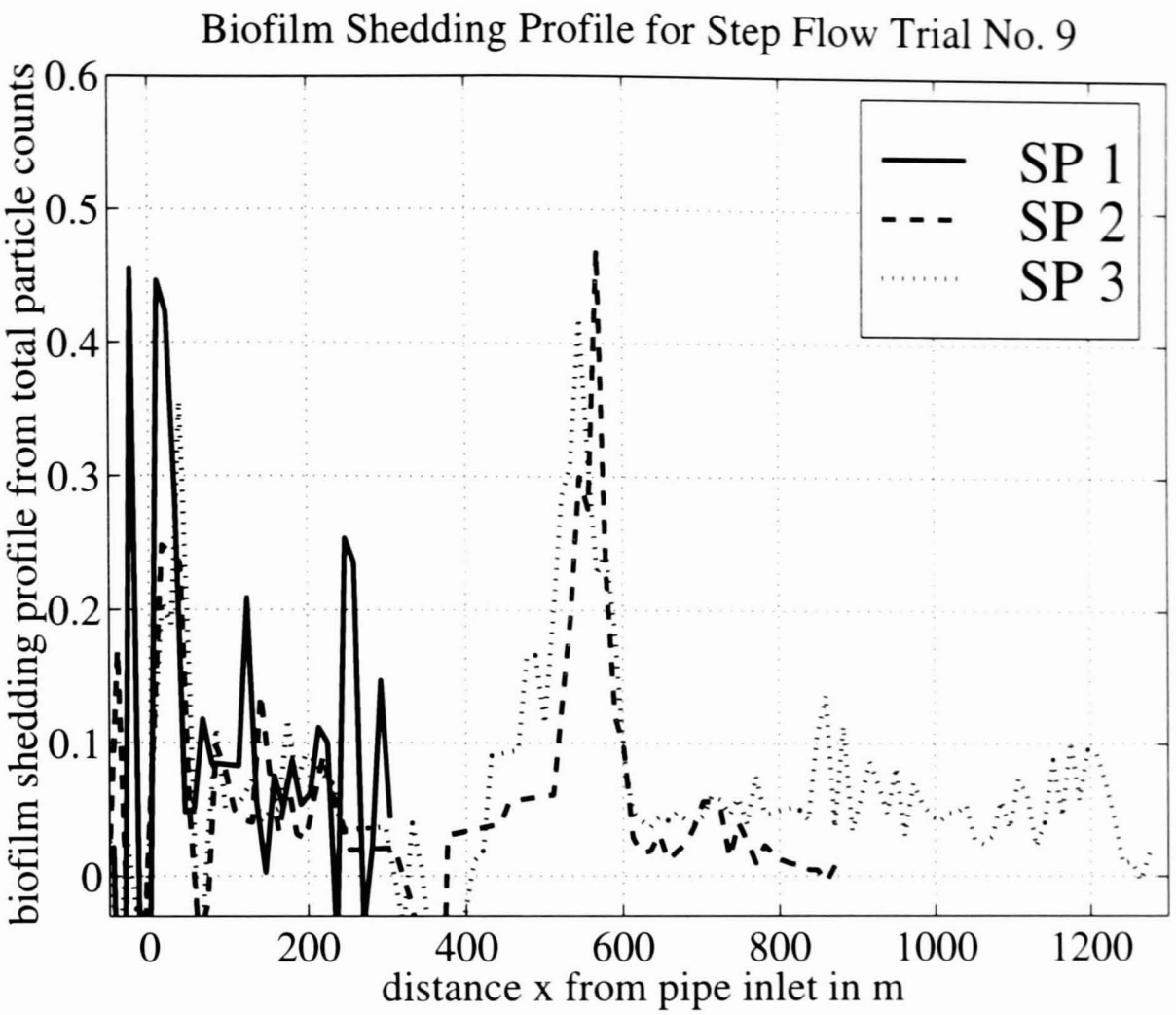


**Figure 6.29:** *Apparent initial biofilm shedding profile obtained from total particle counts of step flow trial 9, 30 October 1996. Filter window size is 15.*

sient response of particles to a step in flow. The dynamics involved in biofilm detachment are generally reduced to a linear time dependency in the literature, as is discussed in the literature review in section 2.4.3 on page 17, cf. [137, 115, 122, 28, 61, 6]. However, in the case considered in this thesis the transient shear-off did have an important impact on the biofilm in the pipe rig. Not only does it dominate the 10–20 hours of the particle counts response, but it also reduces the amount of biofilm in the pipe rig noticeably. The exponential dynamics as used in this model are an important part of the new approach of this thesis.

Thus, the model presented in this chapter was shown to be a useful tool for understanding the underlying processes of biofilm detachment and the dynamics of suspended particles in the pipe rig. Its parameters and the initial biofilm

shedding profile give information about the condition of the system and the likely locations of the origin of high particles incidents. The measurement of biofilm thickness *in situ* is currently still a major challenge (cf. section 2.4.5), with this model, step flow trials and the initial biofilm shedding profile provide together an indirect (and destructive) measure of the biofilm shedding potential which can give valuable information about the condition of the distribution system.

## 6.9 Validation and Limitations

The validity of the parametric particle counts model developed in this chapter cannot be proven, since its development is based on data, however, evidence of the validity of the model can be shown.

- The inlet particle counter response matches the assumed shear-off function $s(t)$ (cf. section 6.4.1.7).
- The resulting Biofilm Shedding Profile has a meaningful interpretation.
- The errors between the exponential tail data and the fitted exponential function are small.

A possible further validation of the model would be to install *in-situ* biofilm sensors to monitor the thickness and, thus, the shear-off from biofilms. However, this technology is not currently available. Another option would be to freeze and cut out the pipes and analyse the amount of biofilm left on the surface. It would be possible to obtain only sparse results using this method and although feasible it is not very practical. The most practical way for improved validation are more experiments of the kind reported in this thesis.

It is also important to be understand clearly the limitations of this model.

- The model is valid for a step flow input only.
- The parameters $k_1(f)$ and $k_2(f)$ depend on the magnitude of the flow step.
- It may be necessary to extend the basic model of the Slow Signal to match data (see 'Extended Model of the Slow Signal,' section 6.4.1.4).

- Absolute values of different particle counters do not agree well (see section 5.2) and therefore it is necessary to fit $k_1(f)$ and $k_2(f)$ for each counter.

## 6.10 Implementation

All calculations presented in this chapter are included in the Water Quality Toolbox for Matlab (cf. appendix C).

The numerical statistical simulations of section 6.3.1 are done in the Matlab scripts `st_tpc1` (figures 6.3 and 6.4), `st_tpc2b` (figure 6.5), `st_tpc3a` (figure 6.6) and `st_tpc4` (figure 6.8). The calculations for the particle counter size distributions (section 6.3.2) are done in `st_sdpc1` and `st_sdpc2`.

The analysis of the total particle counts as discussed in sections 6.4 to 6.8 is implemented in `bioprofi`. This function calls several other functions during execution, i.e `peakdetect` is used for the detection of peaks (cf. section 6.5.1.2), `wfitfun` is the error function for the identification of the parameters $c_1(T)$, $c_2(T)$ and $a$ of the exponential tail (see section 6.5.2) and `bioapprox` is used for the determination of the parameters $k_1(f)$ and $k_2(f)$ as discussed in section 6.5.3. The function `bspinvsim` simulates the inverse system to obtain the biofilm shedding profile as introduced in section 6.6.

A data file `shdata.mat` containing the step heights of the occasional particle steps was generated before using `bioprofi`. This is done by `dostepheight`. This script uses the function `findstepheight`, which is interactive, for that purpose. This function is also called automatically from `bioprofi` if the file `shdata.mat` does not exist in the search path.

The script `bioscript`, that employs `bioprofi`, was used to generate the results presented in section 6.7. The script `biogiveout` produces the body of the tables given in that section for inclusion in this thesis.

## 6.11 Conclusions

This chapter discussed the particle counts response to a step increase in flow. For that both non-parametric (i.e. numerical and statistical) and parametric models of total particle counts were presented and a brief discussion of a numerical statistical model of particle counter size distributions was included.

All models are based on observed data. Thus, the difficult issue of the determination of the model structure was solved via specifications derived from data and assumptions validated by model fitting.

The basic parametric model covers the 'Slow Signal' of the particle counter response. Specifications that have to be fulfilled in this case for the model to match the data are provided in section 6.2, specifications for an extended model are presented as well in that section. The assumptions of sections 6.4.1.3 and 6.4.1.4 set the foundation for the development of the model. They introduce a local shear-off density and the separation of the effects of biofilm over distance and time dynamics. In addition the dynamics are assumed to be exponential. The mathematical model for a step increase of flow (see section 6.4.2) becomes a linear model (a convolution) which allows for parameter identification despite incomplete knowledge of the input signal.

Results include parameters that describe the net effect of the sheared-off biofilm over the length of the rig and the dynamics associated with the shear-off process. The initial biofilm shedding profile (BSP) is another important result, it gives a profile of the locations of sheared-off material along the rig and therefore provides a tool for the assessment of the condition of the pipe rig.

Particles and biofilm are an important indicator of water quality. The model presented in this section gives some more insight into the processes associated with flow increases and particle shear-off from biofilms. Another frequently used indicator of water quality, the disinfectant, will be the object of the next chapter.

# Chapter 7

# Comparison of Models of Monochloramine Decay

## 7.1 Introduction

The aim of this chapter is to investigate two commonly used chlorine decay models in detail, i.e. a single decay coefficient model and the combined bulk and wall demand model used in Epanet [123]. These models are adapted for the use of monochloramine as disinfectant and compared to each other. In addition, data from bottled samples are presented and compared to results obtained from the pipe rig.

An introduction to chlorine or monochloramine as disinfectant and an overview of the relevant literature was given in section 2.6.2 on page 34. Section 5.3 on page 101 provides an account of the preprocessing procedure that was done prior to the calculations given in this chapter.

The publication by the author together with R. S. Powell and C. A. Woodward of 1997 [97] gives an account of earlier results, using the same or very similar methods. Additional analyses are included in this chapter. Note that, however, a different correction procedure (i.e. reverse-calibration with no further windowing) was used for the preprocessing of the data considered in this chapter (see section 5.3.2).

## 7.2 Review of Chlorine Kinetics

Most work on disinfection kinetics is concerned with free chlorine ($Cl_2$ or $HOCl^-$). It is frequently assumed that free chlorine decays according to first order reaction kinetics [25, 60]. A chlorine concentration $c(x,t)$ that is decaying with time in a flow system is described by the general partial differential equation given in eq. (2.7) on page 35 [126]

$$\frac{\partial c(x,t)}{\partial t} + \frac{f}{A}\frac{\partial c(x,t)}{\partial x} = -Kc(x,t). \tag{7.1}$$

This equation is valid for a constant velocity $v = \frac{f}{A}$, where $f$ is the volumetric flow rate and $A$ is the area of a pipe cross-section. The variables $x$ and $t$ represent distance along the rig and time, respectively, and $K$ is the decay coefficient of chlorine. If $K$ is constant this type of decay is referred to as first order.

For the simple one-dimensional system that is considered in this thesis, eq. (7.1) is solved by

$$c(x_2,t_2) = c(x_1,t_1)\cdot \mathrm{e}^{-K(t_2-t_1)} \tag{7.2}$$

with

$$x_2 - x_1 = v\cdot(t_2 - t_1), \tag{7.3}$$

where $t_1$, $t_2$ represent time, $x_1$, $x_2$ represent distance along the pipe and $v$ is the constant velocity of water in the pipe. Therefore, the decay of free chlorine is characterised by just one (constant) decay coefficient $K$. The travel time between points $x_1$ and $x_2$ is $\tau = \frac{x}{v} = t_2 - t_1$. For discrete time, eq. (7.2) can be rewritten in the following form

$$c(x + v\cdot\Delta t, t + \Delta t) = c(x,t)\exp(-K\Delta t). \tag{7.4}$$

This equation is equivalent to eq. (7.2), however it allows us to deal with varying parameters $v$ and $K$ since they need to be constant only within the hydraulic

time step $\Delta t$, which in the case considered here is chosen to be equivalent to the sampling time.

In particular, a possible variation of the decay coefficient $K$ may be required, since in recent years more evidence has been published that shows that simple first order kinetics do not fully match the behaviour of free chlorine in a distribution system. Lungwitz *et al.* [92] investigated booster (impulse) chlorination and found that they had to postulate several decay coefficients depending on the chlorine gradient. Schneider *et al.* [128] concluded that the decay coefficient (and possibly other parameters) are flow dependent. Woodward *et al.* [160] found experimentally that the monochloramine decay coefficient changes with flow rate. Heraud *et al.* [67] used different decay coefficients depending on pipe materials and diameter to fit their model to the data.

Simulation packages reflect these findings to some extent. In Piccolo [127] it is possible to use a chlorine decay coefficient, $K_{H_20}$, which depends on total organic carbon and temperature or to use diameter dependent decay coefficients within the distribution system. Epanet [123, 124] includes a wall demand and a flow dependent mass transfer coefficient. Thus, it replaces the constant decay coefficient $K$ with

$$K = k_b + \frac{k_f k_w}{R_H(k_f + k_w)} \tag{7.5}$$

where $k_f$ is a flow dependent mass transfer coefficient, $k_b$, $k_w$ are constants representing bulk and wall demand respectively and $R_H$ is the hydraulic radius.

The mass-transfer coefficient $k_f$ is calculated as

$$k_f = Sh\frac{D}{d} \tag{7.6}$$

$$Sh = 0.023 Re^{0.83} Sc^{0.333} \quad \text{for } Re \geq 2300 \tag{7.7}$$

$$Sh = 3.65 + \frac{0.0668\frac{d}{L}ReSc}{1+0.04\left(\frac{d}{L}ReSc\right)^{0.67}} \quad \text{for } Re < 2300 \tag{7.8}$$

where $k_f$ mass transfer coefficient [m/s],

$Sh$ Sherwood number,

(or Nusselt number for mass transfer),

$Re = \frac{fd}{A\nu}$ Reynolds number.

$Sc = \frac{\nu}{D}$ Schmidt number,

$d$ pipe diameter [m],

$L$ pipe length [m],

$f$ flow rate [$m^3/s$],

$A$ cross-sectional flow area of pipe [$m^2$],

$D$ molecular diffusivity of substance in fluid [$m^2/s$],

$\nu$ kinematic viscosity of fluid [$m^2/s$].

Compare p. 17 in [124], pp. 128 and 142 in [50] or p. 176 in [68] to validate these equations. The kinematic viscosity $\nu$ of water is $10^{-6}\frac{m^2}{s}$, the Schmidt number of diluted chlorine in water at $68^0$F is $Sc = 824$. These numbers and the above units are given for $k_w$ in m/s and $k_b$, $K$ in 1/s. In the implementation a factor of 3600 seconds/hour converts the term that includes $k_w$ to the unit 1/h such that $k_b$ and $K$ can be used in 1/h, while $k_w$ remains in m/s.

## 7.3 Total Chlorine Kinetics

In the present study monochloramine is investigated since it is used in the London distribution system, and it also finds application in other water networks worldwide, e.g. [141]. Monochloramine ($NH_2Cl$) is generally believed to behave in the same fashion as free chlorine, only that it reacts more slowly than free chlorine [156], also it was suggested that monochloramine is more efficient against biofilms than free chlorine [85, 151].

To date, it is impossible to measure monochloramine directly online. Thus, total chlorine, which includes free chlorine, monochloramine and organic chloramines, is measured using online meters. When ammonia is added in the correct ratio to free chlorine residuals, there will be no free chlorine left. However, organic chloramines, in addition to monochloramine, are generally still present in the wa-

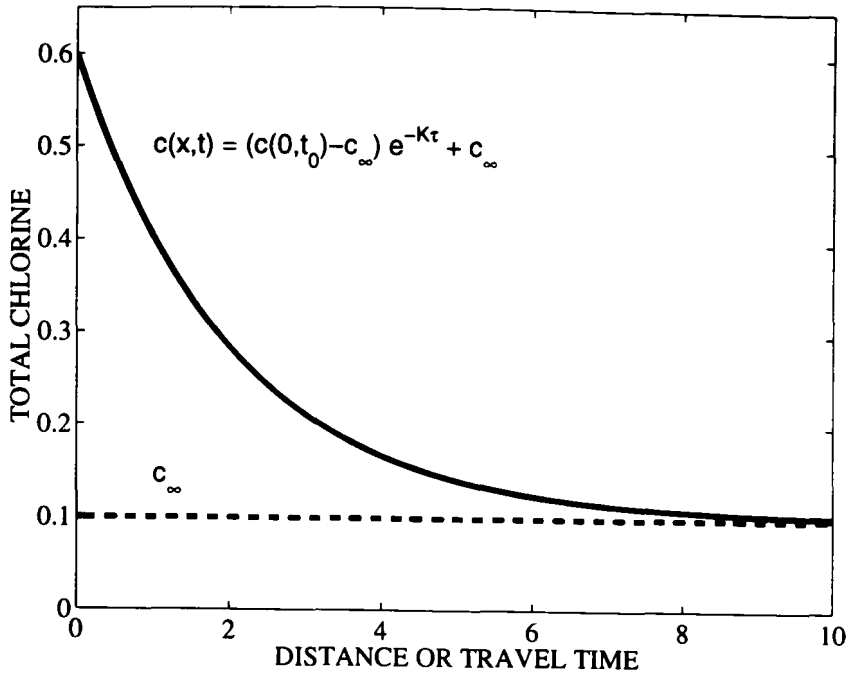


**Figure 7.1:** *Simple first order decay of total chlorine.*

ter. These organic chloramines are relatively stable and have a very low bacterial action [52] and thus are considered as a constant fraction of total chlorine in this work.

Thus, first order kinetics as in fig. 7.1 are obtained, which can be described as

$$c(x_2, t_2) = (c(x_1, t_1) - c_\infty) \cdot \mathrm{e}^{-K(t_2 - t_1)} + c_\infty. \tag{7.9}$$

Note that $c(x, t)$ is the total chlorine concentration at $x, t$. Monochloramine is the reactive fraction of total chlorine, or $c(x, t) - c_\infty$, while $c_\infty$ is the non-reactive fraction of total chlorine, i.e. the organic chloramines.

To simplify notation in the following only the pipe rig inlet will be considerd as reference point $x_1 = 0$. To signify this, $t_0$ is written instead of $t_1$ and the index 2 is dropped from the left hand side of eq. (7.9). As before, the travel time $\tau = t_2 - t_1 = t - t_0$ can be used in the argument of the exponential function. With these changes eq. (7.9) becomes

$$c(x, t) = (c(0, t_0) - c_\infty) \cdot \mathrm{e}^{-K\tau} + c_\infty. \tag{7.10}$$

As elaborated earlier, it may be more realistic to replace the constant coefficient $K$ in eq. (7.10) by a function depending on flow, pipe materials, and possibly other variables. In sections 7.4 and 7.6, the dependencies of $K$ on flow and inlet chlorine concentration are investigated.

## 7.4 Determination of Decay Coefficients

Two possible descriptions of monochloramine decay as in eq. (7.10) were studied.

1) $K = \text{const.}$, and

2) $K = k_b + \frac{k_f k_w}{R_H(k_f + k_w)}$, as used in Epanet.

To calibrate both models the unknown parameters $K$ and $c_\infty$ (case 1) or $k_b$, $k_w$ and $c_\infty$ (case 2) have to be found such that the data fits a model according to eq. (7.10).

### 7.4.1 Parameter Estimation for the Single Decay Coefficient Model

If only free chlorine and a single decay coefficient as in case 1 are considered, it is possible to reduce this problem to a linear regression by taking the natural logarithm on both sides of eq. (7.2) and estimating $\ln c(x_1, t_1)$ or $\ln c(0, t_0)$ and $K$. A weighted least-squares algorithm has to be used to remove the bias introduced by taking the logarithm. This approach may also be suitable for the monochloramine problem eq. (7.10) if $c_\infty$ is known or otherwise estimated, however, data values that are smaller than the final value $c_\infty$ can not be included in the estimation since they would lead to a logarithm of a negative value, which is a complex number.

To apply this approach, first the natural logarithm of eq. (7.10) has to be taken to obtain

$$\tilde{c}(x, t) = \tilde{c}(0, t_0) - K\tau. \tag{7.11}$$

with

$$\tilde{c}(x,t) = \ln\left(c(x,t) - c_\infty\right), \tag{7.12}$$

$$\tilde{c}(0,t_0) = \ln\left(c(0,t_0) - c_\infty\right). \tag{7.13}$$

A standard weighted least-squares error function $J_1$ has to be minimised over $K$ and $\tilde{c}(0,t_0)$ with

$$J_1 = \sqrt{\sum_{j=1}^{n_1}\sum_{i=1}^{n_2}\left(w(i,j)\left[\tilde{c}_c(x_j,t_i) + K\tau(i,j) - \tilde{c}(0,t_{0,i})\right]\right)^2} \tag{7.14}$$

The index $i$ of $t_i$, $t_{0,i}$ indicates that chlorine readings at $n_2$ time instants are considered, the index $j$ of $x_j$ implies that $n_1$ locations along the rig are used to obtain a best estimate of $K$. The upper limits $n_1$ and $n_2$ define the size of the sample used for estimating $K$, in general a larger sample will give a better estimate. In the case of the pipe rig $n_1 = 3$, since there are three sample points in the pipe rig. The weights $w(i,j)$ and the travel time $\tau(i,j)$ depend on distance and point in time. The total chlorine reading $\tilde{c}_c(x_j,t_i)$ is the corrected meter reading as opposed to calculated values which are not indexed.

The weight $w(i,j)$ for an unbiased estimate is found by considering an approximation of the derivative of the logarithm. It is

$$\frac{\mathrm{d}\ln x}{\mathrm{d}x} = \frac{1}{x} \approx \frac{\ln(x+\Delta x) - \ln x}{\Delta x} = \frac{\Delta \ln x}{\Delta x}. \tag{7.15}$$

The error function $J_1$ contains for $w(i,j) = 1$ a difference of logarithms of $c(x,t)$ as in the above equation. An unbiased estimate, however, has to include a difference of $c(x,t)$. This difference of $c(x,t)$ relates to the difference of logarithms according to eq. (7.15) as $\Delta c(x,t) = c(x,t) \cdot \Delta \ln c(x,t)$, and thus

$$w(i,j) = c_c(x_j,t_i). \tag{7.16}$$

Due to the fact that data values smaller than $c_\infty$ have to be excluded, this approach does not necessarily perform well, instead, solving a nonlinear optimisation problem is preferable.

Then, the problem is reformulated to find the minimum over $K$ and $c_\infty$ of

$$J_2 = \sqrt{\sum_{j=1}^{n_1}\sum_{i=1}^{n_2}(c_c(x_j,t_i) - g_1(j,i;K,c_\infty))^2}, \tag{7.17}$$

with

$$g_1(j,i;K,c_\infty) = (c_c(0,t_{0,i}) - c_\infty)\exp(-K\tau(i,j)\,) + c_\infty, \tag{7.18}$$

where $c_c(x_j,t_i)$ is the corrected chlorine meter reading at time $t_i$ and distance $x_j$, and $\tau(i,j)$ is the travel time between $x_j$ and $x=0$ determined for the aliquot of water that is at time $t_i$ at $x_j$. The measurement $c_c(0,t_{0,i})$ is the corrected meter reading at the inlet for the time when the aliquot of water that reaches $x_j$ at time $t_i$ started its travel. The indices $i$ and $j$ indicate again that several time and distance values are used for estimation. Instead of using the data value $c_c(0,t_{0,i})$ this value could be estimated as well.

To minimise the cost function, $J_2$, a Nelder-Mead type simplex algorithm for nonlinear systems as implemented in MATLAB is employed [107]. It is among the most popular and successful direct search methods which do not require the gradient. Roughly speaking the minimum is found by repetitive 'casting of a net'. In more detail, a simplex of order $n+1$ is constructed among the initial values of the $n$ parameters to be estimated. The initial value is iteratively improved by contracting or expanding the simplex and shifting the corner with the highest cost function toward the minimum, for instance by reflecting the worst corner through an appropriately chosen centroid.

### 7.4.2 Parameter Estimation for the Model With Two Decay Coefficients

In case 2, the decay coefficient $K$ is defined by eq. (7.5), thus it includes the flow and diameter dependent parameters $k_f$ and $R_H$. In this work only the flow dependence is considered (flow is varied in steps during SFTs). Using a decay coefficient as in eq. (7.5) in eq. (7.10) is valid only if for the whole period of investigation $\tau = t - t_0$ the flow does not change. Since the distance between the investigated points $x_j$ is in the considered case relatively large, this condition is not fulfilled. For this reason it is necessary to break up the time interval $\tau$ into small time steps $\Delta\tau \equiv \Delta t$ in which the flow is constant. Thus, eq. (7.10) becomes

$$\begin{aligned} c(x_j, t_i) =& c_\infty + (c(0, t_0) - c_\infty) \times \\ & \times \exp\left(-k_b \tau(i,j) - \sum_{m=0}^{n_3} \frac{k_f(m) k_w}{R_H(m)(k_f(m) + k_w)} \Delta t(m)\right), \end{aligned} \tag{7.19}$$

where $n_3$ is defined by the travel time $\tau(i,j)$ ,

$$\tau(i,j) = \sum_{m=0}^{n_3} \Delta t(m). \tag{7.20}$$

The travel time $\tau(i,j)$ is calculated through the knowledge of distance $(x_j)$ and velocity $v$ (or flow $f$) following eqs. (5.15) and (5.16) on page 110.

Note that in this consideration of the pipe rig, the portions of it with smaller diameter are neglected. Therefore the hydraulic radius does not change, $R_H(m) = R_H = \text{const.}$

The resulting optimisation problem is to find a minimum over all $k_b$, $k_w$ and $c_\infty$ of

$$J_3 = \sqrt{\sum_{j=1}^{n_1} \sum_{i=1}^{n_2} [c_c(x_j, t_i) - g_2(j, i; k_b, k_w, c_\infty)]^2}, \tag{7.21}$$

with

$$g_2(j,i;k_b,k_w,c_\infty) = c_\infty + (c_c(0,t_{0,i}) - c_\infty) \times \\ \times \exp\left(-k_b\tau(i,j) - \sum_{m=0}^{n_3} \frac{k_f(m)k_w}{R_H(k_f(m)+k_w)}\Delta t(m)\right), \tag{7.22}$$

and

$$\tau(i,j) = \sum_{m=0}^{n_3} \Delta t(m), \tag{7.23}$$

where $c_c(x_j,t_i)$, $x_j$, $t_i$, and $c_c(0,t_i)$ are defined as above.

A Nelder-Mead type simplex algorithm is used to minimise $J_3$ as in the case of a single decay coefficient.

### 7.4.3 Issues in Estimation

Minimising these cost functions concerning $c_\infty$ and $k_w$ poses some generic problems. Estimation of $c_\infty$ is very difficult if data points are only available in the initial portion of the exponential decay of fig. 7.1. The sensitivity of the estimate of $c_\infty$ on errors in these data points is very high. This leads in the case of the data considered in this work to spurious results, which include physically impossible solutions like large negative values of $c_\infty$. Generally, it appeared that it is futile to attempt to estimate $c_\infty$ unless the chlorine reading for the largest travel time is close to $c_\infty$.

Hence the problem of obtaining $c_\infty$ has to be investigated from a different source. It is possible to get a fairly reliable estimate of the fraction of organic chloramines from a full chlorine speciation. In particular before ammonia dosing, there is generally assumed to be only free chlorine present besides organic chloramines. A value based on these titrations is used in the following as $c_\infty$.

Estimation of $k_w$ poses a different problem. It is possible only if

$$\sum_{m=0}^{n_3} \frac{k_f(m)k_w}{R_H(m)(k_f(m)+k_w)}\Delta t(m) \neq C \cdot \tau(i,j), \tag{7.24}$$

where $C$ is an arbitrary constant. In other words, either $k_f(m)$ or $R_H(m)$ needs to change within the travel time $\tau(i,j)$. Otherwise, there remains the problem of estimating

$$J_4 = \sqrt{\sum_{j=1}^{n_1}\sum_{i=1}^{n_2}(c_c(x_j,t_i) - (c_c(0,t_i) - c_\infty)\exp[-k_b\tau(i,j) - C\tau(i,j)] + c_\infty)^2}. \tag{7.25}$$

It is not possible to obtain an estimate for both $k_b$ and $C$ from $J_4$, only the sum of both can be identified.

Therefore, in the following it will be attempted to estimate the Epanet decay coefficient (i.e. case 2) only around flow changes, when $k_f$ varies.

## 7.5 Bottled Samples

During September, October and November 1996 bottled samples of disinfected water were taken to evaluate the bulk water chlorine demand independent of the wall demand. The method of sampling is provided in section 3.2.7 on page 58, the schedule of these experiments is given in section 3.3.2 on page 62. Results are discussed quantitatively in section 4.3.2 on page 79. In this section the decay coefficients and other chlorine model parameters of free chlorine and monochloramine as found from these bottled samples are provided.

Figs. 7.3 and 7.2 show the chlorine bottles data as discussed earlier together with the fitted exponential functions. Monochloramine data is presented in fig. 7.2, results of free chlorine bottles are given in fig. 7.3. Three parameters $K$, $c_0$ and $c_\infty$ were estimated by fitting the data $c(t)$ to

$$c(t) = (c_0 - c_\infty)e^{-Kt} + c_\infty. \tag{7.26}$$

The Nelder-Mead type simplex and the Levenberg-Marquardt gradient method, both as implemented in Matlab,[1] were used to find the model parameters. Both

[1] Functions **fmins** and **leastsq** of Matlab 5.

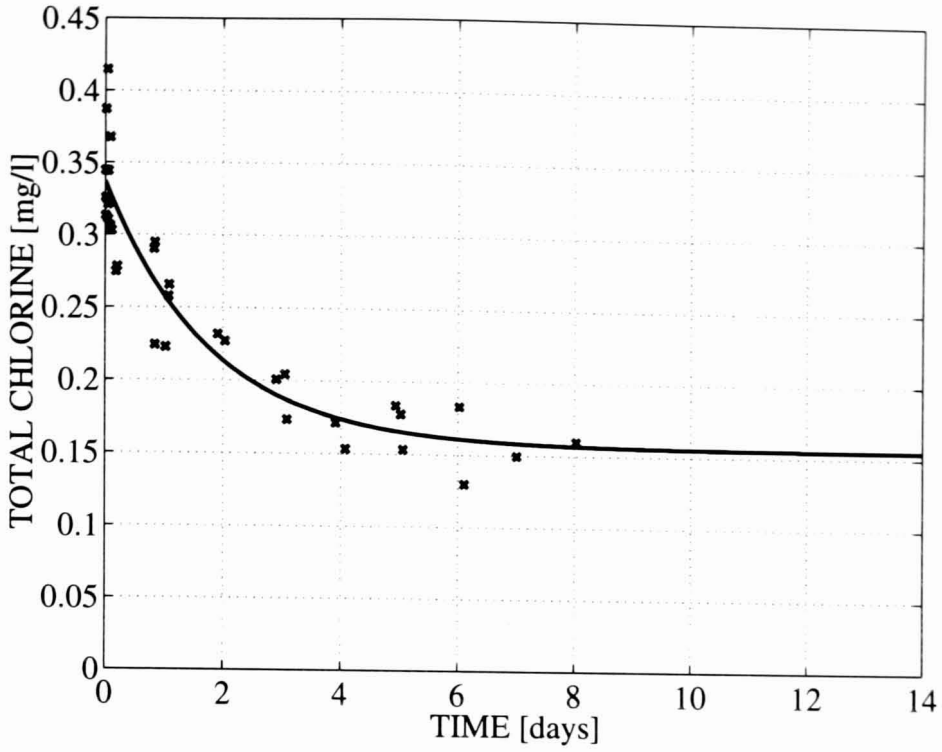


**Figure 7.2:** *Monochloramine in glass bottles and an exponential function is fitted to all data.*

methods yield the same results within an accuracy of at least six digits. The estimated parameters $K$, $c_0$ and $c_\infty$ are provided in table 7.1, values for the decay coefficient $K$ are given in 1/hours and 1/days, and the time constant $T_K = \frac{1}{K}$ is also provided in hours and days. Note that in this case there is no generic problem in estimating $c_\infty$ (as there is in the pipe rig data), because the final data values are close to $c_\infty$. Whereas fig. 7.2 shows a good overall fit to the data, fig. 7.3 has a poorer fit which might affect the estimation of the final value.

**Table 7.1:** *Decay coefficients and other fitted parameters of monochloramine and free chlorine bottled samples.*

| Monochloramine | | | | | |
|---|---|---|---|---|---|
| Decay Coefficient $K$ | | Time Constant $T_K$ | | Initial Value $c_0$ | Final Value $c_\infty$ |
| 1/hours | 1/days | hours | days | mg/l | mg/l |
| 0.0236 | 0.566 | 42.4 | 1.77 | 0.337 | 0.155 |
| Free Chlorine | | | | | |
| Decay Coefficient $K$ | | Time Constant $T_K$ | | Initial Value $c_0$ | Final Value $c_\infty$ |
| 1/hours | 1/days | hours | days | mg/l | mg/l |
| 0.125 | 3 | 8 | 0.333 | 0.343 | 0.0972 |

From table 7.1 it is seen that free chlorine decays much more rapidly than

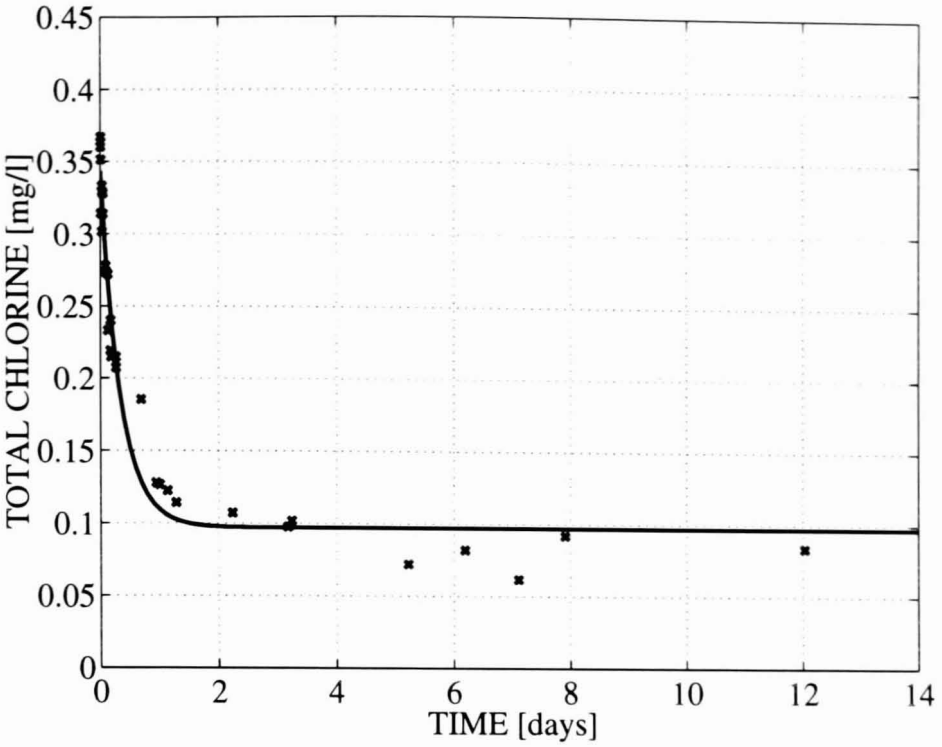


**Figure 7.3:** *Free chlorine in glass bottles and an exponential function is fitted to all data.*

monochloramine (as expected). If this table is compared to table 7.2 on page 198 it is seen, in addition, that the monochloramine decay in bottles is generally smaller than the decay in the pipe rig. Since the same water as in the pipe rig at roughly the same temperature was used the additional decay is most likely due to the influence of the pipe system, notably the biofilm.

## 7.6 Analysis of Pipe Rig Data

### 7.6.1 Single Decay Coefficient

Only step flow trials to 0.6 l/s or less were considered for the calculation of the decay coefficient, since at higher flow (i.e. 0.9 l/s) all chlorine readings throughout the rig are approximately the same.

Single decay coefficients $K$, as in case 1, were calculated within 15 periods of consecutive data with varying length at different flow and chlorine conditions, avoiding outliers in the data where possible. These periods were further divided into 40 samples of approximately equal length (between 39 and 80 decay coef-

**Table 7.2:** *Monochloramine decay coefficient data, sorted into regimes.*

| Period Number | Mean of $K$ $h^{-1}$ | Standard Deviation $h^{-1}$ | Sample Size | Flow l/s | Inlet Chlorine mg/l | Temperature $^0C$ |
|---|---|---|---|---|---|---|
| 1 | 0.0496 | 0.0058 | 57 | 0.081 | 0.39 | 14.4 |
| 2 | 0.0522 | 0.0028 | 57 | 0.081 | 0.39 | 13.9 |
| 3 | 0.0517 | 0.0043 | 57 | 0.081 | 0.38 | 13.7 |
| 4 | 0.0513 | 0.0034 | 57 | 0.081 | 0.36 | 14.0 |
| 5 | 0.0503 | 0.0031 | 60 | 0.082 | 0.37 | 14.4 |
| 6 | 0.0363 | 0.0014 | 50 | 0.083 | 0.37 | 13.3 |
| 7 | 0.0338 | 0.0021 | 51 | 0.083 | 0.39 | 13.0 |
| 8 | 0.0378 | 0.0024 | 50 | 0.079 | 0.39 | 6.4 |
| 9 | 0.0332 | 0.0053 | 50 | 0.079 | 0.40 | 6.1 |
| 10 | 0.0315 | 0.0011 | 52 | 0.080 | 0.40 | 6.7 |
| 11 | 0.0285 | 0.0020 | 39 | 0.080 | 0.37 | 6.9 |
| 12 | 0.0280 | 0.0114 | 58 | 0.079 | 0.36 | 6.5 |
| 13 | 0.0616 | 0.0078 | 58 | 0.080 | 0.36 | 6.8 |
| 14 | 0.0310 | 0.0021 | 56 | 0.085 | 0.36 | 6.2 |
| 15 | 0.0329 | 0.0023 | 56 | 0.086 | 0.34 | 6.5 |
| 16 | 0.0578 | 0.0079 | 56 | 0.086 | 0.35 | 6.6 |
| 17 | 0.0512 | 0.0170 | 56 | 0.085 | 0.36 | 6.6 |
| 18 | 0.0480 | 0.0136 | 56 | 0.085 | 0.37 | 6.6 |
| 19 | 0.0375 | 0.0039 | 56 | 0.084 | 0.38 | 6.6 |
| 20 | 0.0333 | 0.0040 | 57 | 0.087 | 0.35 | 6.6 |
| 21 | 0.0207 | 0.0033 | 63 | 0.079 | 0.67 | 6.8 |
| 22 | 0.0173 | 0.0019 | 64 | 0.079 | 0.61 | 6.5 |
| 23 | 0.0349 | 0.0045 | 59 | 0.308 | 0.36 | 13.2 |
| 24 | 0.0274 | 0.0045 | 59 | 0.306 | 0.34 | 13.6 |
| 25 | 0.0393 | 0.0084 | 59 | 0.306 | 0.35 | 14.0 |
| 26 | 0.0422 | 0.0040 | 59 | 0.306 | 0.32 | 14.0 |
| 27 | 0.0521 | 0.0033 | 61 | 0.306 | 0.32 | 14.0 |
| 28 | 0.0434 | 0.0046 | 62 | 0.308 | 0.31 | 14.2 |
| 29 | 0.0427 | 0.0062 | 62 | 0.309 | 0.31 | 14.0 |
| 30 | 0.0584 | 0.0094 | 62 | 0.308 | 0.32 | 13.6 |
| 31 | 0.0813 | 0.0060 | 62 | 0.308 | 0.34 | 13.5 |
| 32 | 0.0504 | 0.0075 | 63 | 0.302 | 0.66 | 7.6 |
| 33 | 0.0369 | 0.0052 | 64 | 0.298 | 0.66 | 6.9 |
| 34 | 0.0506 | 0.0101 | 72 | 0.452 | 0.35 | 6.8 |
| 35 | 0.0609 | 0.0081 | 72 | 0.448 | 0.31 | 7.0 |
| 36 | 0.0418 | 0.0056 | 70 | 0.449 | 0.61 | 7.5 |
| 37 | 0.0375 | 0.0034 | 70 | 0.448 | 0.59 | 7.5 |
| 38 | 0.0757 | 0.0320 | 80 | 0.604 | 0.34 | 7.0 |
| 39 | 0.0972 | 0.0228 | 40 | 0.606 | 0.35 | 6.8 |
| 40 | 0.0694 | 0.0138 | 54 | 0.609 | 0.61 | 7.1 |

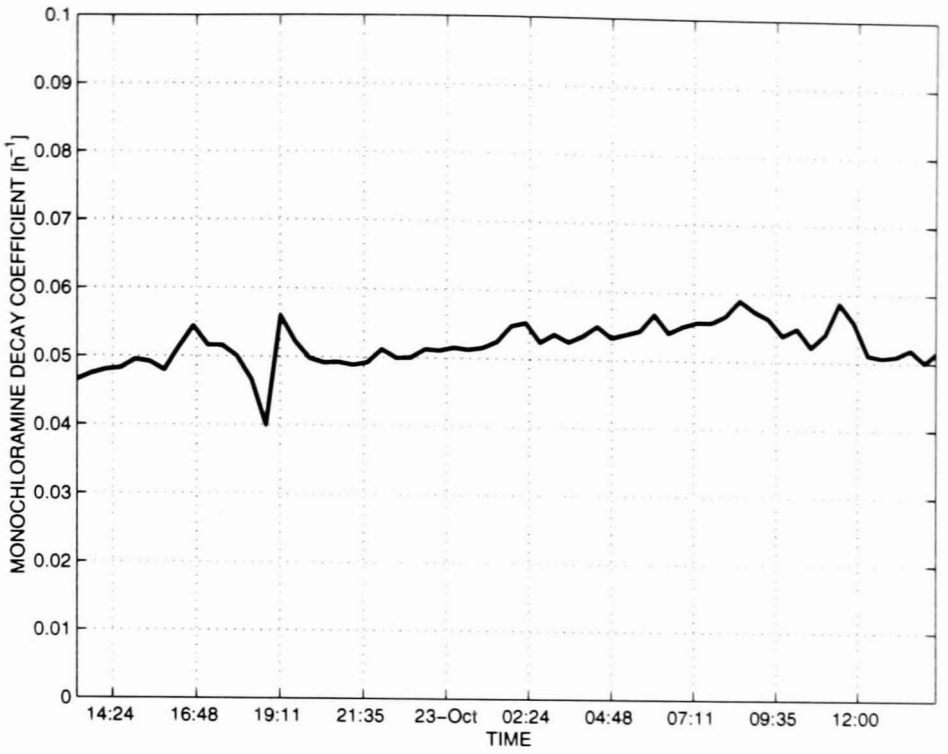


**Figure 7.4:** *Decay Coefficients in period 12 (22/23 October 1996) as example of estimated single monochloramine decay coefficients $K$ of data with low standard deviation (0.0033 $h^{-1}$). Inlet flow is 0.3 l/s, inlet chlorine is 0.32 mg/l and temperature is 14$^0$C.*

ficient estimates per sample), to allow for extensive comparison of periods with similar conditions. The flow rates investigated were 0.08 l/s, 0.3 l/s, 0.45 l/s, and 0.6 l/s, the inlet chlorine concentrations were approximately 0.4 mg/l and 0.65 mg/l of total chlorine, the temperature was either 13–14$^0$C or 6–7$^0$C. In every case, the chlorine readings were preprocessed as described in section 5.3. Each estimate of the decay coefficient is based on five time instants or 15 data points. The final value $c_\infty$ is assumed to be 0.08 mg/l. Two examples of monochloramine decay coefficients are depicted in fig. 7.4 and 7.5, all 40 average decay coefficients together with other relevant data are given in table 7.2.

The presentation of the data in table 7.2 follows regimes (separated by horizontal lines). Thus, sections of table 7.2 that are not separated by a horizontal line have roughly the same flow, inlet chlorine concentration and temperature. The given values for mean decay coefficient, flow, inlet chlorine and temperature are averages over each sample. From the table it is seen that the highest average decay coefficient was found in period 39 ($K$=0.0972 h$^{-1}$), at flow 0.6 l/s,

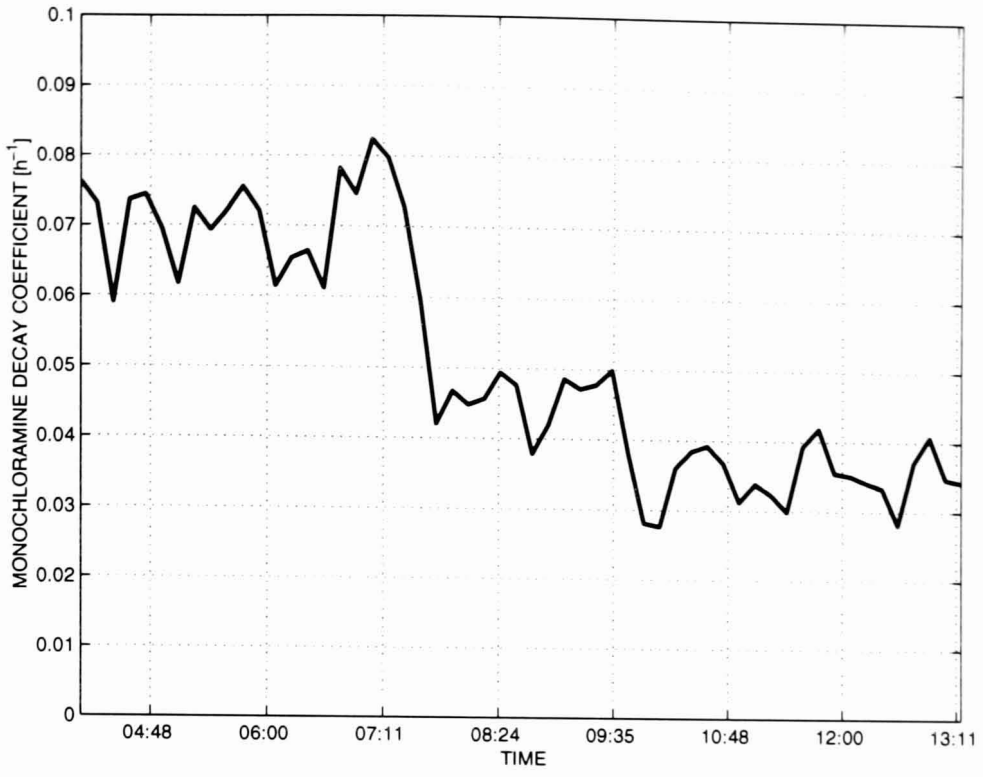


**Figure 7.5:** *Decay Coefficients in period 30 (8 December 1996), as example of estimated single monochloramine decay coefficients K of data with high standard deviation (0.0170 $h^{-1}$). Inlet flow is 0.085 l/s, inlet chlorine 0.36 mg/l and temperature is about 7$^0$C.*

inlet chlorine 0.61 mg/l and temperature 7$^0$C, the lowest decay coefficient is $K$=0.0173 $h^{-1}$ (period 22, 0.08 l/s, 0.61 mg/l and 6.5$^0$C). Note, for comparison, that the monochloramine decay coefficient in bottles with no chlorine demand was found to be 0.0236 h$^{-1}$ in the previous section. Some of the investigated periods have high standard deviations, in particular, during periods 38–40 (all at flow 0.6 l/s) the inlet chlorine meter reading was oscillating which implies that these data have only limited validity. If periods 38–39 are disregard the highest decay coefficient is 0.0813 h$^{-1}$ (period 31, flow 0.3 l/s, inlet chlorine 0.34 mg/l, temperature 13.5$^0$C).

From a first investigation for relationships between flow and monochloramine decay coefficients, there is no clear pattern emerging. Although the highest decay coefficients were achieved at higher flows, even at baseline flow (0.08 l/s) the coefficient may rise to 0.0578 h$^{-1}$ (period 16) and also higher flow rates sustain decay coefficients almost as low as the one found in bottle tests (e.g. $K$=0.0274 h$^{-1}$ in period 24, with a flow of 0.3 l/s).

Investigations of temperature and inlet chlorine lead to similar results. Both at high ($14^0$C) and low ($7^0$C) temperature both relatively large and quite small decay coefficients are observed, and although the lowest decay coefficients are found at an inlet chlorine residual of approximately 0.65 mg/l (and flow 0.08 l/s), very high decay coefficients of 0.0694 $h^{-1}$ (period 40) and 0.0418 $h^{-1}$ (period 36) are also found at that level of inlet chlorine.

Figures 7.4 and 7.5 illustrate this further. Examples of data with low standard deviation (period 12, fig. 7.4) and high standard deviation (period 30, fig. 7.5) are provided. Both figures have the same y-axis limits for better comparison. The main reason for the large drop in decay coefficient in fig. 7.5 is the (continuous) decrease of the chlorine meter reading at sample point 1 during period 30, the smaller fluctuations are probably due a slight oscillatory behaviour, chiefly of the inlet chlorine meter.

A more rigorous investigation of relationships between decay coefficients is the application of the t-test. It can be used to test if the means of two normally distributed samples with unknown, but equal, variance are equal [78, 139].

T-tests on all $\frac{39 \cdot 40}{2} = 780$ possible pairs of the 40 periods given in table 7.2 were performed. If a significance level of 0.05 is applied, then 709 pairs of the 780 pairs show a significant difference in mean, i.e. only 9.1 % or 71 time period pairs have average monochloramine decay coefficient that are *not* signifcantly different amongst the 40 investigated periods. The period numbers, flows, temperatures and inlet chlorine residuals of these 71 period pairs are given in table 7.3 at the end of this section.

Of the 780 possible pairs, 140 compare two average decay coefficients with each one being in the same regime (in terms of flow, inlet chlorine and temperature). Of these 140, only 17 period pairs (12.1 %) show no significant difference in mean (see table 7.3). If only flow regimes are considered, only 31 of 295 pairs with the same flow (or 10.5 %) show no significant difference in mean (and are therefore included in table 7.3). Most of the 71 pairs of time periods given in table 7.3 are pairs of period with different flow, inlet chlorine or temperature conditions (regimes), and most of the pairs of same conditions have a significantly different

mean of the decay coefficient.

Assuming that the requirements for the t-test are fulfilled, the conclution from these results is that there is no clear relationship between monochloramine decay coefficient and flow, inlet chlorine or temperature. Although the t-test did discover sample pairs which exhibit means of only insignificant difference (as given in table 7.3) the results imply that these relationships occur at random, i.e. without a pattern related to either flow, inlet chlorine or temperature.

**Table 7.3**: *Pairs of time periods with average decay coefficients that are* **not** *significantly different (according to a t-test with significance 0.05). Period numbers are the same as in table 7.2, the data is organised in terms of pairs of flows (separated by horizontal lines).*

| Period Numbers | | Flows l/s | | Temperatures $^0$C | | Inlet Chlorine mg/l | |
|---|---|---|---|---|---|---|---|
| 3 | 2 | 0.08 | 0.08 | 13.7 | 13.9 | 0.38 | 0.39 |
| 4 | 1 | 0.08 | 0.08 | 14.0 | 14.4 | 0.36 | 0.39 |
| 4 | 2 | 0.08 | 0.08 | 14.0 | 13.9 | 0.36 | 0.39 |
| 4 | 3 | 0.08 | 0.08 | 14.0 | 13.7 | 0.36 | 0.38 |
| 5 | 1 | 0.08 | 0.08 | 14.4 | 14.4 | 0.37 | 0.39 |
| 5 | 4 | 0.08 | 0.08 | 14.4 | 14.0 | 0.37 | 0.36 |
| 9 | 7 | 0.08 | 0.08 | 6.1 | 13.0 | 0.40 | 0.39 |
| 12 | 11 | 0.08 | 0.08 | 6.5 | 6.9 | 0.36 | 0.37 |
| 14 | 10 | 0.09 | 0.08 | 6.2 | 6.7 | 0.36 | 0.40 |
| 14 | 12 | 0.09 | 0.08 | 6.2 | 6.5 | 0.36 | 0.36 |
| 15 | 9 | 0.09 | 0.08 | 6.5 | 6.1 | 0.34 | 0.40 |
| 17 | 1 | 0.09 | 0.08 | 6.6 | 14.4 | 0.36 | 0.39 |
| 17 | 2 | 0.09 | 0.08 | 6.6 | 13.9 | 0.36 | 0.39 |
| 17 | 3 | 0.09 | 0.08 | 6.6 | 13.7 | 0.36 | 0.38 |
| 17 | 4 | 0.09 | 0.08 | 6.6 | 14.0 | 0.36 | 0.36 |
| 17 | 5 | 0.09 | 0.08 | 6.6 | 14.4 | 0.36 | 0.37 |
| 18 | 1 | 0.09 | 0.08 | 6.6 | 14.4 | 0.37 | 0.39 |
| 18 | 3 | 0.09 | 0.08 | 6.6 | 13.7 | 0.37 | 0.38 |
| 18 | 4 | 0.09 | 0.08 | 6.6 | 14.0 | 0.37 | 0.36 |
| 18 | 5 | 0.09 | 0.08 | 6.6 | 14.4 | 0.37 | 0.37 |
| 18 | 17 | 0.09 | 0.09 | 6.6 | 6.6 | 0.37 | 0.36 |
| 19 | 8 | 0.08 | 0.08 | 6.6 | 6.4 | 0.38 | 0.39 |
| 20 | 7 | 0.09 | 0.08 | 6.6 | 13.0 | 0.35 | 0.39 |
| 20 | 9 | 0.09 | 0.08 | 6.6 | 6.1 | 0.35 | 0.40 |
| 20 | 15 | 0.09 | 0.09 | 6.6 | 6.5 | 0.35 | 0.34 |
| 23 | 7 | 0.31 | 0.08 | 13.2 | 13.0 | 0.36 | 0.39 |

*continued on next page*

*continued from previous page*

| Period Numbers | | Flows l/s | | Temperatures $^0$C | | Inlet Chlorine mg/l | |
|---|---|---|---|---|---|---|---|
| 27 | 2 | 0.31 | 0.08 | 14.0 | 13.9 | 0.32 | 0.39 |
| 27 | 3 | 0.31 | 0.08 | 14.0 | 13.7 | 0.32 | 0.38 |
| 27 | 4 | 0.31 | 0.08 | 14.0 | 14.0 | 0.32 | 0.36 |
| 8 | 25 | 0.08 | 0.31 | 6.4 | 14.0 | 0.39 | 0.35 |
| 9 | 23 | 0.08 | 0.31 | 6.1 | 13.2 | 0.40 | 0.36 |
| 11 | 24 | 0.08 | 0.31 | 6.9 | 13.6 | 0.37 | 0.34 |
| 12 | 24 | 0.08 | 0.31 | 6.5 | 13.6 | 0.36 | 0.34 |
| 32 | 1 | 0.30 | 0.08 | 7.6 | 14.4 | 0.66 | 0.39 |
| 32 | 2 | 0.30 | 0.08 | 7.6 | 13.9 | 0.66 | 0.39 |
| 32 | 3 | 0.30 | 0.08 | 7.6 | 13.7 | 0.66 | 0.38 |
| 32 | 4 | 0.30 | 0.08 | 7.6 | 14.0 | 0.66 | 0.36 |
| 32 | 5 | 0.30 | 0.08 | 7.6 | 14.4 | 0.66 | 0.37 |
| 33 | 6 | 0.30 | 0.08 | 6.9 | 13.3 | 0.66 | 0.37 |
| 33 | 8 | 0.30 | 0.08 | 6.9 | 6.4 | 0.66 | 0.39 |
| 16 | 30 | 0.09 | 0.31 | 6.6 | 13.6 | 0.35 | 0.32 |
| 17 | 27 | 0.09 | 0.31 | 6.6 | 14.0 | 0.36 | 0.32 |
| 17 | 32 | 0.09 | 0.30 | 6.6 | 7.6 | 0.36 | 0.66 |
| 18 | 32 | 0.09 | 0.30 | 6.6 | 7.6 | 0.37 | 0.66 |
| 19 | 25 | 0.08 | 0.31 | 6.6 | 14.0 | 0.38 | 0.35 |
| 19 | 33 | 0.08 | 0.30 | 6.6 | 6.9 | 0.38 | 0.66 |
| 28 | 26 | 0.31 | 0.31 | 14.2 | 14.0 | 0.31 | 0.32 |
| 29 | 26 | 0.31 | 0.31 | 14.0 | 14.0 | 0.31 | 0.32 |
| 29 | 28 | 0.31 | 0.31 | 14.0 | 14.2 | 0.31 | 0.31 |
| 32 | 27 | 0.30 | 0.31 | 7.6 | 14.0 | 0.66 | 0.32 |
| 33 | 25 | 0.30 | 0.31 | 6.9 | 14.0 | 0.66 | 0.35 |
| 34 | 1 | 0.45 | 0.08 | 6.8 | 14.4 | 0.35 | 0.39 |
| 34 | 2 | 0.45 | 0.08 | 6.8 | 13.9 | 0.35 | 0.39 |
| 34 | 3 | 0.45 | 0.08 | 6.8 | 13.7 | 0.35 | 0.38 |
| 34 | 4 | 0.45 | 0.08 | 6.8 | 14.0 | 0.35 | 0.36 |
| 34 | 5 | 0.45 | 0.08 | 6.8 | 14.4 | 0.35 | 0.37 |
| 34 | 17 | 0.45 | 0.09 | 6.8 | 6.6 | 0.35 | 0.36 |
| 34 | 18 | 0.45 | 0.09 | 6.8 | 6.6 | 0.35 | 0.37 |
| 35 | 13 | 0.45 | 0.08 | 7.0 | 6.8 | 0.31 | 0.36 |
| 37 | 8 | 0.45 | 0.08 | 7.5 | 6.4 | 0.59 | 0.39 |
| 37 | 19 | 0.45 | 0.08 | 7.5 | 6.6 | 0.59 | 0.38 |
| 34 | 27 | 0.45 | 0.31 | 6.8 | 14.0 | 0.35 | 0.32 |
| 34 | 32 | 0.45 | 0.30 | 6.8 | 7.6 | 0.35 | 0.66 |
| 35 | 30 | 0.45 | 0.31 | 7.0 | 13.6 | 0.31 | 0.32 |
| 36 | 26 | 0.45 | 0.31 | 7.5 | 14.0 | 0.61 | 0.32 |
| 36 | 28 | 0.45 | 0.31 | 7.5 | 14.2 | 0.61 | 0.31 |
| 36 | 29 | 0.45 | 0.31 | 7.5 | 14.0 | 0.61 | 0.31 |
| 37 | 25 | 0.45 | 0.31 | 7.5 | 14.0 | 0.59 | 0.35 |

*continued on next page*

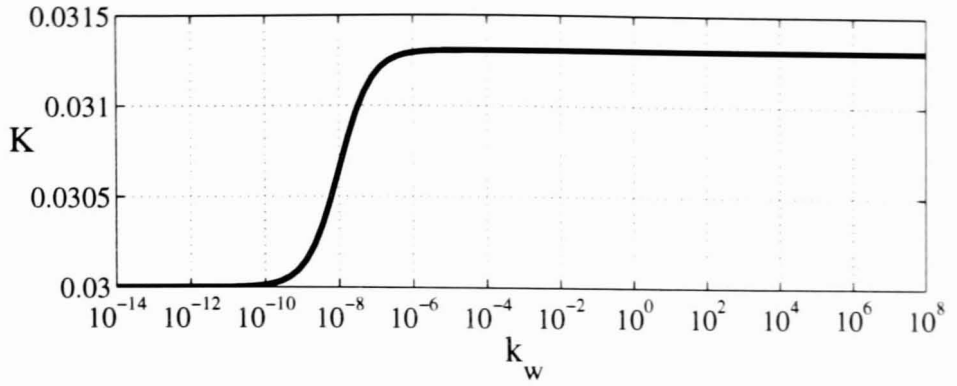


**Figure 7.6:** *The combined decay coefficient $K$ as used in Epanet versus the wall demand $k_w$ (here $k_b = 0.03$ 1/h, $R_H = 0.0275$ m, $k_f = 10^{-7}$ m/s).*

*continued from previous page*

| Period Numbers | | Flows l/s | | Temperatures $^0$C | | Inlet Chlorine mg/l | |
|---|---|---|---|---|---|---|---|
| 37 | 33 | 0.45 | 0.30 | 7.5 | 6.9 | 0.59 | 0.66 |
| 38 | 31 | 0.60 | 0.31 | 7.0 | 13.5 | 0.34 | 0.34 |
| 40 | 38 | 0.61 | 0.60 | 7.1 | 7.0 | 0.61 | 0.34 |

### 7.6.2 Combined Decay Coefficients

The decay coefficients of case 2 were also investigated. If the variation of the decay coefficient followed this model, the fit of that model would be better than that of a single decay coefficient model. For four flow changes both single and combined decay coefficients were calculated for comparison, again assuming $c_\infty$=0.08 mg/l. The investigated flow changes were from 0.08 l/s to 0.3 l/s (period A), from 0.3 l/s to 0.08 l/s, from 0.08 l/s to 0.45 l/s (period C) and from 0.08 l/s to 0.9 l/s (period B). Three optimisation procedures were used for the calculation of the decay coefficients: a Nelder-Mead type simplex, a Levenberg-Marquardt gradient method and a Gauss-Newton gradient based algorithm, all as implemented in Matlab[2]. A maximum of 8000 iterations were done in each case. Within this limit of iterations, the Nelder-Mead method always produced the smallest residual cost function (or root mean square error).

To clarify the expected order of magnitude of values, consider the Epanet

[2]Functions `fmins` for Nelder-Mead simplex and `leastsq` for the other two methods in Matlab 5.

decay coefficient as given in equation (7.5):

$$K = k_b + 3600 \cdot \frac{k_f k_w}{R_H(k_f + k_w)} \tag{7.27}$$

The factor 3600 is introduced for conversion of the term with $k_w$ from 1/seconds to 1/hours. If reasonable approximate values of $k_b \approx 0.03$ 1/h, $R_H = 0.0275$ m and $k_f \approx 10^{-7}$ m/s are used, a plot of $K$ versus $k_w$ as given in fig. 7.6 can be obtained.

From this figure it is obvious that the sensitivity of $K$ towards changes of $k_w$ is negligible for $k_w > 10^{-5}$ and $k_w < 10^{-11}$. This range shifts with varying $k_f$. Note that Rossman [124, p.89] uses 1 foot/day=$3.53 \cdot 10^{-6}$ metre/second in an example in the manual of Epanet.

From the investigated time periods, in one case $k_w$ converged to a negative (i.e. infeasible) value. In three of four cases values of $k_w$ that are between $10^{-8}$ and $10^8$ are obtained. Only time periods with positive $k_w$ are investigated further, they are given in table 7.4. These periods are 18.10.96 00:00 to 19.10.96 12:00 (period A), 14.10.96 12:00 to 15.10.96 12:00 (period B) and 16.12.96 12:00-18:30 (period C).

The results were compared by taking the root mean square error between the $N$ data points $y_j$ and the corresponding model output $\hat{y}$ for each chlorine decay models with decay coefficients $K$ according to case 1 and 2, respectively. The error is defined as

$$RMS\ Error = \sqrt{\frac{1}{N}\sum_{j=1}^{N}(y_j - \hat{y})^2}. \tag{7.28}$$

It is seen from table 7.4 that the decay coefficients of case 2 perform better than a single decay coefficient as in case 1, however, the improvement in period A is neglibile. In periods B and C, however, an improvement of 22.8 % and 17.4 % over the values of case 1 is observed. The results from these periods were not included in [97]. It is important to note again in this context that the sensitivity of the determination of $k_w$ is very small, i.e. in period B, a root mean square error

**Table 7.4:** *Results of the estimation of combined decay coefficients (as in Epanet). All decay coefficients are found through a Nelder-Mead type simplex as implemented in Matlab.*

| Time Period | A | B | C |
|---|---|---|---|
| Data Points | 1728 | 1560 | 2184 |
| Flow Change [l/s] | 0.08→0.3 | 0.08→0.9 | 0.08→0.45 |
| $K$, Case 1 [$h^{-1}$] | 0.0348 | 0.0566 | 0.0309 |
| $k_b$, Case 2 [$h^{-1}$] | 0.0340 | 0.0490 | 0.0242 |
| $k_w$, Case 2 [$h^{-1}$] | $1.95 \cdot 10^{-7}$ | $4.11 \cdot 10^{8}$ | $3.90 \cdot 10^{7}$ |
| RMS Error, Case 1 [mg/l] | 0.012538 | 0.022498 | 0.021032 |
| RMS Error, Case 2 [mg/l] | 0.012534 | 0.017364 | 0.017364 |

that is only $2.70 \cdot 10^{-9}$ mg/l larger than the one given in column 3 of table 7.4 leads to $k_w = 5.93$ m/s, a reduction by a factor of $10^{-8}$. A wall demand of $k_w = 10^{-2}$ m/s in period C (column 4) leads to an increase of the root mean square error of only $5.19 \cdot 10^{-7}$ mg/l, a wall demand of $k_w = 10^{-6}$ m/s would, however, increase to error by $3.85 \cdot 10^{-3}$ mg/l.

In summary, an improvement of model error due to the use of a combined decay coefficient with flow dependence as currently used in Epanet is observed. However, reliability of wall demand $k_w$ estimation results can be very low, i.e. inaccuracies involved in estimating $k_w$ are several orders of magnitude for periods B and C.

## 7.7 Discussion

Although a relatively large variability of the single decay coefficientis is observed, this does not appear to be related to flow, chlorine changes or temperature. However, the results of columns 3 and 4 in table 7.4 give strong evidence that the model with combined bulk and wall decay gives better results than a single decay coefficient. The flow changes in these periods are higher than in period A. This is a likely reason for the improved performance of the Epanet model compared to period A.

But, as pointed out earlier, the sensitvity of the model and cost function to

changes in $k_w$ may be very small. This is the case in periods B and C, where the actual value of $k_w$ is of little importance. As long as it is much larger than $k_f$ (e.g. 1000 times), the flow dependent parameter $k_f$ will determine the second term of the Epanet model.

Although from a discussion of initial results it was concluded that a single decay coefficient describes the monochloramine decay adequately [97], the additional data of periods B and C in table 7.4 implies that a model as used in Epanet (with flow dependence) performs better than a decay coefficient as in case 1.

From the detailed analysis of the single decay coefficient data it emerged, however, that the prime obstacle for the validation of chlorine models are the inaccuracies in the data. Even after performing a preprocessing procedure based on an independent set of measurements (i.e. the titrations), estimated decay coefficients vary significantly even within the same regime. It is noted in this context that the investigated step flow trials were undertaken after a series of prior trials. Thus, if an increase of decay coefficient is due to an increase in entrained particulate matter or erosion of biofilm, the previous step flow trials will have decreased that effect.

## 7.8 Implementation

The decay coefficients in bottled samples presented in section 7.5 were found with `wdecay`. This Matlab function can calculate decay coefficient in 18 different ways. They differ in the type of decay coefficient (single or Epanet), the type of optimisation procedure (least-squares fit with logarithmic approximation, Nelder-Mead type simplex, Levenberg-Marquardt or Gauss-Newton gradient methods) and in the amount of data taken into account (either one estimation per time instant or a cumulative estimation of all in all one coefficient for a whole period). These calculations are either done by calling separate functions (`wdclse`, `wdcepa` for fitting with a logarithmic approximation) or they are done in `wdecay` with the help of a separate error function (`errfundclse`, `errfundclse1`, `errfundclse2`, `fundclse`, `fundclse1`, `errfundcepa`, `errfundcepa1`, `errfundcepa2`, `fundcepa`, `fundcepa2`;

the numbers indicate either (no number) estimation of decay coefficient and final value, (one) additional estimation of initial value, or (two) estimation of decay coefficient only).

The analysis of pipe rig data of section 7.6.1 and section 7.6.2 were done with `calcdecay`, which uses `wdecay` internally. This function calculates a series of subsequent cumulative decay coefficients and saves the result to a Matlab data file. The methods 17 and 18 in `wdecay` or `calcdecay` were used for the calculation of single or Epanet coefficients, respectively (see `help wdecay`).

Matlab scripts were written to calculate the presented results. The script `calcmax` uses `calcdecay` to compute decay coefficients, `chlmeans2` generates all the data provided in tables 7.2 and 7.3 and `chlgiveout` produces ASCII files of that data for the inclusion in this thesis. The function `testepa` uses some of the outputs of `wdecay` to test the performance of different optimisation procedures. It was used in section 7.6.2 together with `rmsechl`, which calculates root mean square errors of chlorine data.

All of the above discussed functions and scripts are part of the Water Quality Toolbox that was written by the author (see appendix C).

## 7.9 Conclusions

The important task of chlorine model calibration was addressed in this chapter. It appeared that the issue of data accuracy is paramount, since the sensitivity of decay coefficient estimates to data inaccuracies is very large.

It was shown that the final value $c_\infty$ cannot normally be estimated. Furthermore, it can only be attempted to estimate the wall demand $k_w$ of the Epanet model if a flow or diameter change takes place, but even then it may be impossible to determine the exact value due to a possibly very shallow cost function.

Finally, no relationships between single decay coefficients and flow, inlet chlorine or temperature could be found, however, some evidence for an improved performance of the Epanet model over single decay coefficients for flow changes by more than 0.3 l/s was presented.

It is concluded that there is a variation of monochloramine decay coefficent due to flow changes, however, because of the frequently high uncertainty associated with chlorine data, a simpler model with only a single decay coefficient may be a good approximation of monochloramine decay in a system like the one investigated in this thesis.

# Part IV

# Conclusion

# Chapter 8

# Discussion and Conclusions

This thesis covered experimental work and analyses of data aimed at the development of water quality models for water distribution networks. A total particle counts model was constructed for a step flow input and two monochloramine decay models were discussed and compared. In this chapter, some of the broader issues that are associated with water quality modelling will be discussed and a summary will conclude this work.

## 8.1 Merits of this Approach to Modelling

In this thesis, techniques of physical modelling were combined with system identification to determine a model of particle counts. The 'hybrid' method that is presented in this work is somewhat different from earlier proposed approaches such as empirical modelling or semi-physical modelling. The system is first split into suitable sub-systems, derived specifications for the model from the data for those sub-systems and then proposed models that are validated through their interpretability and by fitting them to data. Thus, a model was found that lends itself to physical or biological interpretation. The other criterion for a good model is that it should be usable, e.g. for the determination of the biofilm shedding profile.

The approach taken in this thesis (as all methods of system identification) is data oriented, i.e. net effects are captured rather than the fine details of underlying

processes. This has the advantage that the effects that are of the most interest are modelled. This approach is limited by the assumptions, which need to be fulfilled for the model to be valid and therefore might have to change in a trial and error process. Nevertheless, a model structure was derived directly from data. Although as much physical (or biological) knowledge of the underlying processes as possible was incorporated into finding the model structure to avoid a lengthy period of trial and error, this knowledge is only then absolutely required when the meaning of the model is being examined.

## 8.2 Generalisation

Naturally it is desirable to extend the results of this work (which were derived for the "TORUS" pipe rig) to more general water distribution systems, more general flow regimes (i.e. not just step changes) or long-term effects.

One major problem is the impact of different pipe materials. From the results of the pipe rig, it is very difficult to extrapolate information about systems that are not predominately MDPE pipes. The pipe rig has less than 2 % (15 m) of lined or unlined iron pipes. Despite that iron particles are found throughout the system (see [46]), which implies that even these 2 % may influence the particle counts.

Another issue is that flow regimes that do not consist of steps alone will probably make it impossible to find a linear model. This is demonstrated in section 6.4.3, where the negative input slope model is developed. Because the contribution of particles before flow change cannot be neglected (in this case flow decrease), the obtained model is not a convolution anymore and, therefore, nonlinear. This is likely to be even more the case if the flow varies arbitrarily.

For the possibility of long-term predictions, a full model has to include long-term effects as well. Those were studied only briefly in this work, because they lie outside the scope of this thesis. A model of long-term effects will either require several years of experiments or be based on published results and their extrapolation.

The particle counts model of chapter 6 may also be a part of a full model. It would, however, cover short-term effects only. In particular, it would cover shear stress related erosion of biofilm.

## 8.3 Water Industry Perspective

Some of the results of this thesis have implications on the operation of water distribution systems.

The relationships between particle counts and plate counts or epifluorescence microscopy counts as discussed in section 4.5.3 implies that particle counters may give valuable information on the bacteriological condition of the network. More research will be necessary into these findings. From the results presented in this work it is concluded that particle counts can be used effectively to measure suspended bacteria in a high shear stress environment where 'clumps' of biomass dominate.

Apart from the insight in the processes of biofilm detachment and the dynamics of suspended particles, the main use of the particle counts model of chapter 6 is the computation of the biofilm shedding profile. This profile gives information about the state of the system and, in particular, potentially critical areas in terms of high shear-off. With this method, a step flow trial could be used to test a portion of the distribution system to locate the sources of increased shear-off.

The discussions of the peaks (see section 4.1.2.1) are also very relevant. The results give evidence to the effect that high particle incidents originate from valves. Thus, this implies that the maintenance of valves is important for the compliance with water quality standards.

The preprocessing of chlorine meter data of section 5.3 highlighted that it is necessary to take careful account of inaccuracies in the readings of these meters and, therefore, more accurate meters will be necessary for effective calibration of chlorine models. The preprocessing procedure to improve data accuracy with the help of titrations can be used for real distribution systems.

In the comparison between different chlorine decay models of chapter 7, addi-

tional insight is given that is of use if chlorine decay models are to be calibrated for distribution systems; in particular, the difficulties associated with fitting the parameters are discussed in some detail (sections 7.4.3 and 7.6.2). This has implications on the design of experiments for chlorine model calibration: if it is desired to find the wall demand in the Epanet model it will be necessary to consider a time span with a flow change or, alternatively, a network area with change of diameter. In addition, it was seen that even if these constraints are satisfied it may be impossible to find the wall demand due to the poor sensitivity of the model and therefore it might be necessary to obtain it from an alternative source [153] or just assume some reasonable value.

The Reynolds numbers used in this work (see section 3.3.1) are relatively low compared to operational conditions in strategic mains, however, they generally match the conditions in pipes of similar sizes as the pipe rig (i.e. 110 mm diameter). Thus, the results of this thesis are particularly valid for the pipe work near to the customer's tap.

## 8.4 Future Perspective

As already discussed when the extended model was introduced in section 6.4.1.4, a continuation of this work may include a more general particle counts model. This model would cover the suggested extensions to the model of biofilm detachment as measured by suspended particles together with an indication of the biofilm on the pipe walls. In addition, diurnal variations, e.g. input flows that are not steps, or long-term aspects may feature in the model.

A piecewise linear decomposition of a more general input signal could be used to make the current particle counts model applicable to more general inputs, however, it will be required to distinguish between positive and negative slopes in the input and there is likely to be a threshold for the positive slope below which the input signal will not result in a response. In addition, it will be necessary to take into account the dependence of the parameters on the magnitude of the input, e.g. by the generation of a look-up table of parameter values. However,

such a look-up table will require many experiments under similar conditions.

These problems will have to be addressed before the particle counts model can be integrated into a software package. For this integration it may be a natural choice to use the numerical models discussed in section 6.3.1, however, they have similar shortcomings to the parametric model. After reformulation in terms of a numerical model, the parametric model could be adopted as well.

More work on monochloramine will require more and better data. Other model structures should be considered and it is desirable to find a chlorine decay model where the wall demand exhibits a better sensitivity than in the Epanet model.

Other water quality variables, like temperature, free chlorine, bacterial counts and nutrient content (Biodegradable Dissolved Organic Carbon, BDOC) could be investigated in more detail. This will require further literature work and experiments on possibly both the pipe rig and a distribution system (with meters). These experiments could feature longer periods of high flow than in the present work and it would be beneficial to be able to control water temperature in the pipe rig. Simply heating the water may serve that purpose because most of the system is buried underground.

Fuzzy modelling (cf. section 2.10) is probably a natural choice to combine several linear models obtained by these further investigations into one large non-linear model.

Alternatively, a model derived only from already published knowledge (as e.g. in [49]) could be attempted. It is likely that parts of such a model are not described in literature to date, these aspects would have to be investigated separately by similar methods as used in this thesis. Results of modelling from data concerning, for instance, biofilm detachment, the relationship of particle counts and bacterial counts or monochloramine/free chlorine decay may be included symbiotically.

## 8.5 Conclusions

This thesis focused on two aspects of water quality in distribution systems: particle counts and disinfectant. Additional observations of heterotrphic plate counts and epifluorescence microscopy counts are reported.

The response of the particle counts to a step increase of flow was modelled from experimental data. This model introduces the concepts of a local particles shear-off function and an initial biofilm shedding profile. They give insight into the dynamics and the condition of the network. The parameters of this model describe the net effect and the speed of biofilm shear-off. It is observed that the net effect decreases towards the end of the experiment which is likely to be due to repeated shear-off, decrease of temperature and the introduction of a disinfectant. The biofilm shedding profile and the identification of peaks allow to pinpoint potentially critical sections of the system (in terms of high shear-off).

The approach taken in this work uses specifications derived from data and assumptions to obtain a meaningful model structure. In particular, the degree to which it is interpretable, and the fit of the parameters and biofilm shedding profile are used for validation.

Monochloramine is used as disinfectant in the experimental system considered in this work. The chlorine meter readings were first preprocessed with the help of titrations to remove meter drift, and then two different monochloramine decay models are calibrated and compared. The calibration (or parameter identification) highlighted several generic problems that come about due to the mathematical structure of the models, i.e. it is impossible to estimate both the bulk decay coefficient and the wall demand unless there is a flow or diameter change in the considered time or distance interval. The decay coefficients are compared and tested for flow, temperature or inlet chlorine residual dependence, however, only a weak dependence on flow could be found.

It is anticipated that this work will facilitate the assessment of potential danger from biofilm (in terms of high shear-off). Furthermore, the work has shed light on biofilm detachment dynamics and chlorine decay model calibration. A

generalisation of this work will facilitate the incorporation of these findings into a water quality monitoring and control system.

# Bibliography


[1] O. Adam and Y. Kott. Evaluation of water quality as measured by bacterial maximum growth rate. *Water Research*, 23(11):1407–1412, 1989.

[2] S. M. Alexander, N. L. Glenn, and D. W. Bird. Advanced techniques in the mathematical modeling of water distribution systems. *Journal of the American Water Works Association*, pages 343 –346, July 1975.

[3] J. H. Andersen and R. S. Powell. Simulation of water networks containing controlling elements. Submitted for publication to the *Journal of Water Resources Planning and Management*, 1998.

[4] K. J. Åström and B. Wittenmark. *Computer–Controlled Systems*. Prentice Hall International, London, 3rd edition, 1997. Chapter 8.

[5] R. Babuška and H. B. Verbruggen. An overview of fuzzy modeling for control. *Control Engineering Practice*, 4(11):1593–1606, 1996.

[6] R. Bakke, W. G. Characklis, M. H. Turakhia, and A.-I. Yeh. Modelling a monopopulation biofilm system: *Pseudomonas Aeruginosa*. In W. G. Characklis and K. C. Marshall, editors, *Biofilms*, pages 487–520. J. Wiley & Sons, New York, 1990.

[7] R. Bakke and P. Q. Olsson. Biofilm thickness measurements by light microscopy. *J. Microbial. Meth.*, 5:93, 1986.

[8] G. Billen. Protein degradation in aquatic environments. In R. Chrost, editor, *Microbial Enzyme in Aquatic Environments*, pages 348–389. Springer-Verlag, Berlin, 1991.

[9] S. A. Billings. Identification of nonlinear systems—a survey. *IEE Proceedings, Part D*, 127(6):272–285, 1980.

[10] P. Biswas, C. Lu, and R. M. Clark. Particle and chemical transport in drinking water systems. In *Water Quality Modeling in Distribution Systems*, pages 323–361, Cincinnati, Ohio, Feb. 1991. American Water Works Association.

[11] P. Biswas, C. Lu, and R. M. Clark. A model for chlorine concentration decay in pipes. *Water Research*, 27(12):1715–1724, 1993.

[12] J. C. Block, F. Bois, D. J. Reasoner, M. Dutang, L. Mathieu, J. L. Paquin, and J. Maillard. Disinfection of drinking water distribution systems. *Water Supply*, 13(2):1–11, 1995.

[13] J. C. Block, M. Dutang, J. Maillard, and D. Reasoner. Growth of attached bacteria in water distribution systems. *Water Supply*, 12(1/2):SS1–8 - SS1–12, 1994. Special subject: Biological activity in distribution systems.

[14] P. F. Boulos, T. Altman, R. W. Bowcock, A. K. Dhingra, and F. Collevati. An explicit algorithm for modeling distribution system water quality with applications. In *Proceedings of the 2nd International Conference on Water Pipeline Systems*, pages 405–423, Edinburgh, 1994.

[15] P. F. Boulos, T. Altman, P.-A. Jarrige, and F. Collevati. An event-driven method for modelling contaminant propagation in water networks. *Applied Mathematical Modelling*, 18:84–92, Feb. 1994.

[16] M. A. Brdys, H. Puta, E. Arnold, K. Chen, and S. Hopfgarten. Operational control of integrated quality and quantity in water systems. In P. D. Roberts and J. E. Ellis, editors, *IFAC Symposium on Large Scale Systems: Theory and Applications*, volume 2, pages 715–721, London, 1995. Pergamon.

[17] M. A. Brdys and B. Ulanicki. *Operational Control of Water Systems: Structures, Algorithms and Applications.* Prentice Hall, London, 1994.

[18] I. N. Bronstein and K. A. Semendjajew. *Taschenbuch der Mathematik.* B.G. Teubner Verlagsgesellschaft, Stuttgart, 1991.

[19] M. R. W. Brown, R. J. Courcol, and G. P. Testing sensitivity of biofilms to antimicrobial agents. In J. W. T. Wimpenny, W. Nichols, D. Stickler, and H. Lappin-Scott, editors, *Bacterial Biofilms and Their Control in Medicine and Industry*, pages 135–140. BioLine, Cardiff, 1994.

[20] J. D. Bryers. Biologically active surfaces: Processes governing the formation and persistence of biofilms. *Biotechnology Progress*, 3(2):57–68, June 1987.

[21] P. Burgess, P. Clayton, and D. Vitanage. Dynamic water quality modelling in the sydney water board. In *Australian Institute of Engineers WATERCOMP*, pages 363–372, Melbourne, Australia, 30th March - 1st April 1993.

[22] P. L. Burgess, D. C. Vitanage, A. H. Morton, and P. J. Bliss. Determination of kinetic decay factors to model chlorine in water supply distribution systems. In *Hydrotop'94: Colloque 'Mieux gerer l'Eau'. Vol. 2*, pages 143–151. Marseille, France, 1994.

[23] V. K. Chambers. Long term variability of chlorine decay rate in distribution. Technical Report UC 2295, WRc Swindon, Frankland Road, Blagrove, Swindon, Wilts, Apr. 1994.

[24] V. K. Chambers, J. D. Creasey, and J. S. Joy. Modelling free and total chlorine decay in potable water distribution systems. *Journal Water Supply Research and Technology - Aqua*, 44(2):60–69, 1995.

[25] V. K. Chambers and J. S. Joy. Validity of modelling chlorine residuals in distribution. Technical Report UC 1942, WRc Swindon, Frankland Road, Blagrove, Swindon, Wilts, Apr. 1993.

[26] W. G. Characklis. Fouling biofilm development: A process analysis. *Biotechnology and Bioengineering*, 23:1923–1960, 1981.

[27] W. G. Characklis and K. C. Marshall. *Biofilms*. J. Wiley & Sons, New York, 1990.

[28] W. G. Characklis, M. H. Turakhia, and N. Zelver. Transport and interfacial transfer phenomena. In W. G. Characklis and K. C. Marshall, editors, *Biofilms*, pages 265–340. J. Wiley & Sons, New York, 1990.

[29] K. Chen and M. A. Brdys. Set membership estimation of state and parameters of large scale water supply and distribution systems — integrated quantity and quality. In P. D. Roberts and J. E. Ellis, editors, *IFAC Symposium on Large Scale Systems: Theory and Applications*, pages 543–548, London, 1995. Pergamon.

[30] R. M. Clark. Water quality modeling in distribution systems. *Journal of Environmental Science and Health, Part A*, 27(5):1329–1366, 1992.

[31] R. M. Clark, D. J. Ehreth, and J. J. Convery. Water legislation in the U.S.: an overview of the Safe Drinking Water Act. *Toxicology and Industrial Health: An International Journal*, 7(516):43–52, 1991.

[32] R. M. Clark and J. A. Goodrich. Modelling human exposure to contaminants from drinking water. *Journal Water Supply Research and Technology - Aqua*, 41(4):224–230, 1992.

[33] R. M. Clark, J. A. Goodrich, and L. J. Wymer. Effect of the distribution system on drinking-water quality. *Journal Water Supply Research and Technology - Aqua*, 42(1):30–38, 1993.

[34] R. M. Clark, W. M. Grayman, J. A. Goodrich, R. A. Deininger, and K. Skov. Measuring and modeling chlorine propagation in water distribution systems. *Journal of Water Resources Planning and Management*. 120(6):871–887, November/December 1994.

[35] R. M. Clark, W. M. Grayman, R. M. Males, and J. D. Coyle. Predicting water quality in distribution systems. Technical Report EPA/600/D-86/230, Drinking Water Research Division, U.S. Environmental Protection Agency, Cincinnati, Ohio, Sept. 1986.

[36] R. M. Clark, B. W. Lykins, J. C. Block, L. J. Wymer, and D. J. Reasoner. Water quality changes in a simulated distribution system. *Journal Water Supply Research and Technology – Aqua*, 43(6):263–277, 1994.

[37] R. M. Clark, G. Smalley, J. A. Goodrich, R. Tull, L. A. Rossman, J. J. Vasconcelos, and P. F. Boulos. Managing water quality in distribution systems: Simulating TTHM and chlorine residual propagation. *Journal Water Supply Research and Technology – Aqua*, 43(4):182–191, 1994.

[38] J. Cohen. The development of a dynamic calculation model for drinking-water networks. *Journal Water Supply Research and Technology - Aqua*, 39(3):172–187, 1990.

[39] J. Cohen. Further development of a dynamic calculation and simulation model for water distribution. In *Water Quality Modeling in Distribution Systems*, pages 155–181, Cincinnati, Ohio, Feb. 1991. American Water Works Association.

[40] F. Colin and G. Grapin. Design of a hydraulic and water quality model of a meshed distribution network: The case of chemical species in a singel kinetics reaction. In *Water Quality Modeling in Distribution Systems*, pages 141–153, Cincinnati, Ohio, Feb. 1991. American Water Works Association.

[41] F. Colin, G. Grapin, J. Cheron, Y. Levi, E. Pozzoli, J. Miazza, and O. Pascal. Etude de l'évolution de la qualité d'eau potable dans les réseaux de distribution, une approche et des moyens nouveaux. *Techn. Sci. Munic. Eau*, 12:565–574, 1987.

[42] B. Coulbeck and C. H. Orr. A network analysis and simulation program for water distribution systems. *Civil Engineering Systems*, 1(3):139–144, 1984.

[43] B. Coulbeck, B. Ulanicki, and C. H. Orr. Optimal scheduling of water supply taking account of quality and transmission costs. In *Water Quality Modeling in Distribution Systems*, pages 131–139, Cincinnati, Ohio, Feb. 1991. American Water Works Association.

[44] A. Delanoue and D. M. Holt. "TORUS" pipe test rig design and construction. Technical Report Projects R9311 & R9374, Thames Water Plc, Group Research & Development, Spencer House, Manor Farm Road, Reading, RG2 0JN, England, Feb. 1995. Company Confidential.

[45] A. Delanoue, D. M. Holt, H. A. Anderson, S. M. McMath, S. E. Smith, C. A. Woodward, A. R. Fraser, and M. Roe. Analysis of material (biofilm) present on the internal surfaces of a drinking water distribution system. In C. Keevil, editor, *Proceedings of the International Conference on Biofilms in Aquatic Systems*, Coventry, April 13–16 1997. Royal Society of Chemistry.

[46] A. Delanoue, D. M. Holt, S. M. McMath, and S. Smith. "TORUS" pipe test rig strip down 1996. Technical Report Project R19610, Thames Water

Plc, Group Research & Development, Spencer House, Manor Farm Road, Reading, RG2 0JN, England, Dec. 1997. Company Confidential.

[47] J. Dojlido and G. A. Best. *Chemistry of Water and Water Pollution.* Ellis Horwood, Ltd., London, 1993.

[48] R. M. Donlan and W. O. Pipes. Selected drinking water characteristics and attached microbial population density. *Journal American Water Works Association*, 80(11):70–76, Nov. 1988.

[49] S. Dukan, Y. Levi, P. Piriou, F. Guyon, and P. Villon. Dynamic modelling of bacterial growth in drinking water networks. *Water Research*, 30(9):1991–2002, 1996.

[50] D. K. Edwards, V. E. Denny, and A. F. Mills. *Transfer Processes.* McGraw-Hill, New York, 1976.

[51] A. Elton, L. F. Brammer, and N. S. Tansley. Water quality modeling in distribution networks. *Journal of the American Water Works Association*, 87(7):44–52, July 1995.

[52] T. H. Feng. Behaviour of organic chloramines in disinfection. *J. Water Pollut. Control Fed.*, 38(4):614–627, 1966.

[53] J. W. Forrester. *Principles of Systems.* Wright-Allen Press, Cambridge, Massachusetts, 1968.

[54] G. Fransolet, G. Villers, and W. J. Masschelein. Influence of temperature on bacterial development in waters. *Ozone Sci. Engng.*, 7:205–227, 1985.

[55] H. J. Gold. *Mathematical Modeling of Biological Systems—an Introductory Guidebook.* John Wiley & Sons, New York, 1977.

[56] R. C. Gonzalez and R. E. Woods. *Digital Image Processing.* Addison-Wesley, New York, 1992.

[57] M. A. Goshko, H. A. Minnigh, W. O. Pipes, and R. R. Christian. Relationships between standard plate counts and other parameters in water distribution systems. *Journal American Water Works Association*, pages 568–571, Nov. 1983.

[58] K. Gotoh. Residual chlorine concentration decreasing rate coefficients for various pipe materials. *Water Supply*, 1(2/3):SS 21–17 - SS 21–18, 1989.

[59] W. M. Grayman and R. M. Clark. An overview of water quality modeling in a distribution system. In *The 1990 Annual Conference Proceedings*, pages 81–92, Cincinnati, Ohio, 1990. American Water Works Association.

[60] W. M. Grayman, R. M. Clark, and R. M. Males. Modeling distribution-system water quality: Dynamic approach. *Journal of Water Resources Planning and Management*, 114(3):295–312, May 1988.

[61] W. Gujer and O. Wanner. A multispecies biofilm model. *Biotechnology and Bioengineering*, 28:314–328, 1986.

[62] W. Gujer and O. Wanner. Modelling mixed population biofilms. In W. G. Characklis and K. C. Marshall, editors, *Biofilms*. pages 397–443. J. Wiley & Sons, New York, 1990.

[63] C. N. Haas, M. A. Meyer, and M. S. Paller. Microbial alterations in water distribution systems and their relationship to physical-chemical characteristics. *Journal American Water Works Association*, pages 475–481, Sept. 1983.

[64] R. Haber and H. Unbehauen. Structure identification of nonlinear dynamic systems—a survey on input/output approaches. *Automatica*, 26(4):651–677, 1990.

[65] E. E. Hargesheimer and C. M. Lewis. A practical guide to on-line particle counting. Technical report, American Water Works Association Research Foundation, Denver, Colorado, 1995. ISBN 0-89867-785-8.

[66] S. Hatukai, Y. Ben-Tzur, and M. Rebhun. Particle counts and size distribution in sytem design for removal of turbidity by granular deep bed filtration. *Water Science and Technology: A Journal of the International Association of Water Polution Research*, 36(4):225–230, 1997.

[67] J. Heraud, L. Kiéné, M. Detay, and Y. Levi. Optimised modelling of chlorine residuals in a drinking water distribution system with a combination of on-line sensors. *Journal Water Supply Research and Technology - Aqua*, 46(2):59–70, 1997.

[68] A. L. Hines and R. N. Maddox. *Mass Transfer - Fundamentals and Applications*. Prentice-Hall, Englewood Cliffs, NJ, 1985.

[69] D. M. Holt, C. A. Woodward, T. Rachwal, A. Delanaoue, and J. S. Colbourne. A pipe based experimental system to study factors influencing bacterial growth in London's water mains. In *Proceedings of the Water Quality Technical Conference*, San Francisco, 6–10th November 1994. American Water Works Association, Denver.

[70] R. F. Hoskins. *Generalised Functions*. Ellis Horwood Ltd, Chichester, 1979.

[71] P. M. Huck. Measurement of biodegradable organic matter and bacterial growth potential in drinking water. *Journal of the American Water Works Association*, 82:78–86, July 1990.

[72] W. A. Hunt and J. R. Kroon. Model calibration for chlorine residuals in distribution systems. In *Water Quality Modeling in Distribution Systems*, pages 237–261, Cincinnati, Ohio, Feb. 1991. American Water Works Association.

[73] IHD-WHO Working Group on the Quality of Water. *Water Quality Surveys.* UNESCO/WHO, Paris/Geneva, 1978.

[74] Internatioal Water Supply Association. The practice of chlorination: Application, efficacy, problems and alternatives. *Journal Water Supply Research and Technology - Aqua*, 46(4):inserted as The Blue Pages, Aug. 1997.

[75] J. Jass, J. W. Costerton, and H. M. Lappin-Scott. Assessment of a chemostat-coupled modified Robbins device to study biofilms. *Journal of Industrial Microbiology*, 15:283–289, 1995.

[76] T. A. Johansen and B. A. Foss. Empirical modeling of a heat transfer process using local models and interpolation. In *Proceedings of the American Control Conference*, pages 3654–3658, Seattle, Washington, 1995.

[77] R. Johansson. *System Modeling and Identification.* Prentice-Hall, Englewood Cliffs, NJ, 1993.

[78] R. A. Johnson. *Miller and Freund's Probability and Statistics for Engineers.* Prentice-Hall International, London, 1994.

[79] R. P. Kanwal. *Generalised Functions: Theory and Technique.* Academic Press, New York, 1983.

[80] C. W. Keevil. Methods for assesing the activity of biofilm microorganisms *in situ.* In J. W. T. Wimpenny, W. Nichols, D. Stickler, and H. Lappin-Scott, editors, *Bacterial Biofilms and Their Control in Medicine and Industry*, pages 45–47. BioLine, Cardiff, 1994.

[81] M. S. Kennedy, S. Sarikelle, and K. Suravallop. Travel time calibration in water distribution systems. In *Water Quality Modeling in Distribution Systems*, pages 219–233, Cincinnati, Ohio, Feb. 1991. American Water Works Association.

[82] E. Kreyszig. *Advanced Engineering Mathematics.* John Wiley & Sons, New York, 7th edition, 1993.

[83] M. W. LeChevallier. Microbial processes within the distribution system. In *Water Quality Modeling in Distribution Systems*, pages 365–380, Cincinnati, Ohio, Feb. 1991. American Water Works Association.

[84] M. W. LeChevallier, T. M. Babcock, and R. G. Lee. Examination and characterization of distribution system biofilms. *Applied and Environmental Microbiology*, 53(12):2714–2724, Dec. 1987.

[85] M. W. LeChevallier, C. D. Cawthon, and R. G. Lee. Inactivation of biofilm bacteria. *Applied and Environmental Microbiology*, 54(10):2492–2499, Oct. 1988.

[86] M. W. LeChevallier, C. D. Lowry, and R. G. Lee. Disinfection of biofilms in a model distribution system. In M. W. LeChevallier, B. H. Olson, and G. A. McFeters, editors, *Assessing and Controlling Bacterial Regrowth in Distribution Systems*, chapter 1, pages 1–47. American Water Works Association Research Foundation, 1990.

[87] P. Lindskog and L. Ljung. Tools for semi-physical modelling. In T. Söderström and M. Blanke, editors, *Proceedings of the IFAC Symposium on System Identification*, volume 3, pages 1199–1204, Copenhagen, Denmark, 1995. Pergamon.

[88] C. P. Liou and J. R. Kroon. Modeling the propagation of waterborne substances in distribution networks. *Journal of the American Water Works Association*, pages 54–58, Nov. 1987.

[89] L. Ljung. *System Identification: Theory for the User.* Prentice-Hall, Englewood Cliffs, NJ, 1987.

[90] L. Ljung and T. Glad. *Modeling of Dynamic Systems.* Prentice-Hall, Englewood Cliffs, NJ, 1994.

[91] C. Lu, P. Biswas, and R. M. Clark. Simultaneous transport of substrates, disinfectants and microorganisms in water pipes. *Water Research*, 29(3):881–894, 1995.

[92] M. Lungwitz, S. Hopfgarten, K. Chen, M. Brdys, and H. Puta. Modelling and simulation of chlorine concentration in water supply systems for control purposes. In *Proceedings of the 39th International Scientific Colloquium*, Ilmenau, Germany, Sept. 1994.

[93] D. Maier, M. Maier, and J. Ulmer. Automatische Wassergütemeßstationen; Teil I: Stand und Entwicklung von Meßgeräten zur kontinuierlichen Wassergüteüberwachung. *Wasser — Abwasser*, 136(5):242–249, 1995.

[94] S. H. Maier, S. Kaattari, and M. E. Magaña. Analysis of limiting dilution assays conducted under non-saturating conditions. *Journal of Theoretical Biology*, 179(2):173–177, 1996.

[95] S. H. Maier, M. E. Magaña, R. R. Mohler, and S. Kaattari. Modified limiting dilution assay for cell systems. *Applied Mathematics and Computation*, 78:187–195, 1996.

[96] S. H. Maier and R. S. Powell. A systems approach to modelling chlorine deacy in water distribution systems. In *Proceedings of the Doctoral Research Conference 1996*, Uxbridge, 19–20 June 1996. Department of Manufacturing and Engineering Systems, Brunel University.

[97] S. H. Maier, R. S. Powell, and C. A. Woodward. Behaviour of monochloramine in a pipe test rig. In R. S. Powell and K. S. Hindi, editors, *Proceedings of the International Conference on Computing and Control for the Water Industry*, Uxbridge, September 4–5 1997. Research Studies Press.

[98] S. H. Maier, C. A. Woodward, A. Delanoue, D. M. Holt, S. M. McMath, and R. S. Powell. Relationships between total chlorine, particle counts and biofilm detachment in a drinking water distribution system. In C. W. Keevil, editor, *Proceedings of the International Conference on Biofilms in Aquatic Systems*, Coventry, April 13–16 1997. Royal Society of Chemistry.

[99] R. M. Males. Graph-theoretic approaches to hydraulic network issues. In *Water Quality Modeling in Distribution Systems*, pages 95–109, Cincinnati, Ohio, Feb. 1991. American Water Works Association.

[100] K. Marshall, editor. *Microbial Adhesion and Aggregation, Dahlem Konferenzen*, Berlin, 1984. Springer-Verlag.

[101] R. E. Martin, M. Y. Ramirez, and V. P. Olivieri. Attachment of bacteria to surfaces in drinking water distribution systems. In *ASM Meeting '87*, 1987.

[102] B. Massey. *Mechanics of Fluids*. Chapman & Hall, London, 1995.

[103] S. M. McMath, A. Delanoue, D. M. Holt, A. H. L. Chamberlain, and B. J. Lloyd. The optimization of an epifluorescence microscopy technique for the direct counting of clumped bacteria. *Journal of the Chartered Institution of Water and Environmental Management*, 12(2):113, April 1998.

[104] S. M. McMath, A. Delanoue, D. M. Holt, S. H. Maier, and C. A. Woodward. Importance of "clumps" shed from biofilms in a water distribution system. In C. W. Keevil, editor, *Proceedings of the International Conference on Biofilms in Aquatic Systems*, Coventry, April 13–16 1997. Royal Society of Chemistry.

[105] R. Murga, P. S. Stewart, and D. Daly. Quantitative analysis of biofilm thickness variability. *Biotechnology and Bioengineering*, 45:503–510, 1995.

[106] L. A. Nagy and B. H. Olson. Occurence and significance of bacteria, fungi and yeasts associated with distribution pipe surfaces. In *Proceedings of the Water Quality Technical Conference*, Houston, Texas, 1985. American Water Works Association, Denver.

[107] J. A. Nelder and R. Mead. A simplex method for function minimization. *Comput. J.*, 7:308–313, 1965.

[108] O. Nelles, O. Hecker, and R. Isermann. Automatic model selection in local linear model trees (LOLIMOT) for nonlinear system identification of a transport delay process. In Y. Sawaragi and S. Sagara, editors, *Preprints of the 11th IFAC Symposium on System Identification*, volume 2, pages 727–732, Fukuoka, Japan, 1997. Pergamon.

[109] C. D. Norton and M. W. LeChevallier. Chloramination: its effect on distribution system water quality. *Journal of the American Water Works Association*, 89(7):66–77, July 1997.

[110] P. T. O'Shaughnessy, M. G. Barsotti, J. W. Fay, and S. W. Tighe. Evaluating particle counters. *Journal American Water Works Association*, 89(12):60–70, Dec. 1997.

[111] A. Ostfeld and U. Shamir. Optimal operation of multiquality distribution systems: Steady state conditions. In *Water Quality Modeling in Distribution Systems*, pages 111–129, Cincinnati, Ohio, Feb. 1991. American Water Works Association.

[112] P. J. Packer. Water distribution modelling effect on advanced water treatment. Final Report Project R92/C2, Physiology & Biofilms Section, Legionella & Aerobiology, Pathology Division, PHLS-CAMR (Centre for Applied Microbiology and Research), Porton Down, Salisbury, Wilts, SP4 0JT, Mar. 1994.

[113] B. M. Peyton and W. G. Characklis. Kinetics of biofilm detachment. Poster presented at *IAWPRC Conference – Water Quality International'92*, Washington D.C., May 24–30 1992.

[114] B. M. Peyton and W. G. Characklis. Kinetics of biofilm detachment. *Water Science and Technology*, 26(9–11):1995–1998, 1992.

[115] B. M. Peyton and W. G. Characklis. A statistical analysis of the effect of substrate utilization and shear stress on the kinetics of biofilm detachment. *Biotechnology and Bioengineering*, 41:728–735, 1993.

[116] P. Piriou. A new tool for the study of the evolution of water quality in distribution systems: design of a network pilot. In *Proceedings of the Water Quality Technical Conference*, New York, 19–23rd June 1994. American Water Works Association, Denver.

[117] P. Piriou, S. Dukan, and Y. Levi. Piccobio: Modelling bacterial regrowth in drinking water distribution systems. In R. S. Powell and K. S. Hindi, editors, *Computing and Control for the Water Industry*. Research Studies Press Ltd., Taunton, England, 1998.

[118] P. Piriou, Y. Levi, J. Heraud, and L. Kiene. New tools and applications in modelling and monitoring water quality in drinking water distribution systems. *Water Supply*, 15(2):119–135, 1997.

[119] R. S. Powell. WASMACS functional description. Technical Report 3.4, WASMACS Ltd., Control Engineering Centre, Brunel University, UB8 3PH, U.K., Sept. 1994.

[120] N. M. Ram and J. P. Malley Jr. Chlorine residual monitoring in the presence of N-organic compounds. *Journal of the American Water Works Association*, pages 74–81, Sept. 1984.

[121] M. Reike, K. H. Fasol, G. Sinai, and D. Pessen. Hierarchical control of multi-quality water distribution systems. *Computers and Electronics in Agriculture*, 2:1–13, 1987.

[122] B. E. Rittman. Detachment from biofilms. In W. G. Characklis and P. A. Wilderer, editors, *Structure and Function of Biofilms*, pages 49–57. J. Wiley & Sons, New York, 1989.

[123] L. A. Rossman. The EPANET water quality model. In B. Coulbeck, editor, *Integrated Computer Applications in Water Supply. Volume 2 - Applications and Implementations for Systems Operation and Management*, pages 79–93. Research Studies Press Ltd., Taunton, England, 1993.

[124] L. A. Rossman. *EPANET User's Manual, EPA-600/R-94/057.* Risk Reduction Engineering Laboratory, U.S. Environmental Protection Agency, Cincinnati, Ohio, Jan. 1994. Version 1.1.

[125] L. A. Rossman and P. F. Boulos. Numerical methods for modelling water quality in distribution systems: A comparison. *Journal of Water Resources Planning and Management*, 122(2):137–146, March/April 1996.

[126] L. A. Rossman, P. F. Boulos, and T. Altman. Discrete volume-element method for water-quality models. *Journal of Water Resources Planning and Management*, 119(5):505–517, September/October 1993.

[127] SAFEGE, Consulting Engineers. *Piccolo 3.10 Reference Manual*, November/December 1992.

[128] S. Schneider, M. A. Brdys, H. Puta, and S. Hopfgarten. Modelling of chlorine concentration in water systems directed to integrated operational control. In B. Coulbeck, editor, *Integrated Computer Applications in Water Supply*, pages 143–159, 1993.

[129] P. Servais, P. Laurent, and G. Randon. Comparison of the bacterial dynamics in various French distribution systems. *Journal Water Supply Research and Technology - Aqua*, 44(1):10–17, 1995.

[130] U. Shamir and C. D. D. Howard. Water distribution system analysis. *Journal of the Hydraulics Division*, 94(HY1):219–234, Jan. 1968.

[131] U. Shamir and C. D. D. Howard. Topics in modelling water quality in distribution systems. In *Water Quality Modeling in Distribution Systems*, pages 183–192, Cincinnati, Ohio, Feb. 1991. American Water Works Association.

[132] W. W. Sharp, J. Pfeffer, and M. Morgan. Insitu chlorine decay rate testing. In *Water Quality Modeling in Distribution Systems*, pages 311-321, Cincinnati, Ohio, Feb. 1991. American Water Works Association.

[133] R. Sinha, P. Gupta, and P. K. Jain. Water quality modelling of a city water distribution system. *Indian J. Environ. Hlth.*, 36(4):258-262, 1994.

[134] J. Sjöberg, Q. Zhang, L. Ljung, A. Benveniste, B. Deylon, P.-Y. Glorennec, H. Hjalmarsson, and A. Juditsky. Non-linear black-box modelling in system identification: a unified overview. *Automatica*, 31(12):1691–1724, 1995.

[135] T. Söderström and P. Stoica. *System Identification*. Prentice-Hall, Englewood Cliffs, NJ, 1989.

[136] M. Somville and G. Billen. A method for determining exoproteolytic activity in natural waters. *Limnol. Oceanogr.*, 28:190–193, 1983.

[137] P. S. Stewart. A model of biofilm detachment. *Biotechnology and Bioengineering*, 41:111–117, 1993.

[138] P. Stoodley, A. Cunningham, Z. Lewandowski, J. Boyle, and H. Lappin-Scott. Biofilm structure and influence on biofouling under laminar and turbulent flows. In C. Keevil, editor, *Proceedings of the International Conference on Biofilms in Aquatic Systems*, Coventry, April 13–16 1997. Royal Society of Chemistry.

[139] P. T. Strait. *Probability and Statistics with Applications*. Harcourt Brace Jovanovich, London, 2nd edition, 1989.

[140] T. Ta. Analysis of the particle counts and the chlorine decay in PIPE RIG during the step flow trials. Technical report, Thames Water Utilities Ltd., Group R&D, Spencer Hse, Manor Farm Rd, Reading, Berks RG2 0JN, July 1995.

[141] P. M. Thomas. Chloramination of water supplies. Progress report no.1, Urban Water Research Association, State Water Laboratory, Engineering and Water Supply Department, S.A., Australia, Jan. 1988.

[142] R. Todd. Reaction of nitrite with chlorine species. Experimental report, Operational Science, Thames Water Utilities Ltd., Wraysbury, Aug. 1995.

[143] R. E. Train. *Quality Criteria for Water*. Castle House Pub., London, 1979.

[144] M. G. Trulear. Dynamics of biofilm processes in an annular reactor. Master's thesis, Rice University, Houston, Texas, 1980.

[145] M. G. Trulear and W. G. Characklis. Dynamics of biofilm processes. *Journal WPCF*, 54(9):1288–1301, Sept. 1982.

[146] H. Unbehauen. *Regelungstechnik III*. Vieweg Verlag, Braunschweig, 5th edition, 1995.

[147] H. Unbehauen. Some new trends in identification and modeling of nonlinear dynamical systems. *Applied Mathematics and Computation*, 78:279–297, 1996.

[148] H. Unbehauen and G. P. Rao. *Identification of Continuous Systems*. North Holland, Amsterdam, 1987.

[149] D. van der Kooij and H. R. Veenendaal. Assessment of the biofilm formation characteristics of drinking water. In *Proceedings of the American Water Works Association Water Quality Conference*, pages 1099–1110, Toronto. Canada, November 15–19 1992.

[150] D. van der Kooij and H. R. Veenendaal. Biofilm development on surfaces in drinking water distribution systems. *Water Supply*, 12(1/2):SS1–1 - SS1–7. 1994. Special subject: Biological activity in distribution systems.

[151] E. van der Wende and W. G. Characklis. Biofilms in potable water distribution systems. In A. McFeters, editor, *Drinking Water Microbiology*, chapter 12, pages 249–268. Springer-Verlag, 1990.

[152] E. van der Wende, W. G. Characklis, and D. B. Smith. Biofilms and bacterial drinking water quality. *Water Research*, 23:1313–1320, 1989.

[153] J. J. Vasconcelos, L. A. Rossman, W. M. Grayman, P. F. Boulos, and R. M. Clark. Kinetics of chlorine decay. *Journal American Water Works Association*, 89(7):54–65, July 1997.

[154] O. Wable, N. Dumoutier, J. P. Duguet, P. A. Jarrige, G. Gelas, and J. F. Depierre. Modelling chlorine concentrations in a network and applications to Paris distribution system. In *Water Quality Modeling in Distribution Systems*, pages 77–87, Cincinnati, Ohio, Feb. 1991. American Water Works Association.

[155] É. Walter and L. Pronzato. *Identification of Parametric Models*. Springer-Verlag, London, 1997.

[156] G. C. White. *Handbook of Chlorination and Alternative Disinfectants*. John Wiley & Sons Inc., Taunton, England, 1998.

[157] J. W. T. Wimpenny. The spatial organisation of biofilm. In J. W. T. Wimpenny, W. Nichols, D. Stickler, and H. Lappin-Scott, editors, *Bacterial Biofilms and Their Control in Medicine and Industry*, pages 1–6. BioLine, Cardiff, 1994.

[158] S. Wolfram. *The Mathematica Book*. Wolfram Media and Cambridge University Press, Cambridge, Mass., 3rd edition, 1996.

[159] C. A. Woodward, C. T. Ta, J. Colbourne, and D. M. Holt. Behaviour of particles in a large scale experimental pipe system. In *Proceedings of the Water Quality Technology Conference*, New Orleans, 12–16th November 1995. American Water Works Association.

[160] C. A. Woodward, C. T. Ta, D. M. Holt, and J. Colbourne. Relationship between observed monochloramine decay rates and other physical and chemical parameters. In *Proceedings of the Water Quality Technology Conference*, New Orleans, 12–16th November 1995. American Water Works Association.

# Appendix

# Appendix A

# Model-Relevant Data

This appendix contains graphs of the data most relevant for the development of a water quality model. In particular it covers the particle counter data for the twelve step flow trials of the 1996 experiment. Both total particle counts and size distributions are included. This appendix is meant as a reference to allow the visual verification of the characterisation of data as given in chapter 4, which is the basis of the models obtained in chapter 6.

All graphs given in this appendix are generated with the Matlab function `plotallpc` that is part of the Water Quality Toolbox.

## A.1 Total Particle Counts

Observations from the total particle counter data presented in this section are given in section 4.1 on page 67.

Figs. A.1 to A.12 present total particle counts, i.e. the number of all particles $\geq 2\mu$m, for inlet shed (if appropriate), sample points 1, 2 and 3 together with flow rate (for reference) versus time. All graphs are split into four plots according to sample point. Note that some of the peaks are not visible in these graphs as the graphs have been scaled to show the slow pattern better. All times are in days since 1 January 1995.

Note that after step down at of SFT 1 (fig. A.1) there was a treatment plant failure. Therefore the flow rate is interrupted (i.e. zero) for several hours.

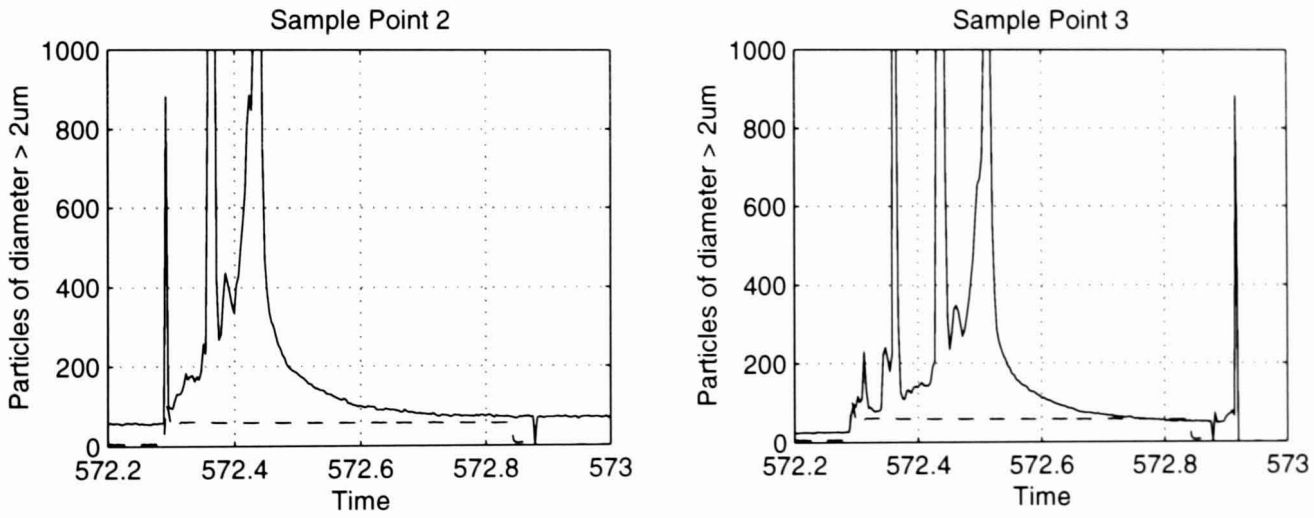


**Figure A.1:** *Step flow trial 1, 25 July 1996: total particle counts data during high flow period; time is in days since 1 January 1995, flow (dashed line) is multiplied by 100 and included for reference. Inlet particle counter data was not yet installed.*

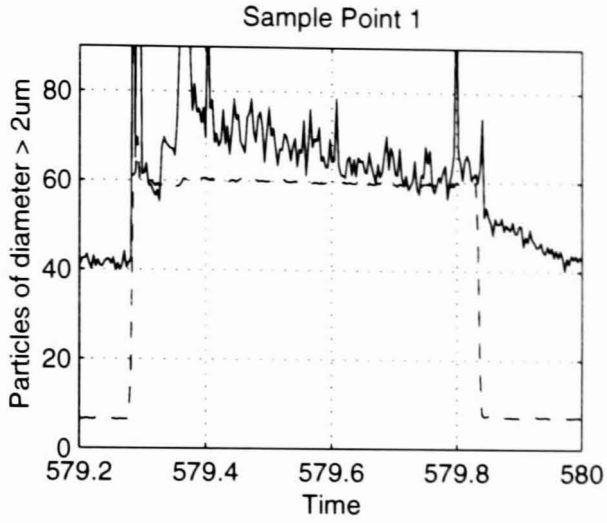


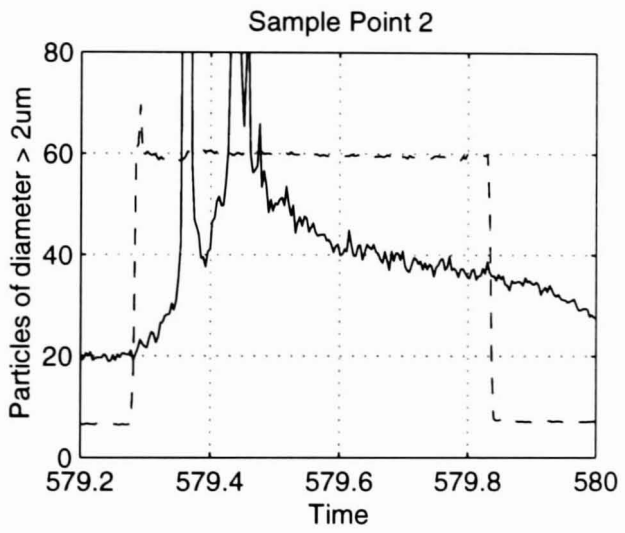


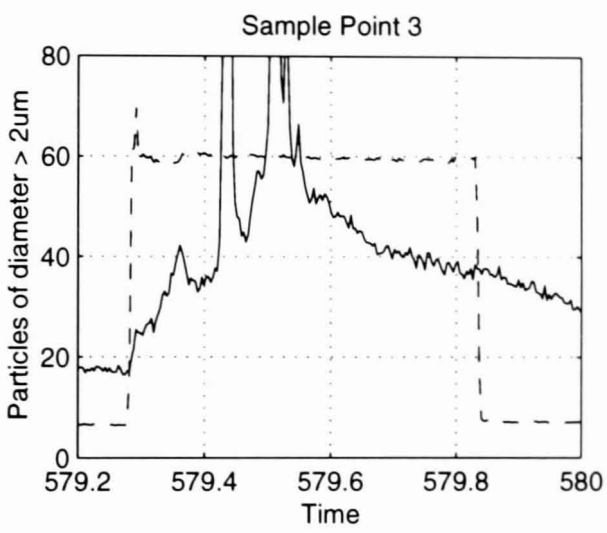


**Figure A.2:** *Step flow trial 2, 1 August 1996: total particle counts data during high flow period; time is in days since 1 January 1995, flow (dashed line) is multiplied by 100 and included for reference. Inlet particle counter data was not yet installed.*

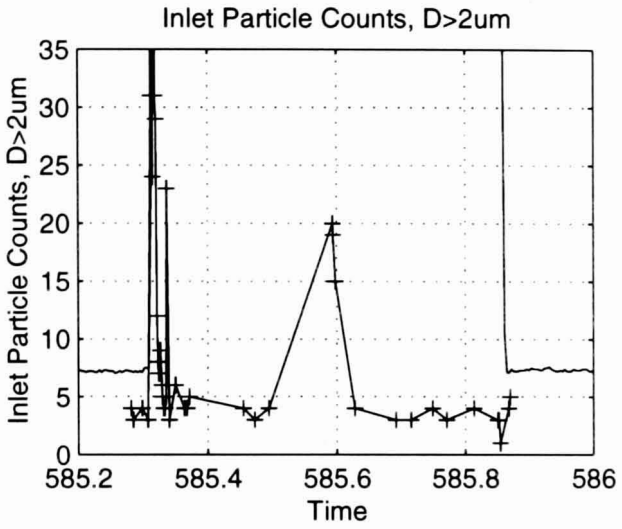


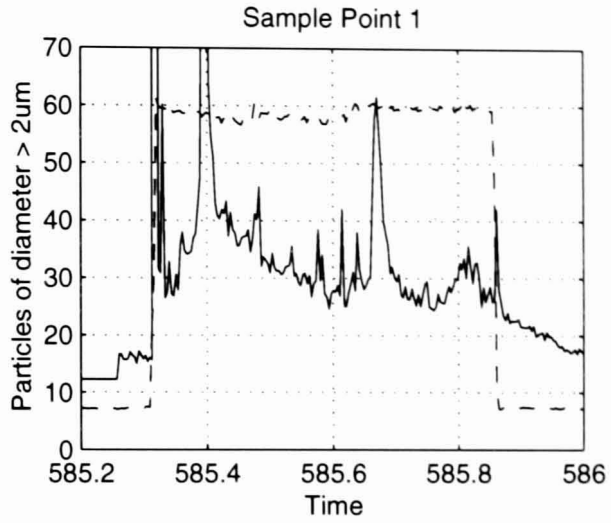


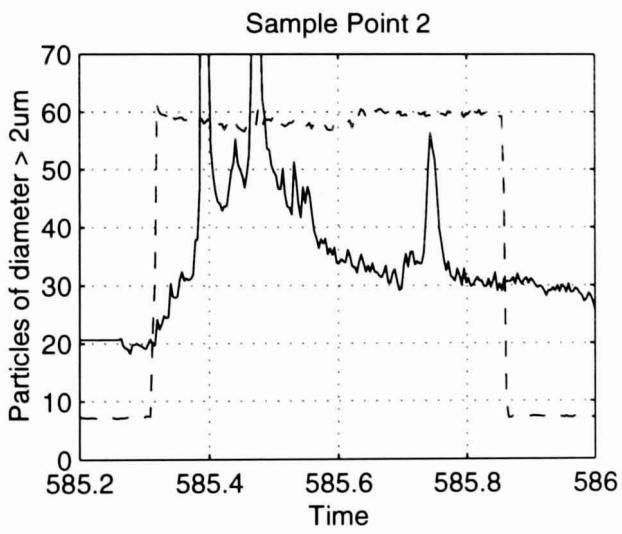


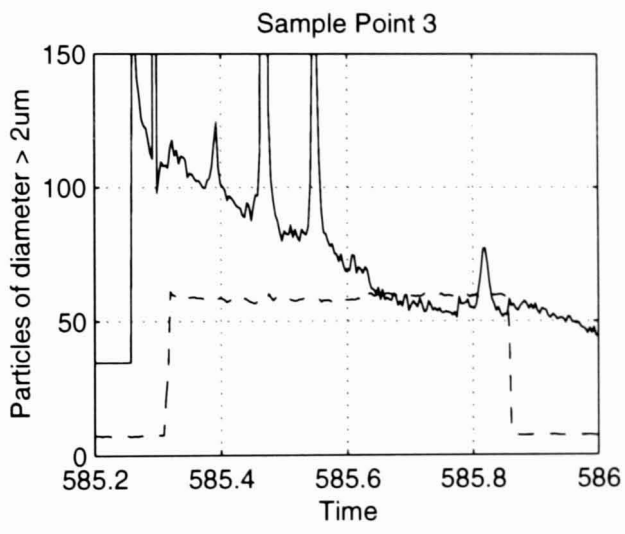


**Figure A.3:** *Step flow trial 3, 7 August 1996: total particle counts data during high flow period; time is in days since 1 January 1995, flow (dashed line) is multiplied by 100 and included for reference. Inlet particle counter data was not yet computer logged (hand-logged data is shown).*

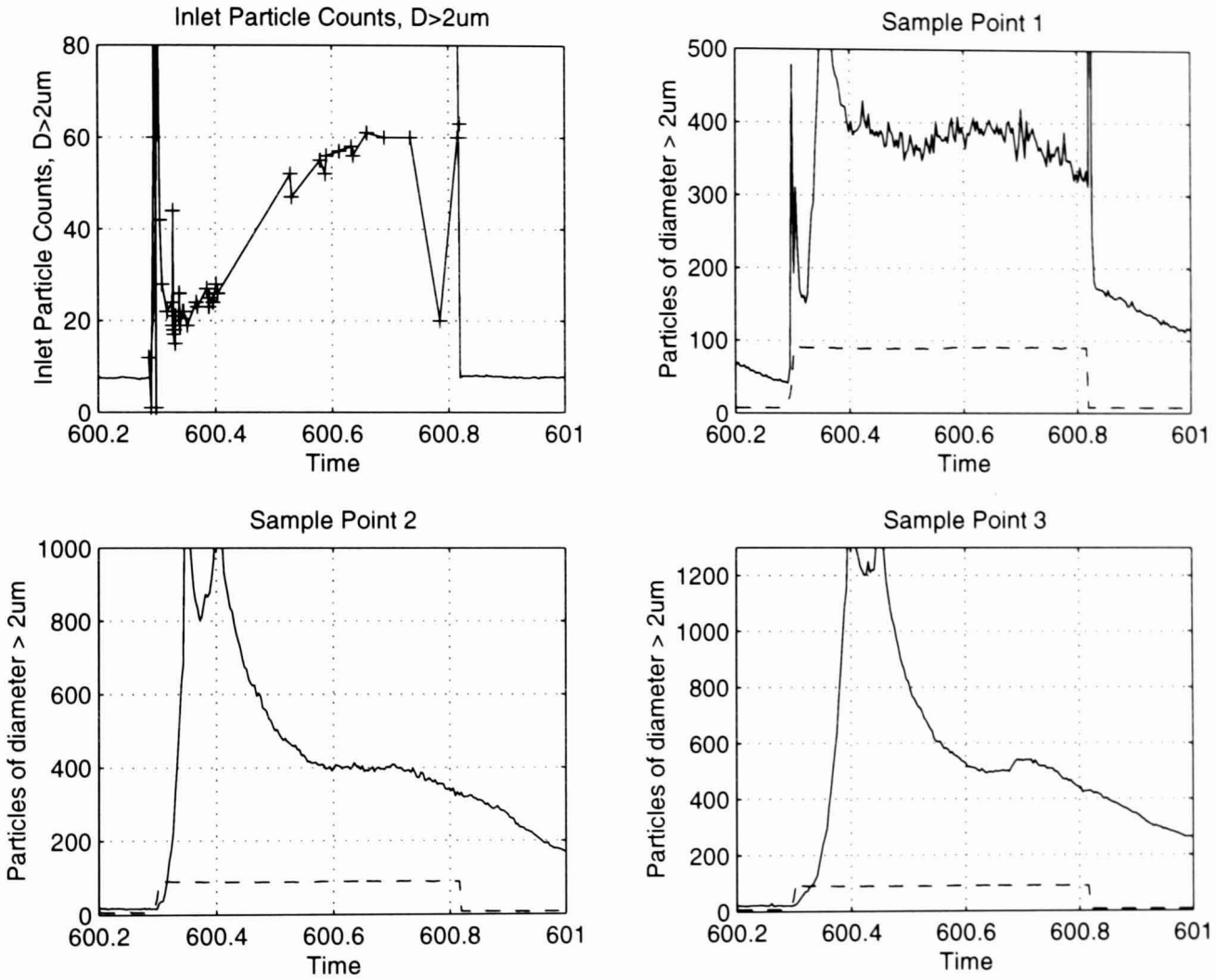


**Figure A.4:** *Step flow trial 4, 22 August 1996: total particle counts data during high flow period; time is in days since 1 January 1995, flow (dashed line) is multiplied by 100 and included for reference. Inlet particle counter data was not yet computer logged (hand-logged data is shown).*

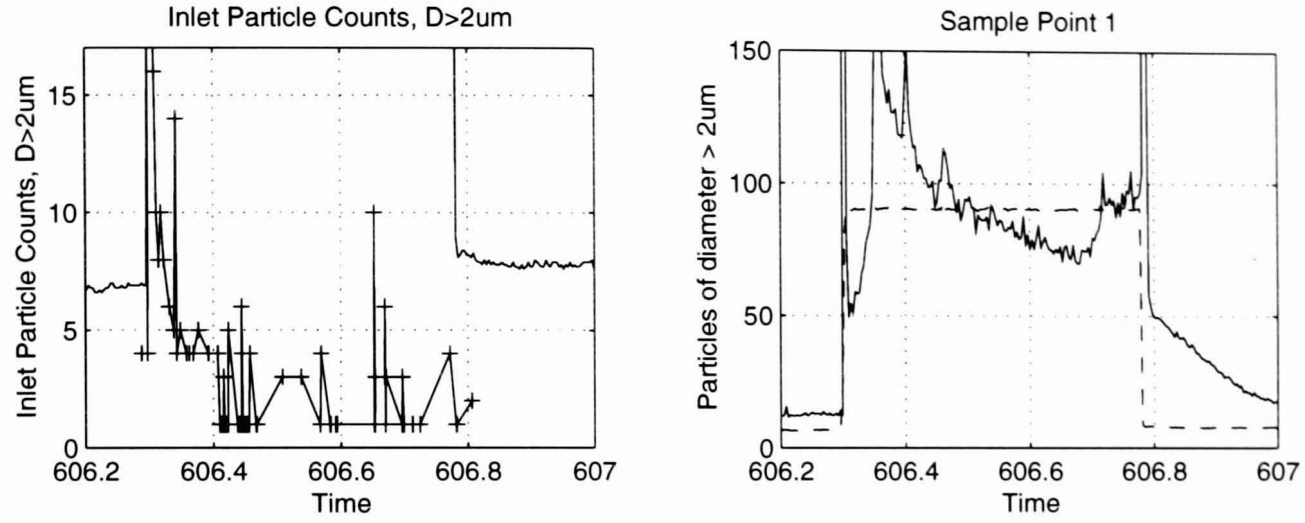


**Figure A.5:** *Step flow trial 5, 28 August 1996: total particle counts data during high flow period; time is in days since 1 January 1995, flow (dashed line) is multiplied by 100 and included for reference. Inlet particle counter data was not yet computer logged (hand-logged data is shown).*

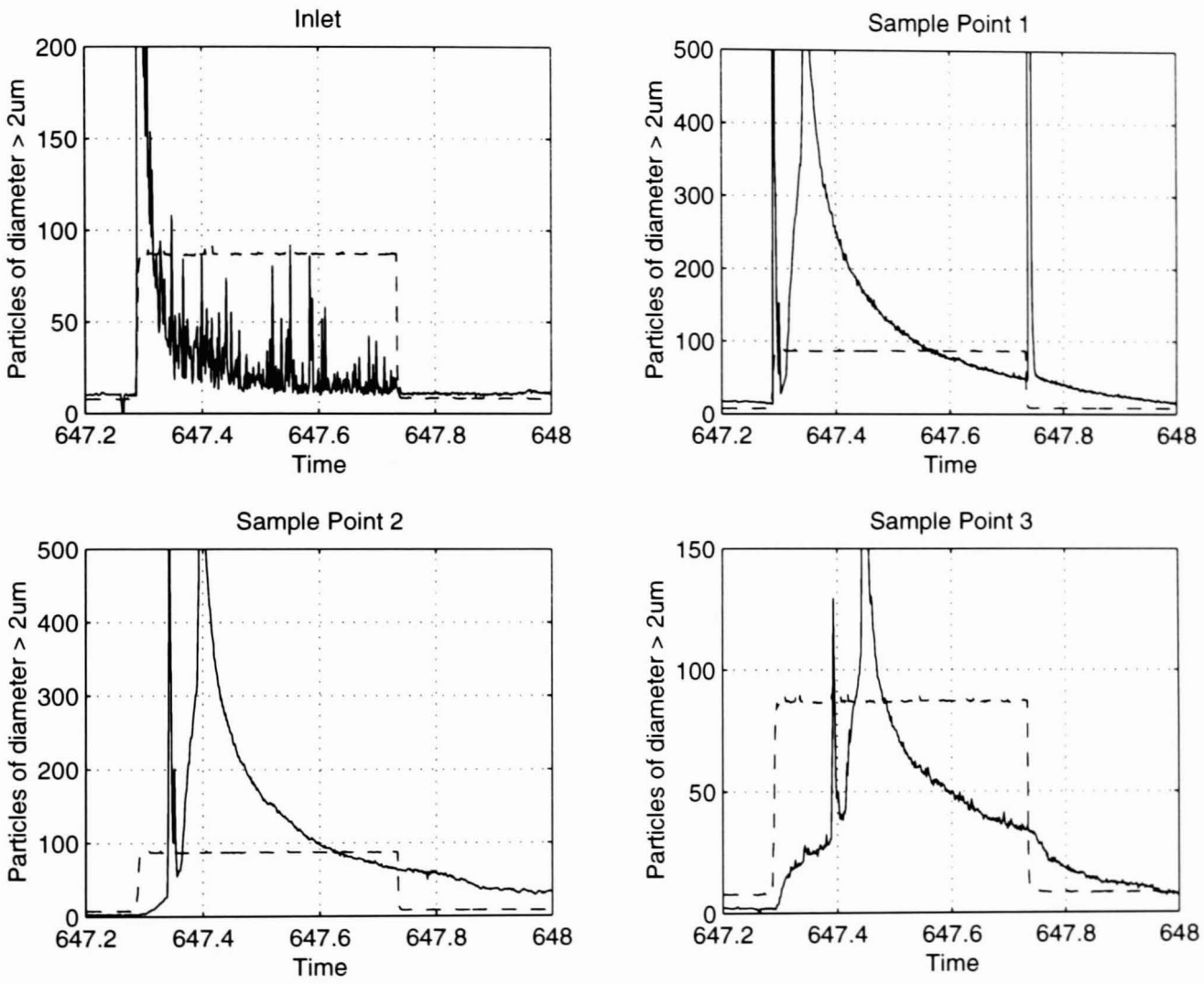


**Figure A.6:** *Step flow trial 6, 8 October 1996: total particle counts data during high flow period; time is in days since 1 January 1995, flow (dashed line) is multiplied by 100 and included for reference.*

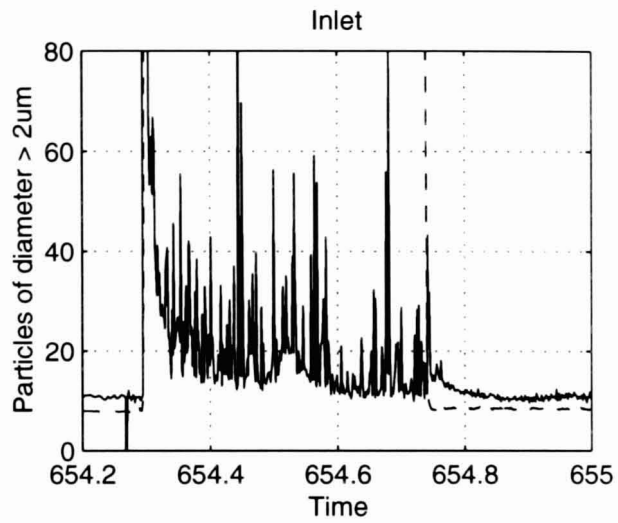


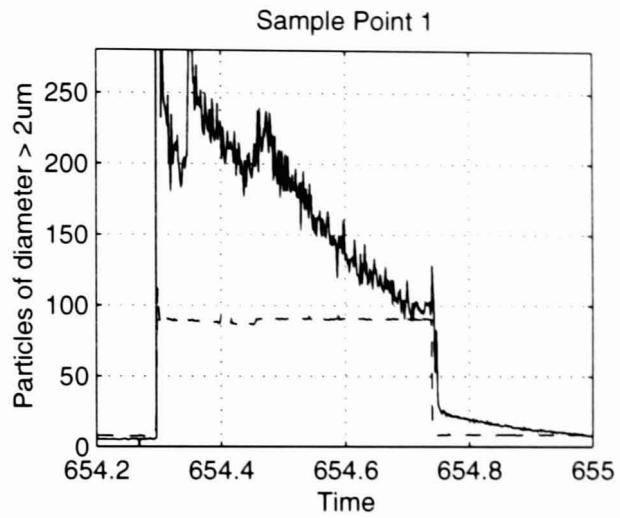


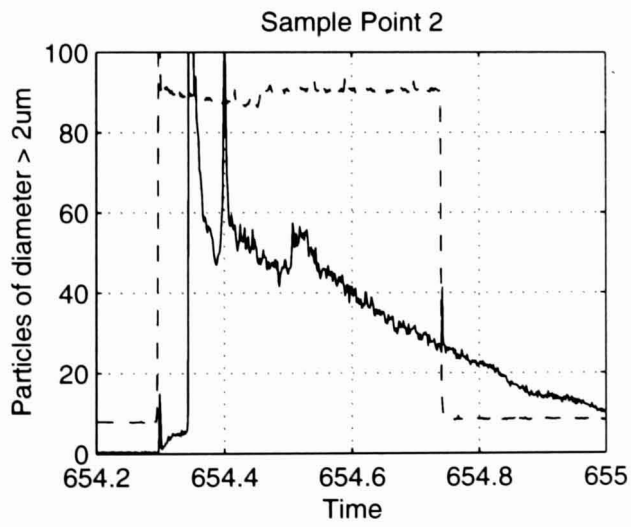


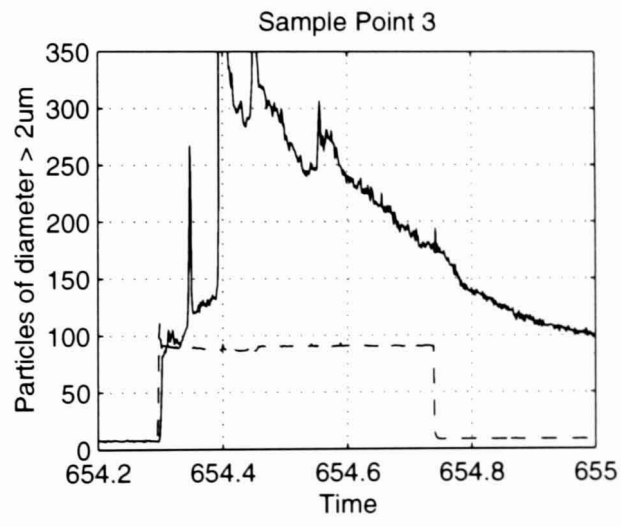


**Figure A.7:** *Step flow trial 7, 15 October 1996: total particle counts data during high flow period; time is in days since 1 January 1995, flow (dashed line) is multiplied by 100 and included for reference.*

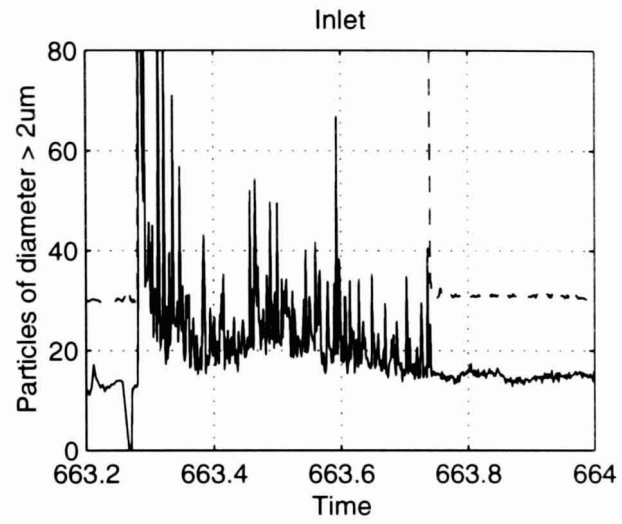


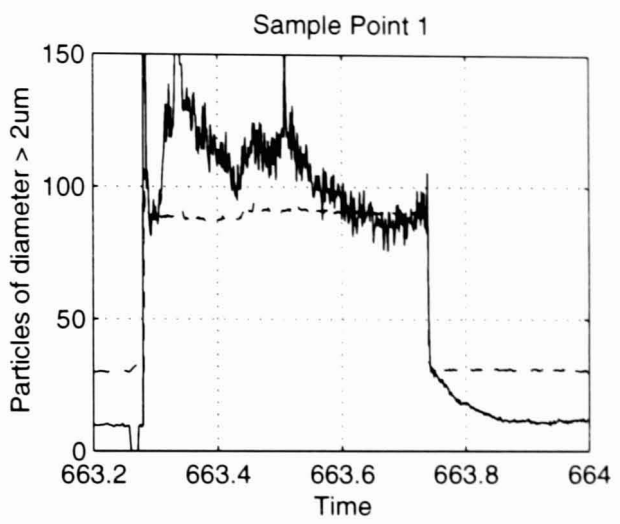


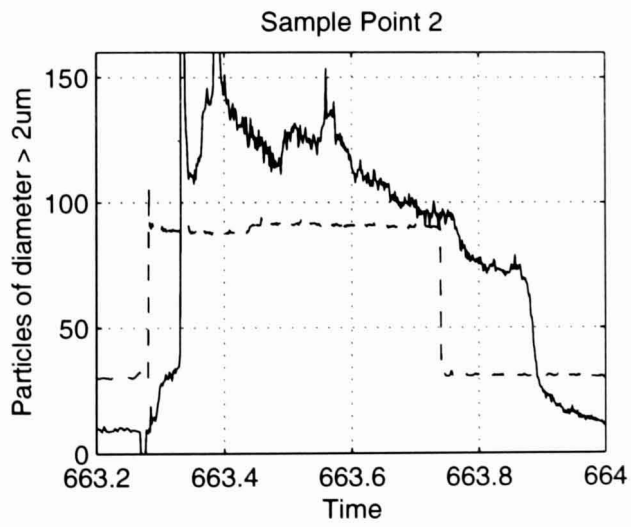


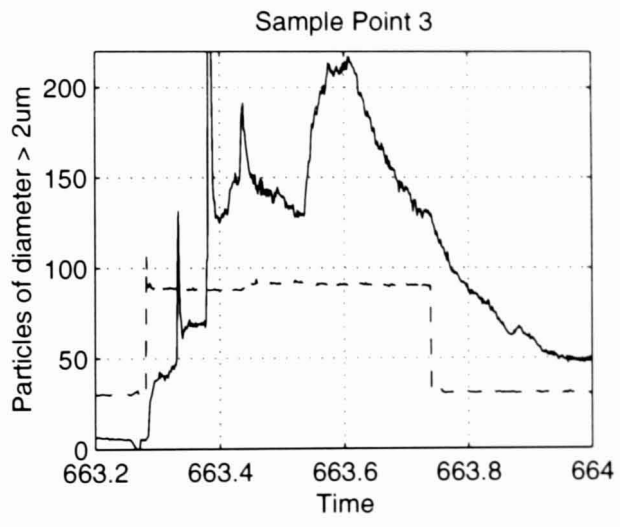


**Figure A.8:** *Step flow trial 8, 24 October 1996: total particle counts data during high flow period; time is in days since 1 January 1995, flow (dashed line) is multiplied by 100 and included for reference.*

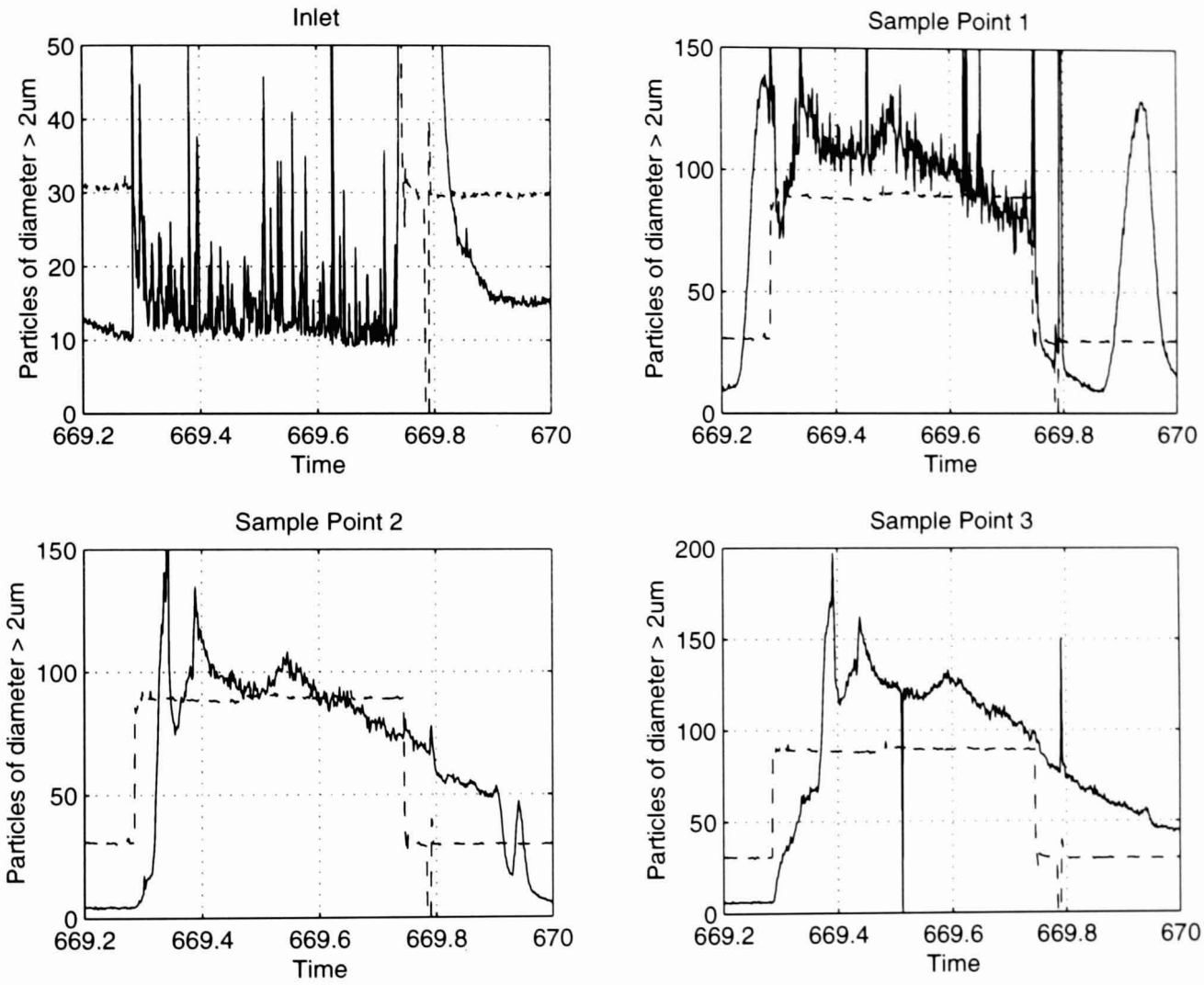


**Figure A.9:** *Step flow trial 9, 30 October 1996: total particle counts data during high flow period; time is in days since 1 January 1995, flow (dashed line) is multiplied by 100 and included for reference.*

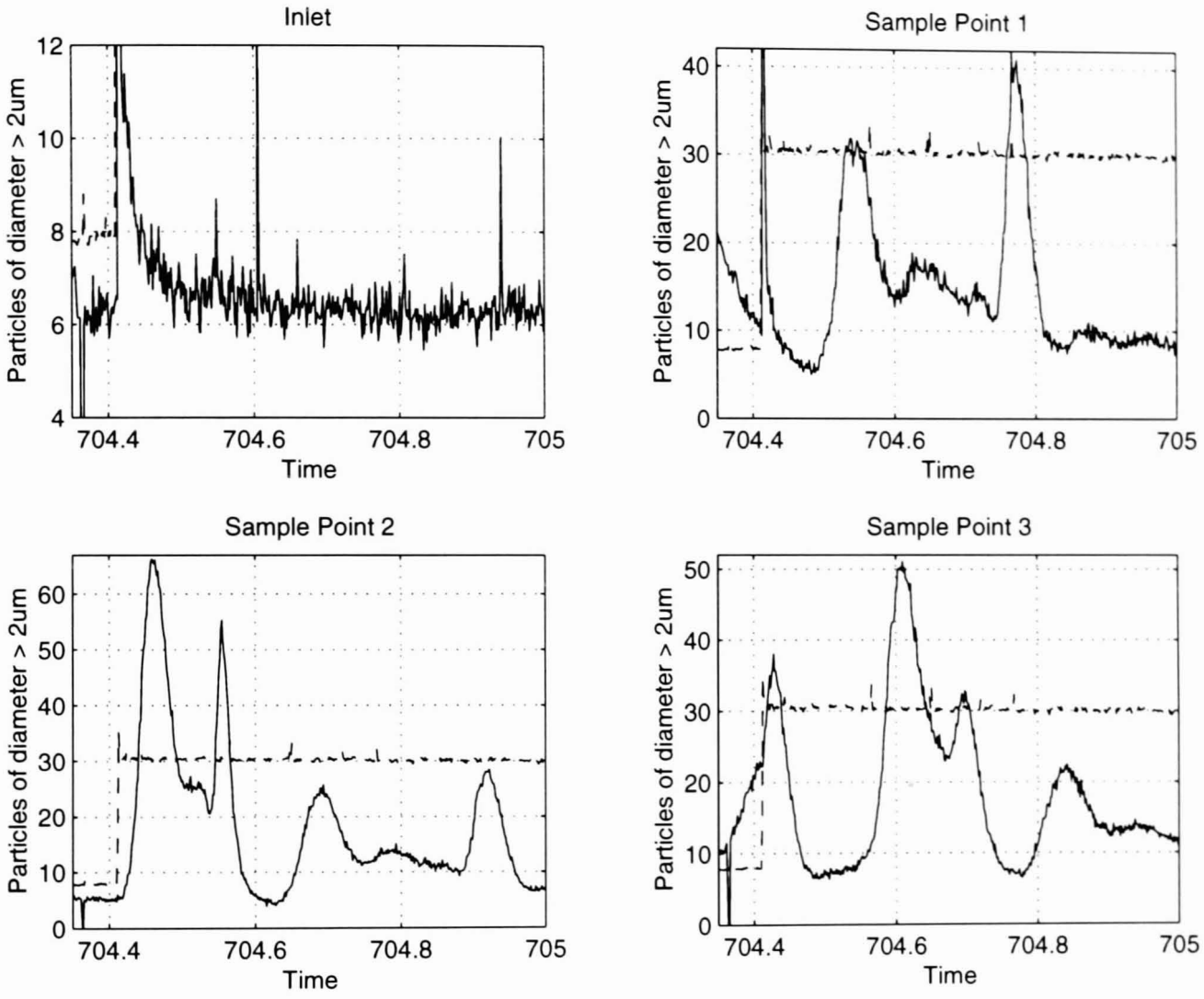


**Figure A.10:** *Step flow trial 10, 4–5 December 1996: total particle counts data during high flow period; time is in days since 1 January 1995, flow (dashed line) is multiplied by 100 and included for reference.*

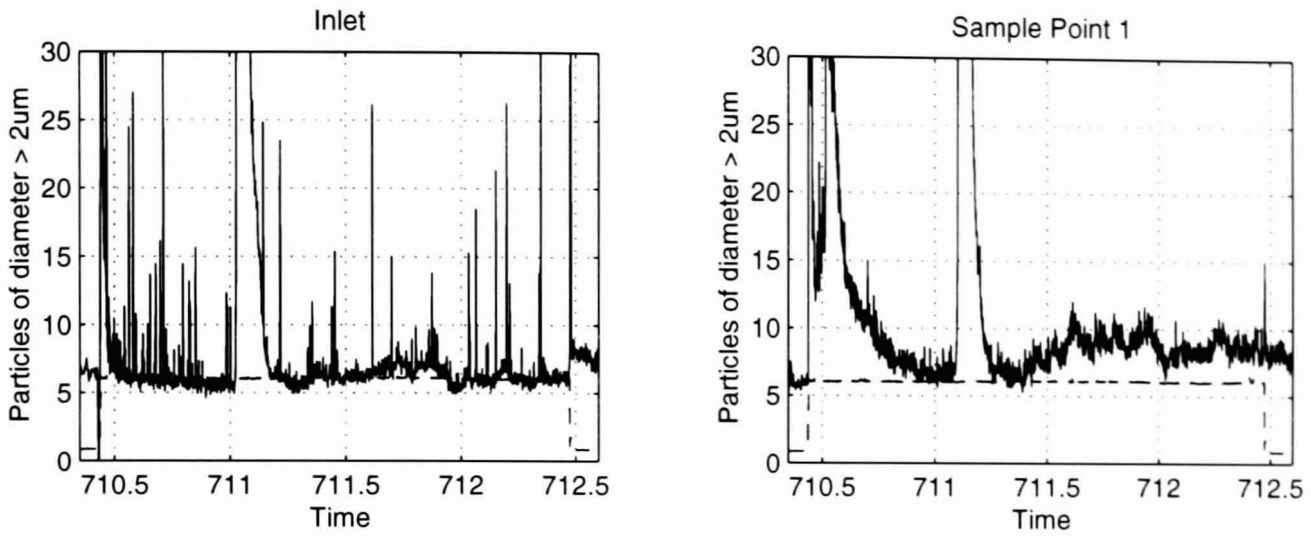


**Figure A.11:** *Step flow trial 11, 10–12 December 1996: total particle counts data during high flow period; time is in days since 1 January 1995, flow (dashed line) is multiplied by 10 and included for reference.*

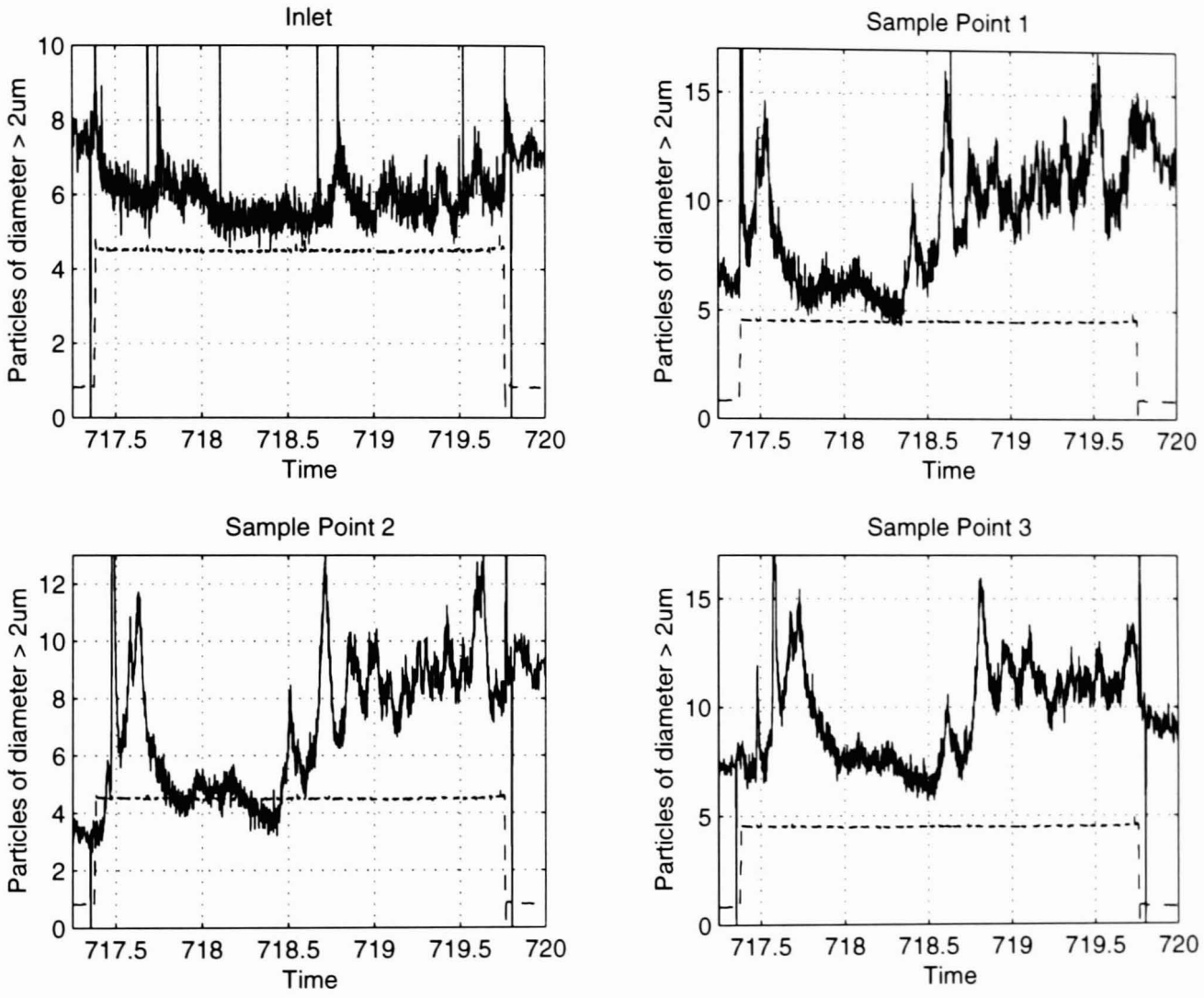


**Figure A.12:** *Step flow trial 12, 17–19 December 1996: total particle counts data during high flow period; time is in days since 1 January 1995, flow (dashed line) is multiplied by 10 and included for reference.*

## A.2 Size Distributions of Particle Counts

Observations from the particle counter size distributions presented in this section are given in section 4.2 on page 74.

The figures A.13 to A.24 show particle counter size distributions, one subplot per sample point, with percentages on the y-axis and time in days since 1.1.1995 on the x-axis. Flow is given for reference as a dashed line, its value in litre per second is multiplied by 100 to fit on the same scale as the percentages. In addition, a vertical dashed-dotted line marks the elapse of one travel time since the start of the step flow trial to the respective sample point. The lines depicted on the graphs show (from larger to smaller values) particles in the range 2–5$\mu$m, 5–10$\mu$m, 10–15$\mu$m and 15–20$\mu$m (cf. fig. 4.3 on page 75).

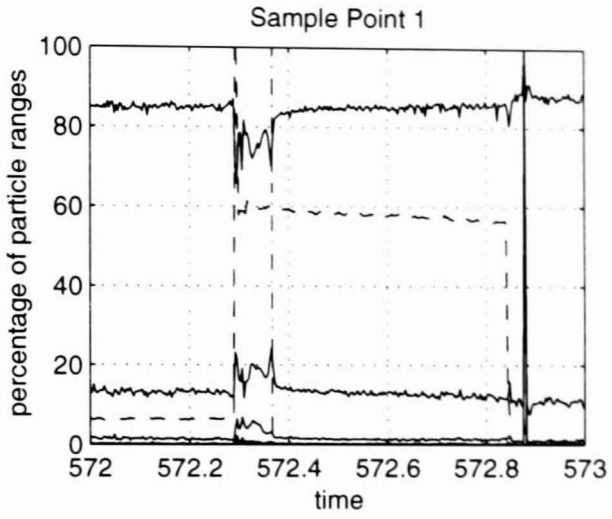


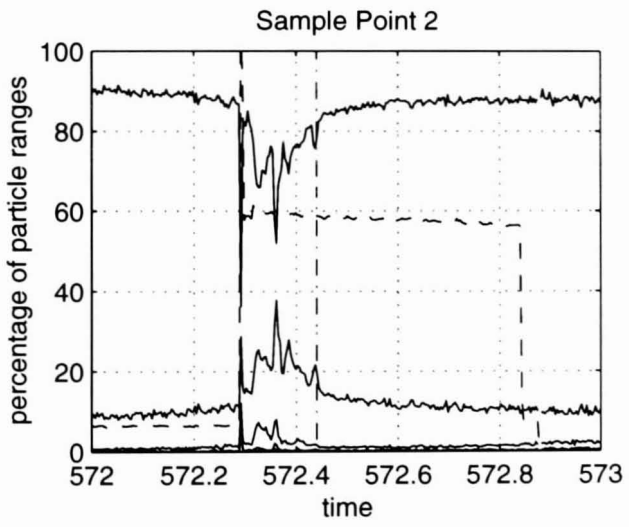


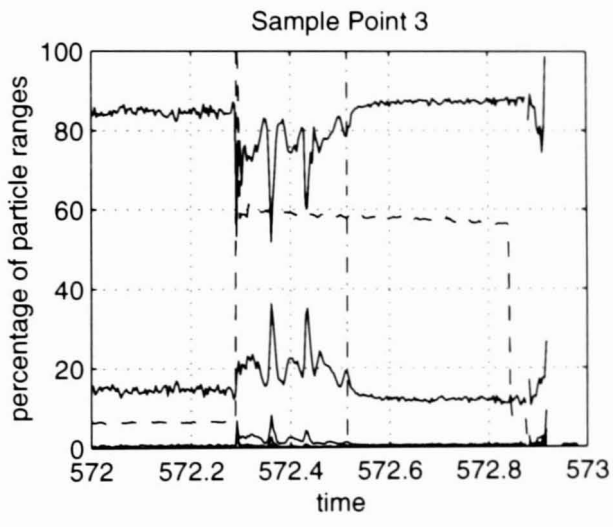


**Figure A.13:** *Step flow trial 1, 25 July 1996: particle counter size distributions; time is in days since 1 January 1995, flow (dashed line) is multiplied by 100, the elapse of one travel time is indicated by a vertical dashed-dotted line, both are included for reference. Inlet particle counter size distribution data is not available for this step flow trial.*

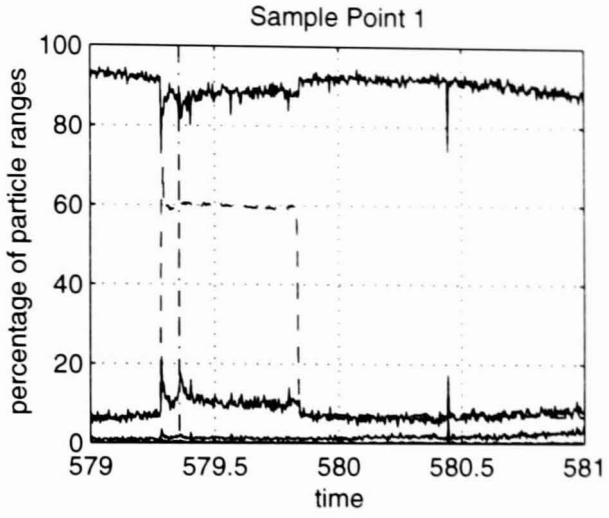


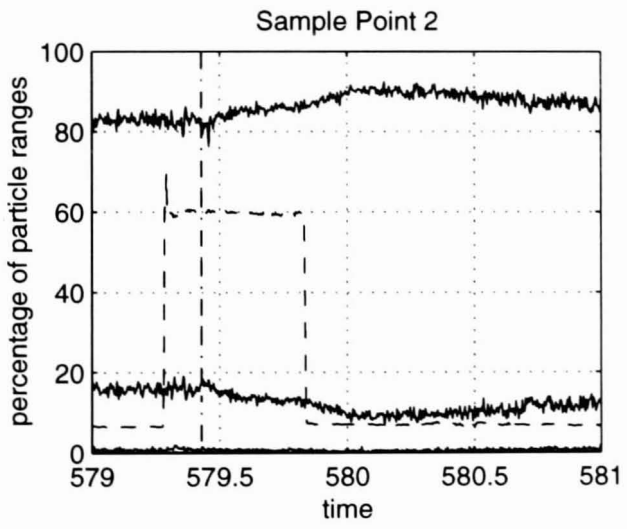


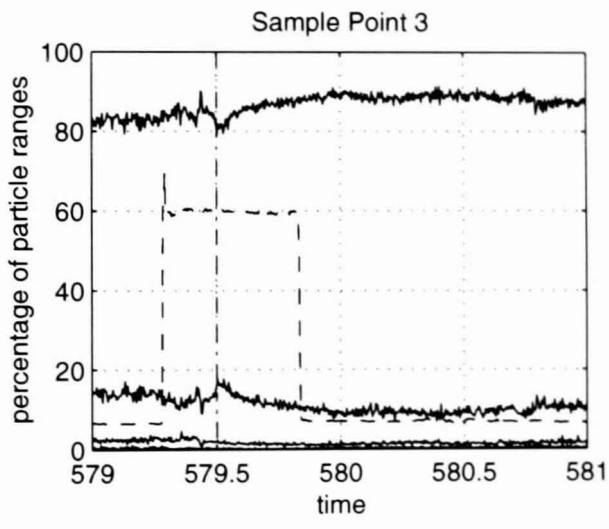


**Figure A.14:** *Step flow trial 2, 1 August 1996: particle counter size distributions; time is in days since 1 January 1995, flow (dashed line) is multiplied by 100, the elapse of one travel time is indicated by a vertical dashed-dotted line, both are included for reference. Inlet particle counter size distribution data is not available for this step flow trial.*

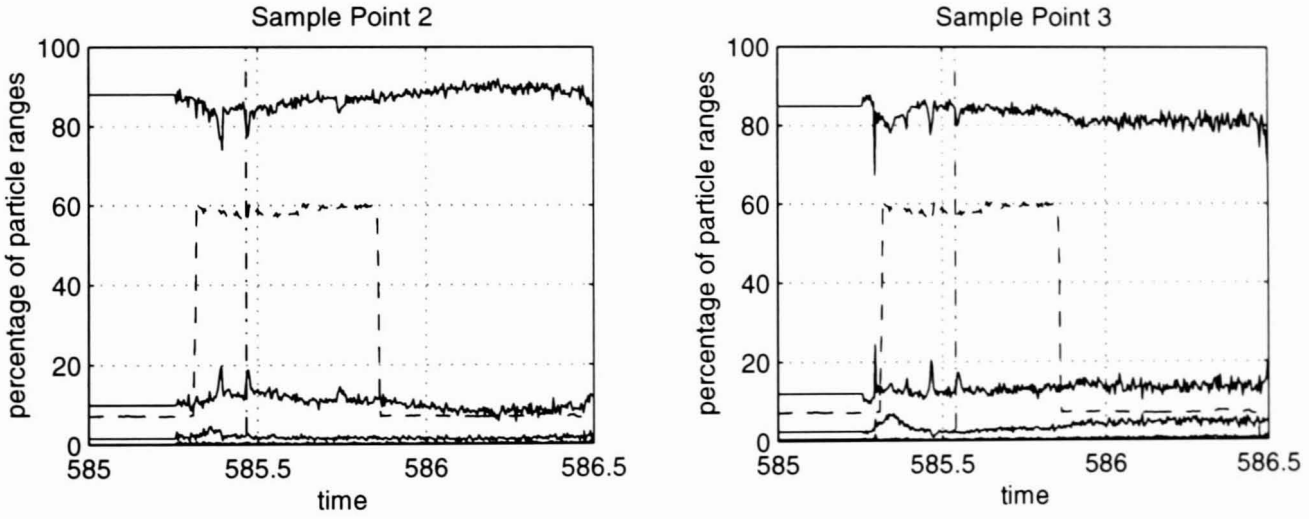


**Figure A.15:** *Step flow trial 3, 7 August 1996: particle counter size distributions; time is in days since 1 January 1995, flow (dashed line) is multiplied by 100, the elapse of one travel time is indicated by a vertical dashed-dotted line, both are included for reference. Inlet particle counter size distribution data is not available for this step flow trial.*

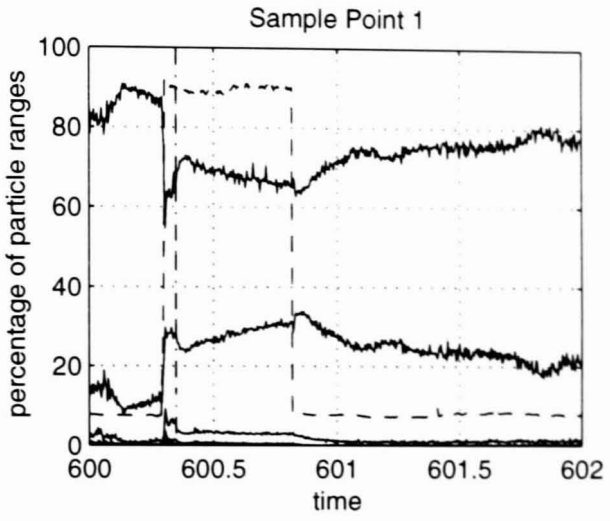


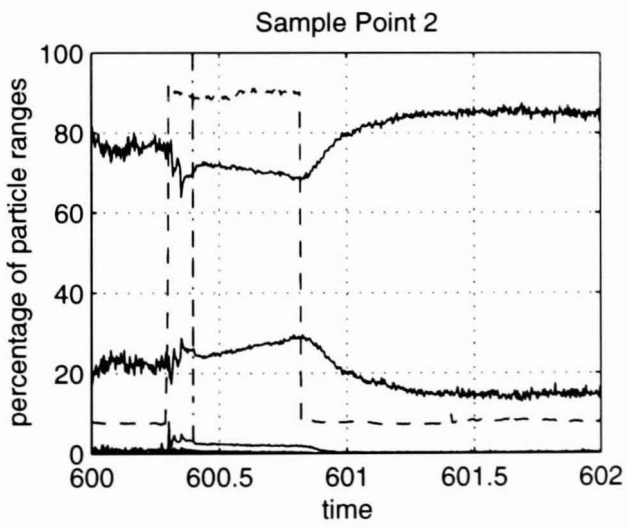


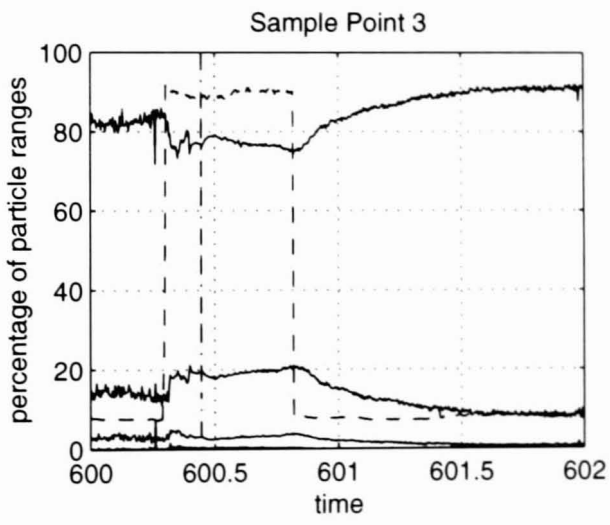


**Figure A.16:** *Step flow trial 4, 22 August 1996: particle counter size distributions; time is in days since 1 January 1995, flow (dashed line) is multiplied by 100, the elapse of one travel time is indicated by a vertical dashed-dotted line, both are included for reference. Inlet particle counter size distribution data is not available for this step flow trial.*

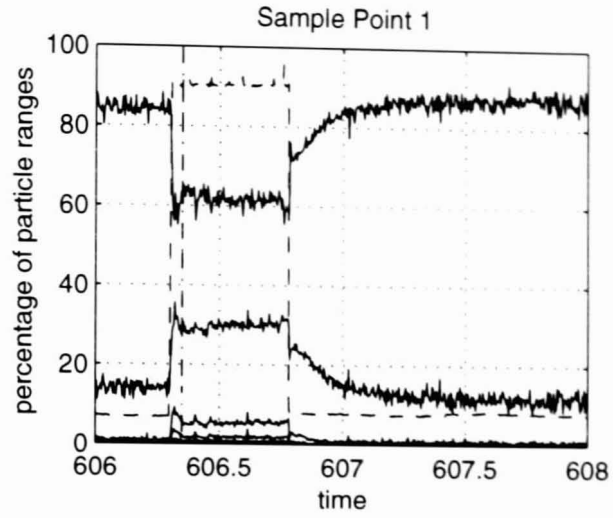


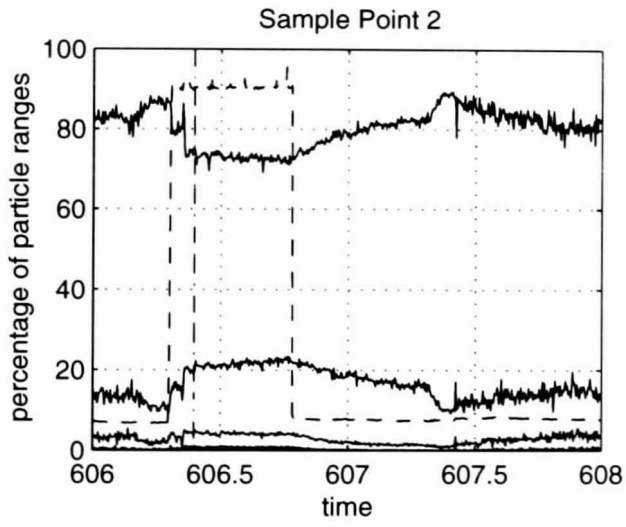


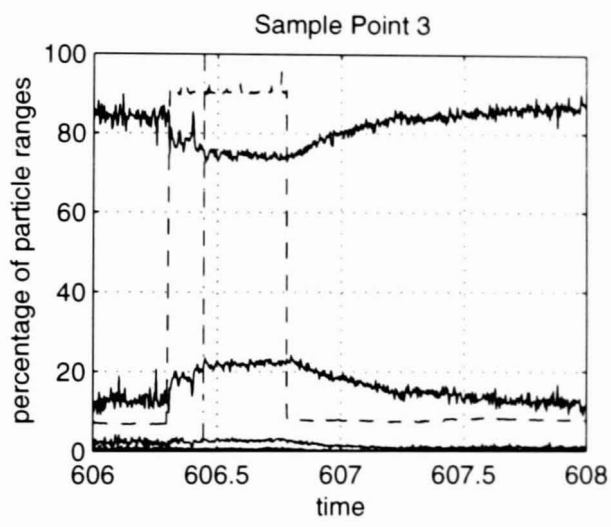


**Figure A.17:** *Step flow trial 5, 28 August 1996: particle counter size distributions; time is in days since 1 January 1995, flow (dashed line) is multiplied by 100, the elapse of one travel time is indicated by a vertical dashed-dotted line, both are included for reference. Inlet particle counter data was not yet computer logged (hand-logged data is shown). Inlet particle counter size distribution data is not available for this step flow trial.*

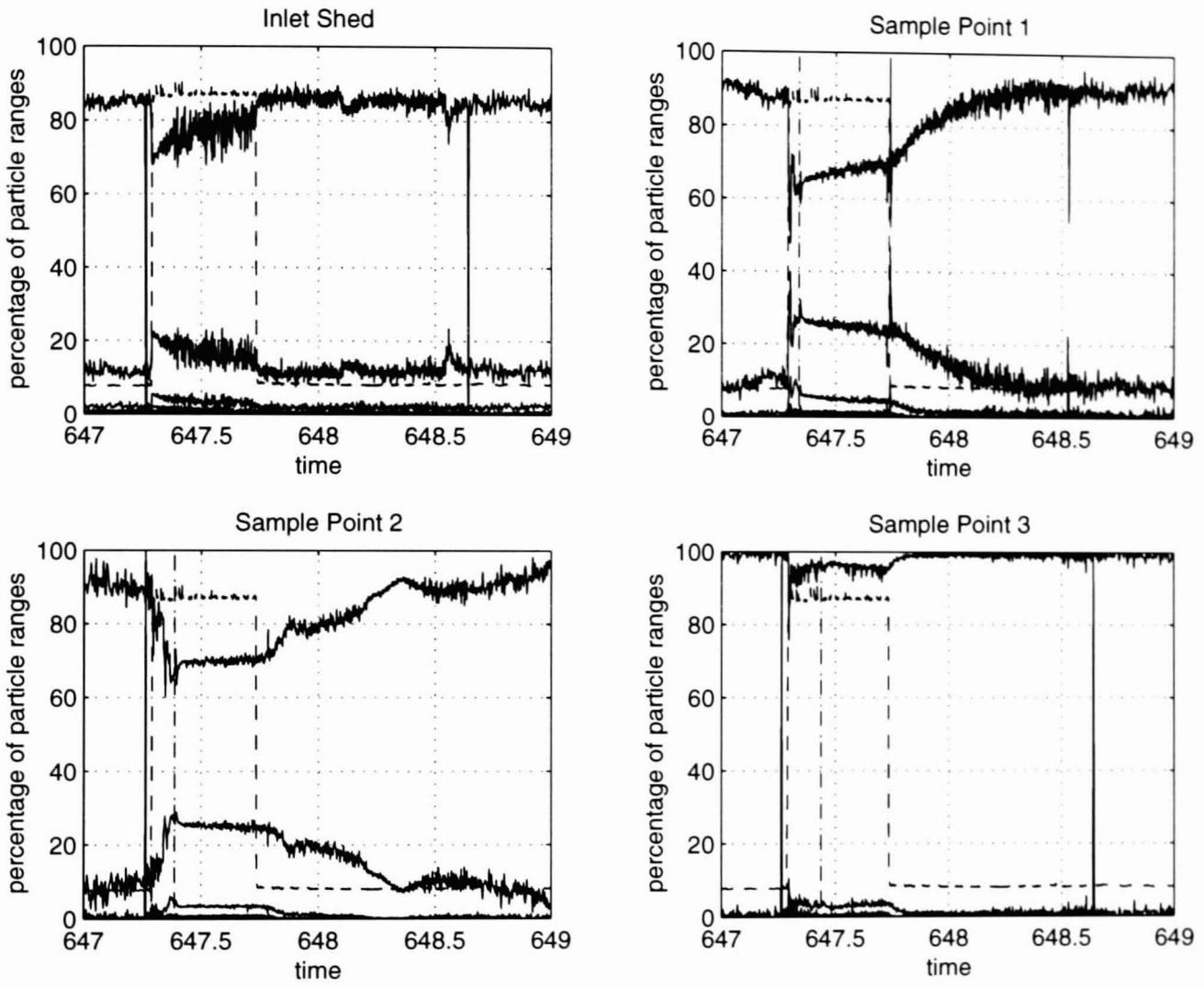


**Figure A.18:** *Step flow trial 6, 8 October 1996: particle counter size distributions; time is in days since 1 January 1995, flow (dashed line) is multiplied by 100, the elapse of one travel time is indicated by a vertical dashed-dotted line, both are included for reference.*

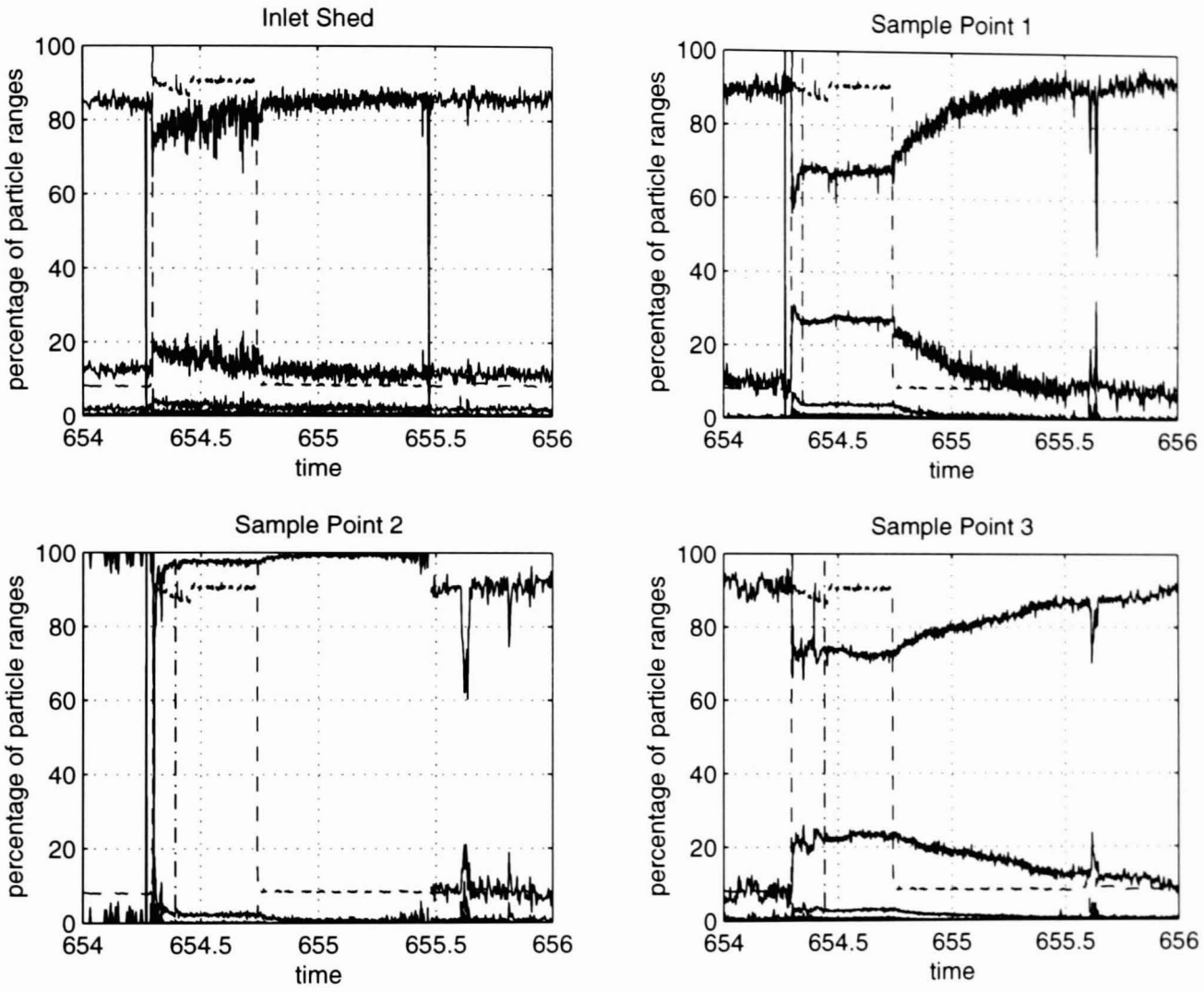


**Figure A.19:** *Step flow trial 7, 15 October 1996: particle counter size distributions; time is in days since 1 January 1995, flow (dashed line) is multiplied by 100, the elapse of one travel time is indicated by a vertical dashed-dotted line, both are included for reference.*

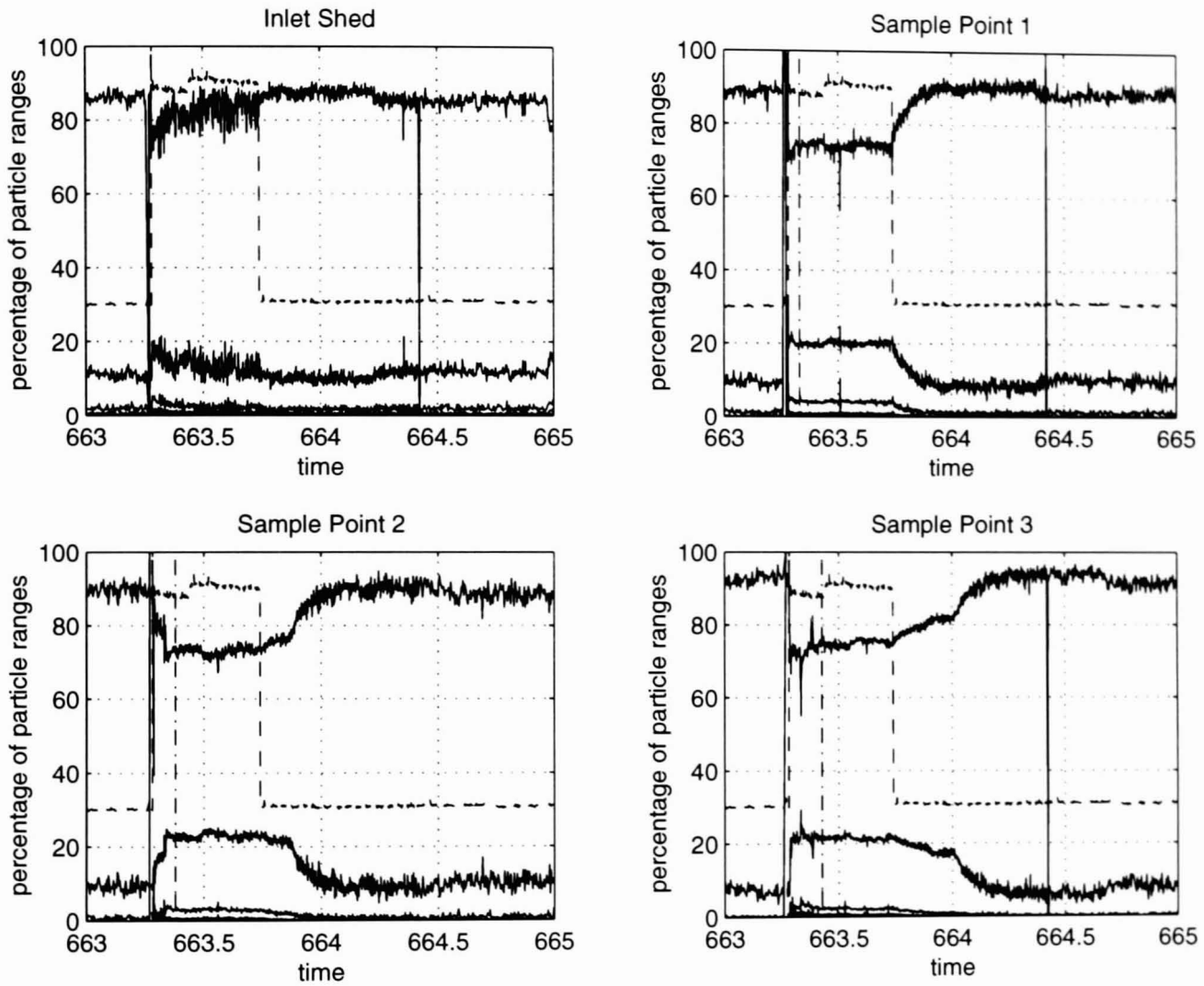


**Figure A.20:** *Step flow trial 8, 24 October 1996: particle counter size distributions; time is in days since 1 January 1995, flow (dashed line) is multiplied by 100, the elapse of one travel time is indicated by a vertical dashed-dotted line, both are included for reference.*

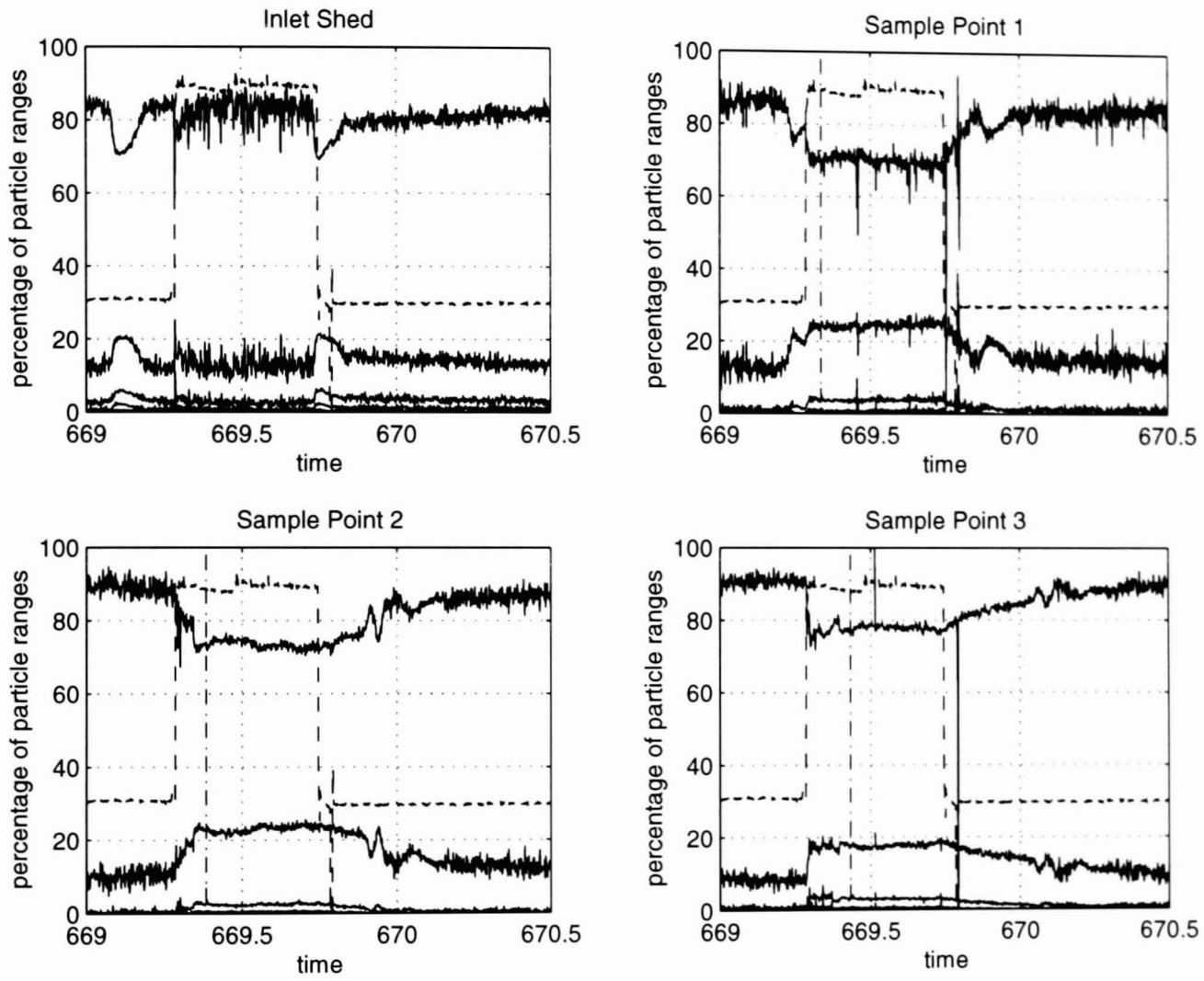


**Figure A.21:** *Step flow trial 9, 30 October 1996: particle counter size distributions; time is in days since 1 January 1995, flow (dashed line) is multiplied by 100, the elapse of one travel time is indicated by a vertical dashed-dotted line, both are included for reference.*

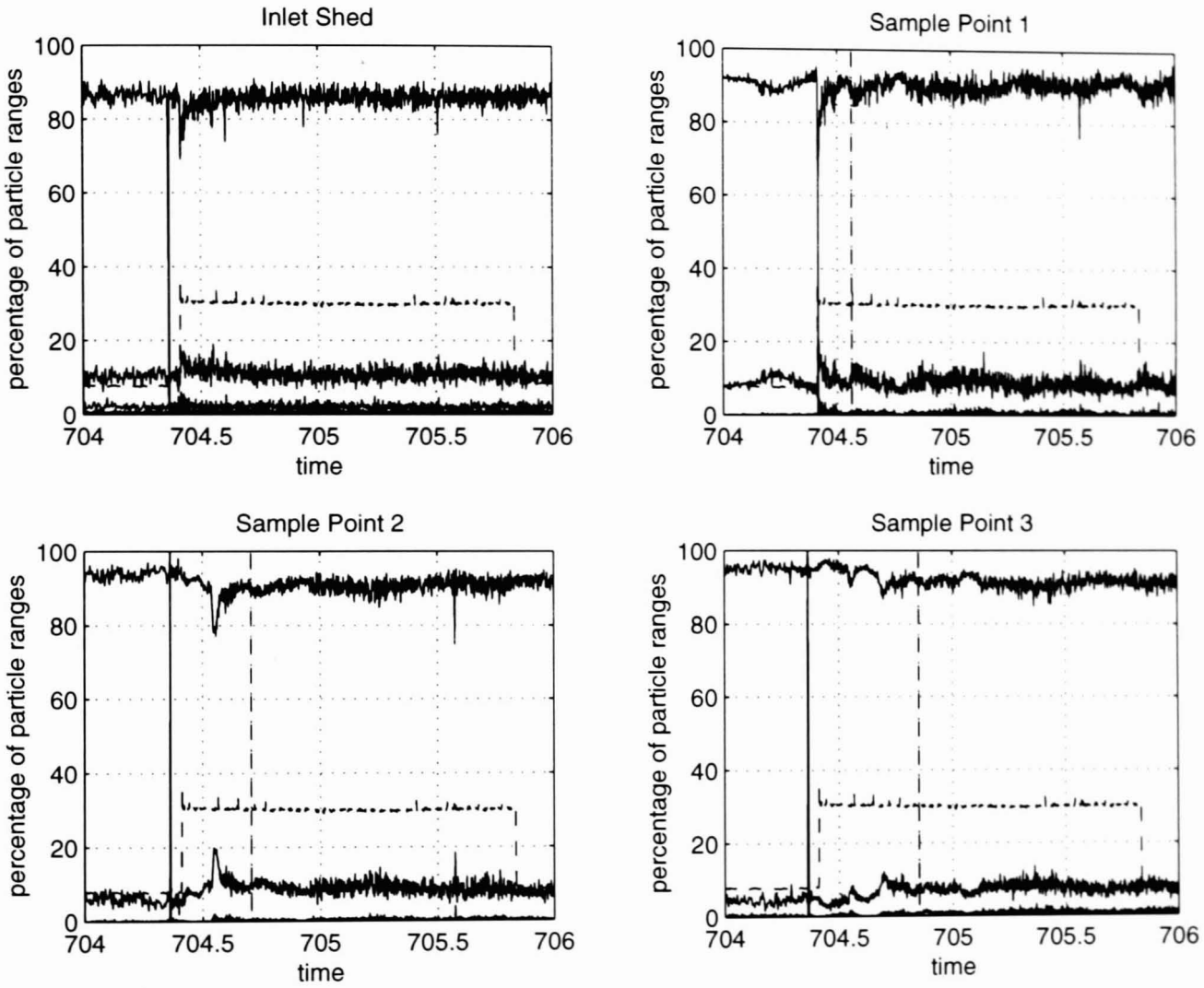


**Figure A.22:** *Step flow trial 10, 4–5 December 1996: particle counter size distributions; time is in days since 1 January 1995, flow (dashed line) is multiplied by 100, the elapse of one travel time is indicated by a vertical dashed-dotted line, both are included for reference.*

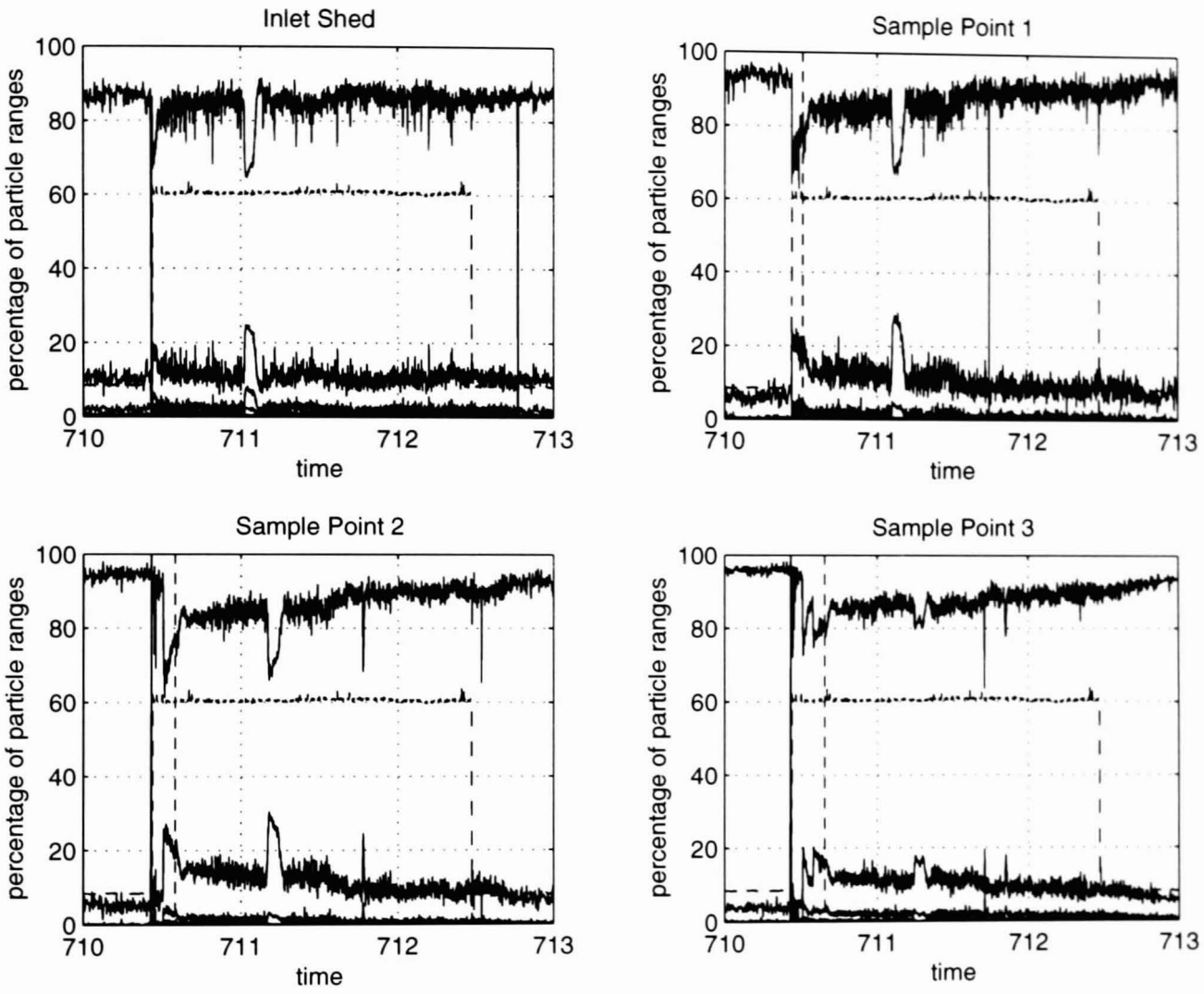


**Figure A.23:** *Step flow trial 11, 10–12 December 1996: particle counter size distributions; time is in days since 1 January 1995, flow (dashed line) is multiplied by 100, the elapse of one travel time is indicated by a vertical dashed-dotted line, both are included for reference.*

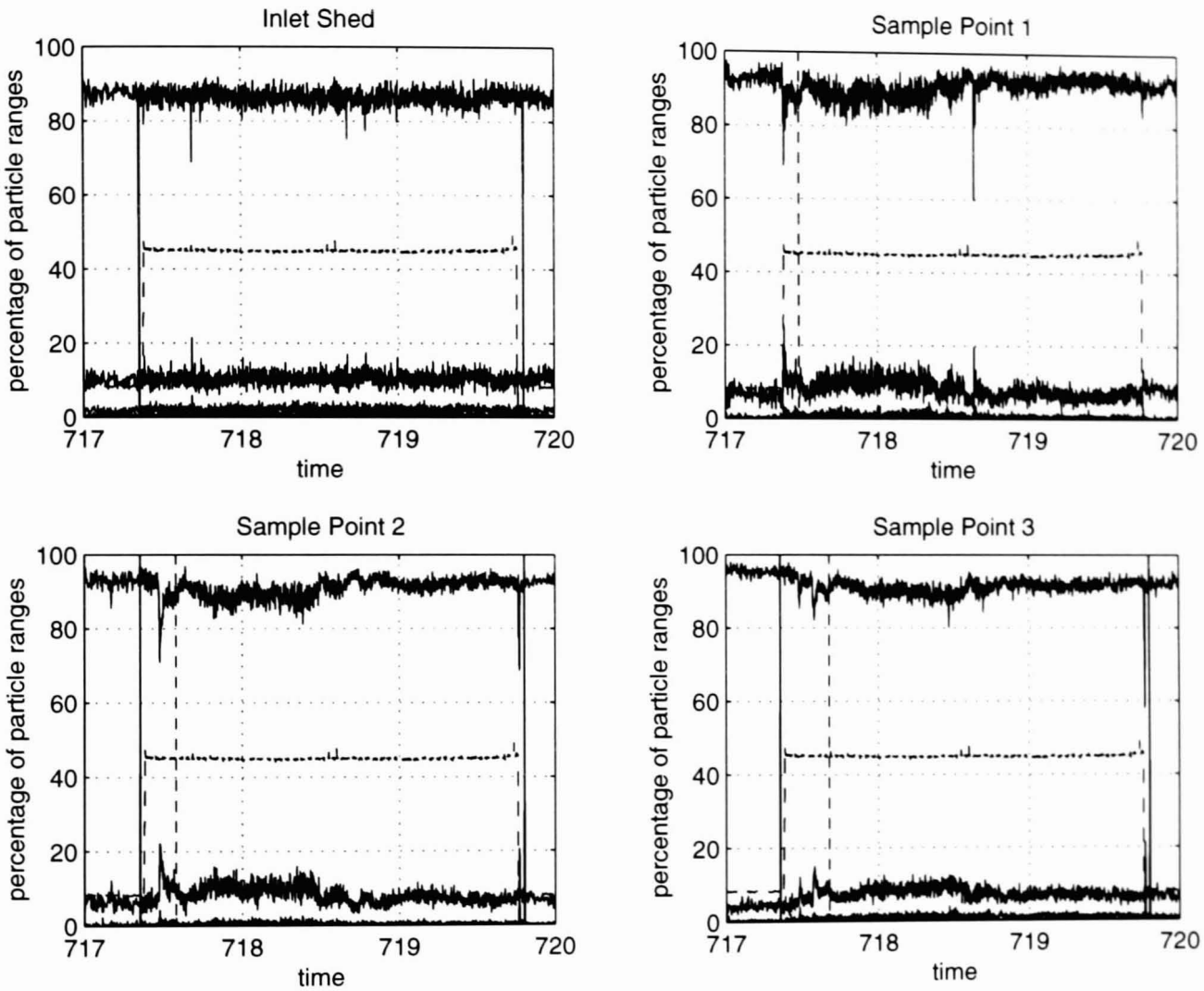


**Figure A.24:** *Step flow trial 12, 17–19 December 1996: particle counter size distributions; time is in days since 1 January 1995, flow (dashed line) is multiplied by 100, the elapse of one travel time is indicated by a dotted line, both are included for reference.*

# Appendix B

# Calculations for the Determination of $k_1(f), k_2(f)$

## B.1 Introduction

In section 6.5.3 an outline of the calculations that were used to determine the parameters $k_1(f)$ and $k_2(f)$ of the model of the response of particle counts to a step increase in flow is given. To maintain the flow of thought intermediate equations were omitted there, but are provided in this appendix.

Let us recall the particle counts model eq. (6.9) on page 149:

$$p(t) = v \int_{\vartheta=0}^{T} b^*(\vartheta) \left(k_1(f)\mathrm{e}^{-a(t-\vartheta)} + k_2(f)\right) 1(t-\vartheta)\,\mathrm{d}\vartheta, \tag{B.1}$$

with

$$1(t) = \begin{cases} 1 & \text{if } t > 0 \\ 0 & \text{otherwise} \end{cases} \tag{B.2}$$

From this it follows that for $t > T$ ($1(t)$ not necessary) the parameters $c_1(T)$

and $c_2(T)$ can be calculated,

$$c_1(T) = vk_1(f) \int_{\vartheta=0}^{T} b^*(\vartheta) \mathrm{e}^{a\vartheta} \, \mathrm{d}\vartheta. \tag{B.3}$$

$$c_2(T) = vk_2(f) \int_{\vartheta=0}^{T} b^*(\vartheta) \, \mathrm{d}\vartheta. \tag{B.4}$$

which can be found independent of these equations directly from the particle counter data.

In addition, the inverse $S^{-1}(s)$ of the Laplace transform $S(s)$ of the shear-off function $s(t)$ is used. The Laplace back-transform of $S^{-1}(s)$ is denoted by $s_{inv}(t)$. It is

$$b^*(\vartheta) = \frac{1}{v} \int_0^{\vartheta} p(t) s_{inv}(\vartheta - t) \, \mathrm{d}t. \tag{B.5}$$

with

$$s_{inv}(t) = \mathcal{L}^{-1} \left\{ \frac{1}{S(s)} \right\}. \tag{B.6}$$

## B.2 Calculation of the Laplace Back-Transform

The aim is to find

$$\begin{aligned} s_{inv}(t) &= \mathcal{L}^{-1} \left\{ \frac{s(s+a)}{s(k_1(f)+k_2(f))+ak_2(f)} \right\} \\ &= \mathcal{L}^{-1} \left\{ \frac{s^2}{s(k_1(f)+k_2(f))+ak_2(f)} \right\} + \mathcal{L}^{-1} \left\{ \frac{as}{s(k_1(f)+k_2(f))+ak_2(f)} \right\}. \end{aligned} \tag{B.7}$$

With $\mathcal{L}\{f(t)\} = F(s)$, the well known theorem [18, 82] can be written as

$$\mathcal{L}\left\{f^{(n)}(t)\right\} = s^n F(s) - s^{n-1} f_0 - \cdots - s f_0^{(n-2)} - f_0^{(n-1)}. \tag{B.8}$$

with

$$f_0^{(\nu)} = \lim_{t \to +0} \frac{\mathrm{d}^\nu f(t)}{\mathrm{d}t^\nu} \tag{B.9}$$

Thus (since the Laplace transform is linear)

$$\begin{aligned} \mathcal{L}^{-1}\{sF(s)\} &= \mathcal{L}^{-1}\{sF(s) - f_0\} + \mathcal{L}^{-1}\{f_0\} \\ &= f'(t) + f_0\delta(t) \qquad \text{(B.10)} \\ \mathcal{L}^{-1}\{s^2F(s)\} &= \mathcal{L}^{-1}\{s^2F(s) - sf_0 - f_0'\} + \mathcal{L}^{-1}\{sf_0\} + \mathcal{L}^{-1}\{f_0'\} \\ &= f''(t) + f_0\delta'(t) + f_0'\delta(t), \qquad \text{(B.11)} \end{aligned}$$

where prime denotes differentiation, so that $f'(t)$ is the first and $f''(t)$ the second derivative of $f(t)$ with respect to $t$. In eqs. (B.10) and (B.11) Dirac's delta impulse is used [70, 79]. The validity of the use of the Dirac impulse in this context can be seen from pp. 92/93 in [70] or p. 202 in [79]. However, it can also be calculated. Consider the definition of the Laplace transform to find:

$$\begin{aligned} \mathcal{L}\{\delta'(t-a)\} &= \int_0^\infty \mathrm{e}^{-st}\delta'(t-a)\mathrm{d}t \\ &= \left[e^{-st}\delta(t-a)\right]_{t=0}^{\infty} - \int_0^\infty \frac{\mathrm{d}}{\mathrm{d}t}e^{-st}\delta(t-a)\mathrm{d}t \\ &= se^{-sa}, \qquad \text{(B.12)} \end{aligned}$$

where integration by parts and the fact that $\delta(t-a) = 0$ for $t = 0$ and $e^{-st} = 0$ for $t \to \infty$ is used. Hoskins [70] remarks at this point "... that strictly this last step does involve a tacit appeal to the pointwise behaviour of the delta function. However, all that we are really saying is that the operational property of $\delta$ is confined absolutely to the point $t = 0$. At any other points it has no effect, and this is what is really meant by saying that it 'evaluates to zero' at such points" (p.53/54). Then by formally setting $a = 0$, the following is obtained:

$$\mathcal{L}\{\delta'(t)\} = s. \tag{B.13}$$

Note that the respective integral is not defined for $a = 0$, but this result is consistend within the framework of the Laplace transform and therefore generally adopted (see p. 202 in [79] or p. 82/83 in [70]).

With the help of on eqs. (B.10) and (B.11) eq. (B.7) can be solved:

$$\begin{aligned}
&\mathcal{L}^{-1}\left\{\frac{s^2}{s(k_1(f)+k_2(f))+ak_2(f)}\right\}+\mathcal{L}^{-1}\left\{\frac{as}{s(k_1(f)+k_2(f))+ak_2(f)}\right\}= \\
=&\frac{\mathrm{d}^2}{\mathrm{d}t^2}\left[\frac{1}{k_1(f)+k_2(f)}\mathrm{e}^{-\frac{ak_2(f)}{k_1(f)+k_2(f)}t}\right]+\frac{1}{k_1(f)+k_2(f)}\delta'(t)-\frac{ak_2(f)}{(k_1(f)+k_2(f))^2}\delta(t)- \\
&\frac{\mathrm{d}}{\mathrm{d}t}\left[\frac{a}{k_1(f)+k_2(f)}\mathrm{e}^{-\frac{ak_2(f)}{k_1(f)+k_2(f)}t}\right]+\frac{a}{k_1(f)+k_2(f)}\delta(t) \\
=&\left[\frac{a^2k_2(f)^2}{(k_1(f)+k_2(f))^3}-\frac{a^2k_2(f)}{(k_1(f)+k_2(f))^2}\right]\mathrm{e}^{-\frac{ak_2(f)}{k_1(f)+k_2(f)}t}+\frac{ak_1(f)}{(k_1(f)+k_2(f))^2}\delta(t)+ \\
&+\frac{1}{k_1(f)+k_2(f)}\delta'(t)
\end{aligned} \tag{B.14}$$

Therefore, the inverse shear-off function is obtained to be

$$\begin{aligned}
s_{inv}(t) =& -\frac{a^2k_1(f)k_2(f)}{(k_1(f)+k_2(f))^3}\mathrm{e}^{\frac{-ak_2(f)}{k_1(f)+k_2(f)}t}+\frac{ak_1(f)}{(k_1(f)+k_2(f))^2}\delta(t)+ \\
&+\frac{1}{k_1(f)+k_2(f)}\delta'(t).
\end{aligned} \tag{B.15}$$

as given in eq. (6.29) on page 161. This result was also double-checked with Mathematica [158].

## B.3 Calculation of the Full Integral

Now eqs. (B.3) and (B.4) will be solved.

However, first the abbreviation is introduced

$$g_i(\vartheta) = \begin{cases} e^{a\vartheta}, & i = 1 \\ 1, & i = 2 \end{cases} \tag{B.16}$$

and calculate the following integral:

$$\begin{aligned}
&\int_{t=0}^{\vartheta} p(t)\frac{1}{k_1(f)+k_2(f)}\delta'(\vartheta-t)g_i(\vartheta)\mathrm{d}t = \\
&=\frac{g_i(\vartheta)}{k_1(f)+k_2(f)}\left[-p(t)\delta(\vartheta-t)\right]_{t=0}^{\vartheta} - \int_0^{\vartheta} -p'(t)\frac{1}{k_1(f)+k_2(f)}\delta(\vartheta-t)g_i(\vartheta)\mathrm{d}t \\
&=p'(\vartheta)\frac{1}{k_1(f)+k_2(f)}g_i(\vartheta).
\end{aligned} \tag{B.17}$$

Note that the minus signs in front of $p(t)$ and $p'(t)$ within the integration by parts originate from the argument of the delta impulse, which is negative in $t$. The above result is only valid for $p(0) = 0$ and the interpretation of the limit at $t = \vartheta$ follows the argumentation of eqs. (B.12) and (B.13).

Now, for $i = 1, 2$, eqs. (B.3) and (B.4) can be written as

$$\begin{aligned}
c_i(T) =& k_i \int_{\vartheta=0}^{T}\int_{t=0}^{\vartheta} p(t)s_{inv}(\vartheta-t)g_i(\vartheta)\,\mathrm{d}t\,\mathrm{d}\vartheta \\
=& k_i \int_{\vartheta=0}^{T}\int_{t=0}^{\vartheta} p(t)\left(-\frac{a^2k_1(f)k_2(f)}{(k_1(f)+k_2(f))^3}\mathrm{e}^{-\frac{ak_2(f)}{k_1(f)+k_2(f)}(\vartheta-t)}+\right. \\
&\left.+\frac{ak_1(f)}{(k_1(f)+k_2(f))^2}\delta(\vartheta-t)+\frac{\delta'(\vartheta-t)}{k_1(f)+k_2(f)}\right)g_i(\vartheta)\,\mathrm{d}t\,\mathrm{d}\vartheta \\
=& k_i \int_{\vartheta=0}^{T}\int_{t=0}^{\vartheta} -p(t)\frac{a^2k_1(f)k_2(f)}{(k_1(f)+k_2(f))^3}\mathrm{e}^{-\frac{ak_2(f)}{k_1(f)+k_2(f)}(\vartheta-t)}g_i(\vartheta)\,\mathrm{d}t\,\mathrm{d}\vartheta + \\
&+ k_i \int_0^{T} p(\vartheta)\frac{ak_1(f)}{(k_1(f)+k_2(f))^2}g_i(\vartheta)\,\mathrm{d}\vartheta + \\
&+ k_i \int_{\vartheta=0}^{T}\int_{t=0}^{\vartheta} p(t)\frac{1}{k_1(f)+k_2(f)}\delta'(\vartheta-t)g_i(\vartheta)\mathrm{d}t\,\mathrm{d}\vartheta \\
c_i(T) =& k_i \int_{\vartheta=0}^{T}\int_{t=0}^{\vartheta} -p(t)\frac{a^2k_1(f)k_2(f)}{(k_1(f)+k_2(f))^3}\mathrm{e}^{-\frac{ak_2(f)}{k_1(f)+k_2(f)}(\vartheta-t)}g_i(\vartheta)\,\mathrm{d}t\,\mathrm{d}\vartheta + \\
&+ k_i \int_0^{T}\left(p(\vartheta)\frac{ak_1(f)}{(k_1(f)+k_2(f))^2}+\frac{\mathrm{d}p(\vartheta)}{\mathrm{d}\vartheta}\frac{1}{k_1(f)+k_2(f)}\right)g_i(\vartheta)\,\mathrm{d}\vartheta.
\end{aligned} \tag{B.18}$$

Eq. (B.18) is the same as eq. (6.31) on page 162.

## B.4 A Test of Validity

A simple test of the validity of eq. (B.18) can be performed by calculating a known case. This obviously does not prove that the equation is valid, however, it gives some evidence to that effect. Take a step response of $S(s)$, i.e. a flat biofilm profile with magnitude 1 is the input of the system $S(s)$. In that case, eq. (B.5) leads to:

$$\frac{1}{v}\int_0^{\vartheta} p(t)s_{inv}(\vartheta - t)\,\mathrm{d}t = 1. \tag{B.19}$$

Furthermore, the response of the system for $t < T$ is known to be

$$p(t) = \frac{vk_1(f)}{a}\left(1 - \mathrm{e}^{-at}\right)\,1(t) + vk_2(f)t\,1(t), \quad t < T \tag{B.20}$$

$$p'(t) = vk_1(f)\mathrm{e}^{-at}\,1(t) + vk_2(f)\,1(t), \quad t < T \tag{B.21}$$

Note, that the condition $p(0) = 0$ is fulfilled in this case. Thus, for $t < T$ (i.e. $\vartheta < T$)[1]

$$\begin{aligned}
1 =& \frac{1}{v}\int_{t=0}^{\vartheta} -p(t)\frac{a^2k_1(f)k_2(f)}{(k_1(f)+k_2(f))^3}\mathrm{e}^{-\frac{ak_2(f)}{k_1(f)+k_2(f)}(\vartheta-t)}\,\mathrm{d}t + \\
&+ \frac{1}{v}p(\vartheta)\frac{ak_1(f)}{(k_1(f)+k_2(f))^2} + \frac{1}{v}p'(\vartheta)\frac{1}{k_1(f)+k_2(f)} \\
=& \int_{t=0}^{\vartheta} -\frac{ak_1(f)^2k_2(f)}{(k_1(f)+k_2(f))^3}\mathrm{e}^{-\frac{ak_2(f)}{k_1(f)+k_2(f)}(\vartheta-t)} + \frac{ak_1(f)^2k_2(f)}{(k_1(f)+k_2(f))^3} \times \\
&\times \mathrm{e}^{-\frac{a}{k_1(f)+k_2(f)}(k_1(f)t+k_2(f)\vartheta)} - \frac{a^2k_1(f)k_2(f)^2}{(k_1(f)+k_2(f))^3}t\mathrm{e}^{-\frac{ak_2(f)}{k_1(f)+k_2(f)}(\vartheta-t)}\,\mathrm{d}t + \\
&+ \left(\frac{k_1(f)}{a}\left(1-\mathrm{e}^{-a\vartheta}\right) + k_2(f)\vartheta\right)\frac{ak_1(f)}{(k_1(f)+k_2(f))^2} + \frac{k_1(f)\mathrm{e}^{-a\vartheta}+k_2(f)}{k_1(f)+k_2(f)}.
\end{aligned} \tag{B.22}$$

[1] Note that eq. (B.18) is only concerned with $0 \le \vartheta \le T$

Using integration by parts, the following is obtained

$$\begin{aligned}
&\int_0^{\vartheta} -\frac{a^2 k_1(f) k_2(f)^2}{(k_1(f)+k_2(f))^3} t \mathrm{e}^{\frac{ak_2(f)}{k_1(f)+k_2(f)}(t-\vartheta)}\,\mathrm{d}t = \\
&\qquad = -\frac{ak_1(f)k_2(f)}{(k_1(f)+k_2(f))^2}\vartheta + 0\cdot\frac{ak_1(f)k_2(f)}{(k_1(f)+k_2(f))^2}\mathrm{e}^{-\frac{ak_2(f)}{k_1(f)+k_2(f)}\vartheta} + \\
&\qquad\quad + \frac{ak_1(f)k_2(f)}{(k_1(f)+k_2(f))^2}\frac{k_1(f)+k_2(f)}{ak_2(f)}\left(1-\mathrm{e}^{-\frac{ak_2(f)}{k_1(f)+k_2(f)}\vartheta}\right).
\end{aligned} \tag{B.23}$$

With this result:

$$\begin{aligned}
1 = &\int_{t=0}^{\vartheta} -\frac{ak_1(f)^2k_2(f)}{(k_1(f)+k_2(f))^3}\mathrm{e}^{-\frac{ak_2(f)}{k_1(f)+k_2(f)}(\vartheta-t)} + \frac{ak_1(f)^2k_2(f)}{(k_1(f)+k_2(f))^3}\times \\
&\times \mathrm{e}^{-\frac{a}{k_1(f)+k_2(f)}(k_1(f)t+k_2(f)\vartheta)}\,\mathrm{d}t - \frac{ak_1(f)k_2(f)}{(k_1(f)+k_2(f))^2}\vartheta + \frac{k_1(f)}{k_1(f)+k_2(f)} \\
&- \frac{k_1(f)}{k_1(f)+k_2(f)}\mathrm{e}^{-\frac{ak_2(f)}{k_1(f)+k_2(f)}\vartheta} + \frac{k_1(f)^2}{(k_1(f)+k_2(f))^2}\left(1-\mathrm{e}^{-a\vartheta}\right) + \\
&+ \frac{ak_1(f)k_2(f)}{(k_1(f)+k_2(f))^2}\vartheta + \frac{k_1(f)}{k_1(f)+k_2(f)}\mathrm{e}^{-a\vartheta} + \frac{k_2(f)}{k_1(f)+k_2(f)} \\
= &-\frac{ak_1(f)^2k_2(f)}{(k_1(f)+k_2(f))^3}\frac{k_1(f)+k_2(f)}{ak_2(f)}\left(1-\mathrm{e}^{-\frac{ak_2(f)}{k_1(f)+k_2(f)}\vartheta}\right) + \\
&+ \frac{ak_1(f)^2k_2(f)}{(k_1(f)+k_2(f))^3}\frac{k_1(f)+k_2(f)}{-ak_1(f)}\left(\mathrm{e}^{-a\vartheta}-\mathrm{e}^{-\frac{ak_2(f)}{k_1(f)+k_2(f)}\vartheta}\right) + \\
&+ \frac{k_1(f)+k_2(f)}{k_1(f)+k_2(f)} - \frac{k_1(f)(k_1(f)+k_2(f))}{(k_1(f)+k_2(f))^2}\mathrm{e}^{-\frac{ak_2(f)}{k_1(f)+k_2(f)}\vartheta} + \\
&+ \frac{k_1(f)^2}{(k_1(f)+k_2(f))^2} + \left(\frac{k_1(f)}{k_1(f)+k_2(f)} - \frac{k_1(f)^2}{(k_1(f)+k_2(f))^2}\right)\mathrm{e}^{-a\vartheta} \\
= &\ 1,
\end{aligned} \tag{B.24}$$

as expected.

# Appendix C

# Implementation in Matlab

## C.1 Overview

The Water Quality Toolbox written during the work for this PhD contains over 100 Matlab functions and scripts. Its current version is 2.3 and it is written for Matlab 5. The purpose of this toolbox is to facilitate the analyses necessary for modelling water quality in the "TORUS" pipe rig of Thames Water. It contains function for reading data into Matlab, has its own time format, contains several functions for visualisation and graphical input, includes the preprocessing (as discussed in section 5.5), is capable of finding the parameters of the particle counts model and the biofilm shedding profile (see section 6.10) and does the calculations of various chlorine decay coefficients (cf. section 7.8).

A discussion of the functionality of the relevant functions is given at the end of each chapter in part III (as indicated in the previous paragraph). In addition a full on-line help is available for each function, a list of all functions is available through `help wqt`. A list of required data files is provided through `wqt_data`, a brief on-line introduction is given through `wqt_info`.

The following section explains briefly the most important functions and script. It is not a full tutorial of the Water Quality Toolbox. For more information see the on-line help.

## C.2 Using the Water Quality Toolbox

### C.2.1 Reading Data and Time Formats

An executable file, **datapre** (source in C++), does some initial conversions on the ASCII output file of the pipe rig computer (extension **wlf**). The converted files have the extension **swlf** and are the input of the load function of the Water Quality Toolbox, **wload**. This function can load pipe rig data between January 1995 and July 1997. If new data is to be analysed, only **wload** of all the functions in the Water Quality Toolbox needs to be modified.

Since the work on this Toolbox started in 1996, this function was originally written for Matlab 4 and no cell arrays were available. This implies that there is a need for four data matrices, one for each sample point (Inlet, SP 1, SP 2, SP 3), because the sizes do not always agree (mainly due to errors or meter failures in single sample points). These variables are declared global and are called **yraw0** (Inlet), **yraw1** (SP 1), **yraw2** (SP 2) and **yraw3** (SP 3). In addition there is **yraw4** which contains the inlet flow readings.

In addition to the logged pipe rig data several bench analyses were done. These results are provided in files with the extension **dat** (see the file **readme** or **wqt_data** in Matlab for a complete list of **swlf** and **dat** files). These data files are loaded through **wxload**.

The Water Quality Toolbox used two time formats of its own. The 'internal' format is days in the year since 1 January 1995 (used in **swlf**-files and all visualisation), the 'external' format is (generally) of the form yyddmm.hhmm with yy=year, dd=day, mm=month, hh=hour, mm=minute. The year is optional, the default is 1996. This format is used in all **dat**-files. The function **wdate** converts into and from these time formats.

### C.2.2 Processing of Raw Data, Visualisation and Graphical Input

A lot of the data processing is done in **wcreate**. This function splits the raw

data matrices `yraw0...yraw4` into columns, depending on which variable is of interest. The columns are referred to by numbers. e.g. 3=total particle counts, 23=total chlorine, 24=temperature. A full list of column numbers and their meaning is obtained with `wcreate('?')`. Use any column>24 with care since calculations may take very long. It is generally better to calculate the chlorine decay coefficients with `wdecay`.

It is also possible to generate a matrix of indices in data vectors created by `wcreate` or in the raw data. These matrices are referred to as minmax-matrices and are generated by `wminmax`.

Visualisation of data is frequently done with the script `lookat`. This script uses `wcreate` internally. This script can plot `swlf`-data and external data (`dat`-files), it can input via a crosshair, plot in subplots, do axes adjustments and change the x-axis labels, among other things. The plot functions `wplot` or `wlog` are used.

Other functions that take graphical input (generally a crosshair) are `finddate`, `findindex`, `findttime`, `finddistance` and `findstepheight`.

The size distributions are no column in the raw data matrices, therefore they have to be calculated separately in the function `sizedistr` and are not included in `wcreate` or `lookat`.

### C.2.3 Data Analysis

The functions and scripts used for the analysis of data as discussed in part III of this thesis are already given in the appropriate chapters (as indicated above). Thus, the implementation of the preprocessing as presented in chapter 5 is given in section 5.5 on page 120, the Matlab functions for the particle counter models and their implications as shown in chapter 6 are provided in section 6.10 on page 183 and the part of the Water Quality Toolbox that is concerned with modelling monochloramine decay (chapter 7) is discussed in section 7.8 on page 207.

These sections together with rest of the respective chapters and the on-line help should give sufficient information for the usage of these functions and scripts.

### C.2.4 Starting a Session

Typically a session of using the Water Quality Toolbox would be started by invoking `wload` (obviously after starting Matlab), e.g. `wload([19 20 22])` to load July, August and October 1996. Subsequently preprocessing is necessary, e.g. it is necessary to run `preproc` (no input arguments). This will set the global variable `preprocessing` to 1 if run successfully, or to 0 otherwise.

After this any of the above mentioned functions or script can be used, e.g. type `lookat` and give as '`dmin`' 572, as '`dmax`' 573 and as '`col`' 3 to see a plot of the total particle counts of SFT 1. Type `?` at the prompt '`Do you wish to see another plot?`' to obtain a list of capabilities of `lookat`. Alternatively, use `wdecay` or `calcdecay` for chlorine decay coefficients or `bioprofi` for the particle counts model and the biofilm shedding profile. See the scripts `calcmax` or `bioscript` for examples of how to use `calcdecay` or `bioprofi`.

## C.3 Summary

This appendix gave a brief overview and introduction into the Water Quality Toolbox written for Matlab 5. A full on-line help complements the above given deliberations. These functions and scripts form a powerful tool for the analysis of "TORUS" pipe rig data and possibly other water quality data. In addition they can be used to reproduce all the data given in this thesis and most of the graphs.

# Appendix D

# Reynolds Numbers

This appendix gives in figure D.1 the Reynolds numbers versus the volumetric flow rate in litres/second for the "TORUS" pipe rig. The Reynolds number $Re$ is calculated as

$$Re = \frac{vd}{\nu} = \frac{f}{250\pi d\nu}. \tag{D.1}$$

where $v$=velocity of water in m/s, $d$=pipe diameter in m, $\nu$=kinematic viscosity of water in $m^2/s$ and $f$=volumetric flow rate of water in l/s. The pipe diameter is in the case of this work assumed to be uniformely 0.11 m.

The kinematic viscosity changes with temperature (see p.337 in [50]). Generally it is assumed that for Reynolds numbers below 2000 the flow is laminar and for Reynolds numbers larger than 4000 it is turbulent (see p.142 in [102]), although these numbers may increase drastically for very smooth pipes.

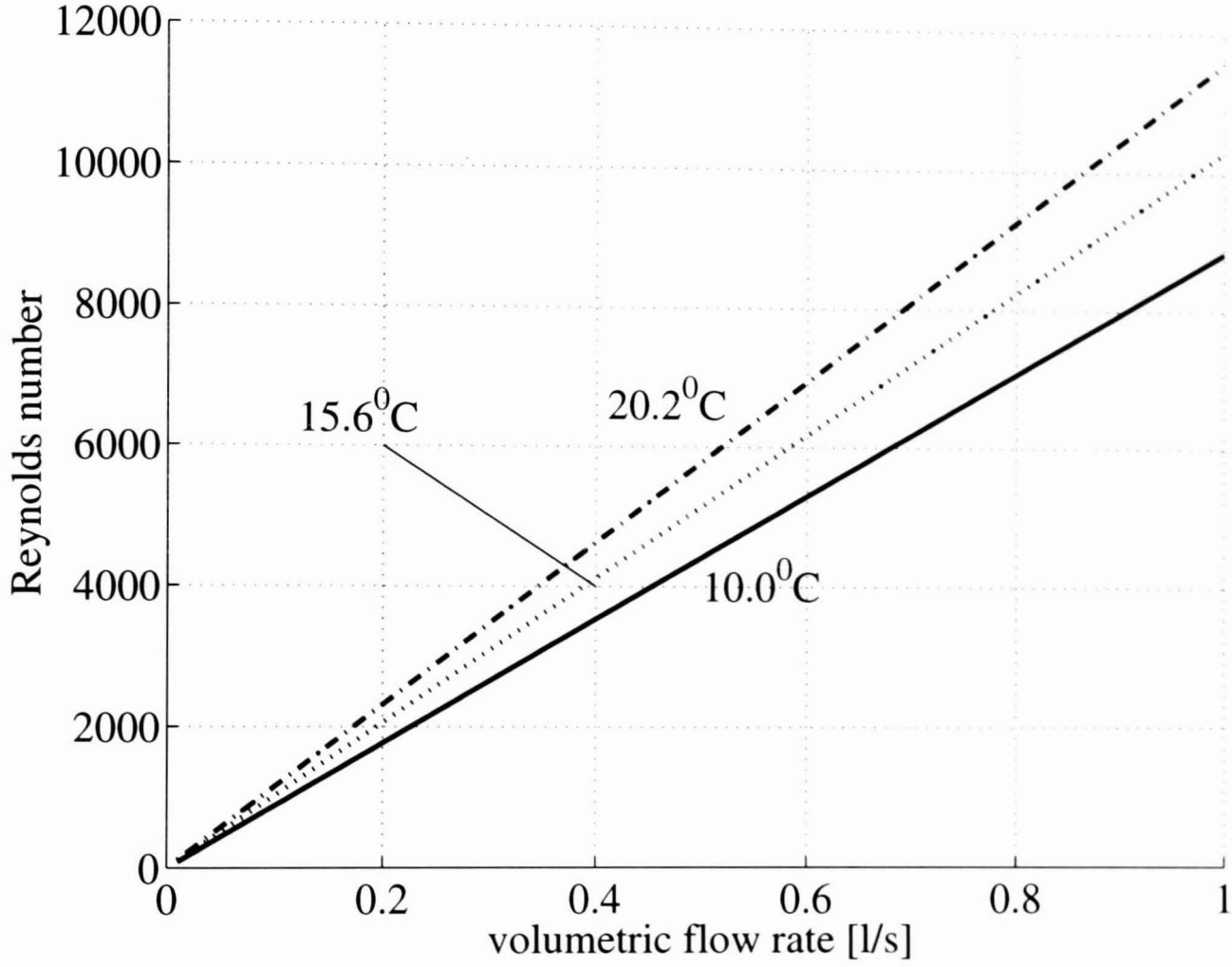


**Figure D.1:** *Reynolds numbers versus volumetric flow for the "TORUS" pipe rig (diameter 110mm). Change in Reynolds number due to change in viscosity with temperature is indicated.*